Magnetic White Dwarf Stars

Thesis by
Angela Putney

In Partial Fulfillment of the Requirements
for the Degree of
Doctor of Philosophy

California Institute of Technology
Pasadena, California

1996
(Submitted October 30, 1995)

©1996
Angela Putney
All Rights Reserved

Acknowledgements

I have often read the acknowledgements of theses and books and wondered why they were so long and thanked so many people. Now I understand.

First, I should thank all the people who made this thesis technically possible. I wish to thank Marshall Cohen, my advisor, for allowing me to pursue a topic so distant from his usual work and for supporting me in the endeavor. I wish to thank Bob Goodrich for teaching me all the ins and outs of optical spectropolarimetry and for answering my questions, no matter how dumb they may have seemed. I wish to thank Jim McCarthy and Neill Reid for answering questions and reading manuscripts. I wish to thank Brad Hansen and Yanqin Wu for helping me with various aspects of white dwarf theory. I wish to thank Patrick Ogle and Hien Tran for help with the observations. I wish to thank the entire Robinson staff. I wish to thank the entire Palomar staff, both on campus and on the mountain, with special thanks going to Juan Carrasco, who served as my night assistant for the majority of my observing runs. I wish to thank our wonderful librarians, Helen Knudsen and Anne Snyder, who managed to find everything I needed, no matter how obscure. I wish to thank Stefan Jordan, my collaborator in white dwarf modeling, who also answered many questions which may have seemed trivial. I wish to thank Prof. Volker Weidemann and his wife Helga for all their hospitality during my extended stay in Kiel, Germany.

Next, I wish to thank everyone at Caltech who helped me keep my sanity while undertaking all this work. In the 5+ years I have been here, I have made a lot of friends and to list them all seems impractical (and if I accidentally left someone off of that list . . .), so I will only list a few (in no particular order). John Cromer, Bill Douglas, Hal Petrie, Ernest Croner, and Fred Barnum who came by regularly to keep the students in the basement from being lonely. The Astronomy softball and soccer teams for getting me out in the fresh (?) air. The professors for throwing parties and BBQs, with extra thanks to the Sargents and Readheads for allowing me to care for their homes and hot tubs. Petra de la Paz, Chris Tinney,

Jamie Schlessman, Neill Reid, Donna Womble, Rudi Danner, John Gizis, Gautam Vashist, Lin Yan, Peter Bryant, Todd Small, Brad Hansen, Rachel Akeson, Chris Fassnacht, John Conway, and Sponger for often putting up with me off campus. Erik Leitch and Rob Langston, my fellow kitchen conspirators and general sanity regulators. Extra thanks goes to Erik Leitch.

I also wish to thank all those not at Caltech who helped me to keep my sanity. Laura Johnston and Cathy Hoffman for all the phone calls, letters, visits, and being friends for so long. Simone Missirian for showing me that there is more to LA than Pasadena. Julie Neugebauer (Davis) for allowing me to crash at her place in San Diego when I needed to get out of town. My mother, my father, my brother Alex, and my Aunt Angela, for always supporting me and encouraging me, no matter what, even if they didn't understand (like how I got paid for doing my research) and it means that I won't be settling down anywhere soon. I wish to thank my grandmother and Mrs. Ellis. Both of these women have been an inspiration to me all my life. They also feel that you are never too old to learn something new. I dedicate this to them.

Abstract

Three aspects of magnetic white dwarf stars are studied to aid in the understanding of stellar evolution.

A survey of $\sim$ 50 DC white dwarf stars was conducted in circular spectropolarimetry to search for magnetic fields $\gtrsim$ 30 kG. Four DC stars were discovered with magnetic fields above 30 kG: G 111-49 with $B_e \sim -220$ MG, G 183-35 with $B_e = +6.8 \pm 0.5$ MG, G 256-7 with $B_e = +4.9 \pm 0.5$ MG, and G 234-4 with $B_e = +39.6 \pm 11.6$ kG. A new magnetic DB white dwarf was also discovered, LB 8827 with $B_e = 1.0 \pm 0.5$ MG. A total of 15% of the white dwarfs in the survey have a magnetic field > 30 kG. This value is far larger than the 2% of DA stars, but more than half of the DC stars were originally misclassified. Only 5% of the re-classified DC stars have magnetic fields above 30 kG.

Three magnetic stars from the DC white dwarf survey were re-observed to investigate the possibility of rotation. Two are definitely rotating: LHS 1734 with 16 min $\lesssim P < 1$ yr and G 158-45 (=LHS 1044) with a probable period $P \sim 11$ hr but a definite period $P \leq 1$ d or $P \sim$ a few days. G 183-35 might be rotating with 50 min $\lesssim P <$ a few yr. From all the white dwarf rotations known, it is clear that angular momentum is lost before a star becomes a white dwarf, but not clear that the loss is greatly enhanced by magnetic fields.

The isolated magnetic white dwarfs G 99-47, KUV 813-14 (KUV 23162-1220), and G 227-35 were observed in linear and circular spectropolarimetry and then compared to calculated theoretical spectra to find a model for the magnetic field strength and structure. The comparisons were to Stokes' V/I (circular polarization) spectra in addition to total flux F_λ, and these add many constraints to the possible solutions. An off-centered dipole or a dipole+quadrupole configuration best fits the observations.

The results of the survey and the modeling are consistent with the theory that the magnetic Ap stars are the predecessors of magnetic white dwarfs.

Contents

List of Tables

List of Figures

CHAPTER 1

Introduction

1.1 General Information on White Dwarfs

1.1.1 Discovery

Many of the bright stars we see are actually binary star systems with one bright star and one dim star, and it was among a few of these systems that the first white dwarfs were found: Sirius B, 40 Eridani B, Van Maanen 2. As binary companions of nearby stars, their mass and luminosities could be accurately determined; they were found to have low masses and low luminosities and therefore thought to be red. However, when spectra were taken, they were found to be blue objects (Sirius B: Adams 1915; 40 Eridani B: Adams 1914, Hertzsprung 1915; Van Maanen 2: van Maanen 1917). From the above data and the relation $L = 4\pi\sigma T_{eff}^4 R^2$, these stars were found to have radii smaller than expected for "normal" stars; as Eddington described Sirius B in 1926: "Apparently we have a star of mass about equal to the sun and of radius much less than Uranus...I think it has generally been considered proper to add the conclusion 'which is absurd.'"

The idea of matter as dense as 10^6 g cm^{-3} was considered absurd at this time since an atom was believed to be a rigid sphere. However, the works of Fermi (1926) and Dirac (1926), Fermi-Dirac statistics, were applied to white dwarfs by Fowler (1926) and an explanation was found. Fowler claimed that the electron degeneracy pressure inside a white dwarf is halting its gravitational collapse. This was revolutionary at the time, but it is well established now as the solution to the densities reached in a white dwarf.

Well over a thousand more white dwarfs have been identified (McCook and Sion 1987) since that time, both with and without companions. White dwarfs are intrinsically dim, thus only those close by or those located in binaries are identified. Parallax surveys, proper motion surveys, and faint blue object surveys have been the most fruitful ways of discovering new white dwarfs.

1.1.2 Basic Description

A white dwarf is one of the end products of stellar evolution. It is a star which no longer burns hydrogen, helium, or anything else; its luminosity is mainly derived from thermal cooling. Its spectral shape is very nearly a black body for the majority of its life. White dwarfs have been observed with temperatures > 60000 K (Sion et al. 1992) and < 6000 K (e.g., Bergeron, Ruiz, and Leggett 1992) and they will eventually cool down enough to no longer be visible, approximately ten gigayears after formation (D'Antona and Mazzitelli 1990, hereafter DM). The theoretical maximum mass attainable is 1.4 $M_\odot$ (using $\mu_e = 2$, instead of 2.5, in Chandrasekhar 1931), although no white dwarf has been identified as being that massive (1.31 $M_\odot$ has been reported by Schmidt et al. 1992 for PG 1658+441). The average mass of DA white dwarfs has been measured at 0.56 $M_\odot$, evenly distributed about this value with 75% of DA white dwarfs falling within ± 0.1 $M_\odot$ of 0.56 $M_\odot$ (Bergeron, Saffer, and Liebert 1992). They typically have radii similar to that of the earth (see below for further explanation). In fact, the more massive a white dwarf is, the smaller its radius is (see Equation 1.6). Their mean densities are on the order of 10^6 g cm^{-3} and they are composed of electron degenerate material, typically carbon and oxygen.

A white dwarf's interior can be described by a polytrope. A polytrope is a gaseous sphere whose pressure-density relation is

$$P = K\rho^\gamma \tag{1.1}$$

where K is a constant depending upon the actual make-up of the polytrope, $\gamma = (n+1)/n$ and n is the polytropic index. If we define

$$\rho \equiv \lambda\phi^n, \tag{1.2}$$

where λ is a scaling parameter and $\phi \propto$ temperature T, and use these values in the equation for hydrostatic equilibrium,

$$\frac{dP}{dr} = -\rho\frac{GM_r}{r^2}\frac{dM_r}{dr}, \tag{1.3}$$

we then have the following relations for the total mass and radius of a polytropic star:

$$R = \sqrt{\frac{(n+1)K}{4\pi G}}\,\lambda^{\frac{1-n}{2n}}\xi_1, \tag{1.4}$$

$$M = -4\pi\left[\frac{(n+1)K}{4\pi G}\right]^{\frac{3}{2}}\lambda^{\frac{3-n}{2n}}\left(-\xi_1^2\frac{d\phi}{d\xi}|_{\xi_1}\right), \tag{1.5}$$

where the ξ_1 is a dimensionless radius and are solved for by the Lane-Emden equation (see, e.g., Clayton 1983). If $2.5\times10^{-8}T^{\frac{3}{2}}$ g cm$^{-3} < \frac{\rho}{\mu_e} < 7.3\times10^{6}$ g cm^{-3} (lower limit is the non-degenerate/degenerate matter boundary and the upper limit is the non-relativistic/relativistic degeneracy boundary), where μ_e is the electron molecular weight, then the best polytrope is the non-relativistic degenerate n=1.5, $\gamma = \frac{5}{3}$ polytrope. In this case,

$$MR^3 = -4\pi\left[\frac{5K}{8\pi G}\right]^3\xi_1^3\left(-\xi_1^2\frac{d\phi}{d\xi}|_{\xi_1}\right) = constant. \tag{1.6}$$

This means that the heavier the white dwarf, the smaller the radius. For a white dwarf with $\frac{\rho}{\mu_e} = 7.3\times10^{6}$ g cm^{-3}, a relativistic electron degenerate polytrope (n=3, $\gamma = \frac{4}{3}$) is the best description. In this case,

$$M = -4\pi\left[\frac{K}{\pi G}\right]^{\frac{3}{2}}\left(-\xi_1^2\frac{d\phi}{d\xi}|_{\xi_1}\right) = 1.457\left(\frac{2}{\mu_e}\right)^2 M_\odot, \tag{1.7}$$

$$R = \left[\frac{K}{\pi G}\right]^{\frac{1}{2}}\lambda^{-\frac{1}{3}}\xi_1 = 3.347\times10^{4}\left[\frac{\lambda}{10^6\text{g cm}^{-3}}\right]^{-\frac{1}{3}}\left(\frac{2}{\mu_e}\right)^{\frac{2}{3}}\text{km} \tag{1.8}$$

(values from Shapiro & Teukolsky 1983). For any mass greater than Equation 1.7, gravity wins and a neutron star is born.

The atmosphere of a white dwarf is composed of non-degenerate and partially degenerate layers of gas. This envelope can be approximated as a perfect gas in radiative equilibrium; however, it is actually much more complicated than this simple picture (DM). Using the approximation of a perfect gas in radiative equilibrium, the depth of the atmosphere can be calculated by determining the

depth at which the degenerate matter begins. If $\xi = \frac{r}{R}$ where r = radius at which degeneracy starts, then

$$\left(\frac{1}{\xi} - 1\right) \gg 5.08 \left[\frac{\mu_e^2 L}{\mu M}\right]^{\frac{2}{7}} \frac{R}{\mu M} \tag{1.9}$$

where μ is the mean molecular weight, and R, M, and L are in solar units (Motz 1970). Thus for a white dwarf of $R = 10^{-2} R_\odot$, $M = 0.56 M_\odot$, and $L = 10^{-2} L_\odot$, $\left(\frac{1}{\xi} - 1\right) \gg 0.011$ which means the atmospheric thickness is $\sim 0.01 R_{WD}$. The white dwarf atmosphere has a period of convection, which depends upon the temperature of the star (see Section 1.1.5.3).

1.1.3 Rotation

One of the hardest characteristics to measure for a white dwarf is its rotation period (I will refer to both rotation period and velocity, depending on which is actually measured). Rotational velocities cannot be measured from line widths as they are for main sequence stars, since the line broadening from the high surface gravities (Stark broadening) is typically one or two orders of magnitude larger than rotational Doppler broadening. There are 15 DA white dwarfs which have line cores sharp enough to make rotational velocity measurements (Pilachowski & Milkey 1987), and most of these measurements are not actual detections. Except for this handful of stars, the only white dwarfs with measured rotation periods are those with strong magnetic fields ($> 10^6$ G) and ZZ Ceti stars. These periods fall into two categories: between hours and days (Liebert 1980) and what appear to be longer than 100 years (Chanmugam 1992). The stars with fastest periods are spinning very much slower than the maximum, or break-up, speed of $v = \sqrt{\frac{GM}{R}} = 3.7 \times 10^8 \sqrt{(\frac{M}{M_\odot})(\frac{R}{R_9})^{-1}}$ cm/s, which corresponds to a period $P = (\frac{R}{v}) = 2.7 \sqrt{(\frac{R}{R_9})^3 (\frac{M}{M_\odot})^{-1}}$ s. It is very curious as to why there is a bimodal distribution of rotational periods (velocities) in white dwarf stars. Section 1.2.3.2 and Chapter 3 discuss this in more detail.

1.1.4 Spectral Types

When white dwarfs were first observed spectroscopically, they were identified as any other star would have been, e.g., as an "A" or "B" star (Schatzman 1958). Eventually, they were given this spectral type with a "D" placed in front to denote degenerate, and extra subscripts were added at the end to denote other qualities like polarization, e.g., DAp (Greenstein 1960). Some were classified by a wavelength, e.g., λ4135, to denote an absorption feature at this wavelength. Such wavelengths were often unidentified. This started to get very complicated. Thus a revised classification system was introduced about ten years ago (Sion et al. 1983) and has been in use since then (see Table 1.1).

1.1.5 Evolution

1.1.5.1 From Main Sequence to White Dwarf

A star with an initial mass between ~ 0.08 $M_\odot$ and ~ 8 $M_\odot$ shall eventually become a white dwarf, assuming "normal" evolution (abnormal evolution includes the evolution of systems involving mass transfer or contact binaries). The upper limit is generally considered to be between 5 and 9 $M_\odot$ and depends upon how much convective overshooting is taken into account in the models; 8 $M_\odot$ comes from a moderate amount of overshooting (Meynet 1991). The lower limit is actually the lower limit on hydrogen burning, i.e., the smallest mass which can support hydrogen burning. The inital mass is the biggest factor in determining the evolutionary path a star will take; another major factor is whether the star is isolated or in a binary – I shall be assuming isolation from now on.

For initial stellar masses between ~ 0.5 and ~ 8 $M_\odot$, the star will burn hydrogen and then become a red giant. For initial masses $\lesssim 2$ $M_\odot$, the helium core is electron degenerate and the star will undergo a helium flash and burn helium along the horizontal branch (HB). Then, if the remaining core mass $\gtrsim 0.5$ $M_\odot$, it will ascend the asymptotic giant branch (AGB), eject its envelope, become a planetary nebula (PN), and finally become a white dwarf with a carbon-oxygen

core. If the star's core mass is $\lesssim 0.5$ $M_\odot$ at the end of the HB (sdB and sdBO stars, for field stars), the star will continue along the HB and evolve directly to a white dwarf (see below). For initial masses $\gtrsim 2$ $M_\odot$, the helium core is non-degenerate and therefore it can ignite helium on its own and burn it while on the HB. It then follows a path similar to a star with a core mass $\gtrsim_{0.5}$ $M_\odot$.

While a star is on the giant branch or the AGB, it is believed to undergo angular momentum transfer from the core to the envelope, and when the envelope is blown off, the transferred angular momentum goes with it. If this or some other means to remove some angular momentum did not exist, conservation of angular momentum would cause the white dwarf to spin faster than its break-up velocity (Villata 1992).

For initial masses between ~ 0.08 and ~ 0.5 $M_\odot$, the star burns hydrogen, but becomes electron degenerate before helium can ignite, in the same way that brown dwarfs never ignite hydrogen (Meynet 1991). The star then evolves directly to the white dwarf region of the H-R diagram from the extreme horizontal branch (Heber 1986, 1987). The actual processes involved in this direct evolution are unclear. The probable scenario is that once all the core hydrogen has been burned and the helium does not ignite, the radiation pressure decreases until it is much lower than the gravitational pressure. Thus the star collapses until the electron degeneracy pressure is equal to the gravitational pressure. Then, as helium white dwarfs, they end their existence.

1.1.5.2 White Dwarf Cooling

Once a star reaches the white dwarf phase it has lost all its ability to produce new energy, so instead it just releases all the energy it has left as it cools. The original description of this process, e.g., Mestel (1952), uses residual ion thermal energy as the only source of luminosity for the white dwarf's lifetime. For this case, it can be easily shown that the time a white dwarf has been a white dwarf is

$$t = \frac{3}{5}\frac{kTM}{Am_pL} \tag{1.10}$$

where T is the internal temperature:

$$T = 5 \times 10^7 \left[\frac{L}{M}\right]^{\frac{2}{7}} \tag{1.11}$$

(Mestel 1965), and A = baryon number. Mestel (1965) calculates the age of Sirius B as $1.5 \times 10^9/A$ years. Shapiro & Teukolsky (1983) make the analogous calculation to Equation 1.10, but add in the lattice potential energy and the latent heat of crystalization. Their lifetime is a factor of ~ 3 longer than Mestel's calculation.

The hot, newborn white dwarf takes some time to settle down. What this involves is not fully understood although it does vary depending on which route the star took to become a white dwarf (e.g., planetary nebula or sub-dwarf). Eventually the white dwarf becomes dominated by neutrino cooling, at which point all white dwarfs have the same thermal structure, regardless of evolutionary path. This stage ends when $\log \frac{L}{L_\odot} \sim -1.5$, which is about $\sim 7 \times 10^7$ years after the white dwarf was born (DM). At this point thermal cooling begins and Mestel's description is valid. When the interior temperature reaches the gas-liquid phase boundary, $T_g \sim 3 \times 10^4 \rho^{\frac{1}{3}} Z^{\frac{5}{3}}$ K (Z is the ion charge), the matter starts to liquify. It continues to thermally cool, but "crystallizing" effects need to be added as well, which cause the cooling time to increase over the previous stage of cooling by a factor of 2 ($t = \frac{6}{5} \frac{kTM}{Am_pL}$). When the interior has cooled down to the melting point ($\log \frac{L}{L_\odot} \sim -3.8$ for hydrogen envelopes, ~ -3 for helium envelopes; DM), it begins to crystallize. The start and end times of the crystallization process vary depending upon composition. To reach $\log \frac{L}{L_\odot} = -4.5$, the approximate point of invisibility, a carbon core, medium opacity model takes $\sim 8.7 \times 10^9$ years, whereas an oxygen core, low opacity model will take $\sim 3.5 \times 10^9$ years (DM). The final phase, like the first, is very poorly understood. When the star reaches the Debye temperature, $\theta_D \simeq 4 \times 10^3 \sqrt{\rho}$ K, it should undergo "fast" Debye cooling. However, it is believed that this rarely, if ever, happens since the outer layers have been cooling more slowly than the inner ones and the overall $\frac{\theta_D}{T}$ ratio is too small for the "fast" cooling.

1.1.5.3 Observed

It is not possible to follow one white dwarf as it evolves due to the brief lifetime of humans. However, we can observe many white dwarfs of different ages and determine a possible evolutionary path for all white dwarfs much in the same way as we could attend a family reunion and determine the aging process of humans by observing the infants through the elderly. For the humans, we can just ask the age of each family member and determine a time line from that. For the white dwarfs, we measure a temperature and piece together an approximate time line where decreasing temperature is increasing age. For humans we might look at size, strength, coordination, elasticity of skin, amount and color of hair as a function of time to determine what aging does to the family in question. For white dwarfs we observe composition (spectral type and abundances), luminosity, magnetic field, and rotation (if possible). In both cases we are only observing the exterior features. They are usually related to the interior features, although the local environment will affect the exterior as well. For example, cousin Bob from Phoenix will probably have more wrinkles at age 35 than cousin Tess from Buffalo will due to increased sun exposure and dry air much in the same way a 10,000 K DZ white dwarf will have more calcium in its atmosphere than a 10,000 K DA white dwarf due to accretion of local dust (see, e.g., Koester & Chanmugam 1990). Thus although the interiors of the white dwarfs will all cool similarly, the exteriors will act differently.

Originally it was thought that a white dwarf atmosphere was mainly hydrogen (DA), helium (DB or DO), or a combination of the two (DAO, DAB), and as the star cooled, the other constituents, e.g., carbon (DQ) and calcium (DZ), would be seen as these atoms and molecules recombined and hydrogen and/or helium lines became weaker. Finally, the star would be so cool that the spectrum would appear continuous (DC) (Liebert 1980). However, the data do not allow these parallel evolutionary tracks (Liebert 1991). Present theories claim that there is settling in the atmosphere by atomic weight, thus slowly obscuring all elements except hydrogen. In fact, there is a gap of DB stars from 45,000 K to 30,000 K.

However, at about 30,000 K, convection begins in the atmosphere and the heavier elements are dredged up. At this point DB stars are once again in existence. Around 10,000 K, the convection goes deep enough in some stars to dredge up carbon, thus introducing the DQ stars. DZ stars are thought to be products of accretion of the local interstellar medium and these appear when enough material has been accreted, typically around 10,000 K. As before, DC stars are believed to be the end results for all white dwarfs. This occurs at around 11,000 K for DB stars and below 4500 K for DA stars (see Chapter 2, Table 2.5 for examples; 4500 K is the coolest temperature of DA white dwarfs in the sample).

Schematically, white dwarf evolution can be seen on the H-R diagram. The white dwarfs occupy the bottom, left-hand corner of the diagram. As they cool, they will follow tracks of constant mass, travelling diagonally from the upper left to the lower right.

1.2 Magnetic Fields in White Dwarfs

One of the topics not covered in the previous section was that of magnetic fields. This is almost an entire field unto itself and I am treating it as such. Again, I am only concerning myself with the isolated white dwarf. Also, the term "magnetic white dwarf," or MWD, will be used to refer to a white dwarf with a surface magnetic field strength $> 10^6$ G (= 1 MG).

All stars have a magnetic field; however, we cannot measure it in most cases because it is too weak. If there is no dynamo in the star to keep the magnetic field going, it is expected to decay with time (see Appendix 1.A; our own sun has a dynamo). Most calculations (e.g., Chanmugam & Gabriel 1972 and Fontaine, Thomas, & Van Horn 1973) place the decay time in a white dwarf between 10^9 and 10^{11} years. This happens to also be the approximate age of a white dwarf when it has reached invisibility.

1.2.1 Discovery

Minkowski (1938) analyzed a spectrum he took of the white dwarf Grw +70°8247. He noticed wide absorption bands at $\sim$ 4135 Å and at $\sim$ 4470 Å, but no absorption at the wavelengths expected for hydrogen, helium, carbon, or any other element or molecule of which he could conceive. Kemp & Swedlund (1970) and Kemp et al. (1970) made circular polarization measurements of Grw +70°8247 and found $\sim$ 3% circular polarization. This now explained the oddly placed absorption features — they were due to hydrogen in a strong magnetic field. Wickramasinghe & Ferrario (1988) modeled this star with a field strength of ~320 MG. Since that time more than 40 isolated white dwarfs have been identified as having fields > 1 MG (Schmidt & Smith 1995; Putney 1995). Also, with the aid of spectropolarimetry, fields < 1 MG are now being accurately identified (Schmidt et al. 1992; Schmidt & Smith 1995; Chapter 2).

1.2.2 Origins

One of the big questions concerning magnetic fields on white dwarfs is "how did it get there?" Present theories (e.g., Chanmugam 1992) suggest that they were born with them, i.e., the magnetic field the star had during the main sequence phase remained. This could explain the distribution of magnetic fields observed (Chanmugam 1992). There are 4.0±1.5% of DA stars with magnetic fields between 30 kG and 1000 MG (Schmidt & Smith 1995).

Conservation of the magnetic flux, $\propto BR^2$, implies that a decrease in radius will cause an increase in magnetic field strength. A magnetic Ap star has a surface field strength on the order of 10^4 G, so if it decreases in radius by a factor of 100 between the main sequence and the white dwarf regime, it will have a surface magnetic field strength on the order of 10^8 G. Similarly, if our own sun shrank by a factor of 100 and kept its magnetic flux, it would have a field strength of $\sim 10^4$ G when it became a white dwarf. The present space density and death rate of Ap stars, assuming they have not changed with time, are estimated to be consistent with the observed space density of magnetic white dwarf stars (Angel,

Borra, & Landstreet 1981). Thus Ap stars could be the progenitors of the magnetic white dwarfs while the other main sequence stars are the progenitors of the white dwarfs with far smaller fields strengths. However, it is possible that many rapidly rotating main sequence stars have forced their magnetic fields below their surfaces (Mestel & Moss 1977) and thus have inhibited our ability to accurately determine the number of main sequence stars with relatively strong fields ($\gtrsim 10^3$ G). On the other hand, Liebert (1988) points out that the magnetic white dwarfs have larger masses than the average as well as smaller tangential space velocities. This points to the conclusion that the magnetic white dwarfs come from the more massive progenitors, namely A and B stars. This dilemma may not be solved until many more white dwarfs have their magnetic fields measured (the surveys of Schmidt & Smith and Putney (Chapter 2) have greatly improved these statistics) and the space densities can be better determined for both white dwarfs and their progenitors.

It has also been suggested that many of the white dwarfs are born with high field strengths which decay before we can observe them. As previously mentioned, calculations show that the magnetic field decays by about a factor of 2 during the white dwarf's lifetime (see Appendix 1.A for calculation). These calculations are for the dipole field, a quadrupole or higher multipole field will decay faster (Chanmugam 1992) and therefore only dipolar fields are expected on the oldest white dwarfs.

1.2.3 Effects of a Magnetic Field on a White Dwarf

1.2.3.1 Gravity

An interesting effect that a strong magnetic field has on a white dwarf is to increase the radius slightly. Chapter 7 of Shapiro and Teukolsky (1983) explains this as "reducing" the the gravitational constant:

$$G' = G(1 - \delta) \tag{1.12}$$

with

$$\delta \equiv \frac{M}{|W|}, \tag{1.13}$$

where M = magnetic energy = $\frac{1}{8\pi}\int B^2 d^3x$ and W = gravitational potential energy = $\frac{1}{2}\int \rho(\mathbf{x})\Phi(\mathbf{x})d^3x$. A non-relativistic degenerate white dwarf will then have a radius

$$R = R_o(1-\delta)^{-1}, \tag{1.14}$$

where $R_o = R(B=0)$; an extreme relativistic degenerate star will have

$$R = R_o \exp(\frac{3\delta}{3-n}), \tag{1.15}$$

where n = polytropic index. The magnetic field will also increase the maximum mass a white dwarf can have:

$$M_{max} = M_{CH}(1+\frac{3}{2}\delta), \tag{1.16}$$

where $M_{CH} = \frac{5.80}{\mu_e}M_\odot$.

1.2.3.2 Rotation

As previously mentioned, the angular momentum is expected to be transferred from the core to the envelope of a post-main sequence star. If the star has a strong magnetic field, then the field should aid in the transfer of the angular momentum by coupling the core and the envelope (Schmidt & Norsworthy 1991). Therefore, the stronger the magnetic field, the slower the white dwarf should be rotating (adding to that the fact that magnetic Ap stars are rotating more slowly than many other stars; Ryabchikova 1991). The rotation periods of magnetic white dwarfs should also be slowing down as they cool due to magnetic braking ($\dot{\Omega} = -\frac{B_P^2 R^6 \Omega^3 \sin^2\alpha}{6Ic^3}$, where B_p = polar field, I = moment of inertia, and α = angle between rotation and dipole axes). This implies that the older and stronger a magnetic field that a white dwarf has, the slower it should be rotating.

Both of these effects might be true, but it is not entirely clear from the observations. Figure 3.6 (Chapter 3) shows the distribution of rotation periods as

a function of polar field strength for 16 magnetic white dwarfs and 15 non-magnetic white dwarfs (see also Tables 3.3 and 3.4). There is almost a correlation between high field and long period, except PG $1031+234$ and RE J$0317-853$ have among the highest field and the shortest periods. Similar discrepancies can be found, with greater frequency, when comparing ages (temperatures) with the rotation periods (see Figure 3.5). It is possible, but not likely (Schmidt & Norsworthy 1991), that each of the stars which appear to be non-rotating either have periods $\lesssim$ 10 min (present limit of time-resolution) or are rotationally symmetric with respect to the magnetic field. In any case, the distribution of rotations is clearly not understood.

1.2.3.3 Absorption Features

The most noticeable effect of a strong magnetic field on a white dwarf is the displacement, in wavelength, of the hydrogen, helium, etc., absorption (emission) features. This effect increases with increasing magnetic field strength from a slight (linear) perturbation, to a stronger (quadratic) perturbation, to even larger changes as the atom's potential is dictated more and more by the magnetic forces instead of the Coulombic forces. These changes in the spectrum make it possible to measure the magnetic field strength from the flux spectrum, as well as the circularly polarized spectrum (see below).

For field strengths $\lesssim 10^6$ G, the magnetic field causes a small perturbation on the atom's potential. This effect is known as the linear Zeeman effect. This causes a shift of the absorption lines of

$$\Delta\lambda_{linear} = \frac{Be}{4\pi m_e c^2}\lambda^2(g''_L m''_j - g'_L m'_j) \tag{1.17}$$

(Condon & Shortly 1951), where $g_L = 1 + \frac{J(J+1)+S(S+1)-L(L+1)}{2J(J+1)}$, B is magnetic field strength, the primes refer to upper (double prime) and lower (single prime) states, and n, m_j, J, K, and L are quantum numbers. For transitions where $\Delta m_j = 0$, the components are linearly polarized parallel to the magnetic field when observing the field perpendicularly (i.e., looking at the equator of a stellar dipolar field), they are also not shifted very far from the zero-field line ($g'_L = g''_L$

the line is not shifted at all). For transitions where $\Delta m_j = \pm 1$ (the selection rules only allow for $\Delta m_j = 0, \pm 1$), the components are linearly polarized perpendicular to the field when observing the field perpendicularly and circularly polarized when observing the converging field (i.e., looking down the pole of a stellar dipolar field). The transition due to $\Delta m_j = +1$ is shifted towards longer wavelengths and yields one sense of circular polarization (a positive circular polarization when observing the north magnetic pole; terms right- and left-handed circular polarization are avoided due to the different conventions of optical and radio astronomers). The transition for $\Delta m_j = -1$ is shifted towards shorter wavelengths and yields the opposite sense of polarization. These polarizations lead to a distinct diagnostic for identifying a magnetic field in a white dwarf even if the magnetic field is only strong enough to broaden, but not split, an absorption feature (the gravitational broadening is large, often obscuring the magnetic broadening, see Section 1.1.3). The finer the resolution, the lower the magnetic field measurable. Figures 2.58 and 2.59 show stars with this effect.

As the magnetic field increases, it introduces a larger perturbation on the atomic potential. This is known as the quadratic Zeeman effect and it becomes noticeable or dominant for fields between $\sim 10^5$ and 10^7 to 10^8 G. This is still treated as a perturbation, thus the absorption becomes

$$\Delta\lambda_{observed} = \lambda_0 + \Delta\lambda_{linear} + \Delta\lambda_{quadratic} \tag{1.18}$$

and

$$\Delta\lambda_{quadratic} \approx -\frac{B^2 e^2 a_0^2}{8 m_e c^3 h Z^2} \lambda_0^2 n''^4 (1 + m_j''^2) \tag{1.19}$$

(Van Vleck 1932; Preston 1970), where λ_0 is the unshifted transition wavelength, a_o = Bohr radius, Z is the atomic number, and n''^4 and $m_j''^2$ are quantum numbers of upper state. The polarization senses of these transitions are the same as for the linear effect, since this effect is an addition to the linear effect. The quadratic effect shifts all lines bluewards. For cases such as the Balmer series, the m_j dependence creates more than the three transitions Δm_j allows. Hα becomes

15 separate transitions, Hβ becomes 18, etc. Kemic (1974) has calculated the transitions for Hα, Hβ, Hγ, Hδ, and several He II lines more precisely than the approximation in Equation 1.19 for magnetic fields through 10^7 to 10^8 G (the maximum field strength depends on the transition). Figure 2.37 is a prime example of this splitting.

For both Zeeman effects, a magnetic field strength can be determined easily by measuring the absorption feature wavelength and inverting equation 1.18 to solve for B. The magnetic field of a star is not single valued, thus the magnetic field calculated by this method is a mean field strength of the observable hemisphere. The strength of magnetic field on the surface of a star with a centered dipolar field will vary by a factor of two from the pole (highest value) to the equator. An offset dipole or dipole+quadrupole will vary by more than that. Models can be calculated to find the field structure (see Chapter 4). However, an average field strength is adequate for most purposes (see Chapter 2).

For fields above 10^7 or 10^8 G, the linear and quadratic Zeeman calculations are insufficient to describe the transitions. This is because at these field strengths the magnetic and Coulombic forces are similar in strength, but very different geometrically. The magnetic forces are cylindrically symmetric and the Coulomb forces are spherically so, making analytic formulae impossible. A theoretical group in Tübingen, Germany, have calculated the transition wavelengths for hydrogen for field strengths from 4.7×10^6 G to 4.7×10^{12} G (Forster et al. 1984, Wunner et al. 1985). These calculations explain the inexplicable absorption bands Minkowski saw in Grw +70°8247. Above 10^9 G the magnetic forces are dominant and the equations become analytic again, but they will not be discussed here since no white dwarf has been discovered in this regime.

The method for magnetic field determination in this regime is similar to that of the Zeeman effect. Namely the wavelengths of the absorption features can be matched to calculations and the best determinations are from models. Section

2.4.2.1 discusses this procedure in more detail and Figure 2.14 is an example of a star in this magnetic field range.

1.2.3.4 Continuum Emission Mechanisms

Most of the effects of a magnetic field on the continuum of a white dwarf are manifested in the linear and circular polarization spectra as opposed to the total flux spectrum. One feature that is expected in the flux spectrum is a cyclotron absorption line feature at the cyclotron frequency, $\nu_c = \frac{eB}{2\pi m_e c}$, which is in the near infrared and optical for B$\geq 10^8$ G; however, no such absorption feature has yet been positively identified (Angel 1978). The polarization effects are mainly due to birefringence in the free-free and bound-free opacities (West 1989). Other effects which need to be considered, particularly when making models, are the Faraday and Voigt effects (Jordan, O'Connell & Koester 1991) and Thompson scattering (Whitney 1991a,b; Chou & Chen 1990).

Bound-free absorption in a large magnetic field reacts to the fact that the structure of the atom has changed, and the higher the field, the more drastic the change. For field strengths $\leq 10^7$ G, Lamb & Sutherland (1974) give a simple description of the bound-free transitions. The bound-free absorption coefficient breaks up into three components corresponding to the three values the magnetic quantum number, m_j, can take. The effect is to create a rise to the red in polarization, depending upon field orientation:

$$\frac{V(\theta)}{\bar{\tau}} = -4(\frac{\omega_L}{\omega})\cos\theta, \tag{1.20}$$

$$\frac{p_{max}(\theta)}{\bar{\tau}} = 5(\frac{\omega_L}{\omega})^2 \sin^2\theta \tag{1.21}$$

(Lamb & Sutherland 1974), where $\bar{\tau}$ = mean optical depth of the absorption layer, θ = angle between the direction of propagation and the magnetic field, and ω_L = Larmor frequency = $\frac{eB}{2m_e c}$. For field strengths $\geq 10^{12}$ G, the entire structure of the atom has changed such that it is almost a cylinder aligned with the magnetic field (Rösner et al. 1984), as opposed to the classical sphere in the

absence of a magnetic field. This causes an overlapping of continuum states and therefore large dichroism in photoabsorption. For field strengths in between these two extremes, fairly unrealistic approximations have been made while calculating the cross-sections (Kara & McDowell 1981), namely the Coulomb forces have been poorly represented, even though, for fields between 10^8 and 10^9 G, the Coulomb forces play a large role. The physics behind these absorptions is poorly understood, and therefore the polarization effects are even less so, although from what I've read, I gather the basic continuum polarization shape is rising to the red with discontinuities at multiples of the cyclotron frequency.

Bremsstrahlung absorption is affected by the presence of a large magnetic field. In a magnetoplasma, the ordinary and extraordinary radiation modes propagate separately. The cyclotron orbit of an electron has the same direction and nearly the same shape as the extraordinary radiation mode, and therefore the electron absorbs the extraordinary mode more often than the ordinary mode. This causes the bremsstrahlung absorption to be effectively polarized across the continuum. Kemp (1970) shows that the circular polarization $\propto \frac{\omega_c}{\omega}$, and the linear polarization $\propto (\frac{\omega_c}{\omega})^2$ (Kemp 1977). West (1989) points out that magneto-bremsstrahlung needs very high collision rates ($\omega_c/\nu \gg 1$, where ν = collision rate) which are found deep in the atmosphere of the white dwarf and therefore we can only see this polarization after it has been reprocessed, perhaps repeatedly.

Cyclotron absorption is the quantized free-free absorption by an electron. The electron, rotating around a field line, will absorb a photon of energy $= nh\nu_c$ (n = an integer) and move into a higher Landau state. This absorption is peaked around ν_c with a width $\frac{\Delta\nu}{\nu_c} \approx \sqrt{\frac{2k_BT}{m_ec^2}}|\cos\theta|$. The polarization produced exists only in a frequency range $\Delta\nu$ around ν_c and can be described by:

$$\frac{V(\theta)}{\bar{\tau}} = -\frac{2\cos\theta}{1+\cos^2\theta}, \tag{1.22}$$

$$\frac{p_{max}(\theta)}{\bar{\tau}} = -\frac{\sin^2\theta}{1+\cos^2\theta} \tag{1.23}$$

(Lamb & Sutherland 1974). West (1989) mentions that since the cyclotron absorption has a large cross section, we observe it from high in the atmosphere and therefore it should be a strong narrow peak at the fundamental frequency.

There are a few other effects which should be considered when making a complete description of the polarization of white dwarfs. The first is the Faraday effect; this is due to the fact that the indices of refraction are different for left and right circular polarization in the presence of a magnetic field. The position angle of the linear polarization as a function of frequency and magnetic field:

$$\frac{d\theta}{dl} = \frac{\omega}{2c}(n_+ - n_-) = \frac{\omega_p^2 \omega_c}{2c(\omega^2 - \omega_c^2)} \tag{1.24}$$

(from Jordan et al. 1991) where l = path length and ω_p = plasma frequency $= \sqrt{4\pi N_e e^2/m_e}$. Another effect is the Voigt effect, which is a phase shift between the electric field components parallel and perpendicular to the magnetic field. What we see is a change in the ellipticity by an amount:

$$\frac{d\phi}{d\tau} = -\frac{\omega}{2c\kappa_R}(n_\parallel - n_\perp) = \frac{\omega_p^2 \omega_c^2}{2c\omega\kappa_R(\omega^2 - \omega_c^2)} \tag{1.25}$$

(from Jordan et al. 1991) where κ_R = Rosseland absorption coefficient and τ = optical depth. A third effect is Thomson scattering in a magnetic field. In the zero magnetic field case, Thomson scatter is the scattering of a photon off of an electron with a cross section of $\sigma_T = 8\pi/3r_o^2$, where r_o is the classical electron radius. In a strong magnetic field, the cross section becomes a function of the cyclotron frequency (see Whitney (1991a) for the dependence). This change in cross section is due to the rotation of the electrons around the magnetic field. Whitney (1991b) does many simulations of what happens polarimetrically as functions of angle from the magnetic axis and ω_c/ω. The polarization seems to be highly dependent upon viewing angle and can reach 100% polarization in some scenarios. Whitney does point out, however, that this may not be very important in white dwarfs since electron scattering is probably not significant in their atmospheres.

The effects of a strong magnetic field on a white dwarf continuum are not well understood. Theorists have been using the above mentioned processes to

try to simulate the conditions on white dwarfs with only limited successes (e.g., Jordan 1992, Wickramasinghe & Ferrario 1988). Portions of the observed polarized continuum will be reproduced by the theoretical model but other regions will be far off (see Chapter 4). The situation may soon change with the newly calculated bound-free opacities from a group in Bochum, Germany (Merani, Main, & Wunner 1995).

1.3 Polarization Measurements

Spectropolarimetry shows both the continuum and the line polarizations, which is useful for comparisons with models of field strength and orientation (e.g., Wickramasinghe & Ferrario 1988, Jordan 1992). Circular spectropolarization measurements also allow measurements of field strengths lower than can be found with flux-only measurements at the same resolution (Schmidt et al. 1992). Thus this method was employed to increase the body of data known about magnetic fields in white dwarf stars.

The details of spectropolarimetry data taking, data analysis, and the instruments used can be found in Miller, Robinson, & Goodrich (1988), Goodrich (1991), and Goodrich, Cohen, & Putney (1995). However, a brief description will be given here to make this thesis more self-contained. The data taking and instruments are described in more detail in Chapters 2 and 4.

1.3.1 The Polarimeter and Obtaining of Data

The polarimeter consists of a wave plate, either quarter-wave or half-wave, which can be rotated to any angle, and a calcite prism which splits incoming light into two parallel, orthogonally polarized beams. The wave plate is placed above the beam splitter and they, in turn, are placed above the entrance slit of the spectrograph. If a half-wave plate is used, a 45° rotation of the wave plate will rotate the plane of polarization (linear) by 90 degrees. A quarter-wave plate

converts the incoming light from circular to linear polarization and, for some wave plate fast axis angles, linear to circular polarization.

Each Stokes' parameter Q, U, V requires two observations with our polarimeter. For Q and U, the two observations are different by a 45° rotation of the half-wave plate, and the initial U observation has a difference of 22.5° in the wave plate angle from the initial Q observation. The V observation needs a 90° difference in quarter-wave plate angle and the first position is such that the fast axis of the wave plate is parallel to the plane of polarization of one of the beam splitter beams. Thus the two observations for each Stokes' parameter produces 4 spectra, which I will call A_o, A_e, B_o, and B_e. The A's refer to the first observation, the B's, to the second, and the o refers to the ordinary ray, and the e, the extraordinary ray.

1.3.2 The Equations Behind the Method

Light and optics, particularly polarized light, can be treated mathematically using one of several different methods. One of the popular methods, and the one used here, is Mueller calculus. Several textbooks describe the method in full (e.g., Shurcliff 1962). Simply put, it is a matrix method for describing the input and output beams through optical equipment and the optical equipment itself. The polarization of a beam of light can be described by the four Stokes' parameters

$$\begin{bmatrix} I \\ Q \\ U \\ V \end{bmatrix}$$

where

$$I = I_x + I_y = I_s + I_t = I_R + I_L = I_e + I_u, \tag{1.26a}$$

$$Q = I_x - I_y = I_e \cos 2\beta \cos 2\theta, \tag{1.26b}$$

$$U = I_s - I_t = I_e \cos 2\beta \sin 2\theta, \tag{1.26c}$$

$$V = I_R - I_L = I_e \sin 2\beta, \tag{1.26d}$$

and (I_x, I_y) are the intensities of perpendicular to the propagation direction and to each other, (I_s, I_t) are the intensities 45° to (I_x, I_y), (I_R, I_L) are the intensities of right and left circular polarization, (I_e, I_u) are the intensities of the polarized and unpolarized light, θ is the angle of the plane of polarization, and β is a measure of ellipticity of the polarization, where $r = \tan^{-1}\beta$ = axial ratio ($\beta = 45°$ = completely circular polarized, $\beta = 0°$= completely linearly polarized, and $0° < \beta < 45°$ is elliptically polarized). Generally, linearly polarized light is described by p (= $\sqrt{((Q^2+U^2)/I^2)}$ = the percentage polarization) and θ (= $\frac{1}{2}\tan^{-1}(U/Q)$).

Each optical element in the polarimeter can be described by a matrix. The wave plate matrix, M_{WP} =

$$\begin{bmatrix} 1 & 0 & 0 & 0 \\ 0 & \cos^2(2\theta) + \sin^2(2\theta)\cos R & \sin(2\theta)\cos(2\theta)(1 - cosR) & -\sin(2\theta)\sin R \\ 0 & \sin(2\theta)\cos(2\theta)(1 - cosR) & \sin^2(2\theta) + \cos^2(2\theta)\cos R & \cos(2\theta)\sin R \\ 0 & \sin(2\theta)\sin R & -\cos(2\theta)\sin R & \cos R \end{bmatrix} \tag{1.27}$$

where R is the retardance of the wave plate (90° for quarter-wave and 180° for half-wave) and θ is the angle of the wave plate fast axis. A half-wave plate is used for linear polarization measurement (Q and U) and a quarter-wave plate for circular polarization measurement (V). The beam splitter matrix is

$$M_{BS} = \begin{bmatrix} 1 & \pm 1 & 0 & 0 \\ \pm 1 & 1 & 0 & 0 \\ 0 & 0 & 0 & 0 \\ 0 & 0 & 0 & 0 \end{bmatrix} \tag{1.28}$$

where the positive terms are for the extraordinary ray (e-ray), in calcite, and the negative terms for the ordinary ray (o-ray). With these matrices we can calculate the Stokes' vector transmitted, S_t, through the polarimeter:

$$S_t = M_{BS} M_{WP} S_0 \tag{1.29}$$

where S_0 is the initial Stokes' vector. The value actually measured by the polarimeter is Stokes' parameter I_t. It can be shown that from two observations an initial Stokes' parameter, say V_0, can be calculated by

$$\frac{V_0}{I_0} = \frac{S_t(\theta_A) - S_t(\theta_B)}{S_t(\theta_A) + S_t(\theta_B)} \tag{1.30}$$

for perfect wave plates, where S_t's refer to either the e-ray or the o-ray, θ_A is the angle of the wave plate fast axis of the first observations, and θ_B is the angle of the second observation. For Q, $\theta_A = 0°$ and $\theta_B = 45°$; for U, $\theta_A = 22.5°$ and $\theta_B = 67.5°$; and for V, $\theta_A = 45°$ and $\theta_B = 135°$. Equation 1.29 is not exact if the wave plates are not perfect, i.e., if the retardance is not precisely 90° or 180° at all wavelengths or the fast axis is not constant in wavelength. The corrections needed are discussed in Miller et al. (1988), Goodrich (1991), and Goodrich et al. (1995).

1.3.3 The Anaylsis

Each of the four observed spectra contains a lot of information. The four spectra can be factored as follows:

$$A_e = I_A p_0 g_e, \tag{1.31a}$$

$$A_o = I_A p_{90} g_o, \tag{1.31b}$$

$$B_e = I_B p_{90} g_e, \tag{1.31c}$$

$$B_o = I_B p_0 g_o, \tag{1.31d}$$

where I_A is the incoming intensity during the A observation, including sky variations and slit losses, I_B is similar except for the B observation, the p's are the fractions of polarization exiting the beam splitter for each sense, and the g's are the gains for each beam, which includes the efficiencies of the beam splitter, grating, and detector for each polarization sense. A Stokes' parameter can be calculated for each beam:

$$V_e = \frac{A_e - B_e}{A_e + B_e} = \frac{I_A p_0 - I_B p_{90}}{I_A p_0 + I_B p_{90}}, \tag{1.32a}$$

$$V_o = \frac{B_o - A_o}{B_o + A_o} = \frac{I_B p_0 - I_A p_{90}}{I_B p_0 + I_A p_{90}}. \tag{1.32b}$$

These equations eliminate the gain factors g_e and g_o which, by experience, have been found to be unstable during a night of observing. If there are, e.g., any sky

transparency changes from observation to the next (clouds) or guiding problems, $I_A \neq I_B$. In order to eliminate this problem, the following factor has been created:

$$\omega = \sqrt{\frac{A_o A_e}{B_o B_e}} = \frac{I_A}{I_B} \tag{1.34}$$

This then gives the Stokes' parameter calculation:

$$V = \frac{p_0 - p_{90}}{p_0 + p_{90}} = V_e = \frac{A_e - \omega B_e}{A_e + \omega B_e} = V_o = \frac{\omega B_o - A_o}{\omega B_o + A_o}. \tag{1.35}$$

Please note that V_e and V_o are not independent estimates of V due to the use of ω. Assuming only photon shot noise and CCD readout noise in each of the four observed spectra, σ, the noise in the calculated Stokes' parameter is

$$\sigma^2(V_o) = \frac{4\omega^2}{(A_o + \omega B_o)^4}[A_o^2\sigma^2(B_o) + B_o^2\sigma^2(A_o)]. \tag{1.36}$$

Linear polarization has the added problem of the instrument Q and U rotated with respect to the sky Q and U. This can be easily remedied:

$$\begin{bmatrix} Q_{sky} \\ U_{sky} \end{bmatrix} = \begin{bmatrix} \cos 2\phi & \sin 2\phi \\ -\sin 2\phi & \cos 2\phi \end{bmatrix} \begin{bmatrix} Q_{inst} \\ U_{inst} \end{bmatrix} \tag{1.37}$$

where ϕ is the angle between the instrument position angle and the sky position angle.

It is possible to calculate a Stokes' parameter with only one exposure, i.e., $V \sim (A_e - A_o)/(A_e + A_o)$; however, this requires knowing the gain ratio g_e/g_o in advance. This is not constant from night to night and not necessarily constant during a night (it has been seen to vary slowly during the night). Therefore, two exposures are needed for a Stokes' parameter calculation. However, if something prohibits two exposures for one object (e.g., sudden thickening of clouds, instrument failure), it is possible to calculate a Stokes' parameter for the object using the preceding object's gain ratio. This has been done for one object in Chapter 2.

References

Adams, W.S. 1914, PASP, 26, 198

—— 1915, PASP, 27, 236

Angel, J.R.P. 1978, ARAA, 16, 487

Angel, J.R.P., Borra, E.F., & Landstreet, J.D. 1981, ApJS, 45, 457

Bergeron, P., Ruiz, M., & Leggett, S.K. 1992, ApJ, 400, 315

Bergeron, P., Saffer, R.A., & Liebert, J. 1992, ApJ, 394, 228

Chandrasekhar, S. 1931, ApJ, 74, 81

Chanmugam, G. 1992, AARA, 30, 143

Chanmugam, G. & Gabriel, M. 1972, A&A, 16, 149

Chou, C. & Chen, H. 1990, ApSpSci, 74, 217

Clayton, D.D. 1983, Principles of Stellar Evolution and Nucleosynthesis (Chicago: The University of Chicago Press), 160

Condon, E.U. & Shortly, G.H. 1951, The Theory of Atomic Spectra (Cambridge: Cambridge University Press)

D'Antona, F. & Mazzitelli, I. 1990, ARAA, 28, 139

Dirac, P.A.M. 1926, Proc Roy Soc Lon, Ser A, 112, 661

Eddington, A.S. 1926, The Internal Constitution of the Stars (New York: Dover Publications, Inc., 1959), 171

Fermi, E. 1926, Zts f Phys, 36, 902

Fontaine, G., Thomas, J.H., & Van Horn, H.M. 1973, ApJ, 184, 911

Forster, H., Strupat, W., Rösner, W., Wunner, G., Ruder, H., & Herold, H. 1984, J Phys B: At Mol Phys, 17, 1301

Fowler, R.H. 1926, MNRAS, 87, 114

Goodrich, R.W. 1991, PASP, 103, 670

Goodrich, R.W., Cohen, M.H., & Putney, A. 1995, PASP, 107, 179

Greenstein, J.L. 1960 in Stars and Stellar Systems, Vol. 6, Stellar Atmospheres, ed. J.L. Greenstein (Chicago: University of Chicago Press), 676

Heber, U. 1986, A&A, 155, 33

—— 1987, in The Second Conference on Faint Blue Stars, IAU Colloquium No. 95, eds. A.G.D. Philip, D.S. Hayes, & J.W. Liebert (Schenectady, N.Y.: L. Davis Press), 79

Hertzsprung, E. 1915, ApJ, 42, 92

Jordan, S. 1992, A&A, 265, 570

Jordan, S., O'Connell, R.F., & Koester, D. 1991, A&A, 242, 206

Kara, S. M. & McDowell, M.R.C. 1981, J Phys B: At Mol Phys, 14, 1719

Kemic, S.B. 1974, JILA report # 113

Kemp, J.C. 1970, ApJ, 162, 169

—— 1977, ApJ, 213, 794

Kemp, J.C. & Swedlund, J.B. 1970, ApJ, 162, L67

Kemp, J.C., Swedlund, J.B., Landstreet, J.D., & Angel, J.R.P. 1970, ApJ, 161, L77

Koester, D. & Chanmugam, G. 1990, Rep Prog Phys, 53, 837

Lamb, F.K. & Sutherland, P.G. 1974, in Physics of Dense Matter, IAU Symposium 53, ed. C.J. Hansen (Dordrecht: D. Reidel Publishing Company), 265

Liebert, J. 1980, ARAA, 18, 363

—— 1988, PASP, 100, 1302

—— 1991, in Evolution of Stars: the Photospheric Connection, IAU Symposium 145, eds. G. Michaud & A. Tutukov (Dordrecht: Kluwer Academic Publishers), 411

McCook, G.P. & Sion, E.M. 1987, ApJS, 65, 603

Mestel, L. 1952, MNRAS, 112, 583

Mestel, L. 1965, in Stars and Stellar Systems, eds. L.H. Aller & D.B. McLanchlin (Chicago: University of Chicago Press), 297

Mestel, L. & Moss, D.L. 1977, MNRAS, 178, 27

Meynet, G. 1991, Ann Physiq, 16, 459

Miller, J.S., Robinson, L.B., & Goodrich, R.W. 1988, in Instrumentation for Ground-Based Astronomy, ed. L.B. Robinson (New York: Springer), 157

Minkowski, R. 1938, Ann Rep Dir Mt Wilson Obs, 28

Motz, L. 1970, Astrophysics and Stellar Structure (Waltham, MA: Ginn and Company)

Pilachowski, C.A. & Milkey, R.W. 1987, PASP, 99, 836

Preston, G.W. 1970, ApJ, 160, L143

Putney, A. 1995, ApJ, 451, L67

Rösner, W., Wunner, G., Herold, H., & Ruder, H. 1984, J Phys B: At Mol Phys, 17, 29

Ryabchikova, T.A. 1991, in Evolution of Stars: the Photospheric Connection, IAU Symposium 145, eds. G. Michaud & A. Tutukov (Dordrecht: Kluwer Academic Publishers), 149

Schatzman, E. 1958, White Dwarfs (Amsterdam: North-Holland Publishing Company)

Schmidt, G.D., Bergeron, P., Liebert, J., & Saffer, R.A. 1992, ApJ, 394, 603

Schmidt, G.D. & Norsworthy, J.E. 1991, ApJ, 366, 270

Schmidt, G.D. & Smith, P.S. 1995, ApJ, 448, 305

Shapiro, S.L. & Teukolsky, S.A. 1983, Black Holes, White Dwarfs, and Neutron Stars (New York: John Wiley & Sons),

Shurcliff, W.A. 1962, Polarized Light Production and Use (Cambridge: Harvard University Press)

Sion, E.M., Bohlin, R.C., Tweedy, R.W., & Vauclair, G.P. 1992, ApJ, 391, L29

Sion, E.M., Greenstein, J.L., Landstreet, J.D., Liebert, J., Shipman, H.L., & Wegner, G.A. 1983, ApJ, 269, 253

van Maanen, A. 1917, PASP, 29, 258

Van Vleck, J.H. 1932, Theory of Electric Magnetic Susceptibilities (Oxford: Oxford University Press), pp. 172-178

Villata, M. 1992, MNRAS, 257, 450

West, S.C. 1989, ApJ, 345, 511

Whitney, B.A. 1991b, ApJS, 75, 1293

—— 1991a, ApJ, 369, 451

Wickramasinghe, D.T. & Ferrario, L. 1988, ApJ, 327, 222

Wunner, G., Rösner, W., Herlod, H., & Ruder, H. 1985, A&A, 149, 102

Table 1.1 White Dwarf Spectral Type Classifications

Symbol	Definition
DA	Only Balmer lines; no HeI or metals
DB	HeI; no H or metals
DC	Continuous, no lines deeper than 5%
DO	HeII strong; HeI or H present
DZ	Metal lines only, no H or He
DQ	Carbon, either atomic or molecular
Extra Symbols	
P	Polarized (magnetic)
H	Magnetic, no detectable polarization
X	Peculiar or unclassifiable
V	ZZ Ceti or other variable
number	Number is $50400/T$

Note: Letters can be used in conjunction to denote secondary characteristics

Appendix 1.A

Derivation of Magnetic Field Decay Times in a White Dwarf

Starting with the Maxwell equations in the MHD approximation ($\frac{\partial \mathbf{D}}{\partial t} \ll \frac{4\pi}{c}\mathbf{J}$):

$$\nabla \times \mathbf{B} = \frac{4\pi}{c}\mathbf{J}, \tag{1.A1}$$

$$\nabla \cdot \mathbf{B} = 0, \tag{1.A2}$$

$$\nabla \times \mathbf{E} = -\frac{1}{c}\frac{\partial \mathbf{B}}{\partial t}, \tag{1.A3}$$

$$\mathbf{J} = \sigma \mathbf{E}. \tag{1.A4}$$

Take the curl of (A1):

$$\nabla \times (\nabla \times \mathbf{B}) = \frac{4\pi}{c}\nabla \times \mathbf{J}. \tag{1.A5}$$

If σ is constant, then

$$\nabla(\nabla \cdot \mathbf{B}) - \nabla^2 \mathbf{B} = \frac{4\pi}{c}\sigma \nabla \times \mathbf{E}, \tag{1.A6}$$

$$-\nabla^2 \mathbf{B} = \frac{4\pi}{c}\sigma(-\frac{1}{c})\frac{\partial \mathbf{B}}{\partial t}, \tag{1.A7}$$

$$\nabla^2 \mathbf{B} = \frac{4\pi}{c^2}\sigma \frac{\partial \mathbf{B}}{\partial t}, \tag{1.A8}$$

since

$$\nabla^2 \mathbf{B} \sim \frac{B}{r^2}, \tag{1.A9}$$

we have

$$\frac{\partial \mathbf{B}}{\partial t} \approx \frac{c^2}{4\pi\sigma r^2}B, \tag{1.A10}$$

$$B(t) = B_0 \exp(t/t_D), \tag{1.A11}$$

where

$$t_D = \frac{4\pi}{c^2}\sigma r^2. \tag{1.A12}$$

The Wiedemann-Franz law estimates the electrical conductivity as

$$\sigma \simeq (\frac{e}{k})^2 \frac{\nu}{T} \tag{1.A13}$$

(Mestel 1965), where ν is the thermal conductivity. Mestel then calculates $\sigma \simeq 10^{16}\rho$ which yields $t = 2 \times 10^{10}(\frac{M}{M_\odot})(\frac{R}{R_\odot})^{-1}$ years. Using the more accurately calculated values for σ in Hubbard & Lampe (1969), Chanmugam & Gabriel (1972) find $t \sim 10^{11}$ years.

CHAPTER 2

Survey of DC Stars

Abstract

A survey of ~ 50 DC white dwarf stars was conducted in circular spectropolarimetry to search for magnetic fields $\gtrsim_{30}$ kG. Four DC stars were discovered with magnetic fields above 30 kG: G 111-49 with $B_e \sim -220$ MG, G 183-35 with $B_e = +6.8 \pm 0.5$ MG, G 256-7 with $B_e = +4.9 \pm 0.5$ MG, and G 234-4 with $B_e = +39.6 \pm 11.6$ kG. A new magnetic DB white dwarf was also discovered, LB 8827 with $B_e = 1.0 \pm 0.5$ MG. A total of 15% of the white dwarfs in the survey have a magnetic field > 30 kG. This value is far larger than the 2% of DA stars, but more than half of the DC stars were originally misclassified. Only 5% of the re-classified DC stars have magnetic fields above 30 kG. Non-white dwarfs were also observed: the two BL Lacs are unpolarized in circular polarization and an extreme carbon star was discovered.

2.1 Introduction

Stellar evolution is a major astronomical topic. Since we, the scientists, are unable to form a star and experiment with it in our labs to find out how it evolves, we must resort to observing as many stars as possible and piece together the evolutionary process from these data. As seen in Chapter 1, the evolution of a star to the white dwarf stage and within the white dwarf star is mostly understood. However, the existence of magnetic white dwarf stars could greatly upset the present evolutionary scenarios.

The present theory on the formation of magnetic white dwarfs (MWDs) assumes that there is not a large number of them (see Chapter 1). They are presumed to be descended from magnetic Ap stars (where these evolved from should be the topic of someone else's thesis) mostly because the field strengths and the observed number of each are consistent with this scenario.

This does not solve all the problems MWDs impart to stellar evolution. One such problem is the very wide spread of rotation periods. Some have rotation periods of less than 3 weeks (typically a few hours to days (Schmidt & Norsworthy 1991)) and others appear not to rotate at all (Grw+70°8247 has shown no change since its first observation by Minkowski (1938)). There is no correlation between rotation period and temperature (age) or between period and field strength (Schmidt & Norsworthy). Chapter 3 discusses the topic of white dwarf rotation in more detail.

The magnetic field's importance to stellar evolution in general cannot be determined until the relative distribution of field strengths is known. The only way to know this distribution is to survey white dwarfs, in an unbiased manner, to look for magnetic fields. Previous surveys for magnetic fields were typically broadband circular polarization surveys, which measure the continuum polarization. These surveys were only sensitive to strong magnetic fields (> 50 MG). Circular spectropolarimetry is a more sensitive method, since it can measure the two oppositely polarized σ-components of the Zeeman split absorption features. Schmidt & Smith (1995) were able to measure a magnetic field as low as 88 kG. Lower fields could be achieved with much higher resolution, but this becomes impractical due to the faint nature of most white dwarfs.

At present, 42 isolated white dwarfs are known to possess magnetic fields in excess of 10^6 G and an additional three have fields stronger than 10^5 G (Schmidt & Smith 1995; SS). The number of isolated white dwarfs known is probably over 1000, but that is not certain. Many of the magnetic white dwarfs discovered recently have been found in quasar surveys or from UV or other high energy surveys. However, until these surveys are complete, we only hear of the MWDs found, not of the other white dwarfs found. This means that we do not have an unbiased sample to work from. However, SS made a survey of DA white dwarfs that is close to being unbiased. I have made a similar survey of DC white dwarfs.

Sections of this chapter have been published separately as a Letter to the Astrophysical Journal (Putney 1995). They are included in this chapter since this is where they logically belong.

2.2 Survey

The survey sample was taken entirely from the McCook & Sion 1987 Catalog of Spectroscopically Identified White Dwarfs. The catalog is a compilation of all known surveys to that time and lists 1279 white dwarf stars. The surveys which identified white dwarfs were typically proper motion surveys and faint blue object surveys (usually searching for quasars). From the catalog, I chose all stars which were identified as DC (or at least one of its identifications was DC), not listed as a binary, had a magnitude ≤ 16.5, and had a declination $> -20°$. The last two criteria allowed for acceptable signal-to-noise in a one hour exposure at Palomar. This left 52 stars, see Table 2.1. (Note: Many white dwarfs have more than one name. I chose the earliest name that had a finding chart from which I could identify the star, thus ensuring that I looked at the named object. Some objects have come to be known in the literature by a different name and in these cases both names will be used in the text.) Table 2.2 lists the other stars which were observed. Table 2.3 lists more information on the observed objects from various literature sources.

The initial sample was whittled down due to a variety of reasons. This left 46 stars in the final sample. After the survey was begun, two stars were identified as BL Lac objects, LB 2449(=PG 1246+586) and PG 1424+240 (Fleming et al. 1993). Ton 1137 has turned out to be a hot subdwarf rather than a white dwarf. WD 0310+1853, LP 414-120, and Rwt 103 were not observed, but other stars were observed in their stead. In McCook & Sion, WD 0310+1853 has the identical coordinates to LP 414-120 (WD 0410+1853), except that the right ascension is different by one hour. WD 0310+1853 also had LP 414-120 listed as an alternate name, although all the other names that were listed for LP 414-120 were not listed for WD 0310+1853. The nearest object to WD 0310+1853 of appropriate

magnitude is LP 412-13. The only information available on LP 412-13 was from Luyten (1979) which called it type m+. Even though this information indicated that it is probably not a white dwarf, it was observed. It turned out not to be a white dwarf, but rather a dM3 star. Due to confusion at the telescope, the objects observed as LP 414-120 and Rwt 103 were not the expected white dwarfs. Instead, three neighboring objects were observed (Putney 1 = object near LP 414-120; Putney 2 = object near Rwt 103; and IRAS 04193+4959, near Rwt 103). All these objects will be described in more detail in section 2.5.3. In any case, this leaves 46 white dwarfs which were observed in circular spectropolarimetry. An additional 11 stars were observed, mostly to check on the reliability of the measurements. Three were known, or expected, to have magnetic fields and be polarized (GD 90, LB 8827, and PG 1658+441). Five were expected to be unpolarized and were observed to check the performance of the polarimeter. They were three flux standards (G 191B2B, G 24-9, and G 138-31) and two random main sequence stars (SAO 59965 and SAO 61549). An additional three were accidentally observed (Putney 3, Putney 4, and Putney 5), i.e., they were supposed to be target stars, but were neighboring ones instead. These 11 will also be discussed with the target objects.

2.3 Observations and Reductions

The majority of the observations were taken at the Palomar Observatory, although a few were taken at the W.M. Keck Observatory. Table 2.4 summarizes the observations. A brief weather description is given: clr=clear, fog=fog, cldy=cloudy, and vcdy=very cloudy. Several objects were observed more than once because either the weather was poor the first time and the data were inconclusive, or a magnetic field was detected and further observations were needed to check for rotation. Some of the stars with magnetic fields are known to be rotating, and others may be as well, so the exposure start times are given for all objects.

Observations at the Palomar Observatory were taken on the Hale 200 inch telescope using the polarimeter (Goodrich 1991) mounted on the double spectrograph (DBSP; Oke & Gunn 1982). A 300 g/mm grating was used in the blue

camera, which yielded 2.2 Å/pixel and a 316 g/mm grating in the red camera, yielding 3.1 Å/pixel. This gives wavelength coverage from $\sim$ 3700 Å to $\sim$ 8000 Å. The slit width was 2″. The resolution was 12.6 Å in the red and 11.7 Å in the blue, but the blue camera data have been smoothed to match the red resolution in the figures. Details of the method used to take and reduce this circular polarization data are in Goodrich et al. (1995). Briefly, the light first passes through a rotatable quarter-wave plate which converts any circular polarization into linear. Then the beam passes through a calcite prism which splits it into two parallel, orthogonally polarized beams. Two observations are required for the Stokes' parameter V – the first observation with the wave plate fast axis at 45° to the axis of the calcite prism, and the second at 135°. The four spectra produced from these two observations are extracted and combined to produce the Stokes' parameters V and I.

The Palomar polarimeter has gone through many changes since it was first installed. Most of these were much needed improvements; however, one series of changes, which were thought to be improvements, actually introduced errors in polarization. Due to the design of the polarizing beam splitter (a modified Glan-Taylor prism), each beam has a different path length in the prism, i.e., the two emerging beams have different foci. This makes it impossible to focus both beams at the same time on the CCD chip. To get around this, we first attached a thin plano-convex lens to the prism where the e-ray (shorter path length beam) emerged. However, this caused great changes in the illumination profile of that beam and vignetting. Next, we removed the thin lens and tried a thick lens, with a convex input and concave output, where the o-ray emerged (more details about these lenses can be found in Goodrich 1991). This lens was in place during the June 1993 observing run. This lens shifted the pupil which caused vignetting. This vignetting introduced a polarization of up to 1%. The object's position on the slit, exposure length, and seeing conditions varied the magnitude of the effect. Also, null polarization standards were not always measured as null (often 1%) and polarization standards (in linear polarization) were often up to 1% different from

the published value. We could find no way to correct for this, so we decided to remove the lens entirely. For all observing runs after December 1993, a focus in between the best focus for each beam is used in the spectrograph. Since then, all null polarization standards have measured polarizations of less than 0.2% and polarized standards (in linear polarization) are always measured at the published value to within 0.1% or 0.2%. The errors introduced by the lens were either constant in wavelength or a smoothly varying function of wavelength, i.e., no feature resembling a line feature would appear. Thus the data from June 1993 have much higher errors than the statistical errors calculated, but only the continuum polarization shape and strength are affected.

The observations at the Keck Observatory 10 m telescope were taken with the polarimeter (similar to the Palomar polarimeter; Goodrich et al. 1995) mounted inside the Low Resolution Imaging Spectrometer (LRIS; Oke et al. 1995). The 300 g/mm grating was used yielding 2.49 Å/pixel and a wavelength coverage from $\sim$ 3900 Å to $\sim$ 8900 Å. The slit width was 1.0″. The resolution was 11.1 Å. We used a new procedure to measure V, the "dual wave plate method" discussed by Goodrich et al. (1995). A comparison of data taken of Grw+70°8247 at both Palomar and Keck indicates that this method worked well, and a brief description follows. A stationary quarter-wave plate is placed above a rotatable half-wave plate. The quarter-wave plate converts the circular polarization to linear, which is then analyzed with the half-wave plate in a method analogous to the method described above for the Palomar data. However, there are two possible contaminants to the data from Keck.

The first possible contaminant is due to cross-talk, i.e., a coupling between the circular and linear polarization, in the dual wave plate method. If the incident light contains any linear polarization, there may be a leakage into the circular polarization measurement if either wave plate is not perfect. Numerical simulations have shown that for V/I $\gg$ p ($= \sqrt{(Q^2 + U^2)/I^2}$), the leakage is less than 0.02 V/I; for V/I $\sim$ p, the leakage can be as high as 0.1 V/I; and for V/I $\ll$ p, the

leakage is large and possibly non-correctable (Goodrich et al. 1995). Tests with Grw+70°8247 confirm these calculations.

The second possible contaminant of the data is second order blue light. Presently the Keck LRIS has only one camera, although a second camera is planned, which would make it similar to the Palomar DBSP. The existing camera is the red camera, which is functional from about 3700 Å to about 11000Å. The wavelength range used for the survey objects covered more than a factor of two in wavelength and no order blocking filter was used. This led to second order light contaminating the red end of the spectrum in all observations. However, due to the low temperature of the white dwarfs observed (and therefore the relatively flat spectral shape in the wavelength range in question), this effect is minimal. In all objects except G 111-49, the continuum polarization was $0.0 \pm 0.1\%$, thus they do not appear to be affected by 2nd order light. G 111-49 might have some effect, but an analysis of Grw+70°8247 (a similar magnetic star) shows that the effect is as high as 10% at 8000 Å, i.e., not very large. Most nights, the flux standards used at Keck were of similar spectral shape to the survey objects (in fact, they were survey objects), so the flux shape of the target objects should have minimal 2nd order effect due to the flux standards. However, one night, 1994 December 31, the DA0 star G 191B2B was used. This star decreases in F_λ by more than a factor of 30 from 3700 Å to 8000 Å. When using this as the flux standard, it was clear from the flux calibrated spectrum of G 158-45(=LHS 1044) and LHS 1734 that 2nd order light was contaminating the spectrum of the flux standard. The flux standards Feige 110 and G 191B2B have nearly identical continuum shapes. Feige 110 was observed both with and without an order blocking filter during an observing run at Keck in May 1995. From these two observations, a curve was calculated to correct for the 2nd order light and used on the 1994 December 31 data.

There was a third problem with some of the data taken at Keck. The angle of the spectrograph's entrance slit must remain fixed to the sky for both exposures of each object when taking polarization measurements (the linear polarization has

a fixed angle to the sky). The optimal angle is the parallactic angle; however, this cannot always be used (e.g., another star would fall on the slit if the parallactic angle were used). If the star is at 1.0 airmasses, there is no effect. At any other airmass, the star is differentially refracted along the parallactic angle, and the higher the airmass, the stronger the effect. For high airmasses ($\gtrsim$1.8) the differential refraction can be as far as 1″ at 4000 Å and at 7000 Å. Combining this refraction with a slit width of 1″ means that blue and red light does not enter the slit. In December 1994, both observations of G 158-45(=LHS 1044) and the observation of Putney 2 were taken at slit position angles much different from the parallactic angles. The effect can be seen in the observed spectra, i.e., depressions in the flux at the red and blue ends of the spectrum.

The spectrophotometric standards of Oke (1990) were used for flux calibration. Corrections were made to the flux spectra for atmospheric H_2O and O_2, using the DC flux standards of Oke (1990) as templates.

2.4 Method to Determine $\vec{B}$

There are several steps involved in accurately determining the magnetic field strength of isolated white dwarfs. The first step is to determine which magnetic field range the star is in: (1) > 50 MG, (2) 1 MG $\leq$ B $<\sim$ 50 MG, (3) < 1 MG, or (4) indeterminable. The second step is a determination of the effective magnetic field, B_e, i.e., the mean line of sight component of the magnetic field (see, e.g., Landstreet 1992). The method for determinating B_e is particular to the magnetic field range and will be explained below. The last step is to calculate theoretical model spectra and determine the whole surface magnetic structure of the star. This has not been done for the stars in this survey; however, Chapter 4 makes these calculations for three other magnetic stars. The effective field is, at most, a factor of two below the actual dipolar magnetic field strength, so it is an adequate measure for this survey.

2.4.1 Range Determination

The field range determination uses a combination of the flux and circular polarization spectra. The 1 MG $\leq$ B $<\sim$ 50 MG field range is the easiest to classify. This is the field range where the quadratic Zeeman effect is dominant, thus the hydrogen or helium lines will be split into three (or more) components with separations up to a few hundred Angstroms (e.g., Figure 2.1). In the majority of cases the three components will be visible as absorption features in the flux spectrum. In a small fraction of cases the absorption features may not be visible because the temperature is too low, or the abundance of the element in question is too low (to allow the σ components to be detectable), or the field structure is such that the σ or π components are too broad to be detectable in flux. However, in all but two cases there is a positive circular polarization feature for one σ-component and a negative feature for the other component (a Zeeman signature). The first exception to this rule is a star with a very low temperature ($T \lesssim_{4000}$ K). A white dwarf this cold cannot form line features in either flux or polarization. The second exception is rare, but possible. If the magnetic configuration of the star is an equator-on view of a centered dipole, the polarization features will not be detectable. The probability of this occurring is about 0.79%[1]. The Zeeman signature is especially useful in identifying magnetic fields in stars with shallow σ components (e.g., PG 1312+099=PG 1312+098, Fig. 2.29). The continuum polarization in white dwarfs with magnetic fields between 1 and 50 MG is typically $< 0.5\%$ (although 1% and greater has been observed). Combining this with the fact that the two σ components have the same strength in polarization, but opposite polarization senses renders searches in broadband (several hundred Å wide) circular polarization inconclusive.

---

[1] One out of 11 magnetic white dwarfs has a magnetic field consistent with a centered dipole (Chapter 4). A viewing angle up to $\sim \pm 5°$ around the equator will act like an equator on view. Thus P= (1/11)*($2\pi(\cos 85° - \cos 95°)$ steradians/4π steradians).

The B > 50 MG range is the next easiest range to classify. This is the magnetic field range where the magnetic and Coulombic forces in an atom are of similar strength and therefore the results of detailed quantum mechanical calculations are required to make line identifications. Also in this regime, the continuum will show circular polarization, although it may be < 1% for equatorial or near equatorial viewing angles of the stars with field strengths close to 50 MG. All stars with continuum polarization stronger than 1% or a structured (not constant in wavelength) polarization spectrum will fall in this category (e.g., Figure 2.14). These stars may have absorption features in flux at wavelengths not usually associated with hydrogen, helium, carbon, calcium, etc. A comparison of these features to the above mentioned calculations may identify them as hydrogen in a very strong magnetic field, e.g., Grw +70°8247 (Minkowski 1938, Kemp et al. 1970, Angel, Liebert, & Stockman 1985).

Stars with no detectable features nor any continuum polarization are placed in the indeterminable range. Since there is no continuum polarization, they cannot have a field above ~ 20 MG.[2] Also, if there are no absorption features, then there is no way to search for the Zeeman effect. For reasons explained in Section 2.4.2.4, white dwarfs whose only absorption features are due to C_2 are placed in this category as well.

The final category is for all the stars with identifiable absorption features, e.g., H, He, or Ca, which are not visibly split into separate Zeeman components (at the resolution of this survey). The magnetic field strength of these stars is less than 1 MG. If the field is strong enough, a star in this category will have a distinct Zeeman signature in circular polarization, e.g., WD 0009+501 (SS).

---

[2] This number is determined by comparing the broadband circular polarization measurements of several stars with field strengths > 1 MG from Angel, Borra, & Landstreet (1981) to the field strengths of the same stars in the SS list of high field stars. The 20 MG limit is conservative.

2.4.2 Field Strength Determination by Individual Field Range

2.4.2.1 $B > 50$ MG

At the present time, precise measurements of the effective magnetic fields in the range of B > 50 MG cannot be made. However, a good approximation can be obtained.

This is the magnetic field range where the magnetic and Coulombic forces are of comparable strength. An analytic solution is not possible here due to different symmetries of the forces – magnetic forces are cylindrically symmetric and Coulombic forces are spherically symmetric. A group in Tübingen, Germany, have made numerical calculations of the transition wavelengths for several hydrogen lines from 4.7 MG to 4700 MG (Wunner et al. 1985; Ruder et al. 1994). No such calculations have been published for helium. The curves of λ as a function of B wander around in wavelength, often by huge amounts, e.g., some of the Paschen β terms are in the ultra-violet at 10^9 G. However, many of these transitions have extrema, or "stationary points," where a transition occurs at a particular wavelength, or over a very small wavelength range (e.g., 50 Å), for a large range of magnetic fields (e.g., 100 MG; see the middle panel of Figure 2.14). A spectral feature may develop at the wavelength of a stationary point if a large enough fraction of the star is covered with the corresponding magnetic field strength. The transitions which have "stationary points" are typically those which correspond to the σ_--components of the Zeeman effect, although a few correspond to the π-components. The σ-like, and many π-like, features are circularly polarized. A comparison of the flux and circular polarization spectra to the curves of λ vs. B yields the range of magnetic field strengths on the observed hemisphere. Often the features are very shallow in flux but very strong in polarization (see Figure 2.14). Some features are stronger than others (usually noticeable in circular polarization) indicating that a larger area of the star's observed hemisphere is covered in the field strength responsible for the feature. This must be taken into account when determining B_e, since B_e is

a weighted average of the observed field. This is not a precise measurement, but it is descriptive and yields a starting point for calculating models.

There are cases in which the observed spectral features do not correspond to any of the calculated hydrogen features, e.g., GD 229 (Schmidt, Latter, & Foltz 1991). The most likely explanation for this is that the atmosphere is dominated by an element other than hydrogen. The most probable culprit is helium since helium is the second most common element to dominate a white dwarf atmosphere (the number of DB + DO stars in the McCook & Sion catalog outnumber the DZ +DQ stars by a factor of about three). If this is the case, the field cannot presently be determined, although lower limits can be found. This is due to the lack of knowledge about helium in a strong magnetic field. Precise calculations of helium lines have not been made for fields beyond that which causes quadratic Zeeman splitting (20 MG; Kemic 1974; Ruder et al. 1994), but the star Feige 7 has split hydrogen and helium lines in a field of about 35 MG (Martin & Wickramasinghe 1986; Achilleos et al. 1992). This means that helium can be identified to field strengths of about 40 or 50 MG.

At present, the continuum polarization as a function of magnetic field strength is not well understood. Kemp (1970) theorized that the continuum of a stellar object, or even a plasma, with a magnetic field of 10^6 G or greater will emit circularly polarized light proportional to magnetic field strength. Many calculations have been made since then (e.g., Lamb & Sutherland 1974 and Merani, Main, & Wunner 1995) which show that circular polarization in the continuum exists and its strength and spectral shape is a function of magnetic field strength. Thus we might expect that the continuum circular polarization will reveal the magnetic field strength through its spectral shape and intensity. However, this does not work as expected. The reason for this is that the mechanisms which produce the circular polarization are not understood well enough to be able to determine the field strength directly from the continuum polarization (see Chapter 4).

2.4.2.2 1 MG < B < 50 MG

Magnetic field determination is straight forward in this regime. A very quick, reliable estimate to the observed field strength can be obtained by comparing the wavelengths of the Hα (or Hβ) triplet to calculations by Kemic (1974). Then, depending on how accurate a value is needed, or how much time is allotted to the task, another method can be used to get a more precise measure of the magnetic field, including the structure of the field over the star.

The most precise field strength determination method is to run a magnetic white dwarf atmospheric modeling code, e.g., the code described in Putney & Jordan (1995) and Chapter 4. Such a computer program will yield the complete magnetic structure of the star, i.e., the dipolar field strength, the viewing angle of the star, and whether it is a centered dipole, or off-set dipole, and if offset, by how much. This is the best method to use; however, it can take weeks or months of running models to find one that fits well.

Less sophisticated modeling routines to find magnetic field strengths have also been used, e.g., Bergeron et al. (1992), Greenstein & McCarthy (1985), and Liebert, Angel, & Stockman (1975). These routines typically try to reproduce the absorption features in flux only. They leave an ambiguity in the sign of the magnetic field and can be as much as a factor of two incorrect since at least two offset dipole models can be found to match a given flux spectrum and only the polarization spectrum can break the ambiguity. Chapter 4 and Putney & Jordan describe this problem in more detail.

Eventually, a sophisticated modeling program will be used on the stars found in this survey, thus I felt that the method used in Putney (1995) is as accurate as is needed for the survey objects, even though this method also produces values up to a factor of two too low. The method is as follows. Using the wavelengths and line strengths calculated by Kemic (1974), and the spectrograph line shape, I calculated simple Gaussian curves as theoretical models of the Hα absorption features, assuming the star's field is single valued. I then matched the line centers

of these curves to the data. The sense of the σ-components in circular polarization fixes the sign of the star's magnetic field. If the σ_+, shorter wavelength, component has a negative sense, then the field is a north pole, or positive, field. If it has a positive sense, then the observed field is negative, or south polar.

2.4.2.3 $B < 1$ MG

This is the best understood regime, but in some ways it is the hardest one to work in. This is the linear Zeeman region, with the quadratic Zeeman effect being noticeable for the strongest fields. The transitions are understood for all elements (see Chapter 1). Therefore, at the wavelength of each absorption line, the circular polarization can be checked for the existence of the Zeeman signature.

Stenflo (1985) derives an equation for the circular polarization as a function of wavelength and magnetic field for the wings of the line. The outcome of the derivation is:

$$\frac{V_\lambda}{I_\lambda} = \frac{\Delta\lambda_z}{I_\lambda}\left[\frac{\partial I_\lambda}{\partial\lambda} + \frac{1}{6}(\Delta\lambda_z)^2\frac{\partial^3 I_\lambda}{\partial\lambda^3} + \ldots\right] \tag{2.1}$$

where $\Delta\lambda_z = +\frac{e}{4\pi m_e c^2} g\lambda^2 \mathrm{B}$ = the Zeeman splitting. g is the landé factor, B is the magnetic field, and $\frac{\partial I_\lambda}{\partial\lambda}$ is the spectral slope. Stenflo points out that only the first term is needed if $\Delta\lambda_z \ll$ line width. Angel, McGraw, & Stockman (1973) use the first term for their calculations of field strength in the Balmer lines and they use $g = 1$. Mathys & Stenflo (1986), in their work on Ap stars, use the effective Landé factor:

$$g_{eff} = \frac{1}{2}(g_\ell + g_u) + \frac{1}{4}(g_\ell - g_u)(J_\ell(J_\ell+1) - J_u(J_u+1)) \tag{2.2}$$

where g_ℓ (g_u) are the Landé factors for the lower (upper) state and J_ℓ (J_u) are the total angular momentum quantum numbers for the lower (upper) state. Beckers (1969) lists the g_{eff} values for the transitions of astrophysical interest.

For all the stars which fall in this category, the following method was used to determine a magnetic field strength. A Lorentzian was fit to the line in question (hydrogen, helium, calcium, or sodium). $\frac{\partial I_\lambda}{\partial\lambda}$ was calculated as $(I_\lambda - I_{\lambda+\Delta\lambda})/\Delta\lambda$,

where $\Delta\lambda$ is the dispersion of the spectrum. A linear least squares fit was performed to

$$y = a + bx \tag{2.3}$$

where

$$y = \frac{V}{I}(\lambda) \text{ (observed)}, \tag{2.4}$$

$$x = \frac{e}{4\pi m_e c^2} g_{eff} \lambda^2 \frac{dI}{d\lambda} \frac{1}{\lambda}, \tag{2.5}$$

a is the constant continuum polarization over the region, and b is the magnetic field strength. This calculation was made over a small range in wavelength across the line in question, e.g., 6500 Å to 6800 Å for Hα. If possible, several lines were treated in this manner and the final magnetic field strength listed in Table 2.6 is a weighted average of the individual field strengths.

For easy referral in later sections, I am calling this the Low Range method.

2.4.2.4 Indeterminable

In certain ways, this is the easiest regime. The objects which fall into this category have no absorption features and no circular polarization, either in the form of features or continuum. A null circular polarization for the data presented is V< 0.2% (V< 1.0% for June 1993 and February 1994 data) or V< 0.5% with the polarization in the red camera and blue camera having different signs (e.g., G 83-10). For the present survey, these objects are probably helium white dwarfs which are too cool to show any helium absorption. All that can be said with certainty about these stars is that they all have magnetic field upper limit of 20 MG, although the field is probably much lower in most cases.

The stars with molecular carbon bands and no polarization are also added to this indeterminable category. As has been demonstrated with G 99-37 (Angel & Landstreet 1974; Schmidt, Bergeron, & Fegley 1995), the C_2 bands do not shift via Zeeman effect until fairly high fields are reached (value unknown, but $\gg$ 10 MG). G 99-37 has a continuum polarization of $\geq$ 1%, varying as a function of

wavelength, and it has the tell-tale Zeeman σ features in circular polarization for the CH feature only. From this feature Angel & Landstreet calculated a field strength of 3.6 MG (but they expect that the dipolar field is more like 10 MG). It is possible that 20 MG might be too high an upper limit for the DQ stars with a null polarization, but their atmospheres are mainly helium (Wegner & Yackovich 1984) like most of the true DC stars.

2.5 Results

2.5.1 Overview

Each survey object is commented on individually below, in Section 2.5.2. The non-survey objects are commented on in Sections 2.5.3, 2.5.4, and 2.5.5. Tables 2.5 and 2.6 list the general results for all the objects, as described below.

2.5.1.1 Spectral Type

Table 2.5 lists the McCook & Sion spectral type (when applicable; column 2) and the spectral type determined here (column 3). For the white dwarfs, the spectral type follows the classification scheme of Sion et al. (1983) (see Chapter 1). For other objects the source is quoted in the text with the object, but typically they were compared, by eye, with spectra from any of several atlases.

Of the non-white dwarfs, a few objects have no previous classification and, in fact, have no previous name. These may be of some interest to non-white dwarf stellar astronomers.

2.5.1.2 Temperature

The white dwarf temperatures were determined by matching the data to the atmospheric grid points of Bergeron, Saumon, & Wesemael (1995) and an update of the grid points from Bergeron (1995). The Bergeron et al. models consisted of the broadband points UBVRIJHK for white dwarfs of temperatures 4000 to 10,000 K and atmospheric compositions of 100% hydrogen and 100% helium, for

$\log g$=7.5, 8.0, and 8.5, and [He/H]=-1, 0, 1, and 2 for $\log g$=8.0. My data cover the BVRI range and in this range there is very little difference between the different gravities and between 100% hydrogen and [He/H]=-1, 0. There was a problem in fitting with these models, in that the model I band points tended to be too high for the models of mostly hydrogen at the higher temperatures. According to Bergeron (1995), they had already realized that the models did not take proper account of the Paschen lines. He sent revised models of pure hydrogen and pure helium. These unpublished models were the ones actually used to make the temperature determinations. The hydrogen models cover T_{eff} for 4000 K to 100,000 K, in varying step sizes, and $\log g$ for 7.0 to 9.0, in steps of 0.5. The helium models spanned the same gravities, but only went as high as T_{eff}=30,000 K. These new models also had multichannel UBGVRI points (e.g., Greenstein 1976a). These values were used since the observed data are essentially this system.

There were many temperature ranges where one gravity was indistinguishable from another because the spectral range was limited. Also, since high accuracy was not needed (I only wanted a spectral type), no interpolation in between the grid points was done. Thus the temperatures and gravities have an error of the size of the grid spacings. The temperature grid spacings increased with increasing temperatures. For hydrogen, the spacing was 500 K for $T_{eff} < 8000$ K, 1000 K until T_{eff}=17000 K, and 5000 K for the rest. The helium spacings were similar. The temperatures are in Table 2.5 (column 4) as well as the dominant atmospheric constituent (column 5). A set of parentheses around an element implies that I believe that it is a possible constituent.

2.5.1.3 Magnetic Field

A magnetic field is determined for each white dwarf, if possible. The method used for each object is described with the object. Table 2.6 contains the average circular polarization measurements (red region, column 3, 6000 to 8000 Å; blue region, column 4, 3800 to 4600 Å), as well as the calculated magnetic field for the observed objects (column 5).

2.5.2 Individual Survey Objects

G 158-45=LHS 1044=LP 704-1=PHL 6421

This object has Zeeman split Hα and Hβ absorption lines. These split lines were first detected by Bergeron, Ruiz, & Leggett (1992). They modeled it as an offset dipole of B_d=16.7 MG, $T_{\rm eff}$=5820 K, and $\log g$=8.15 in a pure hydrogen atmosphere. I found that a helium atmosphere of $T_{\rm eff}$=6000 K and $\log g$=8 approximated the star well, and matches the Bergeron et al. values within the errors of the grid points I was using. The difference in composition is probably due to the limited spectral range I was using. Using the method described in Sec. 2.4.2.2, I determined an average effective field strength of 9.3±0.8 MG. This average is an average of |B|, since, as can be seen in Table 2.6, half of the observations produced a positive magnetic field and half a negative one. The difference between my value and that of Bergeron et al. is due to their value being the strength of the star's dipolar field (and an offset one at that!) and mine is a hemispheric average (see Section 2.4.2.2).

Six observations of this object were taken in the present survey, since a comparison of the first observation to the data of Bergeron et al. showed a shift in the absorption line positions, which implied rotation. Chapter 3 will go into more detail on the rotation of this and other objects with measured magnetic fields. Figure 2.1 shows all six flux and circular polarization spectra. They are organized in time order with the earliest spectrum on top. The last two spectra, from Keck, suffered severely from differential refraction of the Earth's atmosphere; this explains the difference in continuum shape from the other observations.

G 171-52=Gr 495

G 171-52 was first classified as a DC by Hintzen & Jensen (1979) and later confirmed by Greenstein (1979, 1984a) and Sion, Kenyon, & Aannestad (1990). As can be seen in Figure 2.2, there is a weak Hα feature, but no apparent Hβ feature. Greenstein (1984a) suggests that its atmosphere may contain helium and hydrogen. I found that an atmosphere of hydrogen with $T_{\rm eff}$=5500 K and $\log g$=8.0

fits the continuum adequately, although the addition of helium to the atmosphere should not be ruled out. Using the Low Range method on Hα, a magnetic field of 21.8 ± 46.5 kG was measured.

PG 0156+156

PG 0156+156 is a true DC, as can be seen in Figure 2.3. PG 0156+156 was observed previously in circular polarization by Liebert & Stockman (1980). They took broadband measurements, from $\sim$ 3200 to $\sim$ 8600 Å, of V and found V=$-0.0032 \pm 0.14\%$. I measured $V_r = -0.018 \pm 0.030\%$ and $V_b = +0.004 \pm 0.033\%$. The low values and change in sign lead me to conclude that this has a null polarization and therefore the field is indeterminable. The best fitting atmosphere I found was $T_{\rm eff}$=9750 K, any $\log g$, and helium as the main constituent.

G 272-152

This object was classified as a DC by Liebert et al. (1979), but they added the note that weak features could not be ruled out. They were right. As can be seen in Figure 2.4, helium features are indeed present. I found an atmosphere of helium, $T_{\rm eff}$>11000 K and any $\log g$ to be consistent with the continuum. Thus I re-classify this object as DB4. Using the Low Range method on 4 He I lines, I found a field of 25.1 ± 30.5 kG.

PG 0210+168

This star was classified as a DC by Green, Schmidt, & Liebert (1986). Figure 2.5 shows that the spectrum is actually full of very narrow hydrogen, helium, and metal lines. PG 0210+168 appears to be a composite spectrum of a late F early G star and a white dwarf. The white dwarf is of type DC, although weak H I or He I lines cannot be ruled out. I measured $V_r = +0.121 \pm 0.012\%$ and $V_b = +0.183 \pm 0.021\%$. The polarization differs from zero near the red and blue edges of the dichroic; this is a false polarization due to the dichroic in the blue camera and the potato chip shaped CCD in the red camera. Using the Low Range

method on Hα, Hβ, and two He I lines, I measured a magnetic field of -0.051 ± 2.4 kG on the non-white dwarf. The white dwarf has an indeterminable field strength.

LHS 1415=Gr 471=LP 710-47

This star has had a possible Ca II detection, but it was never confirmed nor was there ever any hydrogen detected. Liebert & Strittmatter call it DF? with a probable Ca II detection and it ends up in McCook & Sion (1987) as DC,DF?. Figure 2.6 shows three observations of the star. There are no Ca II lines detected in either of the two exposures which extend far enough into the blue. There are, however, hydrogen Balmer lines through Hγ and possibly Hδ. A hydrogen atmosphere of T_{eff}= 5250 K and $\log g$=8.5$\pm$0.5 matched fine, although there is a possibility of the atmosphere containing a substantial fraction of helium. Liebert & Stockman (1980) measured a circular polarization of V= +0.002$\pm$0.10%. Table 2.6 lists the three separate polarizations measured in the present survey. The values average to well under 0.1%, implying a null polarization. It should be noted that the November 1994 V/I calculation for this star was made from only one exposure. The V/I plot clearly shows the effect of the use of an improper ratio of the gains of the two beams (see Section 1.3.3). Using the Low Range method on Hα, Hβ, and Hγ, an average magnetic field of -9.9 ± 9.2 kG was measured from the September and October data. The magnetic field strengths of the individual runs changed drastically, implying either fluctuations around a low value, or measurements of a rotating magnetic star (the September data is a 2.5 σ result and the November data is an 8 σ result, but known to be faulty). More observations are required for confirmation.

G 7-16=LHS 1617

G 7-16 is another white dwarf with very narrow hydrogen absorption lines (see Figure 2.7). An atmosphere of hydrogen, with possible helium, of T_{eff}=5250 K and any $\log g$ fit the continuum. The continuum circular polarization is effectively null (see Table 2.6). The Low Range method reveals a field of 4.1 ± 9.5 kG from Hα, Hβ, and Hγ.

G 83-10=LB 1320=EG 169=LP 475-70(=VA 377=HAN 372)

G 83-10 appears to be a true DC star, although I do not rule out the possible existence of very weak Ca II H & K lines (see Figure 2.8). Eggen & Greenstein (1965) call it a DC star, and later Greenstein (1986) updates it to DC8. I found that a hydrogen atmosphere of $T_{\rm eff}$=6500 K and $\log g$=8.5±0.5 fit well. Landstreet & Angel (1971) measured a circular polarization of $-0.03 \pm 0.11\%$. From this value, Angel, Borra, & Landstreet (1981;ABL) calculated a magnetic field $B_e = -220 \pm 810$ kG. I measured $V_r = +0.060 \pm 0.020\%$ and $V_b = -0.038 \pm 0.034\%$, which imply a null polarization. Thus this star's magnetic field is indeterminable.

LHS 1734=LP 777-1

This is another object with Zeeman split lines first noticed by Bergeron et al. (1992). They modelled it with an offset dipole of B_d=7.3 MG, $T_{\rm eff}$=5340 K, and $\log g$=7.61 in a pure hydrogen atmosphere. I found 5000<$T_{\rm eff}$<5500 and any $\log g$ were the best fits. Figure 2.9 shows the three observations taken. The circular polarization spectra clearly show the Hα σ-components changing between the last two observations, implying rotation. More details about its rotation will be discussed in Chapter 3. The effective field measurements for each observation are in Table 2.6 and the average is $3.8\ ^{+0.6}_{-0.3}$ MG.

G 108-42=EG 181

G 108-42 is a DC star with a slim possibility of a metal line at 4196 Å (see Figure 2.10). It is highly probable that the line is due entirely to noise. Eggen & Greenstein (1967) first classified it as DC. I found that a helium atmosphere of $T_{\rm eff}$~10000 K with any $\log g$ best fit the continuum. ABL measured V= -0.11 ± 0.10 and calculated $B_e = 360 \pm 330$ kG. I measured $V_r = +0.014 \pm 0.033$ and $V_b = -0.74 \pm 0.041$. Thus this star has an indeterminable magnetic field.

G 234-4=LP 58-247=Gr 321=GJ 1098

This star has had its white dwarf status questioned on occasion. Greenstein (1974) first classified it as a DK-DC and later (Greenstein 1976a) claimed

that it could possibly be a red subluminous star. Probst (1983) followed up on Greenstein's observations and claims that it could be sdG or sdK. Greenstein et al. (1977) call it a DC and Greenstein (1984a) calls it a DC9 with a possible helium atmosphere. Figure 2.11 shows the star. It is a very cool weak hydrogen lined white dwarf and therefore quite red for a white dwarf. I found that a hydrogen atmosphere, possibly a mix with helium, of $T_{\rm eff} \sim$ 4500 K and any $\log g$ fit well. Using the Low Range method on Hα and Hβ, I found a magnetic field of 39.6 $\pm$ 11.6 kG. The polarization at Hα are suggestive of a Zeeman feature and give more credence to this barely 3 σ detection. Further observations are needed on this object.

G 193-74=Gr 344

This object is a flux standard in Oke (1990). No trace of an absorption feature could be found for this object in either of the two observations taken. Figure 2.12 shows the flux and polarization spectra for both observations. The flux data are offset for clarity. Using the method of temperature determination described above, I found a temperature of $\sim$ 8000 K, any $\log g$, and a helium, and probably some hydrogen, atmosphere best fit the spectra. The circular polarization measured was V_r(Feb94) = $-0.020 \pm 0.025\%$, V_b(Feb94) = $-0.095 \pm 0.032\%$, V_r(Dec94) = $+0.092 \pm 0.014\%$, and V_b(Dec94) = $+0.031 \pm 0.024\%$. These data are consistent with an unpolarized object. The lack of absorption features and lack of polarization places it in the indeterminable category.

G 193-78=Gr 322

Greenstein (1974) classified G 193-78 as a DC star and later (Greenstein 1976b) stated that the colors implied a probable helium atmosphere. Wegner & Yackovich (1982) noted a shallow depression near 4200 Å and classified it as λ4200, i.e., akin to G 195-19, a magnetic white dwarf with unidentifiable absorption features. I detected no such feature, see Figure 2.13. I found that the continuum was best fit by a helium atmosphere of $T_{\rm eff}$=11000 K and $\log g$=8. ABL measured V= $-0.02 \pm 0.05\%$ and determined $B_e = -80 \pm 210$ kG. I measured $V_r = +0.007 \pm$

0.016% and $V_b = -0.006 \pm 0.021\%$. This star is probably not like G 195-19, as Wegner & Yackovich claim, but rather a plain helium atmosphere DC. Its magnetic field is indeterminable.

G 111-49=Gr 428

G 111-49 has a history of spectroscopic misidentification. Greenstein et al. (1977) classified it as a DF-C, meaning possible metal lines present. Later Greenstein (1979) revised that classification to DF: with the possible presence of a 4670Å line (indicative of molecular carbon). Next, Sion et al. (1979) classified it as a λ4670 star (DQ in the present classification scheme; Sion et al. 1983). Then it was back to a DC by both Hintzen & Jensen (1979) and Wegner & Yackovich (1982). Guseinov et al. (1983) included it in their survey of helium white dwarf stars, presumably because a star of its temperature (quoted as 8400 K by Guseinov et al.) should have strong hydrogen lines if it were a DA; however, it does not, therefore they thought it likely to be a helium white dwarf. Greenstein (1984a) gave it the designation DCpec with a helium atmosphere. McCook and Sion (1987) finally list it as DC?6. I am now re-classifying and confirming this star as DAP (or perhaps DCAP, since the absorption features are well below 5% of the continuum, the DC definition (Sion et al. 1983)). Figure 2.14 shows the flux and circular polarization measurements of this star, as well as curves of the hydrogen transitions as a function of field strength (from Wunner et al. 1985). The star is strongly circularly polarized and has features which can be identified as hydrogen transitions in a strong magnetic field.

This star falls in the B > 50 MG range, thus the method used to determine the field strength is that of Sec. 2.4.2.1. In Figure 2.14, three circular polarization features are labelled. Feature "a" is near the stationary point of the hydrogen Hα transition 3p-1 – 2s0 at 200 MG (from Wunner et al. 1985; panel C of Figure 2.14). This extremum is a minimum in wavelength, thus as the magnetic field varies from the value at the extremum, the feature will extend redward. The double humped feature "b" is near both Hα 3d−2 — 2p−1 at 117 MG and Pa β 5p′0 — 3d′0

at 290 MG and is a blend of the two transitions. Feature "c" is near Hα 3d$-$1 — 2p0 around 300 MG. A close inspection of the flux will reveal several wide, shallow absorption features at the same wavelengths as the polarization features. There are three small features in flux between 5400 Å and 6000 Å which do not appear to be due to the hydrogen transitions (see Figure 2.14); they could be due to helium, but there is presently no way to confirm this conjecture. There are also hints of features in flux and polarization due to the Hβ transitions, but these are not at stationary points and are therefore wide, shallow, and a less rigorous measure of magnetic field strength. The circular polarization features described above have the opposite polarization sense to the continuum because they are σ_- transitions and the mechanisms which polarize the continuum produce polarization of the same sense as the σ_+ transitions. However, these continuum polarization mechanisms are not completely understood (Putney & Jordan 1995). Also note the similarities between the circular polarization spectrum of G 111-49 and the spectra of both G 227-35 (Cohen et al. 1993; Putney & Jordan 1995) and Grw+70°8427 (Angel et al. 1985) (see Fig 14). The general shape of the continuum polarization in all three is similar with the strength of the polarization strongest in G 111-49, with $|V|_{max} = 9\%$. The field strength derived from the absorption features of Grw+70°8247 (> 300 MG; Greenstein 1984b; Greenstein, Henry, & O'Connell 1985; Angel, Liebert, & Stockman 1985) is stronger than that in G 111-49, thus the reason for |V| being so much larger in G 111-49 is most likely due to the viewing angle of the two stars, i.e., the closer towards the magnetic pole one views a star, the stronger the circular polarization. Section 2.3 discusses some possible contaminants to the circular polarization data of this star. Leakage of linear polarization into the circular is the biggest fear. In the unlikely event that the worst case is present, i.e., the linear polarization is much larger than the circular, then the analysis of the continuum polarization is invalid (there have been no magnetic white dwarfs observed with this condition to date). If the linear and circular polarizations are of comparable strength, then $|V|_{max} = 9\pm2\%$, which is still larger than that of Grw+70°8247. In any case, the analysis of the

features, from which the field strength was determined, is valid since the leakage conserves features.

With the aid of model fitting, G 227-35 was found to have a dipolar magnetic field of ~180 MG and a viewing angle below the equator (Putney & Jordan 1995), thus implying a view of the negative or southern magnetic hemisphere. Keeping this and Figure 2.14 in mind, I conclude that G 111-49 has an effective magnetic field of about −220 MG. Any detailed modeling of this star will be ineffective, until a more accurate theory of the continuum circular polarization in large magnetic fields (> 100 MG) is found. Also, linear spectropolarimetric measurements need to be taken to determine the existence of and remove any contamination to the circular polarization. Only one observation of this star was taken in the present survey, so it is impossible to know if it is rotating or not. However, the fact that it has been classified as a variety of different types may mean that it is rotating and at some rotational phase an absorption feature appears near the wavelength of carbon, calcium, or iron.

This object appears in Putney (1995).

LB 3013=LP 487-21=PG 0913+104

LB 3013 appears to have very shallow C_2 features on an otherwise continuous spectrum (see Figure 2.15). Green, Schmidt, & Liebert (1986; GSL) classified it as DC6. Wegner et al. (1985) found C_2 bands and then fit a model of T_{eff}=9000 ± 500 K, $\log g$=8 and a predominantly helium atmosphere. I found that a helium atmosphere of T_{eff}~ 9500 K and any $\log g$ fit well. Liebert & Stockman (1980) measured V=+0.043 ± 0.14%. I measured $V_r = -0.118 \pm 0.038\%$ and $V_b = -0.031 \pm 0.049\%$. This has an indeterminable field.

Ton 1061=PG 0924+199

Ton 1061 has a continuous spectrum, except for the possibility of extremely weak Hα and He I 5876Å (see Figure 2.16). I found an atmosphere of helium at T_{eff}=11000 K and any $\log g$ fit the continuum beautifully. Liebert & Stockman

measured V= $+0.058 \pm 0.11\%$. I measured $V_r = +0.079 \pm 0.029\%$ and $V_b = -0.002 \pm 0.037\%$. This star has an indeterminable field.

G 195-42=PG 0946+535=EG 251

This white dwarf has a continuous spectrum, except for the very weak C_2 absorption features. Greenstein (1969) classified this as DC with a possible 4670 Å feature (carbon). Wegner & Yackovich (1982) detected a weak C_2 (0,0) Swan Band in the spectrum (at $\sim$ 5165Å). Such a feature is not very obvious in Figure 2.17, but both the (0,0) and (1,0) features are there amongst the poor subtraction of the San Diego light contamination. I fit an atmosphere of helium, with a possible mix of hydrogen, of $T_{\rm eff}$=9500 K and any $\log g$. Landstreet & Angel (1971) measured a circular polarization of V= $+0.09 \pm 0.10\%$ and ABL calculated a magnetic field of $B_e = +310 \pm 340$ kG from this polarization. I measured a polarization of $V_r = +0.026 \pm 0.043\%$ and $V_b = +0.074 \pm 0.055\%$. This places this star in the indeterminable regime.

G 42-33=EG 252=LTT 12680

G 42-33 appears, to me, to be yet another true DC star. Greenstein (1969) and Eggen (1985) each type it as a DC star. Wegner & Yackovich (1982) claim a probable CH absorption near 4300 Å. My data are not very good in that wavelength range (see Figure 2.18), but I see no sign of a feature of the strength they report. I found an atmosphere of helium, with, perhaps, a slight mix of hydrogen, with $T_{\rm eff}\sim$ 7000 K and $\log g$=7.5±0.5 best matched the continuum. Landstreet & Angel (1971) measured V= $-0.02 \pm 0.11\%$ and later ABL calculated a magnetic field $B_e = -150 \pm 800$ kG from the measurement. I measured $V_r = -0.18 \pm 0.016\%$ and $V_b = -0.080 \pm 0.033\%$. This places the star in the indeterminable range.

G 43-54=LTT 12808=LHS 2273

This star has risen from its humble beginnings as a simple DC white dwarf (Hintzen & Strittmatter 1974; Wegner 1983) to the exciting membership in the class of magnetic white dwarfs (see Figure 2.19). As part of the survey described

in Bergeron, Ruiz, & Leggett (1992), they detected Zeeman split hydrogen lines in the star (unpublished). It is listed in Schmidt & Smith (1995) as having a magnetic field of $\sim$ 10 MG and a temperature of $\sim$ 6000 K. I found that either a hydrogen or hydrogen and helium mix atmosphere of $T_{\rm eff} \sim$ 7000 K and $\log g \sim$ 8.5 fit best. Using the method described in section 2.4.2.2, I measured a magnetic field of $B_e = -8.8^{+0.2}_{-1.8}$ MG. The σ-components of Hα, and less so of Hβ, show one sense of polarization for the wavelengths closest to π-component (the central component), and the opposite sense further away in wavelength. This implies either a viewing angle close to the magnetic equator and most probably a dipolar field offset towards the observer, or a quadrupolar field at any viewing angle (Martin & Wickramasinghe 1984).

GD 122=CSO 50=CBS 22

GD 122 was first classified as DC by Wickramasinghe et al. (1975). Later, Wegner (1983) detected HeI lines as well as Hβ, thus re-classifying it as DB. As can be seen in Figure 2.20, this is a DBA or DBAZ star (possible Ca II H & K lines). I found that a helium atmosphere of $T_{\rm eff}$=13000 K and any $\log g$ fit the continuum beautifully. Using the Low Range method on Hα, Hβ, Hγ and five He I lines, I measured a magnetic field of -5.3 ± 10.4 kG.

G 10-11=PG 1115-029=LFT 792=EG 78

This star was classified as DC by Eggen & Greenstein (1965) and reconfirmed as such by Wegner & Yackovich (1982) and GSL, as well as by Figure 2.21. An atmosphere of helium with $T_{\rm eff}$=10000 K and any $\log g$ fit best. Landstreet & Angel (1971) measured V= $+0.05 \pm 0.17\%$ and ABL calculated $B_e = +250 \pm 850$ kG from the measurement. The circular polarization I measured was $V_r = -0.021 \pm 0.020$ and $V_b = -0.015 \pm 0.031\%$. These measurements are consistent with zero polarization. Thus the magnetic field of the star is placed at indeterminable.

PG 1126+186

This star was classified as DC by GSL along with the comment "comp." As can be seen in Figure 2.22, this star is a composite of a DC and a cool star, probably G or K. The presence of an Hβ and an Hγ feature coupled with nearly non-existent Hα absortion feature implies some hydrogen emission in the stellar system. The white dwarf appears to be of type DC. An atmosphere of helium with T_{eff}>7000 K and any $\log g$ was an acceptable fit to the continuum, but this has little meaning since the spectrum is composite. A polarization of $V_r = +0.025 \pm 0.010\%$ and $V_b = +0.036 \pm 0.022\%$ was measured. Using the Low Range method on the Hα, Hβ, Hδ, Ca II H & K, and Na I lines gave a field of 6.5 ± 3.5 kG on the non-white dwarf star. The white dwarf field is indeterminable.

G 147-65=Gr 388

This star was first classified as DCpec by Hintzen & Strittmatter (1974), who commented "DC in blue, some structure in first order red." Greenstein (1976a&b) observed it with the spectrograph tuned more towards the red and classified it as dM+DC. Figure 2.23 clearly shows it to be a dM+DC. The M dwarf has hydrogen emission lines through at least Hθ. Probst (1983) typed the M star as dM6. I typed it as dM4.5e from a comparison to the spectra of Turnshek et al. (1985). Both determinations make assumptions about the spectrum of the white dwarf. I measured the circular polarization as $V_r = +0.002 \pm 0.012\%$ and $V_b = +0.177 \pm 0.081\%$, placing these two stars' magnetic fields at indeterminable.

G 237-28=Gr 353=LP 63-267

This star has had a few different tentative classifications. Hintzen & Strittmatter (1974) classified it as DFwk, Greenstein (1975) as DC, then DC-G (1976b) and later (1984) as DC9 with a helium atmosphere. Figure 2.24 clearly demonstrates the existence of the hydrogen in the form of the Balmer series. I found that a mixed atmosphere of hydrogen and helium fit best with T_{eff}=5500 K and

$\log g \sim 8.0$. ABL measured a circular polarization of V= $-0.007 \pm 0.108\%$ and calculated $B_e = -50 \pm 830$ kG. Using the Low Range method on Hα, Hβ, and Hγ, I measured a magnetic field of -3.6 ± 8.2 kG.

G 11-23=PG 1145+081=G 57-20

G 11-23 was classified DC6 by Green, Schmidt, & Liebert (1986). I agree with the classification, but add the note that there might be some C_2 present; see Figure 2.25. A helium atmosphere of $T_{\rm eff}$=11000 K and any $\log g$ fits the continuum well. I measured the circular polarization as $V_r = +0.146 \pm 0.064\%$ and $V_b = -0.085 \pm 0.075\%$. This places the object in the indeterminable regime.

LHS 2596=LP 171-40

This star is another DC (Liebert, Dahn, & Monet 1988) turned DA (see Figure 2.26). I found that a hydrogen atmosphere, with, perhaps, a little helium, of $T_{\rm eff}$=6500 K and $\log g$=8.0 fit the continuum best. Using the Low Range method on Hα, Hβ, Hγ, and Hδ, I measured a field of 0.3 ± 5.6 kG.

G 60-54=EG 95=LHS 2661

G 60-54 was classified as DC by Luyten (1952), Eggen & Greenstein (1965), and Greenstein (1976a). Wegner (1983) found very weak Hα and Hβ lines. Figure 2.27 shows the hydrogen lines as well as possible Na I and C_2. I found that a helium atmosphere of $T_{\rm eff}$=6000 K and $\log g$=7 fit the continuum well. Using the Low Range method on Hα and Hβ, I measured a magnetic field of 11.2 ± 18.0 kG. This is also a flux standard from Oke (1990).

G 256-7=LP 7-226=Gr 436=LP 8-46

G 256-7 is another white dwarf whose Zeeman split hydrogen lines were not detected in the early observations. Luyten (1965) gave it a spectral type of g. Giclas et al. (1971) gave it a color class 0. In 1974, Hintzen & Strittmatter called it a DG?. Greenstein et al. (1977) took a Multichannel Spectrograph spectrum and declared it DC. Greenstein (1984a) tacked on a temperature designation, calling it DC9. The observation shown in Figure 2.28 demonstrates that this star does have

hydrogen in its atmosphere and that a strong magnetic field is present. The H_α absorption feature is split into three components via the quadratic Zeeman effect and the two σ components show opposite senses of circular polarization. The observations reveal no Hβ nor higher Balmer transitions. A possible reason for this is the low temperature of the star ($T_{\rm eff}$=5000 K, $\log g$=8.0) being unable to excite hydrogen beyond Hα, or to excite enough hydrogen such that a magnetically split line is strong enough to be observed. An atmospheric mixture of hydrogen and helium or a high gravity (high mass) would also cause Hα to be far stronger than Hβ (Hammond et al. 1993; Liebert & Wehrse 1983), but those atmospheres do not fit as well as pure hydrogen.

This star has a magnetic field in the range 1 MG < B < 50 MG, thus the method described in section 2.4.2.2 was used to determine the effective magnetic field strength. This yielded a value of $B_e = +4.9 \pm 0.5$ MG. Only one observation of the object was taken, thus no information about rotation is known.

This object appears in Putney (1995).

PG 1312+099=PG 1312+098

PG 1312+099 was originally classified DCP by GSL. Schmidt (1987) lists a magnetic field of $B_s \sim 50$ MG on this star. He also noted that it was rotating. Schmidt & Norsworthy (1991) measured its rotation period through broadband flux and polarization variations. They fit an absorption profile due to a dipolar field of 10 MG to the star and they measured a rotation period of 5.43 hours. I took two observations of the object. Figure 2.29 shows the two observations. There is a very shallow Hα Zeeman triplet and a little more pronounced Hβ triplet, as well as Hγ. The rotation is most noticable in the polarization spectra. The observations are 23:13:41 hours apart, or 4.28 rotations. Both the pure helium and pure hydrogen models fit equally well, but neither were perfect, implying, perhaps, a mixed atmosphere of $T_{\rm eff}$=20000 K and $\log g \sim 9$. The shapes of the σ-components in flux, namely their very broad, washed-out shape, imply a dipole offset away from the observer. This means that there is a wide range of magnetic fields on the visible

surface, which makes it difficult to use the magnetic field determination method of Section 2.4.2.2, since the method assumes a single valued field on the star's observable hemisphere. This is clearly a poor approximation for PG 1312+099. However, this method was used and yielded a magnetic field of $+6.5 \pm 2.5$ MG for each observation. The large error bars reflect the problem mentioned. This measured value is consistent with the field determined by Schmidt & Norsworthy.

G 124-20=PG 1415-064

This star was given the spectral type DC by GSL (it should also be pointed out that they accidentally call it G 124-209, which does not exist in the Lowell Observatory lists). As can be seen in Figure 2.30, that classification is probably correct. There is a slim chance of a He I 5876 Å line amongst the San Diego sodium lamps, but the quality of these data are too poor to make definite statements about any absorption features. A helium atmosphere of 12000 K $<$ T_{eff} $<$ 13000 K and any $\log g$ fits the continuum. I measured $V_r = +0.377 \pm 0.169\%$ and $V_b = -0.162 \pm 0.158\%$. Due to the amount of noise in the data I would call these measurements close to null and I am placing the object in the indeterminable category. However, a cleaner observation is necessary to secure its position there.

LHS 378=LP 801-9

This star was first classified DC by Liebert et al. (1979), and retains its DC status. It is among the coolest of the stars in the survey. Figure 2.32 shows the flux and polarization spectra. A helium atmosphere of T_{eff}=5000 K and $\log g$=8.5 fit the continuum best. Ruiz et al. (1990) suggest that there might be some carbon in the atmosphere as well as helium. A circular polarization of $V_r = -0.044 \pm 0.042\%$ and $V_b = -0.884 \pm 0.051\%$ was measured. The red is consistent with a null polarization, and as can be seen from the data in Figure 2.31, the blue is much noiser (V(4500-5200Å)$=-0.272 \pm 0.001\%$). The observation was made in June 1993, when there was often a false continuum polarization; therefore, I must conclude that these data are consistent with a null polarization. This means that this object has an indeterminable magnetic field.

PG 1459+645

This is yet another true DC white dwarf. Figure 2.32 shows the flux and polarization data. A helium atmosphere with T_{eff}=11000 K and any $\log g$ best fit the data. Circular polarization measurements of $V_r = -0.283 \pm 0.025\%$ and $V_b = -0.365 \pm 0.001\%$ were taken. These data are not as consistent with zero as the V measurements for the other true DC stars (e.g., G 193-47, G 10-11, or LHS 378). This would imply that the magnetic field in this star is stronger than in those stars. However, one must remember that the data from June 1993 occasionally showed a false continuum polarization of up to 1%. Also, from the atmospheric continuum fit, this star is clearly a helium star, and it is unclear as to how the continuum polarization reacts to magnetic fields. This star is definitely in the indeterminable magnetic field range. It is possibly closer to the few hundred to one megagauss range than the other true DC white dwarfs observed in this survey. This object merits further observations to confirm or refute this claim.

Ton 246=PG 1539+255=GD 188

This object is a simple weak lined helium white dwarf. GSL classified this as DC5, and Figure 2.33 shows the existence of tiny He I lines. A helium atmosphere of T_{eff}=12000 K and any $\log g$ fit the continuum. Using the Low Range method on 4 He I lines, I measured a magnetic field of -6.5 ± 12.0 kG for this star.

GD 352=Gr 366

GD 352 was first classified as DC in 1975 by Greenstein. In 1977, Greenstein et al. noted that there might be some weak features present, which they could not identify. Wegner (1983) found some weak features which corresponded to the (0,0) and (1,0) Swan bands of C_2. Figure 2.34 does indeed reveal some weak features at the Swan bands. What appear to be features below 4400 Å are most likely due to problems in the CCD chip and are probably false. Neither helium nor hydrogen atmospheres fit the continuum well, but the star would appear to have $T_{eff}\sim$9000 K. I measured $V_r = -0.051 \pm 0.025\%$ and $V_b = -0.086 \pm 0.034\%$. I am placing this star in the indeterminable magnetic field range.

G 170-27

This is another true DC white dwarf. Figure 2.35 shows the data from the two observations. The only odd thing about the earlier classification of this star is its temperature determination. McCook & Sion list the star as DC5, which translates into $T_{eff}\sim$10000 K and Guseinov, Novruzova, & Rustamov list it as 6200 K. I found that 7500 K $< T_{eff} <$ 8000 K, $\log g$=9, and an atmosphere of helium, or helium plus hydrogen, fit best. The polarization measured was, on the second night (the data from the first night were too noisy to be of interest or value), $V_r = +0.088 \pm 0.038\%$ and $V_b = +0.008 \pm 0.066\%$. These are consistent with a null polarization. Therefore, I must conclude that the magnetic field is indeterminable.

PG 1747+451

PG 1747+451 is yet another DC white dwarf, although there is a hint of an Hα feature present. Figure 2.36 shows the flux and polarization spectra. A helium atmosphere of T_{eff}=9000 K and any $\log g$ best fit this object. Polarization measurements of $V_r = +0.164 \pm 0.025\%$ and $V_b = -0.032 \pm 0.001\%$ were taken. The change in sign from blue to red and the known problem with the June 1993 data imply that the polarization measurement of this object is consistent with the polarization being null. Thus I have yet another star with an indeterminable magnetic field.

G 183-35

G 183-35 is a white dwarf star of little acclaim and no pretension. Giclas et al. (1971) discovered it as part of their proper motion survey and gave it a color class of 0. Hintzen & Strittmatter (1974) classified it as DC, but noted there might be some Ca II present. Using a spectrograph with much higher resolution than Hintzen and Strittmatter, we were able to locate the Zeeman triplets for Hα and Hβ in the flux measurements (Putney 1994; see Figure 2.37). Both observations of this star are plotted in this figure. The 1994 data were taken through thin clouds, but this does not affect the circular polarization measurement. The 1993

data suffer from the problem caused by using a lens with the beam splitter, as described in Sec. 2.3. It is possible that this problem may be responsible for some of the -1% continuum polarization in G 183-35 in the 1993 data. The differences in the shapes of the lines in both flux and polarization between 1993 and 1994 suggest that there is rotation in this object. In particular, note the widths of the features in flux at Hα and in polarization at Hβ. Also notice the simple Hα circular polarization σ-components in the 1993 data, whereas they are not so clear in the 1994 data. More observations are needed to confirm this and even more are needed to accurately determine a rotation period. Chapter 3 discusses the rotation of this object in greater detail.

This is another star which I used the section 2.4.2.2 method on. From this technique, I determined an effective magnetic field magnitude of $|B_e| = 6.8 \pm 0.5$ MG. The error reflects the range of magnetic field strengths which fall within the observed line widths. The sense of the Hα σ-components in V/I shows that the magnetic field is positive (north), i.e., $B_e = +6.8 \pm 0.5$ MG.

This star appears in Putney (1995).

G 141-2=L 1208-132=Gr 579=LTT 15423/2

This star was originally classified as DC by Hintzen & Strittmatter (1974). Greenstein (1986) classifies it as DAH?9p and comments that Hα is very broad and shallow, which could be explained by a 3 MG field. Figure 2.38 shows the spectra, and there does not appear to be any splitting nor any polarized Zeeman σ-components. Bergeron (1995) says that one observation of G 141-2 suggests that it is an unresolved binary of a hot DA and a cool DC (it is overluminous). However, a subsequent observation had what appeared to be a split, asymmetric Hα. This star should be monitored in circular spectropolarimetry. It is possible that the star is rotating and has a magnetic field such that at certain phases of the rotation the Hα feature is split, and at other phases it is not.

A hydrogen atmosphere of $T_{\rm eff}$=6000 K and $\log g$=8.0 fit the continuum acceptably, although it is possible that the atmosphere contains some helium as

well. ABL measured V= $+0.015 \pm 0.068\%$ and calculated $B_e = +100 \pm 460$ kG. Using the Low Range method on Hα, I determined a field of 60.7 ± 87.2 kG on the star.

G 227-28=LP 103-294

G 227-28 is one of the coolest white dwarfs in the present survey. As can be seen in Figure 2.39, there are several absorption features, Hα and features at 4869 Å, 4966 Å, and 5183 Å, which I cannot identify. A helium atmosphere of $T_{\rm eff}$=5000 K and $\log g$=8.0 fit well, although a hydrogen atmosphere of $T_{\rm eff} \sim$ 4250 and $\log g$=9.0 cannot be discounted. Using the Low Range method on Hα, I measured a magnetic field of -5.3 ± 16.9 kG. The continuum polarizations is non-zero in the red camera. This is probably false since Hα revealed a weak field and the data were taken in June 1993 when instrumental polarizations of $< 1\%$ were encountered.

G 184-12

As Wegner (1983) pointed out, this star has definite Swan band absorption from the (0,0) and (1,0) bands (see Figure 2.40). Both pure hydrogen and pure helium models fit equally well at $T_{\rm eff}$=8000 K, with hydrogen at $\log g$=9.0 and any $\log g$ for helium. I measured $V_r = -0.323 \pm 0.044\%$ and $V_b = -0.475 \pm 0.001\%$. This places the star in the indeterminable category.

G 125-3=G 208-17=Gr 375

Hintzen & Strittmatter (1974) were the first among many to classify this star as a DC white dwarf. My observations also show that it is a true DC (see Figure 2.41). Neither a pure hydrogen nor a pure helium atmosphere fit this continuum. It is probably a mixture of the two near $T_{\rm eff}$=6500 K. ABL measured a polarization of V= $+0.02 \pm 0.03\%$ and from this calculated $B_e = +100 \pm 160$ kG. I measured a polarization of V_r(Jun93) = $+0.493 \pm 0.028\%$, V_b(Jun93) = $-0.062 \pm 0.001\%$, V_r(Sep94) = $+0.072 \pm 0.020\%$, and V_b(Sep94) = $+0.052 \pm 0.031\%$. These

data are consistent with a null polarization. This places the magnetic field at indeterminable.

LP 575-16

This is one last true DC white dwarf. Figure 2.42 shows the flux and polarization spectra. A helium atmosphere with T_{eff}=9000 K and $\log g$=8.0 are best suited to the data. Liebert & Stockman (1980) measured a polarization of V= $-0.054 \pm 0.07\%$. I measured a polarization of $V_r = +0.121 \pm 0.040\%$ and $V_b = -0.025 \pm 0.001\%$, which implies a null polarization. Thus the magnetic field is indeterminable.

G 187-8=LHS 3589

This is another very cool white dwarf. A hydrogen atmosphere around T_{eff}=4500 K was the best fit, although it wasn't a good fit. A helium atmosphere of about T_{eff}=5000 K also fit. The atmosphere is possibly a mixture of the two. As can be seen in Figure 2.43, an Hα feature is present. ABL measured V= $-0.04 \pm 0.05\%$ and calculated from this $B_e = -320 \pm 400$ kG. Using the Low Range method on Hα, I measured a magnetic field of -13.6 ± 13.7 kG.

G 233-19=Gr 379

G 233-19 has an Hα absorption feature, as can be seen in Figure 2.44. I found that an atmosphere of helium at T_{eff}=10000 K and any $\log g$ fit the continuum very well. Using the Low Range method on Hα, I measured a field of 8.6 ± 35.9 kG.

KUV 813-24=LB 1188=PG 2322+119

This star is a prime example of how a limited spectral range can give a false spectral classification. Wegner & McMahan (1985) observed Hα absorption, but not Hβ nor Hγ, thus classified it as em, assuming Hβ and Hγ were filled in by emission. GSL observed too far to the red and called it DC. Liebert, Wehrse, & Green (1987) looked a little more to the blue and noticed the huge calcium absorption features, as can also be seen in my Figure 2.45. Note as well the Hα,

Hβ, and Hγ features. I found that a helium atmosphere of T_{eff}=11000 K and any $\log g$ fit the continuum very well. Using the Low Range method on Hα, Hβ, and Ca II H & K, I measured a magnetic field of 3.0 ± 2.1 kG.

GD 248=Gr 335

GD 248 is nearly a true DC, but there does exist a weak Hα absorption feature (see Figure 2.46). This makes it very useful as a flux standard, and Oke (1990) includes in his list. Greenstein (1974) first classified it as a DC and later (1976) he mentioned the possibility of a weak Hα feature. What I do find curious about this star is the range of temperatures quoted for it. ABL claim T_{eff}=12000 K, and Guseinov, Novruzova, & Rustamov (1983) claim T_{eff}=8900 K. I found that a helium atmosphere of T_{eff}=10000 K and any $\log g$ fit best. ABL measured V= $0.00 \pm 0.04\%$ and calculated $B_e = 0 \pm 210$ kG. Using the Low Range method on Hα, I measured a field of -2.5 ± 33.3 kG.

2.5.3 Miscellaneous Objects

2.5.3.1 Stars

LP 413-12

As explained above, this is the star nearest the coordinates for the star listed as WD 0310+188 with a comparable magnitude. As can be seen from Figure 2.47, this is not a white dwarf. Luyten (1979) gave it a spectral class of m+. With the aid of *The Atlas of Digital Spectra of Cool Stars* (Turnshek et al. 1985), I have classified it as a dM3.

IRAS 04193+4959

Rwt 103 and IRAS 04193+4959 are $< 10''$ apart from one another. This caused some confusion and IRAS 04193+4959 object was observed instead of Rwt 103. It has proven to be quite interesting. Figure 2.48a shows a finding chart for the object. Rwt 103 is the star just southeast of IRAS 04193+4959. Figure 2.48b shows the flux and continuum spectrum. Several of the CN Q_1 band heads

are marked. There are no ZrO bands, thus it is some sort of carbon star, as opposed to an S star. I have tentatively classified it as an Extreme Carbon Star. It has a spectrum similar to GL 1403 (Trammell, Dinerstein, & Goodrich 1994), except that the IRAS source has no emission in the Balmer lines. Most ECS have emission in the Balmer series, although Cohen (1980) reports on the variable nature of emission in other elements. It is plausible that the Balmer lines could be variable as well. This may also be the wrong classification for the star. More observations need to be taken before final conclusions can be made. There appears to be circular polarization in the red camera at the wavelengths of some absorption features. It is not clear if these are real.

A comparison of the Palomar E-plate, taken in 1954, and the Palomar IR extension plate, taken in 1976, clearly shows that the WD has moved but the IRAS source has not. Thus it is highly doubtful that they are the two components of a binary system.

Putney 1

This is a star near LP 414-120. Figure 2.49a is a finding chart and the coordinates it was observed at are $(\alpha, \delta)_{1950} = (04^h10^m17^s, +18°53'30'')$. Figure 2.49b shows the observed spectra. I have classified this as a late G or early K, star, possibly a giant (comparisons made to Jacoby et al. 1984). The polarization does not appear to be null. The averages are $V_r = -0.418 \pm 0.026\%$ and $V_b = -1.185 \pm 0.123\%$.

Putney 2

This is an object near RWT 103. Its coordinates are $(\alpha, \delta)_{1950} = (04^h19^m25^s, +50°00'58'')$, and Figure 2.50a is a finding chart. The object marked is actually a double star (it is slightly elongated in the image) and the one observed is the northwest component of the two. This appears to be a late A or early F star (see Figure 2.50b), but this spectrum suffers from differential refraction which inhibits a determination of giant, dwarf, etc., or the possibility of identifying a DC companion. This star is very clearly and cleanly polarized at $V_r = +0.374 \pm$

0.004% and $V_b = +0.593 \pm 0.008\%$. The cause of this is unclear. A polarized DC companion is possible; however, one would expect the polarization to vary with wavelength. Another observation of this object is needed before a definite statement can be made.

Putney 3

This is a star near LB 8827, at $(\alpha, \delta)_{1950} = (08^h56^m22^s, +16°11'32'')$. Figure 2.51a has a finding chart. Figure 2.51b shows the spectra. I classified it as early K. It is unpolarized with $V_r = +0.055 \pm 0.016\%$ and $V_b = +0.087 \pm 0.037\%$.

Ton 1137=Gr 905=PG 0956+359=CBS 116

The stellar classification on this star varied for a while. Greenstein (1984a) calls it DC?1, GSL call it sdOB, Wagner et al. (1988) call it sdOC, and Paerels & Heise call it a DC2 and detect soft X-rays emanating from it. Figure 2.52 shows the star with all its He I and He II lines. This star is clearly a sub-dwarf rather than a white dwarf, due to the sharpness of the lines and the number of He II lines (they extend through the whole Balmer-like series). Using the classification description of GSL, I classify this as sdOC, since I find no trace of Balmer lines. Using the Low Range method on several He I and He II lines, I found a field of 4.8 ± 5.8 kG.

Putney 4

This star is a neighbor of Ton 246 at $(\alpha, \delta)_{1950} = (15^h39^m31^s, +25°33'00'')$. Figure 2.53a is a finding chart of the object. The flux and polarization spectra are in Figure 2.53b. Using the Turshek et al. atlas, I have classified it as M0 V. I measured a polarization of $V_r = +0.180 \pm 0.042\%$ and $V_b = +0.217 \pm 0.162\%$, during June 1993 when up to a 1% false polarization often appeared. This star is unpolarized, as expected.

Putney 5

This star is near G 183-35 at $(\alpha, \delta)_{1950} = (18^h14^m13^s, +24°53'19'')$. Figure 2.54a is a finding chart of the object. This star is very similar to Putney 4, as can

be seen from Figure 2.54b. I have also classified this one as M0 V. I measured a polarization of $V_r = +0.009 \pm 0.025\%$ and $V_b = +0.109 \pm 0.162\%$, making this star also unpolarized, as expected.

2.5.3.2 BL Lac Objects

Two objects were thought to be DC white dwarfs and made part of the present survey. Flemming et al. (1993) have identified them as the optical counterparts to two X-ray sources. They took further observations, including optical linear polarimetry, and determined that they are BL Lac objects. The circular polarizations measurements taken may not have been done in vain. If the BL Lac had a large magnetic field, 10 to 100 kG (Valtaoja et al. 1993), a continuum circular polarization could be produced. Valtaoja et al. publish a 2σ result of 0.2% polarization measured in the BL Lac objects 0422+004 and 0735+178. Valtaoja et al. took broadband measurements of the circular and linear polarization in the two objects. The circular polarization measurements switch sign with increasing wavelength, twice in one observation, and get up as high as 1.9% for one measurement. This is inconsistent with any mechanisms known to produce continuum circular polarization. These data are consistent with noise. Valtaoja et al. do point out, however, that a 2σ result is not generally considered significant.

PG 1246+586=LB 2449

This object was the optical counterpart of a ROSAT X-ray source, and Flemming et al. found it to be a BL Lac. No optical absorption features are observed (see Fig. 55). I measured circular polarization of $V_r = +0.057 \pm 0.017\%$ and $V_b = +0.030 \pm 0.039\%$. These values are consistent with a null polarization measurement.

PG 1424+240

Flemming et al. identified this as a BL Lac. They also note that it is positionally coincident with a previously discovered BL Lac (Wilkes et al. 1983; Impey & Tapia 1988). Figure 2.56 shows the flux and circular polarization. I measured

$V_r = +0.225 \pm 0.016\%$ and $V_b = -0.098 \pm 0.001\%$. This was taken while the lens was attached to the beam splitter, thus polarization may have been introduced artificially. The change in sign from one camera to the next is a good indicator of the noise in the system, implying that the polarization is most probably less than 0.1%. Using the criteria used for the white dwarfs in this survey, I would call this object a null circular polarization object.

2.5.4 Star Expected to Show Polarization

GD 90=Gr 348=CBS 71=KUV 0816+3741

Angel et al. (1974) had observed this object and thought its spectrum to be very odd. Follow up observations in spectropolarimetry revealed its magnetic nature. Wickramasinghe & Martin (1979) calculated atmospheric models to match this star. They found a 9 MG dipole off-set 0.1 radii away from the observer and a pole-on view fit best. A broadband average of the circular polarization measured during the course of this survey is $V_r = +0.031 \pm 0.028\%$ and $V_b = +0.087 \pm 0.037\%$. This is a clear case where the opposite polarization senses of the two σ-components completely cancel one another and the continuum polarization averages to zero. Figure 2.57 show the flux and polarization spectra. Both the flux and polarization spectra clearly demonstrate how, at a given magnetic field strength, the higher Balmer lines are more spread out and become intertwined with one another. The polarization spectrum clearly demonstrates the response of the Zeeman σ-components to magnetic field strength and direction. Hα clearly shows a reversal in magnetic field direction through the reversal of polarization sign within each σ-component (referred to as "mixing" in Chapter 3). Using the method of Section 2.4.2.2, I measured a magnetic field of $+5.5^{+2.7}_{-0.7}$ MG. This is a factor of about 2 different from the published value, due to this measurement being a disc averaged value and the published value being the dipolar field strength. I fit an atmosphere of hydrogen with $T_{\rm eff}$=14000 K and any $\log g$.

LB 8827=Gr 904=PG 0853+164

GSL classified this star as DBp2, implying a peculiar spectrum. McCook & Sion list this as DB3/DBP2, leading me to believe that a circular polarization measurement had been taken. No one had measured a field in it before. Figure 2.58 shows the flux and polarization measurements. In the flux, the absorption features are slightly widened with the splitting almost apparent in the He I 5876Å line. A Zeeman signature is apparent for several He I lines. Using the method of section 2.4.2.2, I measured a magnetic field of -1.0 ± 0.5 MG. This is the first helium white dwarf with a measured magnetic field (Feige 7 contains both helium and hydrogen). I find a helium atmosphere with $T_{\rm eff} \sim$20,000 K and $\log g \sim$ 8.5.

PG 1658+441

This star was classified as a DAP2 by GSL. Higher resolution spectra, broadband circular polarization, and circular spectropolarimetric observations were taken by Liebert et al. (1983). They found no broadband polarization, but the flux and circular polarization spectra clearly showed the effects of Zeeman splitting. They find magnetic field strengths of $B_e = 0.7$ MG and $B_s = 2.3$ MG (B_s is mean surface field) and a hydrogen atmosphere of 30,000 K. Figure 2.59 shows my observed flux and polarization spectra. My analysis concludes that this star has $T_{\rm eff}$=30,000 K, $\log g$=7.5, an atmosphere of hydrogen, and a magnetic field of $+2.5^{-1.5}_{+2.0}$ MG.

2.5.5 Stars Expected to Have Null Circular Polarization

G 191B2B=EG 247

This is a well studied star. It is a flux standard for the Hubble Space Telescope (Oke 1990). It has weak hydrogen lines that do not appear to be Zeeman split; therefore, it should have no continuum polarization and work well as a null circular polarization object. Landstreet & Angel (1971) measured its circular polarization as V= $+0.023 \pm 0.037\%$. I measured it as $V_r = -0.016 \pm 0.011\%$ and $V_b =$

$+0.062 \pm 0.010\%$ (see Figure 2.60). Using the Low Range method on Hα, Hβ, Hγ, and Hδ, I measured a magnetic field of 8.4 ± 3.7 kG.

SAO 59965=BD +33° 1501=HD 56355

This A0 star (Cannon & Pickering 1919) was observed to check how accurately a null polarization can be measured at short exposures and how well the measurement can be repeated. Figure 2.61 shows the two exposures (of different exposure times, see Table 2.4). For the longer exposure I measured $V_r = -0.073 \pm 0.008\%$ and $V_b = -0.151 \pm 0.012\%$. The second and shorter exposure gave $V_r = -0.035 \pm 0.010\%$ and $V_b = +0.021 \pm 0.014\%$. These are both consistent with null. As a test of the effectiveness of the Low Range method, I measured a magnetic field from Hα, Hβ, Hγ, and Na I for the first observation of the object. The value I measured was 0.9 ± 0.7 kG.

SAO 61549=BD +32° 1893=HD 82354

This K0 star (Cannon & Pickering) was observed through clouds, as is evident in Figure 2.62. It was expected to be null and it is, especially given the weather conditions under which it was observed. I measured $V_r = +0.130 \pm 0.081\%$ and $V_b = -0.500 \pm 0.417\%$.

G 138-31=Gr 327

This is another of Oke's standards, which I expected to have a null polarization. ABL measured it as V= $+0.093 \pm 0.11\%$ and calculated $B_e = +460 \pm 540$ kG. I measured $V_r = +0.024 \pm 0.032\%$ and $V_b = +0.149 \pm 0.063\%$. It can be viewed in Figure 2.63. A hydrogen atmosphere of $T_{\rm eff}$=7000 K and $\log g$=9.0 best fit the data. Using the Low Range method on Hα, Hβ, Hγ, Hδ, and Hϵ, I measured a magnetic field of 0.1 ± 4.2 kG.

G 24-9=LHS 3532=LTT 15921=EG 138

This white dwarf is also a standard star and of type DC. It was not included in the survey due to its being listed in McCook & Sion as a binary (from Greenstein 1984a). Its spectra are in Figure 2.64. The circular polarization has a high

frequency ripple in it due to the lens attached to the beam splitter. (This is the worst case ever seen of the variable problem mentioned in Sec. 2.3. The neighboring observations did not suffer from this.) ABL measured V= $-0.12 \pm 0.09\%$ and calculated $B_e = -550 \pm 410$ kG. I measured $V_r = -0.143 \pm 0.032\%$ and $V_b = -0.128 \pm 0.001\%$. An atmosphere of either hydrogen or helium or a mix of $T_{\rm eff} \sim 7000$ K and $\log g \sim 8.5$ fit the continuum. Due to the problem in this observation, it is hard to determine the magnetic field. The lack of features and $< 2\%$ circular polarization lead me to believe that this should be placed in the indeterminable category. The circular polarization on this star should be re-measured.

2.6 Discussion

2.6.1 Number of Magnetic White Dwarf Stars

In the end, the survey consisted of 46 white dwarf stars. Broken down into primary spectral types, the classifications consist of 18 DA, 3 DB, 3 DQ, 1 DZ, and 21 DC stars. Broken down into magnetic field ranges, they are 1 with B > 100 MG, 5 with 1 MG < B < 50 MG, 7 with 10 kG < B < 1 MG, 10 with B < 10 kG, and 23 with indeterminable fields. Table 2.7 shows the break down per spectral type per magnetic field range. One of the stars in the 10 kG to 1 MG range has a 3 σ detection, G 234-4 with B = $+39.6 \pm 11.6$ kG, and will be singled out from the rest, which appear to be upper limits.

Raw statistics show that 13% of the stars classified as DC before 1987 have magnetic fields above 1 MG and additional 2% (=G 234-4) have definite fields above 30 kG. This totals to 15% above 30 kG. Schmidt & Smith (1995;SS) observed 169 DA stars from the McCook & Sion list and found 4 with detectable fields above 30 kG, translating into 2%. This is a huge discrepancy. Does this imply that the DC and DA stars, classified previous to 1987, are somehow fundamentally different? Before doing too much speculation, the two samples need to be investigated more fully.

Both samples were drawn entirely from the McCook & Sion catalog, but the selection criteria were a little different, besides the obvious DC versus DA. SS take stars with $\delta > -30°$. If I had used this criterion, I would have added two stars to my sample. If SS had stopped at $\delta > -20°$, they would have lost 7 stars, none of which turned out to be magnetic. SS take stars with $m_v \leq 15.0$ magnitudes. Had I done this, I would be left with 3 stars. I have not ventured to count the number of DA stars between magnitude 15 and 16.5, but it is surely far larger that 169. In general, the SS sample stars are hotter than my stars, and therefore are more luminous, which, in turn, implies that they covered a larger volume of space. There is no reason to suppose that more of the nearby stars have measurable magnetic fields than those a little further out. The SS survey is biased against the higher fields, since a hot DA with a field greater than about 10 MG is easily detected in flux through its Zeeman split Balmer lines, thus would be classified as DAP or DAH, and therefore would not have been included in the SS survey. Perhaps a more proper comparison between the two surveys are all those stars with fields between 30 kG and 1 MG. Then the comparison is 3/168=2% to 1/40=3%. These values are effectively the same; therefore, both surveys yielded the same conclusion for magnetic fields between 30 kG and 1 MG.

The problem can also be looked at from another angle. The DC sample is biased towards cool, high magnetic field stars just as the DA sample is biased against hot, high field objects. The nature of a large magnetic field is to spread out the absorption features. The combination of these magnetically widened features with weak features caused by low temperatures (< 10000 K) causes these sorts of objects to be classified as DC. So, a more proper comparison of the two samples might be made by adding the high field white dwarfs into the count. SS lists all the known high field white dwarfs. Of these 40 stars, 3, possibly 4, fit the SS criteria of being a DA star in the McCook & Sion catalog with $\delta > -30°$, and $m_v \leq 15.0$. These are G 99-47, Grw+70°8247, PG 1031+234, and possibly PG 1658+441 ($m_v = 15.02$). This brings their total to 8/173=5%. Using my criteria on the list of 40 stars adds an additional 4 stars: GD 356, G 195-19,

PG 1015+014, and G 227-35. (This star is listed as DXP; however, the X did not come from observed flux features, but rather from an assumption of their existence deduced from the shape of the circular polarization continuum.) This brings my numbers up to 11/51=22%, which is an even larger discrepancy than before. This implies that a DC star is more likely to have a strong magnetic field than a DA star.

This brings up the question of selection effects. Many of the stars in my survey would have been classified differently from DC, had higher resolution spectrographs been used in the 1960's and 70's and had the classification surveys been searching for Hα lines, the major He I lines, and Ca II lines exclusively. If all the objects with distinct features were removed from my survey, I would be left with 21 objects (those classified as DC for the primary designation in Table 2.5). One of these objects has a magnetic field – G111-49. This brings my percentage of DC stars with measurable magnetic fields to 5%, which is approximately the value for SS's DA stars. Thus it would seem that there is not a glut of magnetic stars among the DC stars.

It is very hard to say how significant all these numbers are, since it is all in the realm of small number statistics. The two surveys combined add up to 215 stars and 11 of these have magnetic fields above 30 kG. This is 5% of about 20% (215/1151) of the isolated white dwarfs listed in the McCook & Sion catalog. If I were to assume that all of the isolated white dwarfs with magnetic fields greater than 1 MG in the McCook & Sion list have been found, then there are 31/1151=3%. However, this assumption cannot be made. Most of the McCook & Sion stars have not been surveyed (nearly 80%), mainly because they are too faint. So an estimate of the value is made here. The present survey observed 48 of the 117 listed isolated DC stars in the catalog (two turned out not to be white dwarfs), if the other listed DC stars have the same 13% detection rate, then another 9 stars should be added to the count, except that 3 of the 31 stars with fields known to be $>$ 1 MG are DC, so I add only 6. If the SS survey is representative of the DA sample, then a further 20 should be added, but subtract

the 10 DAs that are already known. The DB, DQ, DZ, and DO stars have not been surveyed systematically. There are 96 isolated DBs, 22 DQs, 20 DZ, and 19 DOs. Two DQ stars and two DBs are known to be magnetic and are in the 31 stars mentioned above. This brings the number of isolated white dwarf stars with magnetic fields greater 1 MG up to (31+6+10-2-2)/(1151-96-22-20-19) = 43/994 = 4%.

All this is saying is that a very small fraction of isolated white dwarf stars actually have magnetic fields above a megagauss. Further, an even smaller fraction appear to have fields between 30 kG and 1 MG. This is the more interesting point. Magnetic field strengths do not appear to be evenly distributed amongst the white dwarf population, i.e., there is a bimodal distribution of magnetic field strengths with one peak above a megagauss and the other below a kilogauss.

2.6.2 Magnetic Field Distributions

2.6.2.1 Numbers of Stars

The number of white dwarf stars with measured magnetic fields has increased drastically over the past few years. Angel (1978) lists 12 isolated magnetic white dwarfs, Landstreet (1992) lists 26, Chanmugam (1992) lists 27, and this year, SS lists 42. I have added 3 more to the list (G 111-49, G 256-7, and LB 8827; G 183-35 was placed on the SS list from Putney 1994). Figure 2.65 shows the distribution of stars per decade of magnetic field (this figure contains all stars in the MWD list in SS, in addition to the 3 MWDs I discovered). The present survey and that of SS attempted to measure the magnetic field on 206 other white dwarfs and they are included in the graph with the appropriate magnetic field strength. Keep in mind that the magnetic fields of these 206 stars are probably upper limits. From this plot, it would appear that magnetic field strengths are bimodal in white dwarfs, as mentioned above. Main sequence stars are also apparently bimodal in magnetic field strength. The magnetic Ap stars have fields of about 10^4 G and the rest of the

main sequence stars have fields $< 10^2$ G (Landstreet 1992).[3] Thus the bimodal nature of white dwarf magnetic field distribution is consistent with the present evolution theories (see Section 2.7).

There is the possibility that the bimodal distribution of Figure 2.65 is false. Perhaps there is a large peak around 0 G (or some such low value) and distribution tails off smoothly to B > 1000 MG. This would require many more stars to have magnetic fields between 10 kG and 10 MG. Assuming that the sample of stars in the present survey and the survey of SS are representative of all white dwarfs, and there is no reason to think otherwise, this is not possible. Another possibility is that there is one peak in the 10 to 100 MG range and a long tail, either decreasing or constant, down to zero. This cannot be disproven with the present techniques of determining magnetic field strengths in white dwarfs. Neither case disproves the theory of magnetic white dwarfs descending from magnetic Ap stars since the actual magnetic field distribution in main sequence stars is unknown.

2.6.2.2 Temperature of Stars

If the fields on magnetic white dwarf stars are indeed fossil fields, they should decay over time (see Chapter 1). However, Mestel (1952) calculated that the decay time is equal to the observable lifetime of a white dwarf. Figure 2.66 shows the distribution of magnetic field as a function of temperature for all known MWDs. There does appear to be more cooler stars, T < 13000 K, with measurable fields than the hotter stars, but this is expected if there are more cooler stars than hotter stars. A hot white dwarf cools faster than a cool white dwarf cools, i.e., the amount of time it takes a white dwarf to cool from T to T/2 is more than twice as long as it took to cool from 2 T to T (see equations 1.10 and 1.11 and D'Antona & Mazzitelli 1990), therefore there should be more cool white dwarfs than hot white dwarfs.

[3] Many G and later type stars have magnetic fields of similar strength to the Ap stars; however, the G and later type stars' magnetic fields are surface fields powered by dynamos (Landstreet 1992), which require convection. Convection ceases before the white dwarf phase (see Chapter 1).

This is, in fact, true (see, e.g., Wood 1992). There is something striking about the figure – there is a huge spike in magnetic field strength between 14000 K and 16000 K. This sudden increase coincidentally, or not, occurs just prior to the start of the ZZ Ceti instability strip (marked on figure), where oscillations due to convection occurs in many white dwarf stars (see, e.g., Kepler & Nelan 1993). Perhaps a dynamo of some form starts up at this temperature and introduces a magnetic field. Then, perhaps, once the star leaves the instability strip, the dynamo ceases and the new found field decays. Figure 2.66 backs up this idea by suggesting two populations, one of stars with magnetic fields of < 50 MG covering all temperature ranges and a second population of stars with magnetic field strengths > 50 MG and temperatures $\lesssim 16000$ K. The second population contains the stars which have a strong increase in magnetic field strength at about 16000 K and then a decay in field strength over time. I should point out that a solar-type dynamo could not produce a magnetic field of the strengths in the spike (Markiel, Thomas, & Van Horn 1994).

As I have mentioned repeatedly, the field of magnetic white dwarf stars works in the regime of small number statistics, so perhaps this spike is not significant. Figure 2.67 shows the numbers of white dwarfs observed in magnetic field searchs per temperature designation ($= \theta = 50400/\mathrm{T}$). The spike occurs at the temperature with the second most observed stars ($\theta = 3$), and the apparent lack of very high magnetic field white dwarfs also has a very large sample base ($\theta = 2$ and 3). Thus this spike is quite probably significant.

2.7 Conclusions

2.7.1 Individual Objects

Five new isolated magnetic white dwarf stars (B $>$ 30 kG) were discovered during the course of this survey, G 111-49, G 183-35, G 256-7, G 234-4, and LB 8827, bringing the total number of known magnetic white dwarfs to 46. Three stars were found to rotate, G 158-45(=LHS 1044), LHS 1734, and G 183-35 (see

Chapter 3 for more details), bringing the number of known rotating magnetic white dwarfs to 16 (out of 21 monitored stars). Four stars, LHS 1415, G 124-20, PG 1459+645, and G 24-9, need to be re-observed to clarify their position. Just as importantly, 40 white dwarfs were found to have fields below 30 kG or to have indeterminable, but < 20 MG, fields. This brings the number of isolated magnetic white dwarf stars systematically searched for magnetic fields above 30 kG to 218.

2.7.2 The Survey as a Whole

Of the stars classified as DC previous to 1987, 22 % have magnetic fields above 30 kG. This appears to be much higher than the 5% of DA stars; however, the number of DC stars is artificially enlarged by the low resolution classification surveys of the 1960's and 70's.

The present theory on the origin of the magnetic field for a white dwarf is that it is a fossil field. This means that the magnetic flux the star had on the main sequence and later is retained. Some Ap and Bp stars have measured magnetic fields on the order of 10^4 G. No F stars have been found with a magnetic field. Many G and later type stars have dynamos which produce surface fields of B$< 10^3$ G; however, these are driven by convection, which has stopped before the star becomes a white dwarf. Thus one would expect white dwarfs, in general, to have a very small field, but a number of white dwarfs, proportional to the number of Ap and Bp stars, should have a large field. Thus far, all data are consistent with this theory. With the possible exception of some form of dynamo (Section 2.6.2.2), there is no known way to create a magnetic field in a white dwarf star. Additionally, there does not appear to be a smooth distribution of magnetic field strengths of white dwarfs. A smooth distribution, e.g., a gaussian around a low magnetic field, might be expected if the fields were not fossil fields. The apparent binomial nature of the white dwarf magnetic field distribution curve is similar to the distribution of magnetic fields in main sequence stars, once again re-affirming the theory of fossil fields.

The observations in this chapter were taken in collaboration with M.H. Cohen, R.W. Goodrich, P.M. Ogle, and H.D. Tran. I wish to thank M.H. Cohen for comments on the manuscript. I wish to thank P.M. Goldreich and Y. Wu for discussions about magnetic field distributions. This research has made extensive use of the Simbad database, operated at CDS, Strasbourg, France. I also wish to thank D. Kirkpatrick, S.R. Trammel, V.V. Smith, P.J. Green, and M. Jura for aiding me in the classification of IRAS 04193+4959.

References

Achilleos, N., Wickramasinghe, D.T., Liebert, J., Saffer, R.A., & Grauer, A.D. 1992, ApJ, 396, 273

Angel, J.R.P. 1978, ARAA, 16, 847

Angel, J.R.P., Borra, E.F., & Landstreet, J.D. 1981, ApJS, 45, 475 (ABL)

Angel, J.R.P., Carswell, R.F., Strittmatter, P.A., Beaver, E.A., & Harms, B. 1974, ApJ, 194, L47

Angel, J.R.P. & Landstreet, J.D. 1974, ApJ 191, 457

Angel, J.R.P., Liebert, J., & Stockman, H.S. 1985, ApJ, 292, 260

Angel, J.R.P., McGraw, J.T., & Stockman, H.S. 1973, ApJ, 184, L79

Beckers, J.M. 1969, A Table of Zeeman Multiplets (Bedford, MA: Office of Aerospace Research, U.S. Air Force), AFCRL-69-0115

Bergeron, P. 1995, private communication

Bergeron, P., Ruiz, M.-T., & Leggett, S.K. 1992, ApJ, 400, 315

Bergeron, P., Saumon, D., & Wesemael, F. 1995, ApJ, 443, 764

Cannon, A.J. & Pickering, E.C. 1919, The Henry Draper Catalogue (Cambridge: Harvard Observatory)

Chanmugam, G. 1992, ARAA, 30, 143

Cohen, M. 1980, ApJ, 238, L81

Cohen, M.H., Putney, A., & Goodrich, R.W. 1993, ApJ, 405, L67

D'Antona, F. & Mazzitelli, I. 1990, ARAA, 28, 139

Eggen, O.J. 1985, PASP, 97, 1029

Eggen, O.J. & Greenstein, J.L. 1965, ApJ, 142, 925

——— 1967, ApJ, 150, 927

Fleming, T.A., Green, R.F., Jannuzi, B.T., Liebert, J., Smith, P.S., & Fink, H. 1993, AJ, 106, 1729

Goodrich, R.W. 1991, PASP,103, 670

Goodrich, R.W., Cohen, M.H., & Putney, A. 1995, PASP, 107, 179

Giclas, H.L., Burnham, Jr., & Thomas, N.G. 1971, *Lowell Proper Motion Survey, Northern Hemisphere* (Flagstaff: Lowell Observatory)

Green, R.F., Schmidt, M., & Liebert, J. 1986, ApJS, 61, 305 (GSL)

Greenstein, J.L. 1969, ApJ, 158, 281

——— 1974, ApJ, 189, L131

——— 1975, ApJ, 196, L117

——— 1976a, AJ, 81,323

——— 1976b, ApJ, 210,524

——— 1979, ApJ, 227, 244

——— 1984a, ApJ, 276, 602

——— 1984b, ApJ, 281, L47

——— 1986, ApJ, 304, 334

Greenstein, J.L., Henry, R.J.W., & O'Connell, R.F. 1985, ApJ, 289, L25

Greenstein, J.L. & Mc Carthy, J.K. 1985, ApJ, 289, 732

Greenstein, J.L., Oke, J.B., Richstone, D., Van Altena, W.F., & Steppe, H. 1977, ApJ, 218, L21

Guseinov, O.H., Novruzova, H.I., & Rustamov, Yu.S. 1983, Ap&SS, 97, 305

Hammond, G.L., Sion, E.M., Aannestad, P.A., and Kenyon, S.J. 1993, in White Dwarfs: Advances in Observation and Theory, ed. M.A. Barstow (Dordrecht: Kluwer Academic Publishers), 253

Henry, R.J.W. & O'Connell, R.F. 1984, ApJ, 282, L97

———— 1985, PASP, 97, 333

Hintzen, P. & Jensen, E. 1979, PASP, 91, 492

Hintzen, P. & Strittmatter, P.A. 1974, ApJ, 193, L111

Impey, C.D. & Tapia, S. 1988, ApJ, 333, 666

Kemic, S.B. 1974, JILA report #113

Kemp, J.C. 1970, ApJ, 162, 169

Kemp, J.C., Swedlund, J.B., Landstreet, J.D., and Angel, J.R.P. 1970, ApJ 161, L77

Kepler, S.O. & Nelan, E.P. 1993, AJ, 105, 608

Lamb, F.K. & Sutherland, P.G. 1974, in Physics of Dense Matter, ed. C.J. Hansen (Boston: Reidel), 265

Landstreet, J.D. 1992, A&AR, 4, 35

Landstreet, J.D. & Angel, J.R.P. 1971, ApJ, 165, L67

Liebert, J., Angel, J.R.P., & Landstreet, J.D. 1975, ApJ, 202, L139

Liebert, J., Dahn, C.C., Gresham, M., & Strittmatter, P.A. 1979, ApJ, 233, 226

Liebert, J., Dahn, C.C., & Monet, D.G. 1988, ApJ, 332, 891

Liebert, J., Schmidt, G.D., Green, R.F., Stockman, H.S., & McGraw, J.T. 1983, ApJ, 264, 262

Liebert, J. & Stockman, H.S. 1980, PASP, 92, 657

Liebert, J. & Strittmatter, P.A. 1977, ApJ, 217, L59

Liebert, J. & Wehrse, R., 1983, A&A, 122, 297

Liebert, J., Wehrse, R., & Green, R.F. 1987, A&A, 175, 173

Luyten, W.J. 1950, ApJ, 112, 212

—— 1979, *NLTT Catalogue* Vol. 2, (Minneapolis: University of Minnesota)

Luyten, W.J. & Anderson, J.H. 1965, *Proper Motion Survey with the Forty-Eight Inch Schmidt Telescope. IV. Five North Polar Regions* (Minneapolis: The Observatory of the University of Minnesota)

Markiel, J.A., Thomas, J.H., & Van Horn, H.M. 1994, ApJ, 430, 834

Martin, B. & Wickramasinghe, D.T. 1984, MNRAS, 206, 407

——— 1986, ApJ, 301, 177

McCook, G.P. & Sion, E.M. 1987, ApJSup, 65, 603

Merani, N., Main, J., & Wunner, G. 1995, A&A, 298, 193

Mestel, L. 1952, MNRAS, 112, 583

Minkowski, R. 1938, Ann Rep Dir Mt Wilson Obs, p. 28

Oke, J.B. 1990, AJ, 99, 1621

Oke, J.B., Cohen, J.G., Carr, M., Cromer, J., Dingizian, A., Harris, F.H., Labreque, S., Lucinio, R., Schaal, W., Epps, H., & Miller, J. 1995, PASP, 107, 375

Oke, J.B. and Gunn, J.E. 1982, PASP, 94, 586

Paerels, F.B.S. & Heise, J. 1989, ApJ, 339, 1000

Probst, R.G. 1983, ApJS, 53, 335

Putney, A. 1994, BAAS, 24, 1128

Putney, A. 1995, ApJ, 451, L67

Putney, A. & Jordan, S. 1995, ApJ, 449, 863

Ruder, H., Wunner, G., Herold, H., & Geyer, F. 1994, Atoms in Strong Magnetic Fields (Berlin: Springer-Verlag)

Ruiz, M.T., Anguita, C., Maza, J., & Roth, M. 1990, AJ, 100, 1270

Schmidt, G.D. 1987, Mem.Soc.Astron.Ital., 58, 77

Schmidt, G.D., Bergeron, P., & Fegley, B. 1995, ApJ, 443, 274

Schmidt, G.D., Latter, W.B., & Foltz, C.B. 1990, ApJ 350, 758

Schmidt, G.D. & Norsworthy, J.E. 1991, ApJ, 366, 270

Schmidt, G.D. & Smith, P.S. 1995, ApJ, 448, 305 (SS)

Sion, E.M., Fragola, J.L., & O'Donnell, W.C. 1979, PASP, 91, 460

Sion, E.M., Greenstein, J.L., Landstreet, J.D., Liebert, J., Shipman, H.L., & Wegner, G.A. 1983, ApJ, 269, 253

Sion, E.M., Kenyon, S.J., & Aannestad, P.A. 1990, ApJS, 72, 707

Trammell, S.R., Dinerstein, H.L., & Goodrich, R.W. 1994, AJ, 108, 984

Turnshek, D.E., Turnshek, D.A., Craine, E.R., Boeshaar, P.C. 1985, An Atlas of Digital Spectra of Cool Stars (Tucson: Western Research Company)

Valtaoja, L., Karttunen, H., Valtaoja, E., Shakhovskoy, N.M., & Efimov, Yu.S. 1993, A&A, 273, 393

Wagnerm R.M., Sion, E.M., Liebert, J. & Starrfield, S.G. 1988, ApJ, 328, 213

Wegner, G. 1983, AJ, 88, 1034

Wegner, G. & McMahan, R.K. 1985, AJ, 90, 1511

Wegner, G. & Yackovich, F.H. 1982, AJ, 87, 155

——— 1984, ApJ, 284, 257

Wegner, G., Yackovich, F.H., Green, R.F., Liebert, J., & Stocke, J.T. 1985, PASP, 97, 575

Wickramasinghe, D.T., Hintzen, P., Strittmatter, P.A., & Burbidge, E.M. 1975, ApJ, 202, 191

Wickramasinghe, D.T. & Martin, B. 1979, MNRAS 188, 165

Wilkes, B.J., Wright, A.E., Jauncey, D.L., & Peterson, B.A. 1983, PAS Australia, 5, 2

Wood, M.A. 1992, ApJ, 386, 539

Wunner, G., Rösner, W., Herold, H., & Ruder, H. 1985, A&A, 149, 102

Table 2.1 Initial 52 DC survey Objects

Name	RA (1950)	DEC	Spectral Type	Other Names	m_v
G 158-45	00 11 41	−13 27.3	DC8	LP704-1,LHS1044 PHL6421	15.8
G 171-52	00 19 36	+42 20.2	DC9	Gr459	16.44
PG 0156+156	01 56 56	+15 34 16	DC6		15.8
G 272-152	02 03 01	−18 07.8	DC		16.0
PG 0210+168	02 10 10	+16 49 57	DC		14.47[b]
LHS 1415	02 30 15	−14 24.5	DC,DF?	Gr471,LP710-47	15.76
WD 0310+188	03 10 18	+18 53.0	DC		16.5
G 7-16	03 57 46	+08 06.6	DC9	LHS1617	15.9
LP 414-120	04 10 18	+18 53.0	DC	HG7-126,LB228	16.5
RWT 103	04 19 24	+50 01.0	DC5	Gr523	16.2
G 83-10	04 23 07	+12 05.2	DC8	LB1320,EG169 LP475-70,VA377[a],HAN372[a]	15.7
LHS 1734	05 03 39	−17 27.3	DZ9?,DC9?	LP777-1	15.97
G 108-42	06 54 46	+02 45.1	DC5	EG181	16.2
G 234-4	07 28 49	+64 16 06	DC9	LP58-247,Gr321 GJ1098	16.38
G 193-74	07 49 37	+52 37.4	DC7	Gr344	15.68
G 193-78	07 51 55	+57 50.2	DC5	Gr322	15.1
G 111-49	07 56 32	+43 43.4	DC?6	Gr428	16.28
LB 3013	09 13 20	+10 23.7	DC6	LP487-21,PG	15.77
TON 1061	09 24 46	+19 56.8	DC	PG	16.1
G 195-42	09 46 55	+53 29.2	DQ6,DC6	PG,EG251	15.3
TON 1137	09 56 58	+33 54 24	DC?1	Gr905,PG CBS116	15.26
G 42-33	09 59 08	+14 55.9	DC7	EG252,LTT12680	15.4
G 43-54	10 26 39	+11 42.9	DC8	LTT12808,LHS2273	16.5

GD 122	10 29 16 +32 55.6	DC5	CSO50[a],CBS22[a]	16.07
G 10-11	11 15 43 −02 57.8	DC5	PG,LFT0792,EG078	15.3
PG 1126+186	11 26 42 +18 33.2	DC8		13.79
G 147-65	11 33 05 +35 50.9	M+DC	Gr388	15.8
		DCPEC		
G 237-28	11 43 03 +63 22.8	DC9	Gr353,LP63-267	16.4
G 11-23	11 45 24 +08 04.4	DC6	PG,G57-20[a]	16.08[b]
LHS 2596	12 36 55 +45 41 36	DC8	LP171-40	16.44
PG 1246+586	12 46 05 +58 36.8	DC8:	LB2449	15.56
G 60-54	12 57 37 +03 45.3	DC9	EG095,LHS2661	15.8
G 256-7	13 09 59 +85 18.6	DG,DC	LP7-226,Gr436	16
		DC9,DG?	LP8-46	
PG 1312+098	13 12 38 +09 53 05	DC		16.4
G 124-20	14 15 21 −06 26.2	DC5	PG	16.2
PG 1424+240	14 24 44 +24 01 23	DC8		15.41
LHS 378	14 44 41 −17 29.5	DC	LP801-9	16.0[c]
PG 1459+645	14 59 55 +64 28 32	DC		16.1
TON 246	15 39 26 +25 33.0	DC5	PG,GD188	15.63
GD 352	15 50 25 +62 36.2	DC6	Gr366	16.5
G 170-27	17 12 23 +21 30.7	DC5		16.51
PG 1747+451	17 47 00 +45 04.3	DC		15.79[b]
G 183-35	18 14 06 +24 53.7	DC7		16.5?
G 141-2	18 18 13 +12 37.4	DC8	L1208-132,Gr579	16
		DAH?9P	LTT15423/2	
G 227-28	18 20 45 +60 59.9	DC:9	LP103-294	15.65
G 184-12	18 31 49 +19 43.7	DC6		16.45
G 125-3	19 17 15 +38 38.0	DC?8	G208-17,Gr375	14.5
LP 575-16	20 27 37 +07 19.8	DC5		16.3
G 187-8	20 48 13 +26 19.6	DC9	LHS3589	15.6
G 233-19	22 34 36 +52 47.6	DC5	Gr379	16.6

KUV 813-24[a]	23 22 26 +11 51.2	DC	PG,LB1188	16.02[b]
GD 248	23 23 36 +15 43.8	DC5	Gr335	15.1

All data from McCook & Sion (1987) unless noted otherwise.
(a) From the Simbad database in Strasbourg, France.
(b) B magnitude.
(c) R magnitude.

Table 2.2 Other Objects

Name	RA DEC (1950)	Spectral Type	Other Names	m_v
	Known Polarized Stars			
GD 90	08 16 31 +37 40.9	DAH5	Gr348,CBS71[a]	15.7
			KUV0816+3741[a]	
LB 8827	08 53 31 +16 22 39	DB3,DBP2	Gr904,PG	15.83
PG 1658+441	16 58 17 +44 05 23	DAP2		15.02
	Unpolarized Stars			
G 191B2B	05 01 31 +52 44.8	DA1[b]	EG247	11.8
SAO 59965	07 14 54 +33 47 25	A0	BD+33°1501	9.2
			HD56355	
SAO 61549	09 29 19 +32 05 57	K0	BD+32°1893	8.1
			HD82354	
G 138-31	16 25 30 +09 19.2	DC8,DA	Gr327	16.11
G 24-9	20 11 29 +06 34.0	DQ7[b]	LHS3532,LTT15921	15.7
			EG138	
	Miscellaneous Observed Objects[c]			
LP 412-13	03 10 23 +18 57 06	m+		
IRAS04193+4959	04 19 21 +49 59 29			
Putney 1	04 10 17 +18 53 30			
Putney 2	04 19 25 +50 00 58			
Putney 3	08 56 22 +16 11 32			
Putney 4	15 39 31 +25 33 00			
Putney 5	18 14 13 +24 53 19			

All white dwarf data from McCook & Sion (1987) unless otherwise noted. SAO star data from the Simbad database in Strasbourg, France, and only two of the other names of the stars have been listed.
(a) Data from the Simbad database.
(b) Listed as a binary in McCook and Sion.

(c) Data for LP 412-13 is from Luyten (1979). IRAS 04193+4959 from the Simbad database. The coordinates for the Putney objects are the observed coordinates precessed to 1950 and finding charts for these objects are refered to in the text.

Table 2.3 Additional Data on the Observed Objects

Name	M_v	$\pi(''$)	V(%)	μ ($''$/yr)	θ
G 158-45	14.58	0.055		0.97	217
G 171-52	14.64	0.044		0.35	218
PG 0156+156	12.48		-0.32 ± 0.14^a		
G 272-152				0.20	115
PG 0210+168					
LHS 1415		0.063	$+0.002 \pm 0.10^a$	0.7	176
G 7-16	14.62	0.0569		0.52	222
G 83-10	15.05	0.08	-0.03 ± 0.11^b	0.26	210
LHS 1734	14.28	0.0464	-0.212 ± 0.08^a	0.687	156/15.6
G 108-42	12.46	0.026	-0.11 ± 0.10^b	0.026	161
G 234-4	15.09	0.055		0.29	169
G 193-74	13.54			0.27	195
G 193-78	12.55	0.027	-0.02 ± 0.05^b	0.5	187
G 111-49	12.88			0.34	294
LB 3013	12.77		$+0.043 \pm 0.14^a$	0.183	115
TON 1061			$+0.058 \pm 0.11^a$		
G 195-42	12.7	0.044		0.3	264
G 42-33	13.7	0.05	-0.02 ± 0.11^b	0.34	276
G 43-54	13.7			0.6	127
GD 122	11.9			<0.2	215
G 10-11	11.45	0.025	$+0.05 \pm 0.17^b$	0.56	292
PG 1126+186	14.07				
G 147-65		0.0182	-0.09 ± 0.10^b	0.5	261
G 237-28	14.76	0.05	-0.007 ± 0.108^b	0.4	201
G 11-23	B-V=+0.15				
LHS 2596	14.0			0.886	230
G 60-54	14.77	0.082	-0.27 ± 0.21^b	1.0	203
G 256-7	15.24	0.07		0.33	137

PG 1312+098	11.3				
G 124-20	12.26			0.27	226
LHS 378		0.063	$+0.233 \pm 0.09^a$	1.177	252.6
PG 1459+645	11.99				
TON 246	12.09				
GD 352	13.13		-0.17 ± 0.14^b	<0.2	350
G 170-27	13.45			0.32	195
PG 1747+451					
G 183-35	13.76			0.28	172
G 141-2	14.46	0.024	$+0.015 \pm 0.068^b$	0.3	20
G 227-28		0.0789	$+0.066 \pm 0.011^a$	0.68	174
G 184-12	13.18	0.017		0.46	174
G 125-3	13.82	0.08	$+0.02 \pm 0.03^b$	0.28	179
LP 575-16	12.4		-0.054 ± 0.07^a	0.26	135
G 187-8	16.04	0.0503	-0.04 ± 0.05^b	0.63	233
G 233-19	12.13		-0.039 ± 0.07^a	0.29	226
KUV 813-24					
GD 248	12.34		0.0 ± 0.04^b	<0.1	210
			Known Polarized Objects		
GD 90	12.31			<0.1	210
LB 8827	11			0.046	-140
PG 1658+441	10.1				
			Unpolarized Objects		
G 191B2B	10.07	0.021		0.1	160
SAO 59965[b]				μ_α=-0.002	μ_δ=-0.014
SAO 61549[b]				μ_α=0.006	μ_δ=0.006
G 138-31	13.84	0.0453		0.476	191
G 24-9	13.73	0.04		0.633	202
			Miscellaneous Observed Objects		
LP 412-13				0.289	69
IRAS04193+4959					

TON 1137	10.29
PG 1246+586	14.22
PG 1424+240	14.24

All data from McCook & Sion (1987) unless noted otherwise. Column 2 is the absolute magnitude; column 3 is the parallax; column 4 is previously measured circular polarization; columns 5 and 6 are the proper motion rate and direction, respectively.
(a) V$\pm\sigma$ from Liebert & Stockman (1980).
(b) V$\pm\sigma$ from Angel, Borra, & Landstreet (1981).

Table 2.4 Summary of Observations

Name	Telescope	Date (UT)	Exposure Length	Exposure Start (UT)	Weather	Flux Standard
Survey Objects						
G 158-45	Palomar	94-Sep-29	50 min	07:01:41	cldy	GD 248
	Keck	94-Oct-28	16 min	11:10:33	clr	GD 248
	Palomar	94-Nov-8	50 min	03:37:51	fog	GD 248
	Palomar	94-Nov-9	50 min	03:45:00	clr	GD 248
	Keck	94-Dec-30	12 min	07:46:59	clr	G 193-74
	Keck	94-Dec-31	8 min	05:53:28	clr	G 191B2B
G 171-52	Palomar	94-Sep-28	50 min	07:24:56	clr	GD 248
PG 0156+156	Palomar	94-Nov-8	50 min	04:42:40	cldy	GD 248
G 272-152	Palomar	94-Sep-28	50 min	08:32:06	clr	GD 248
PG 0210+168	Palomar	94-Nov-8	50 min	05:40:37	clr	GD 248
LHS 1415	Palomar	94-Sep-28	50 min	09:30:18	cldy	GD 248
	Keck	94-Oct-28	16 min	11:35:44	clr	GD 248
	Palomar	94-Nov-9	25 min	05:17:36	clr	GD 248
G 7-16	Palomar	94-Sep-28	50 min	10:31:18	cldy	GD 248
G 83-10	Palomar	94-Feb-3	50 min	03:57:25	cldy	G 191B2B
LHS 1734	Palomar	94-Sep-28	50 min	11:29:39	cldy	GD 248
	Keck	94-Oct-28	16 min	13:41:43	clr	GD 248
	Keck	94-Dec-31	16 min	09:03:10	clr	G 191B2B
G 108-42	Palomar	94-Feb-3	50 min	05:29:56	cldy	G 191B2B
G 234-4	Palomar	95-Mar-29	50 min	03:33:51	clr	G 138-31
G 193-74	Palomar	94-Feb-3	50 min	06:37:26	cldy	G 191B2B
	Keck	94-Dec-30	12 min	10:49:09	clr	G 193-74
G 193-78	Palomar	94-Nov-9	50 min	12:25:33	clr	GD 248
G 111-49	Keck	94-Dec-30	10 min	10:31:41	clr	G 193-74
LB 3013	Palomar	95-Mar-30	50 min	03:28:00	cldy	G 138-31
TON 1061	Palomar	95-Mar-29	50 min	05:07:17	clr	G 138-31

G 195-42	Palomar	95-Mar-30	50 min	04:26:26 cldy	G 138-31
G 42-33	Palomar	95-Mar-29	50 min	06:04:44 clr	G 138-31
G 43-54	Palomar	95-Mar-30	50 min	05:54:27 cldy	G 138-31
GD 122	Palomar	95-Mar-31	50 min	05:29:19 clr	G 138-31
G 10-11	Palomar	95-Mar-29	50 min	07:05:07 clr	G 138-31
PG 1126+186	Palomar	95-Mar-30	50 min	06:52:32 cldy	G 138-31
G 147-65	Palomar	95-Mar-31	50 min	06:26:33 clr	G 138-31
G 237-28	Palomar	95-Mar-29	50 min	08:13:38 clr	G 138-31
G 11-23	Palomar	95-Mar-30	50 min	07:48:34 cldy	G 138-31
LHS 2596	Palomar	95-Mar-31	50 min	07:23:44 clr	G 138-31
G 60-54	Palomar	95-Mar-30	50 min	08:54:05 cldy	G 138-31
G 256-7	Palomar	95-Mar-31	50 min	08:30:28 clr	G 138-31
PG 1312+098	Palomar	95-Mar-29	50 min	10:08:11 clr	G 138-31
	Palomar	95-Mar-31	50 min	09:31:52 clr	G 138-31
G 124-20	Palomar	95-Mar-30	50 min	09:50:20 cldy	G 138-31
LHS 378	Palomar	93-Jun-18	50 min	04:53:36 clr	G 24-9
PG 1459+645	Palomar	93-Jun-17	50 min	04:57:25 clr	G 138-31
TON 246	Palomar	95-Mar-29	50 min	11:08:59 clr	G 138-31
GD 352	Palomar	93-Jun-18	50 min	06:01:59 clr	G 24-9
G 170-27	Palomar	95-Mar-30	50 min	10:52:51 cldy	G 138-31
	Palomar	95-Mar-31	50 min	10:36:12 clr	G 138-31
PG 1747+451	Palomar	93-Jun-18	50 min	07:08:05 clr	G 24-9
G 183-35	Palomar	93-Jun-17	50 min	07:55:02 clr	G 138-31
	Palomar	94-Sep-29	50 min	03:09:21 vcdy	GD 248
G 141-2	Palomar	93-Jun-19	50 min	08:10:15 vcdy	G 24-9
G 227-28	Palomar	93-Jun-18	50 min	08:09:05 clr	G 24-9
G 184-12	Palomar	93-Jun-17	50 min	09:03:06 clr	G 138-31
G 125-3	Palomar	93-Jun-19	50 min	09:14:08 vcdy	G 24-9
	Palomar	94-Sep-29	50 min	04:19:00 cldy	GD 248
LP 575-16	Palomar	93-Jun-18	50 min	10:24:41 clr	G 24-9

G 187-8	Palomar	94-Sep-28	50 min	04:14:03	clr	GD 248
G 233-19	Palomar	94-Sep-28	50 min	05:24:23	clr	GD 248
KUV 813-24	Palomar	94-Sep-29	50 min	06:03:23	cldy	GD 248
GD 248	Palomar	94-Sep-28	50 min	06:22:25	clr	GD 248
Known Polarized Stars						
GD 90	Palomar	95-Mar-31	50 min	03:28:48	clr	G 138-31
LB 8827	Palomar	94-Feb-3	50 min	07:40:02	cldy	G 191B2B
PG 1658+441	Palomar	93-Jun-17	50 min	06:41:25	clr	G 138-31
Unpolarized Stars						
G 191B2B	Palomar	94-Feb-3	400 sec	05:07:02	cldy	G 191B2B
SAO 59965	Palomar	95-Mar-30	50 sec	02:44:51	cldy	G 138-31
	Palomar	95-Mar-30	30 sec	02:51:01	cldy	G 138-31
SAO 61549	Palomar	94-Feb-2	20 sec	08:48:52	cldy	G 191B2B
G 138-31	Palomar	95-Mar-31	40 min	11:32:22	clr	G 138-31
G 24-9	Palomar	93-Jun-18	50 min	09:19:13	clr	G 24-9
Miscellaneous Observed Objects						
LP 412-13	Keck	94-Dec-30	14 min	09:22:21	clr	G 193-74
IRAS 04193+ 4959	Palomar	94-Nov-9	50 min	11:25:48	clr	GD 248
Putney 1	Keck	94-Dec-30	2 min	09:51:41	clr	G 193-74
Putney 2	Keck	94-Dec-30	10 min	10:08:34	clr	G 193-74
Putney 3	Keck	94-Dec-30	8 min	11:47:26	clr	G 193-74
TON 1137	Palomar	95-Mar-31	50 min	04:46:05	clr	G 138-31
Putney 4	Palomar	93-Jun-19	50 min	05:39:42	vcdy	G 24-9
Putney 5	Palomar	94-Sep-28	40 min	03:23:22	clr	GD 248
PG 1246+586	Palomar	95-Mar-29	50 min	09:10:02	clr	G 138-31
PG 1424+240	Palomar	93-Jun-19	50 min	04:40:28	cldy	G 24-9

Table 2.5 Spectral Types

Name	M&S Type	New Type	Temperature (K)	Atm.
Survey Objects				
G 158-45	DC8	DAP8	6000	H(+He)
G 171-52	DC9	DA9	5500	H(+He)
PG 0156+156	DC6	DC5	9750	He
G 272-152	DC	DB4	>11000	He(+H)
PG 0210+168	DC	DC+F/G		
LHS 1415	DC,DF?	DA9	5250	H(+He)
G 7-16	DC9	DA9	5250	H(+He)
G 83-10	DC8	DC8	6500	H(+He)
LHS 1734	DZ9?,DC9?	DAP9	5250	H(+He)
G 108-42	DC5	DC5	10000	He
G 234-4	DC9	DA9	4500	H(+He)
G 193-74	DC7	DC6	8000	He+H
G 193-78	DC5	DC5	11000	He
G 111-49	DC?6	DCAP9	8500	H
LB 3013	DC6	DCQ5	9500	He(+H)
TON 1061	DC	DC5(A?)	11000	He
G 195-42	DQ6,DC6	DCQ?6	9500	He(+H)
G 42-33	DC7	DC7	7000	He(+H)
G 43-54	DC8	DAP7	7000	H+He
GD 122	DC5	DBAZ4	13000	He
G 10-11	DC5	DC5	10000	He
PG 1126+186	DC8	DC+G/K		
G 147-65	M+DC,DCPEC	dM4.5e+DC		
G 237-28	DC9	DA9	5500	He+H
G 11-23	DC6	DQ4	11000	He(+H)
LHS 2596	DC8	DA8	6500	H(+He)

G 60-54	DC9	DAQZ8	6000	He(+H)
G 256-7	DG,DC,DC9,DG?	DAP9	5000	H
PG 1312+098	DC	DAP3	20000	H+He
G 124-20	DC5	DCB?4	12500	He(+H)
LHS 378	DC	DC9	5000	He
PG 1459+645	DC	DC5	11000	He
TON 246	DC5	DB4	12000	He
GD 352	DC6	DQ6	<9000	He(+H)
G 170-27	DC5	DC7	8000	He(+H)
PG 1747+451	DC	DC6	9000	He
G 183-35	DC7	DAP8	6500	H(+He)
G 141-2	DC8,DAH?9P	DA8	6000	H(+He)
G 227-28	DC:9	DAZ?9	<5000	He(+H)
G 184-12	DC6	DQ6	8000	(H+He)
G 125-3	DC?8	DC8	6500	H(+He)
LP 575-16	DC5	DC6	9000	He
G 187-8	DC9	DA9	4500	H(+He)
G 233-19	DC5	DA5	10000	He
KUV 813-24	DC	DZA4	11000	He
GD 248	DC5	DA5	10000	He(+H)
Known Polarized Stars				
GD 90	DAH5	DAP4	14000	H
LB 8827	DB3,DBP2	DBP3	<20000	He
PG 1658+441	DAP2	DAP2	30000	H
Unpolarized Stars				
G 191B2B	DA1	DA0[a]		
SAO 59965	A0[b]			
SAO 61549	K0[b]			
G 138-31	DC8,DA	DA7	7000	H
G 24-9	DQ7	DC7	7000	H or He

Miscellaneous Observed Objects			
LP 412-13	m+[c]	dM3	
IRAS 04193+4959		carbon star	CN
Putney 1		G/K III?	
Putney 2		A/F	
Putney 3		K0/K1	
TON 1137	DC?1	sdOC	He
Putney 4		M0V	
Putney 5		M0V	
PG 1246+586	DC8:	BL Lac	
PG 1424+240	DC	BL Lac	

M&S type, column 2, is the spectral type from McCook & Sion (1987). Column 5 is the atmospheric composition (see text), where a set of parentheses around an element indicate a possible constituent.
(a) From Oke 1990.
(b) From the Simbad database, Strasbourg, France.
(c) From Luyten (1979).

Table 2.6 Polarization and Magnetic Field Measurements

Name	Date	$\langle V_{red} \rangle$ (%)	$\langle V_{blue} \rangle$ (%)	B_e
Survey Objects				
G 158-45	94/9/29	-0.106 ± 0.056	$+0.117 \pm 0.099$	$+8.8^{+1.2}_{-0.8}$ MG
	94/10/28	-0.107 ± 0.022	$-0.322 \pm 0.048b$	$+8.2^{+0.6}_{-0.4}$ MG
	94/11/8	$+0.190 \pm 0.031$	$+0.318 \pm 0.080$	$-10.0^{+1.4}_{-0.2}$ MG
	94/11/9	-0.053 ± 0.024	-0.252 ± 0.060	$+8.7^{+0.9}_{-0.5}$ MG
	94/12/30	$+0.368 \pm 0.028$	$+0.208 \pm 0.086a$	$-10.0^{+0.6}_{-0.4}$ MG
	94/12/31	$+0.270 \pm 0.020$	$+0.282 \pm 0.052a$	$-10.0^{+0.6}_{-0.4}$ MG
G 171-52	94/9/28	$+0.016 \pm 0.027$	-0.025 ± 0.062	$+21.6 \pm 46.5$ kG
PG 0156+155	94/11/8	-0.018 ± 0.030	$+0.004 \pm 0.039$	I
G 272-152	94/9/28	-0.043 ± 0.027	$+0.004 \pm 0.033$	$+25.1 \pm 30.5$ kG
PG 0210+168	94/11/8	$+0.121 \pm 0.012$	$+0.183 \pm 0.021$	I
LHS 1415	94/9/28	-0.024 ± 0.043	$+0.150 \pm 0.099$	-34.4 ± 13.8 kG
	94/10/28	$+0.044 \pm 0.017$	$+0.162 \pm 0.042b$	$+9.3 \pm 12.2$ kG
	94/11/9	-0.223 ± 0.025	-0.096 ± 0.001	$+39.3 \pm 4.9$ kG[c]
G 7-16	94/9/28	$+0.043 \pm 0.032$	-0.044 ± 0.067	$+4.1 \pm 9.5$ kG
G 83-10	94/2/3	$+0.060 \pm 0.020$	-0.038 ± 0.034	I
LHS 1734	94/9/28	-0.093 ± 0.071	-0.080 ± 0.175	$+3.9 \pm 0.4$ MG
	94/10/28	$+0.054 \pm 0.018$	$+0.098 \pm 0.043b$	$+3.8^{+1.0}_{-0.5}$ MG
	94/12/31	$+0.012 \pm 0.013$	$+0.069 \pm 0.033a$	$+3.8^{+0.4}_{-0.2}$ MG
G 108-42	94/2/3	$+0.014 \pm 0.033$	-0.074 ± 0.041	I
G 234-4	95/3/29	-0.097 ± 0.025	-0.032 ± 0.079	$+39.6 \pm 11.6$ kG
G 193-74	94/2/3	-0.020 ± 0.022	-0.095 ± 0.032	I
	94/12/30	$+0.092 \pm 0.014$	$+0.031 \pm 0.024a$	I
G 193-78	94/11/9	$+0.007 \pm 0.016$	-0.006 ± 0.021	I
G 111-49	94/12/30	-3.497 ± 0.023	$-5.403 \pm 0.035a$	-220 MG
LB 3013	95/3/30	-0.118 ± 0.038	-0.031 ± 0.049	I
Ton 1061	95/3/29	$+0.079 \pm 0.029$	-0.002 ± 0.037	I
G 195-42	95/3/30	$+0.026 \pm 0.043$	$+0.074 \pm 0.055$	I

G 42-33	95/3/29	-0.108 ± 0.016	-0.080 ± 0.033	I
G 43-54	95/3/30	-0.107 ± 0.074	$+0.021 \pm 0.117$	$-8.8^{+0.2}_{-1.8}$ MG
GD 122	95/3/31	$+0.048 \pm 0.043$	$+0.069 \pm 0.051$	-5.3 ± 10.4 kG
G 10-11	95/3/29	-0.021 ± 0.020	-0.015 ± 0.031	I
PG 1126+185	95/3/30	$+0.025 \pm 0.010$	$+0.036 \pm 0.022$	I
G 147-65	95/3/31	$+0.002 \pm 0.012$	$+0.177 \pm 0.081$	I
G 237-28	95/3/29	-0.005 ± 0.027	-0.133 ± 0.077	-3.6 ± 8.2 kG
G 11-23	95/3/30	$+0.146 \pm 0.064$	-0.085 ± 0.075	I
LHS 2596	95/3/31	-0.047 ± 0.034	$+0.068 \pm 0.072$	$+0.3 \pm 5.6$ kG
G 60-54	95/3/30	$+0.045 \pm 0.073$	$+0.092 \pm 0.156$	$+11.2 \pm 18.0$ kG
G 256-7	95/3/31	-0.168 ± 0.027	-0.243 ± 0.093	$+4.9 \pm 0.5$ MG
PG 1312+098	95/3/29	$+0.714 \pm 0.049$	$+0.804 \pm 0.050$	$+6.5 \pm 2.5$ MG
	95/3/31	-0.123 ± 0.052	-0.884 ± 0.051	$+6.5 \pm 2.5$ MG
G 124-20	95/3/30	$+0.377 \pm 0.169$	-0.162 ± 0.158	I
LHS 378	93/6/18	-0.044 ± 0.042	-0.361 ± 0.002	I
PG 1459+645	93/6/17	-0.283 ± 0.052	-0.365 ± 0.001	I
Ton 246	95/3/29	-0.051 ± 0.025	-0.086 ± 0.034	-6.4 ± 12.0 kG
GD 352	93/6/18	$+0.205 \pm 0.054$	$+0.051 \pm 0.001$	I
G 170-27	95/3/30	-0.308 ± 0.137	-0.026 ± 0.219	I
	95/3/31	$+0.088 \pm 0.038$	$+0.008 \pm 0.066$	I
PG 1747+450	93/6/18	$+0.164 \pm 0.025$	-0.032 ± 0.001	I
G 183-35	93/6/17	-1.083 ± 0.096	-1.308 ± 0.002	$+6.8 \pm 0.5$ MG
	94/9/29	-0.328 ± 0.129	$+0.154 \pm 0.151$	$+6.8 \pm 0.8$ MG
G 141-2	93/6/19	$+0.267 \pm 0.040$	-0.132 ± 0.001	$+60.7 \pm 87.2$ kG
G 227-28	93/6/18	$+0.497 \pm 0.022$	$+0.017 \pm 0.001$	-5.3 ± 16.9 kG
G 184-12	93/6/17	-0.323 ± 0.044	-0.475 ± 0.001	I
G 125-3	93/6/19	$+0.493 \pm 0.028$	-0.062 ± 0.001	I
	94/9/29	$+0.072 \pm 0.020$	$+0.052 \pm 0.031$	I
LP 575-16	93/6/18	$+0.121 \pm 0.040$	-0.025 ± 0.001	I
G 187-8	94/9/28	$+0.021 \pm 0.015$	-0.011 ± 0.045	-13.6 ± 13.7 kG

G 233-19	94/9/28	$+0.022 \pm 0.047$	-0.031 ± 0.055	$+8.6 \pm 35.9$ kG
KUV 813-24	94/9/29	$+0.001 \pm 0.030$	$+0.069 \pm 0.034$	$+3.0 \pm 2.1$ kG
GD 248	94/9/28	-0.004 ± 0.015	$+0.037 \pm 0.019$	-2.5 ± 33.3 kG
Known Polarized Stars				
GD 90	95/3/31	$+0.031 \pm 0.028$	$+0.087 \pm 0.037$	$+5.5^{+2.7}_{-0.7}$ MG
LB 8827	94/2/3	$+0.118 \pm 0.069$	-0.114 ± 0.053	-1.0 ± 0.5 MG
PG 1658+440	93/6/17	-0.190 ± 0.024	-0.404 ± 0.000	$+2.5^{-1.5}_{+2.0}$ MG
Unpolarized Stars				
G 191B2B	94/2/3	-0.016 ± 0.011	$+0.062 \pm 0.010$	$+8.4 \pm 3.7$ kG
SAO 59965	95/3/30	-0.073 ± 0.008	-0.151 ± 0.012	$+0.9 \pm 0.7$ kG
	95/3/30	-0.035 ± 0.010	$+0.021 \pm 0.014$	
SAO 61549	94/2/2	$+0.130 \pm 0.081$	-0.500 ± 0.417	
G 138-31	95/3/31	$+0.024 \pm 0.032$	$+0.149 \pm 0.063$	-0.1 ± 4.2 kG
G 24-9	93/6/18	-0.143 ± 0.032	-0.128 ± 0.001	I
Miscellaneous Observed Objects				
LP 412-13	94/12/30	$+0.094 \pm 0.009$	$+0.050 \pm 0.060a$	
IRAS 04193+4959	94/11/9	-0.052 ± 0.023		
Putney 1	94/12/30	-0.418 ± 0.026	$-1.185 \pm 0.123a$	
Putney 2	94/12/30	$+0.374 \pm 0.004$	$+0.593 \pm 0.008a$	
Putney 3	94/12/30	$+0.055 \pm 0.016$	$+0.087 \pm 0.037a$	
Ton 1137	95/3/31	$+0.025 \pm 0.024$	-0.008 ± 0.023	$+4.8 \pm 5.8$ kG
Putney 4	93/6/19	$+0.180 \pm 0.042$	$+0.217 \pm 0.003$	
Putney 5	94/9/28	$+0.009 \pm 0.025$	$+0.109 \pm 0.162$	
PG 1246+586	95/3/29	$+0.057 \pm 0.017$	$+0.030 \pm 0.039$	
PG 1424+240	93/6/19	$+0.225 \pm 0.016$	-0.098 ± 0.000	

The circular polarization is averaged over 6000-8000 Å for red and 3800-4600 for blue.
(a) 3910-4600 Å.
(b) 4000-4600 Å.
(c) Not a trustworthy value, see text.

Table 2.7 Number of Stars per Spectral Type per Magnetic Field Range

Spectral Type	Magnetic Field Strength Range				
	B< 10 kG	>10kG <1MG	>1MG <100MG	> 100 MG	I[a]
DA	6	6	6	0	0
DB	2	1	0	0	0
DC	0	0	0	1	20
DQ	0	0	0	0	3
DZ	1	0	0	0	0

(a) I = Indeterminable Field Strength

Figure Captions

Figures 2.1 to 2.64: These figures are all similar. The top panel shows flux in units of 10^{-15} ergs s^{-1} cm^{-2} $Å^{-1}$. If there were several observations of the object, all are shown in time order (earliest observation on top) and they have been offset for clarity. In many cases there are markings for features due to poor subtraction of night sky lines (a vertical line and a $\oplus$ at the appropriate wavelength). There are also vertical lines at the wavelength positions of the Balmer series, several prominent He I lines, the Ca II H & K doublet, the Mg I b triplet, the Na I 5889 Å line, and for Ton 1137, several He II lines. They are not marked as such but should be obvious to the reader. A few other features may be indicated, but they are marked. The second panel shows the circular polarization in units of percent V/I. The dotted line indicates zero polarization. In the magnetic stars there is a third, bottom panel which shows the hydrogen (or helium) transitions as a function of magnetic field. In most cases these values are from Kemic (1974); otherwise the origin is described below. Also, vertical dotted lines are placed on the figure to aid in identifying the magnetic field strength. Observations taken at Palomar have a gap in the data from 5400 Å to 5600 Å due to the dichroic. Other differences are described below.

Figure 2.14 G 111-49. Panel A is the flux in units of 10^{-15} ergs cm^{-2} s^{-1} $Å^{-1}$. Panel B is the circular polarization for G 111-49. Panel C shows the hydrogen transitions as a function of magnetic field (from Wunner et al. 1985). The dotted lines are to guide the eyes to the transitions labeled a, b, and c (see text). The transitions of heavier line weight, are, from left to right at 100 MG, 3p1 – 2s0, 3d-2 – 2p-1, 3d-1 – 2p0, and 5p′0 – 3d′0. The bottom two panels are circular polarization for D: Grw+70°8247 (unpublished data from Keck) and E: G 227-35 (Cohen et al. 1993).

Figure 2.28 G 256-7. The top panel is the flux spectrum in units of 10^{-15} ergs cm^{-2} s^{-1} $Å^{-1}$. All the data have been convolved with a Gaussian to match the instrumental resolution. The middle panel is the circular polarization. The

horizontal dashed line marks zero for the spectrum. The bottom panel shows the hydrogen transitions as a function of magnetic field (from Kemic 1974). The dotted lines are to guide the eyes to the 3 Hα and 3 Hβ components.

Figure 2.37 G 183-35. The top panel is the flux spectrum in units of 10^{-15} ergs cm^{-2} s^{-1} Å^{-1}. The 1994 data have been multipied by a factor of 4/3. All the data has been convolved with a Gaussian to match the instrumental resolution. The middle panel is the circular polarization, with the left ordinate describing the values for the 1993 data and the right ordinate, the values for 1994. The horizontal dashed lines mark zero for each spectrum. The bottom panel shows the hydrogen transitions as a function of magnetic field (from Kemic 1974). The dotted lines are to guide the eyes to the 3 Hα and 3 Hβ components.

Figure 2.48 Figure (a) is a finding chart of IRAS 04193+4959, which is marked. RWT 103 is the object barely southeast of IRAS 04193+4959. Figure (b) is a plot of the flux and polarization spectra as described above. The data from the DBSP blue camera were not reduced because the object was too faint. Several CN Q_1 band heads are marked as dotted lines on the figure.

Figures 2.49, 2.50, 2.51, 2.53, and 2.54 This subsection of the above figures are split into parts (a) and (b). Figure (a) is a finding chart with the observed object marked. Figure (b) is as described above for Figures 1 through 64.

Figure 2.65 Number of observed white dwarf stars per magnetic decade. Data from the present survey, the DA survey of SS, and the table of magnetic white dwarfs of SS.

Figure 2.66 Magnetic field strength versus temperature for all stars in the magnetic white dwarf table of SS and the new magnetic white dwarf stars discovered here. The temperatures for the edges of the ZZ Ceti instability strip are from Kepler & Nolan (1993). The star at 16000 K and 500 MG, GD 229, is listed in SS as 1000 MG, but Schmidt, Latter, & Foltz (1990) claim that the field strength, derived from an approximation from the polarization measurements, is between

500 and 1000 MG. I have placed the object at a conservative 500 MG due to the lack of understanding of continuum polarization in a magnetic field and in helium stars (the constituents of this stellar atmosphere are unknown but presumed to be helium).

Figure 2.67 Total number of stars observed in magnetic field searches per temperature designation ($\theta = 50400/T_{eff}$). The upper panel, a, includes only the stars in the combined DC and DA surveys. The lower panel, b, includes the magnetic white dwarfs in the SS list.

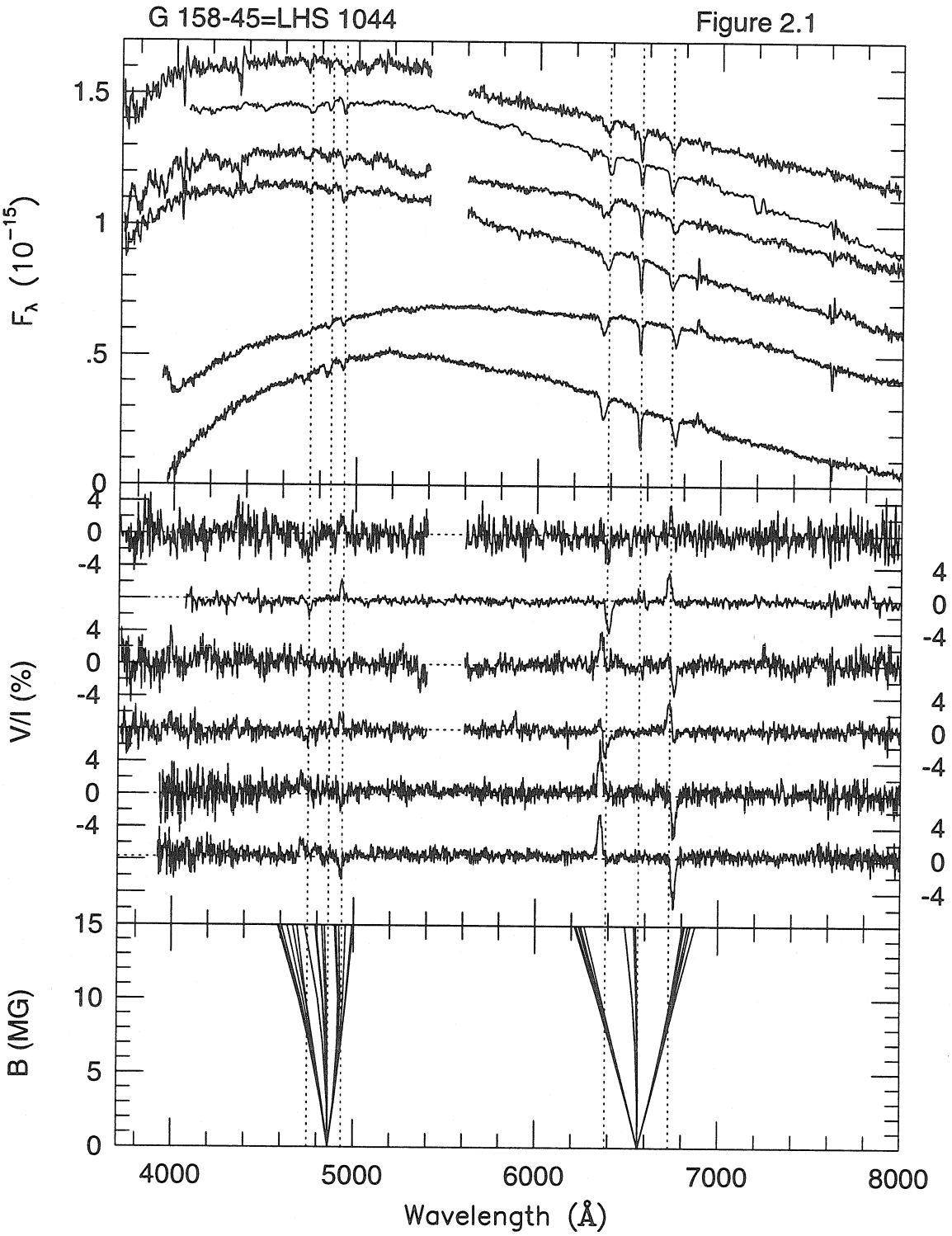
G 158-45=LHS 1044
Figure 2.1
F_λ (10^{-15})
1.5
1
.5
0
V/I (%)
4
0
-4
B (MG)
15
10
5
0
4000
5000
6000
7000
8000
Wavelength (Å)

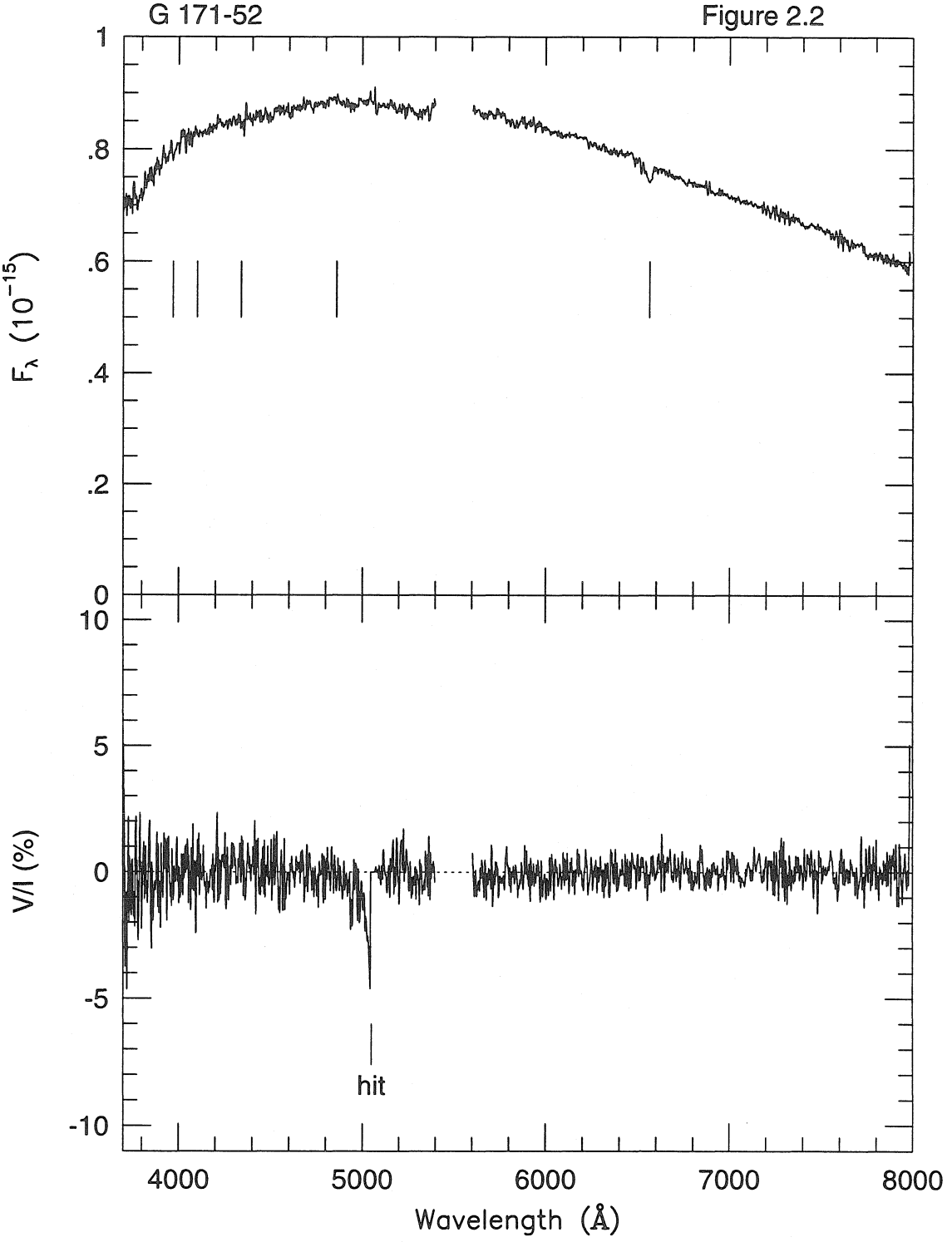
G 171-52
Figure 2.2
1
.8
.6
.4
.2
0
F_λ (10^{-15})
10
5
0
-5
-10
V/I (%)
hit
4000
5000
6000
7000
8000
Wavelength (Å)

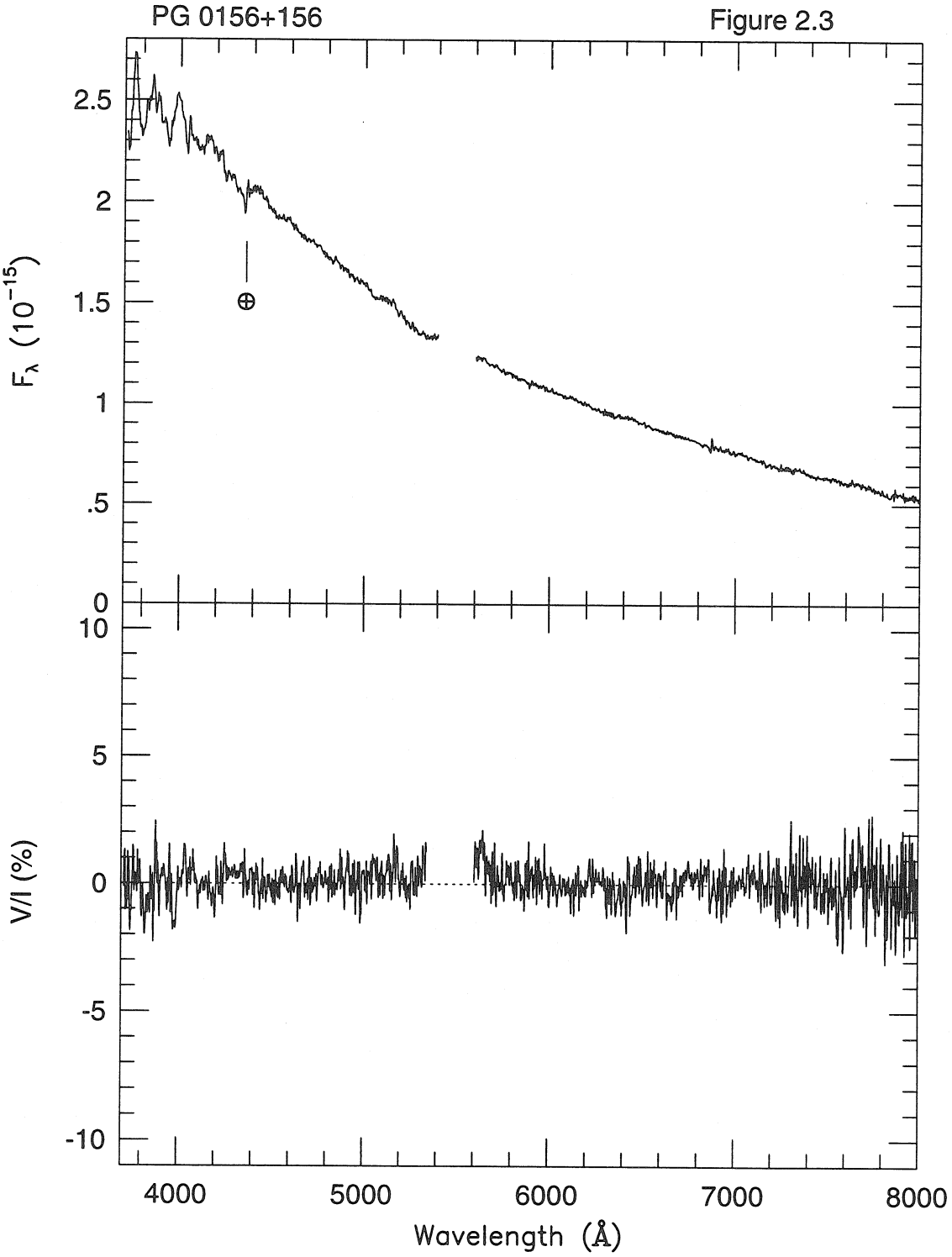
PG 0156+156
Figure 2.3
2.5
2
1.5
1
.5
0
F_λ (10^{-15})
⊕
10
5
0
-5
-10
V/I (%)
4000
5000
6000
7000
8000
Wavelength (Å)

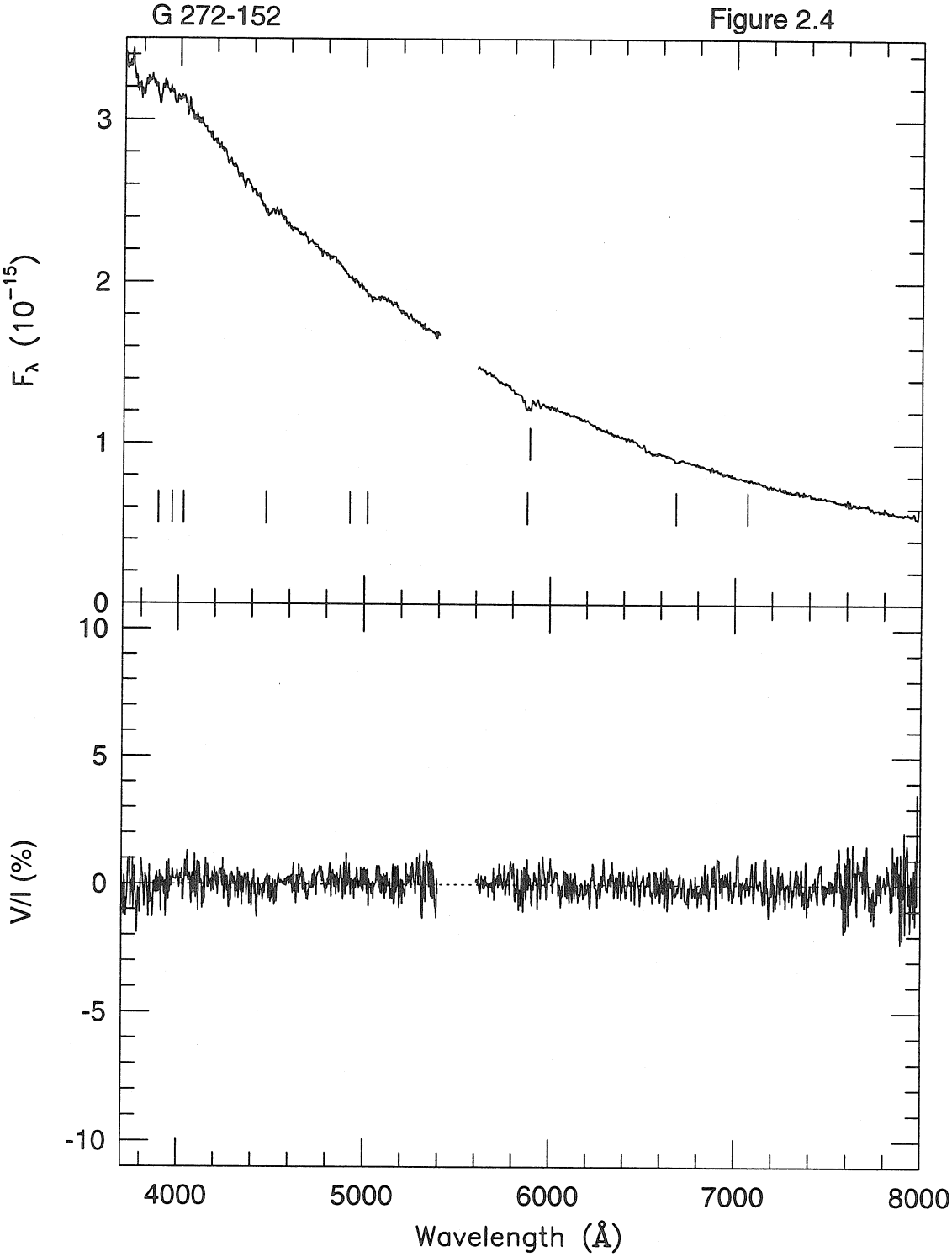
G 272-152
Figure 2.4
F_λ (10^{-15})
3
2
1
0
10
5
0
-5
-10
V/I (%)
4000
5000
6000
7000
8000
Wavelength (Å)

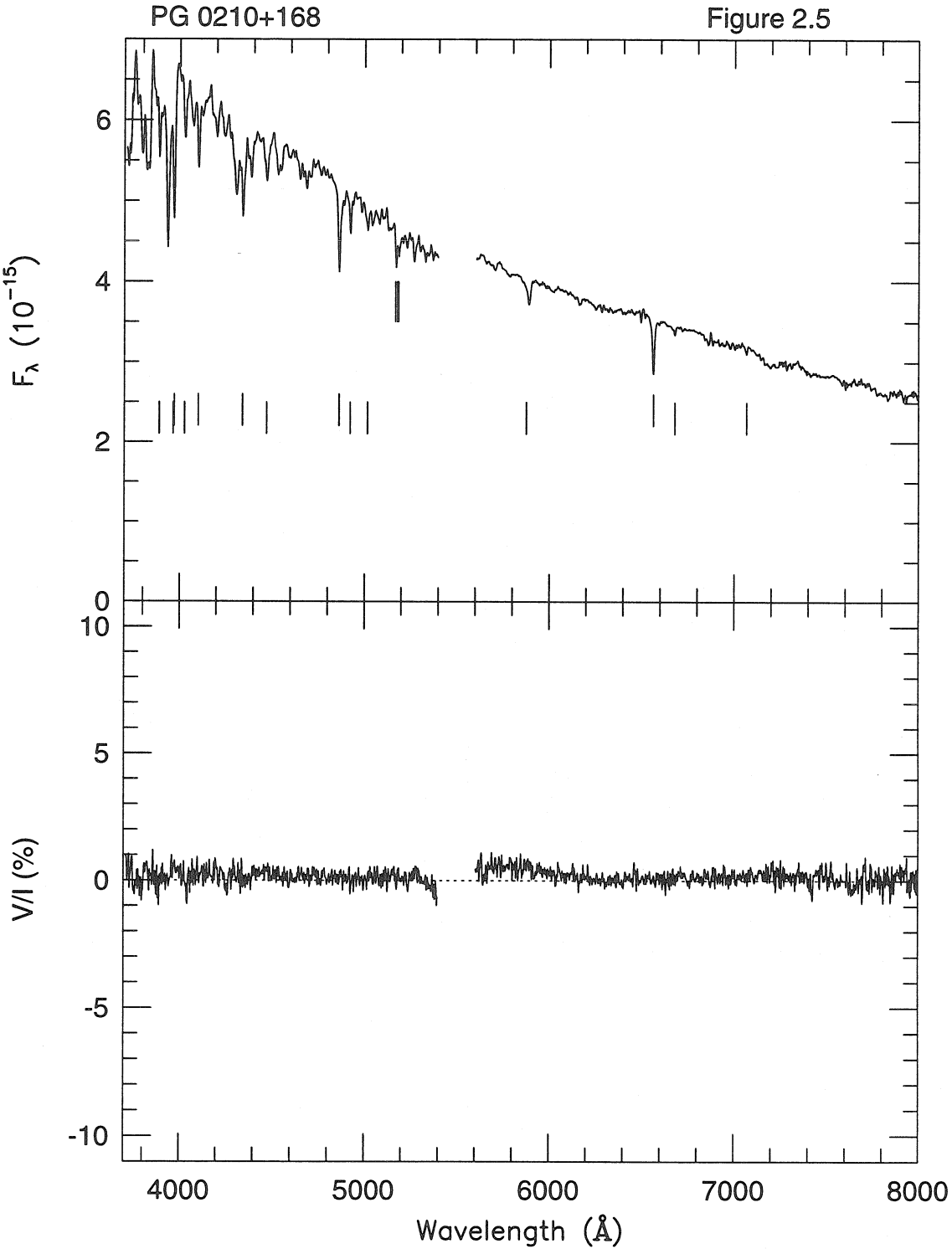
PG 0210+168
Figure 2.5
6
4
2
0
F_λ (10^{-15})
10
5
0
-5
-10
V/I (%)
4000
5000
6000
7000
8000
Wavelength (Å)

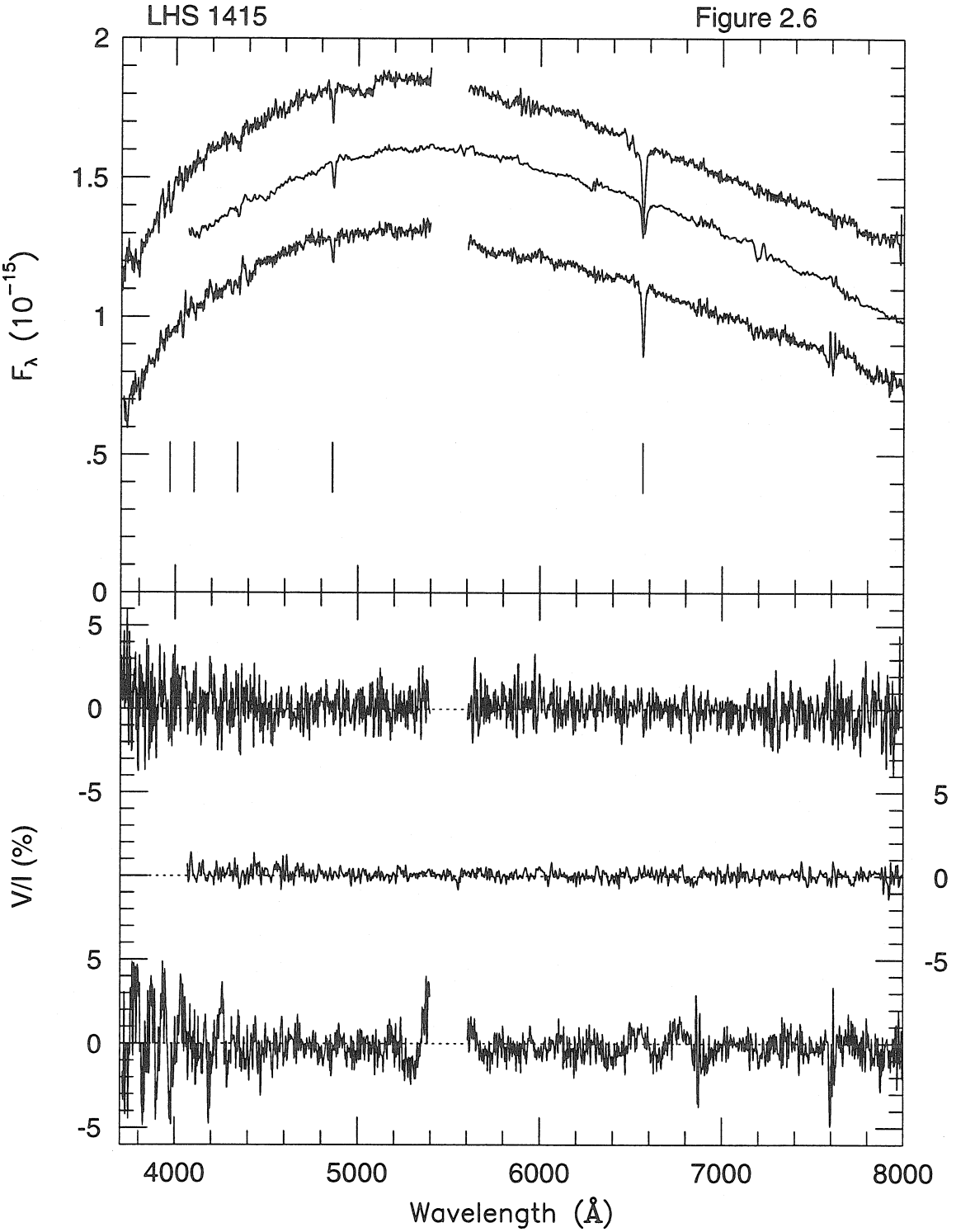
LHS 1415
Figure 2.6
2
1.5
1
.5
0
F_λ (10^{-15})
5
0
-5
5
0
-5
5
0
-5
V/I (%)
4000
5000
6000
7000
8000
Wavelength (Å)

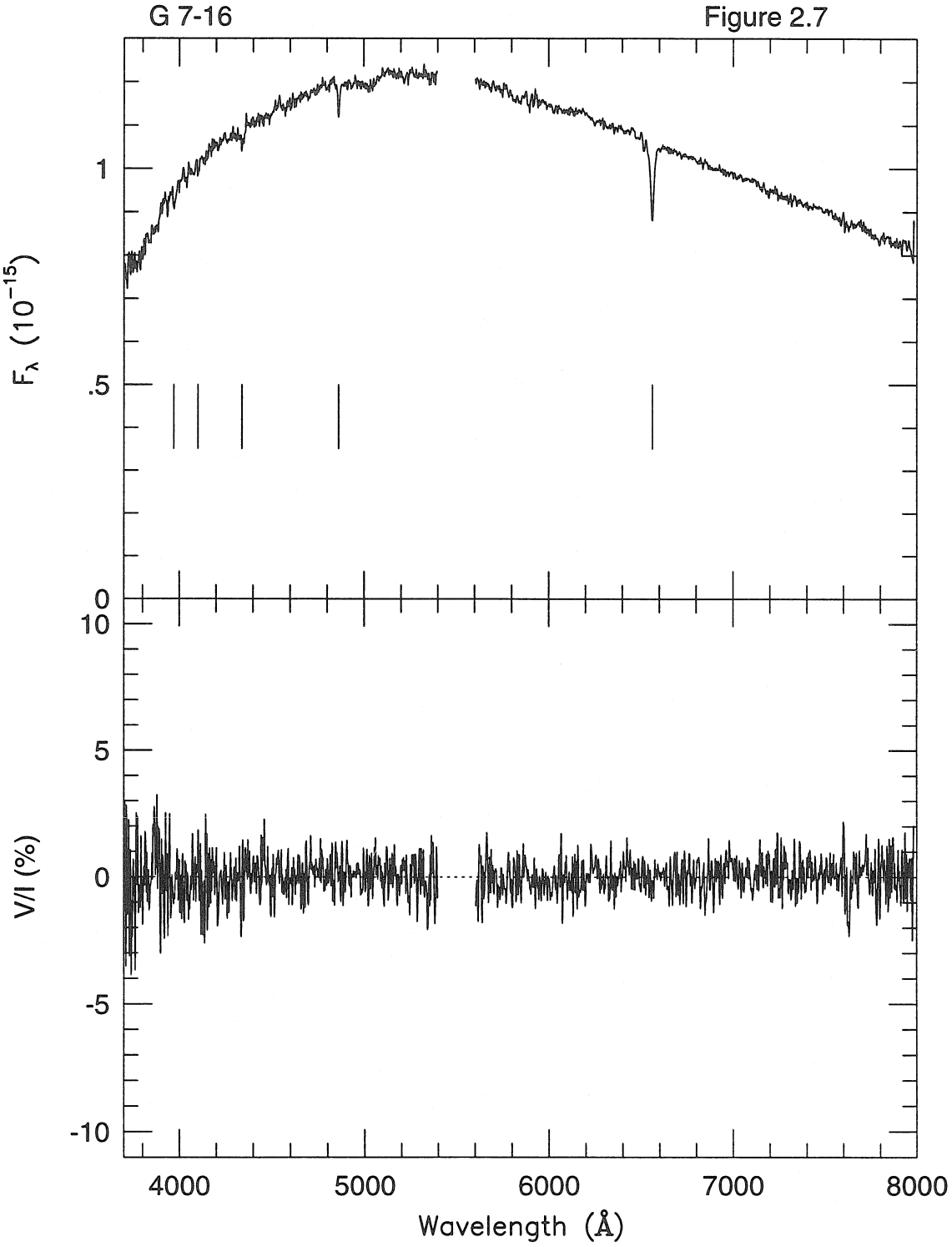
G 7-16
Figure 2.7
1
.5
0
F_λ (10^{-15})
10
5
0
-5
-10
V/I (%)
4000
5000
6000
7000
8000
Wavelength (Å)

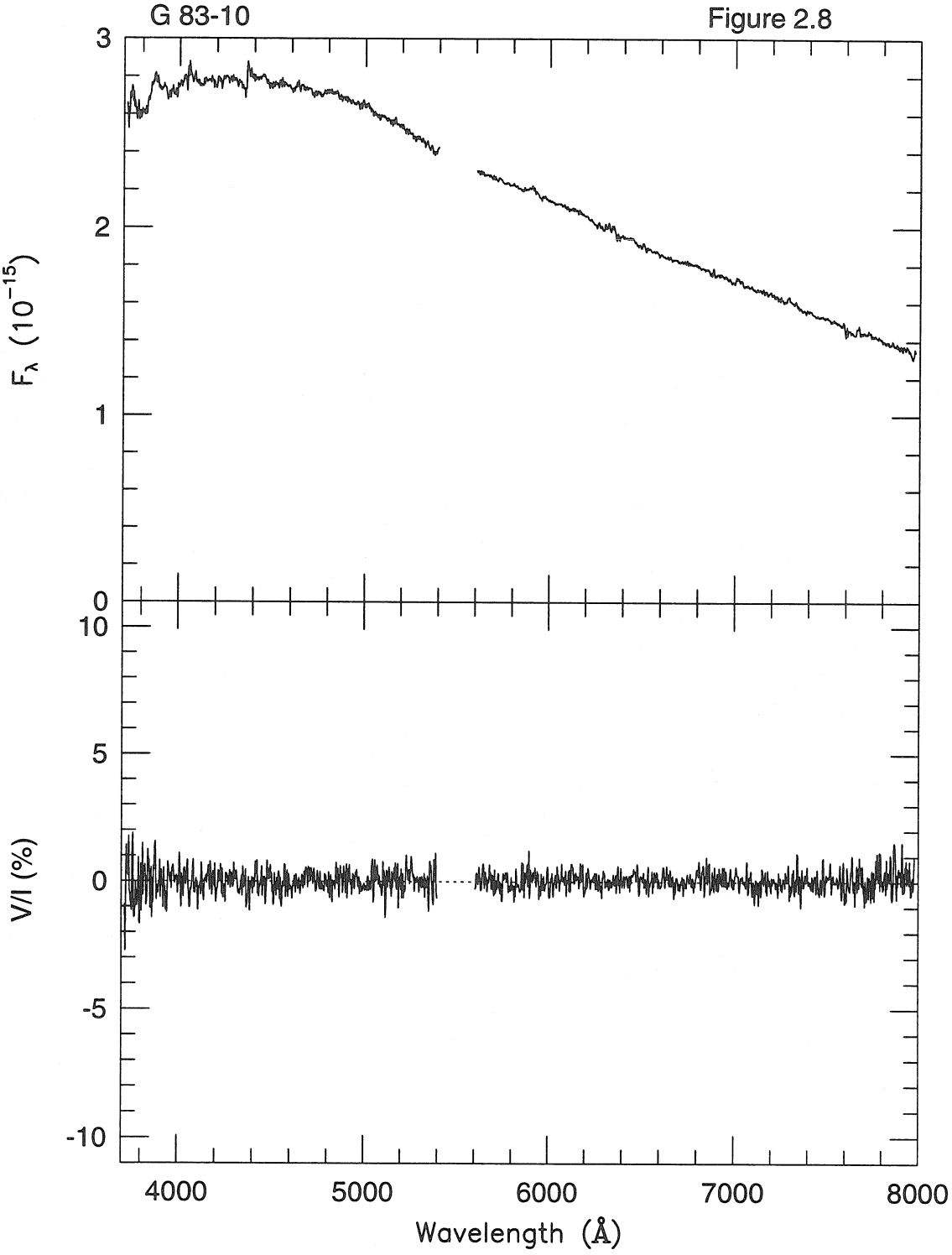
G 83-10
Figure 2.8
3
2
1
0
F_λ (10^{-15})
10
5
0
-5
-10
V/I (%)
4000
5000
6000
7000
8000
Wavelength (Å)

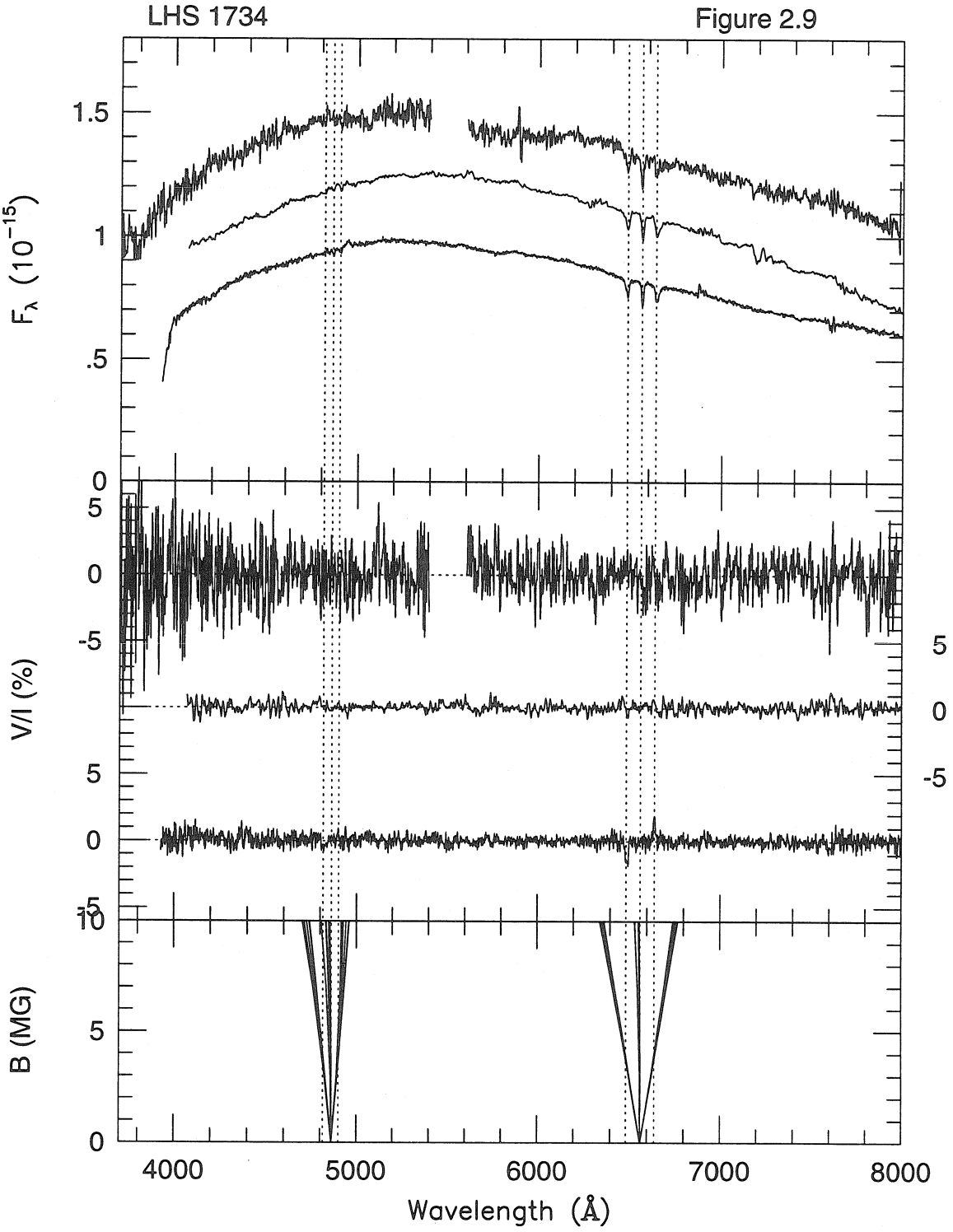
LHS 1734
Figure 2.9
1.5
1
.5
0
F_λ (10^{-15})
5
0
-5
V/I (%)
5
0
-5
5
0
-5
10
5
0
B (MG)
4000
5000
6000
7000
8000
Wavelength (Å)

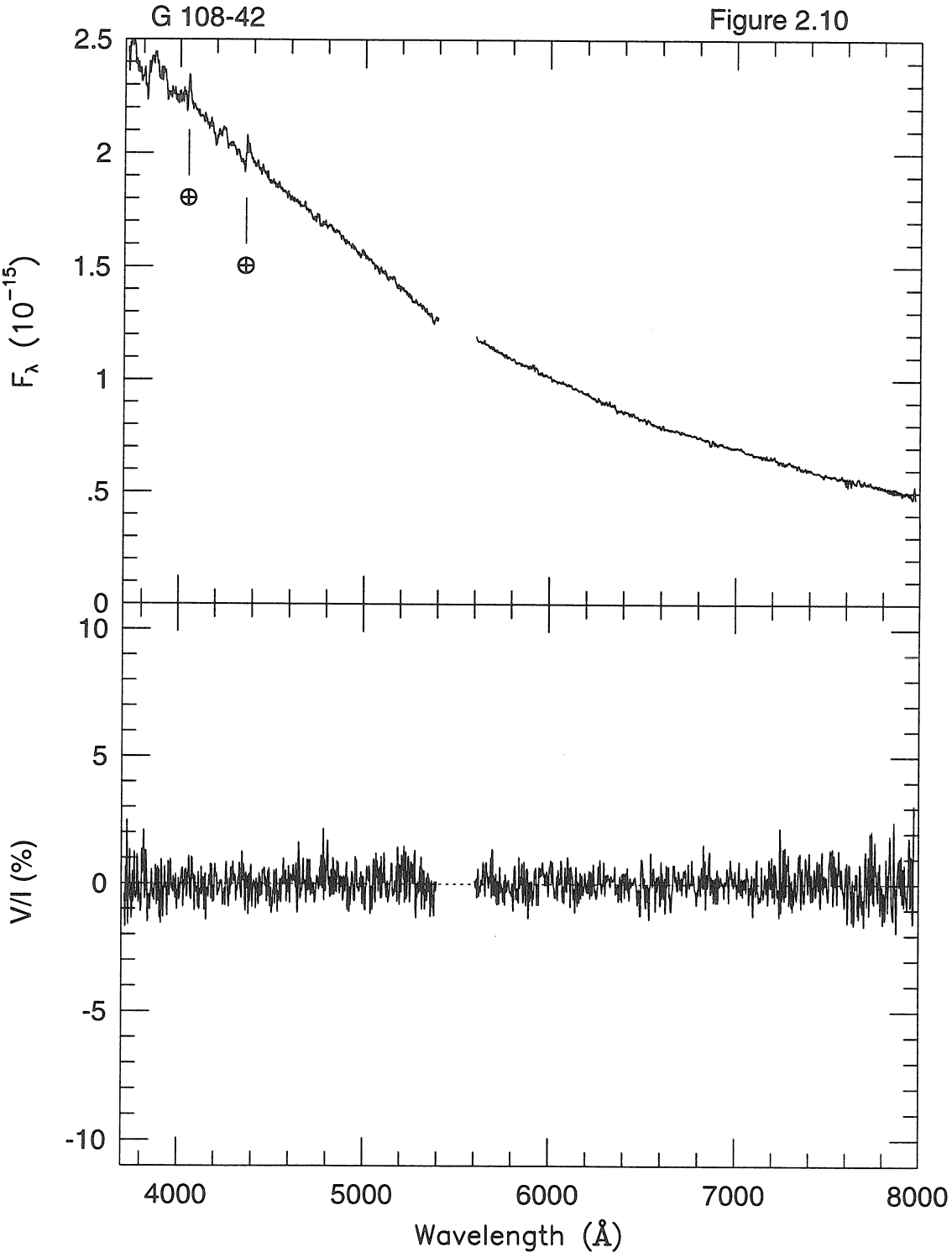
G 108-42
Figure 2.10
2.5
2
1.5
1
.5
0
F_λ (10^{-15})
⊕
⊕
10
5
0
-5
-10
V/I (%)
4000
5000
6000
7000
8000
Wavelength (Å)

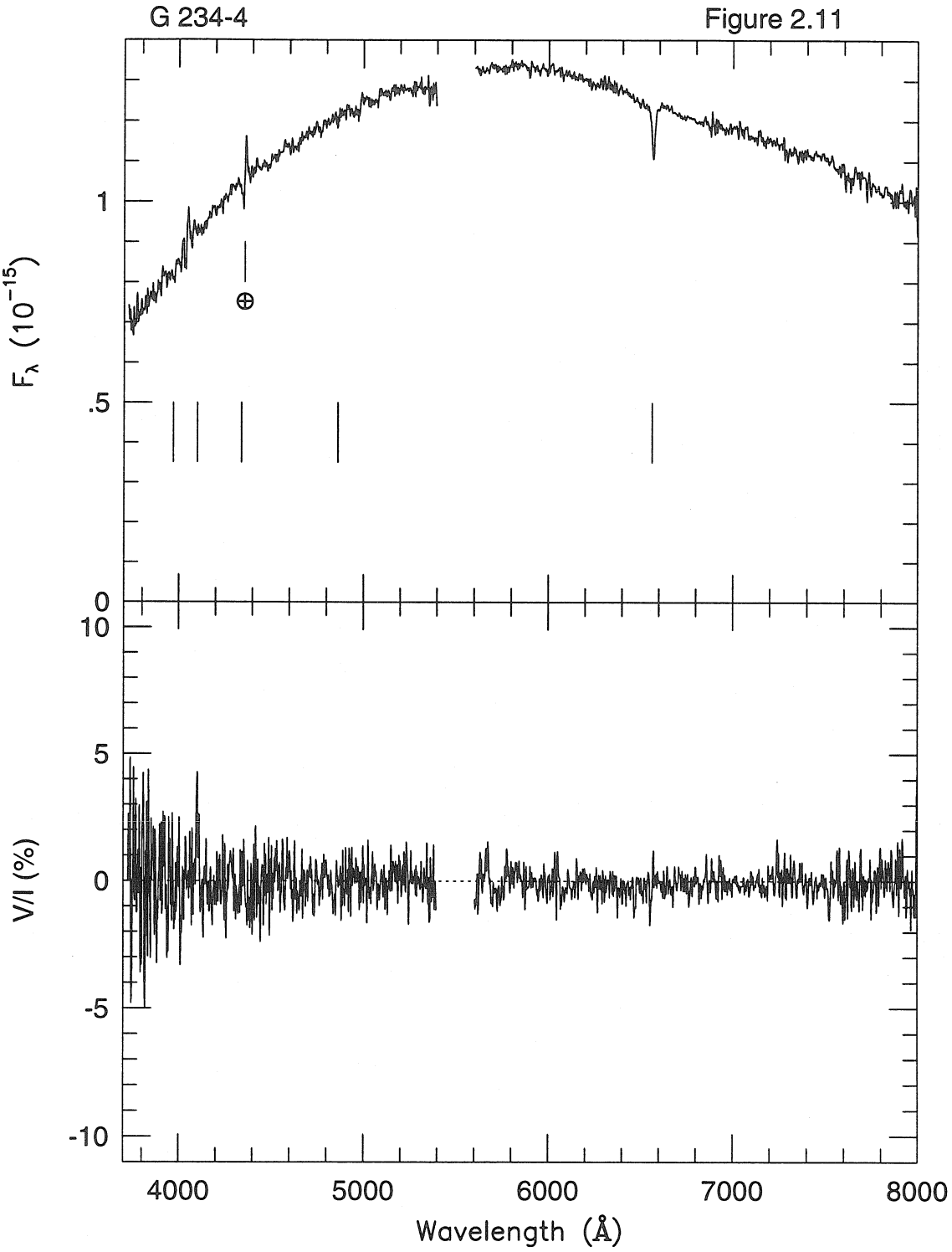
G 234-4
Figure 2.11
F_λ (10^{-15})
1
.5
0
10
5
0
-5
-10
V/I (%)
4000
5000
6000
7000
8000
Wavelength (Å)

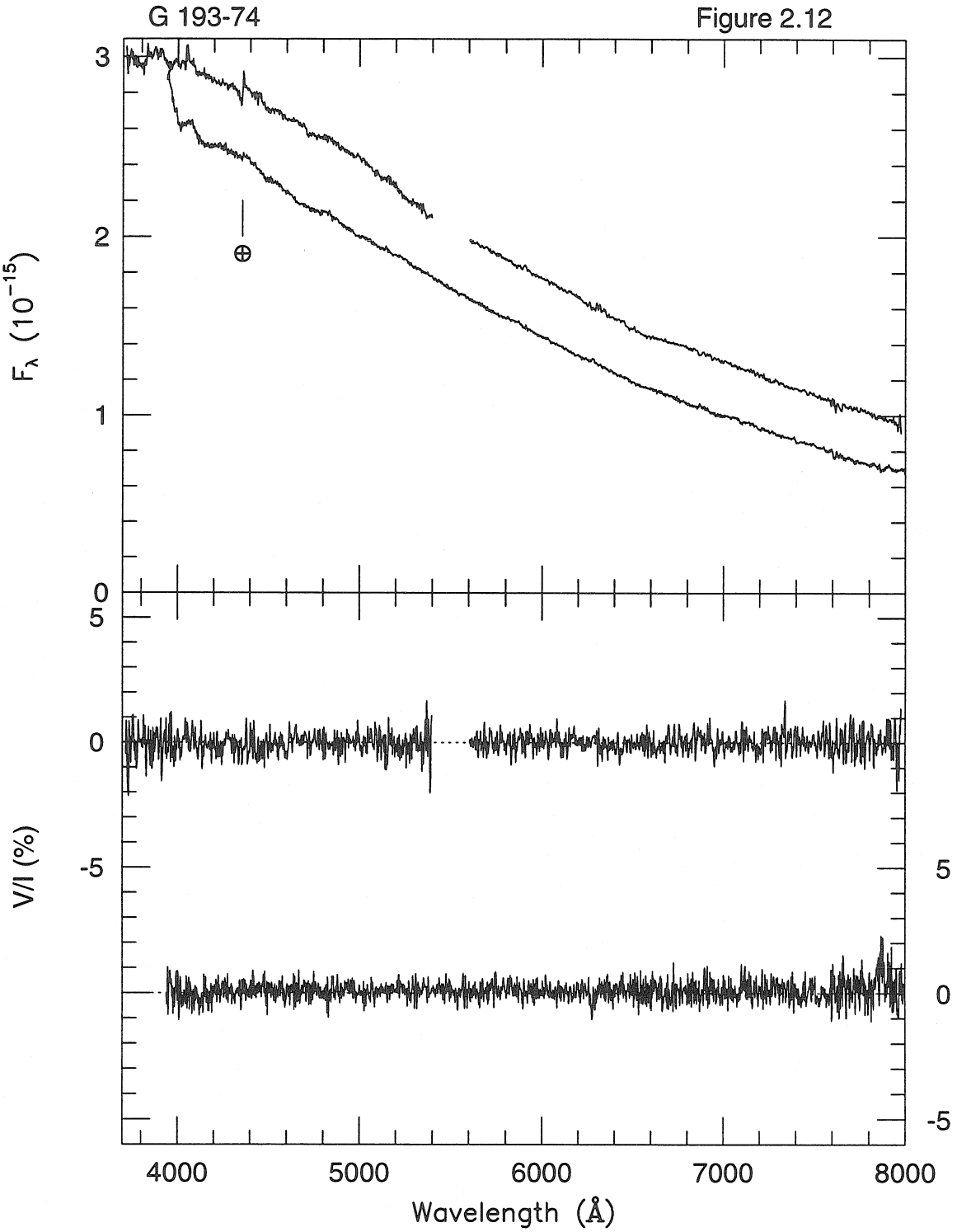
G 193-74
Figure 2.12
3
2
1
0
F_λ (10^{-15})
⊕
5
0
-5
V/I (%)
5
0
-5
4000
5000
6000
7000
8000
Wavelength (Å)

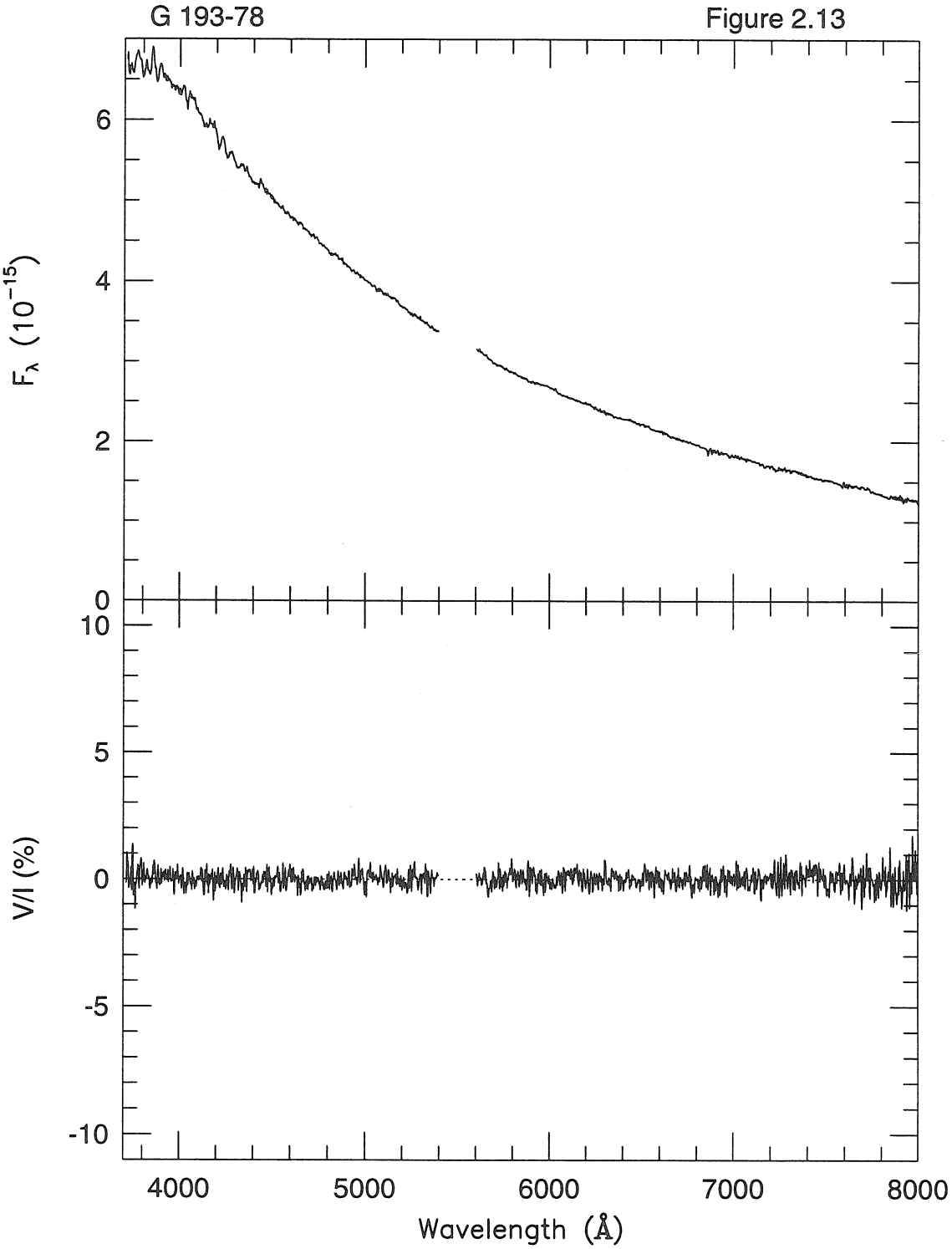
G 193-78
Figure 2.13
6
4
2
0
F_λ (10^{-15})
10
5
0
-5
-10
V/I (%)
4000
5000
6000
7000
8000
Wavelength (Å)

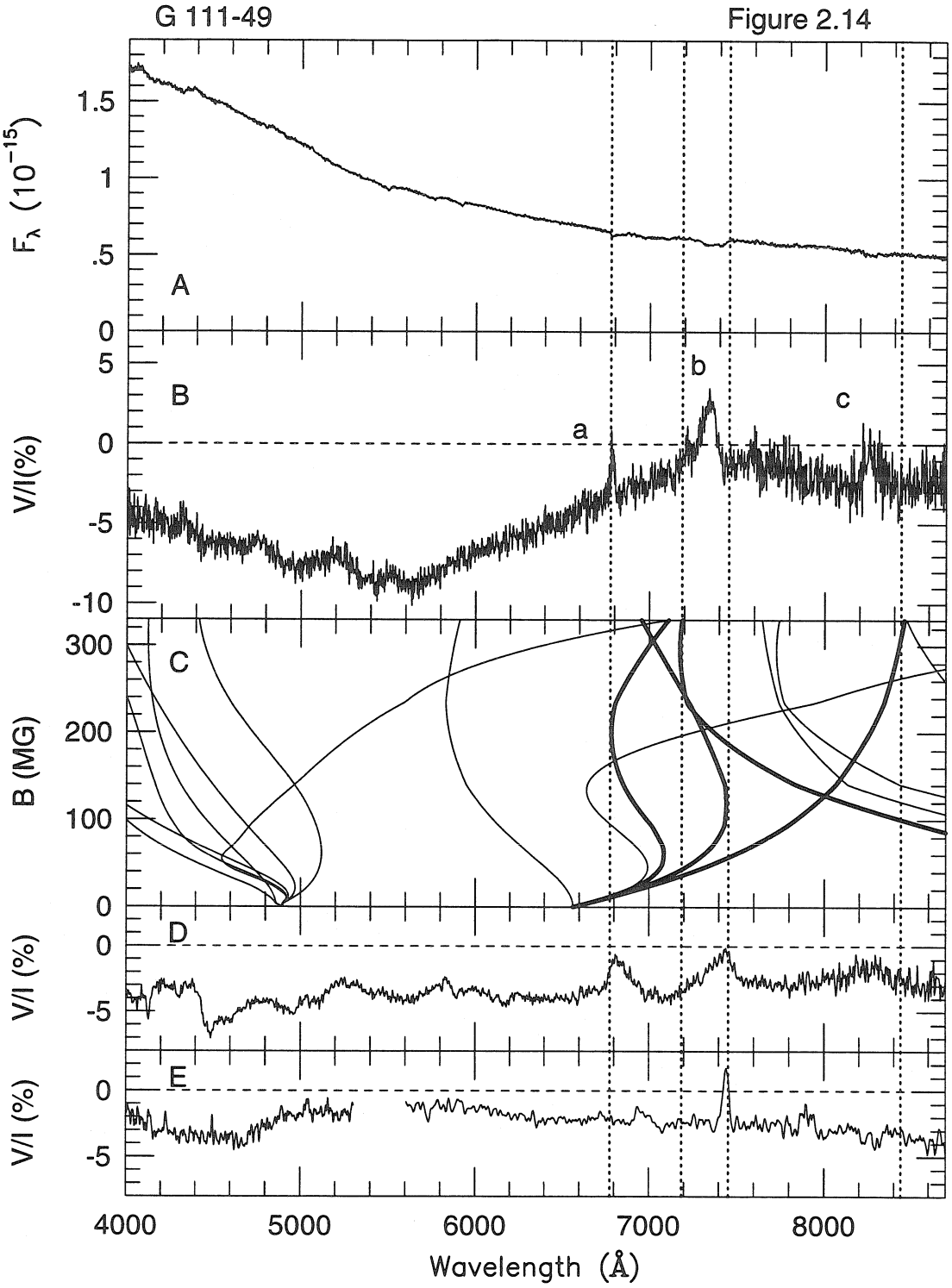
G 111-49
Figure 2.14
F_λ (10^{-15})
1.5
1
.5
0
A
5
0
-5
-10
B
V/I(%)
a
b
c
300
200
100
0
C
B (MG)
0
-5
D
V/I (%)
0
-5
E
V/I (%)
4000
5000
6000
7000
8000
Wavelength (Å)

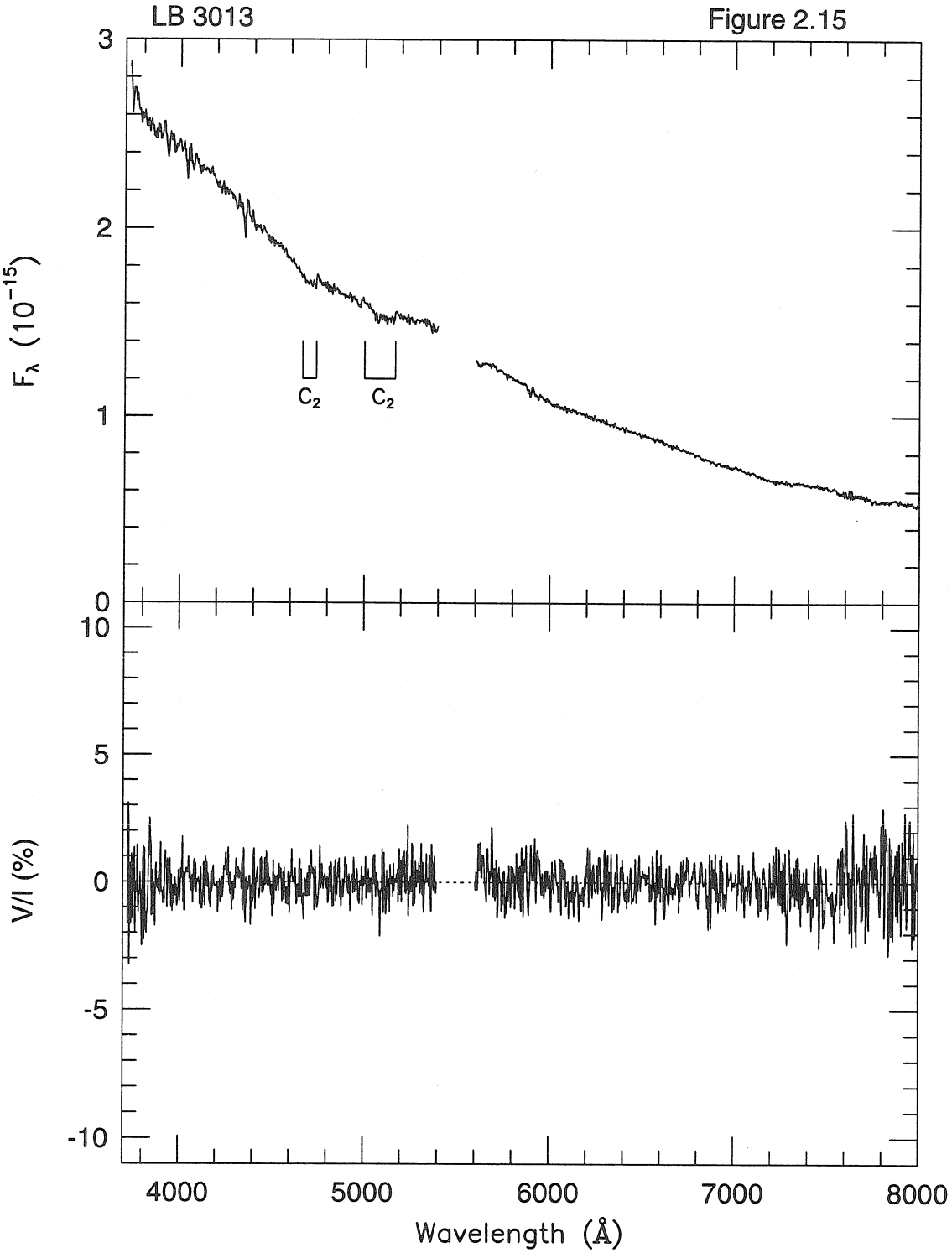
LB 3013
Figure 2.15
3
2
1
0
F_λ (10^{-15})
C_2
C_2
10
5
0
-5
-10
V/I (%)
4000
5000
6000
7000
8000
Wavelength (Å)

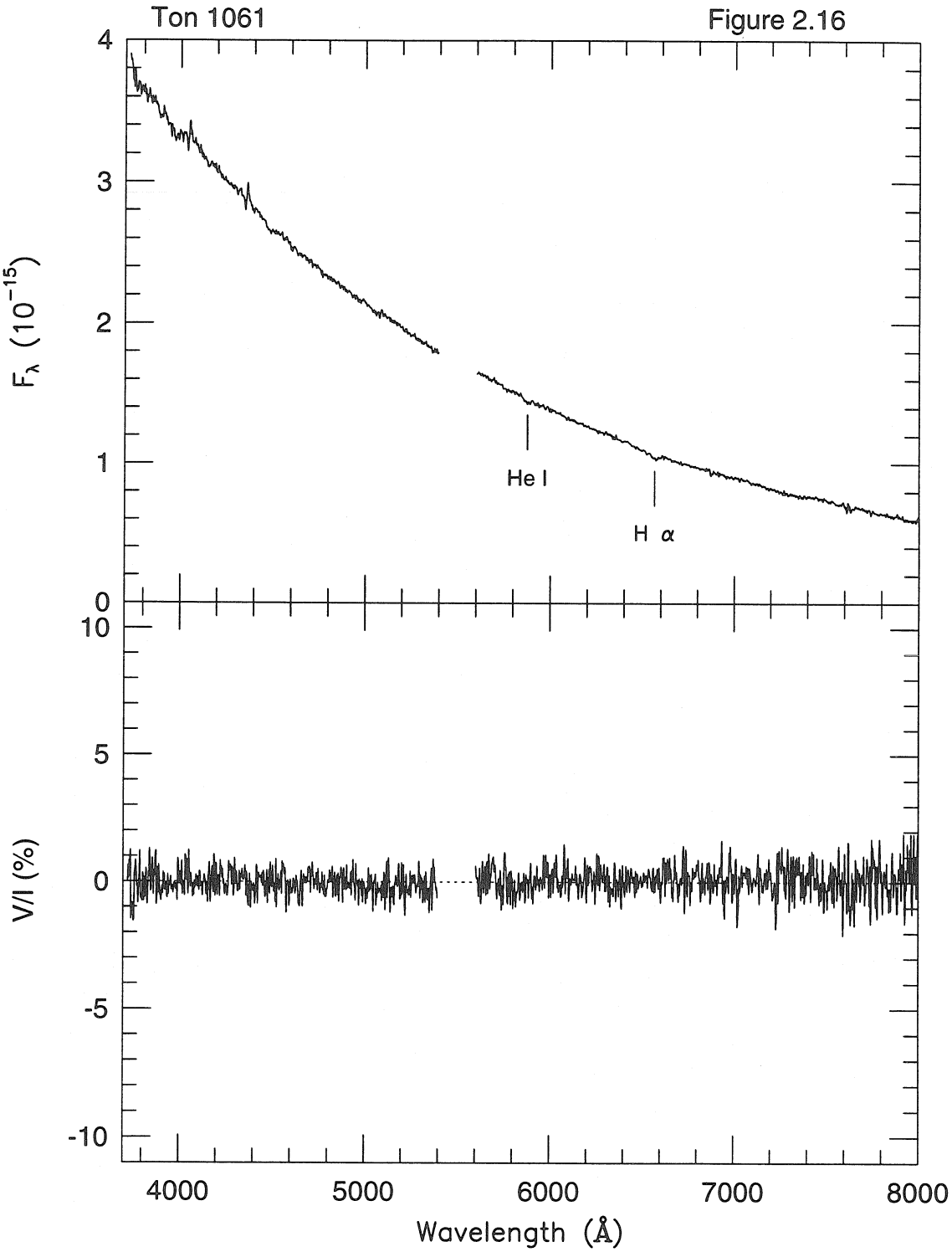
Ton 1061
Figure 2.16
F_λ (10^{-15})
He I
H α
V/I (%)
Wavelength (Å)

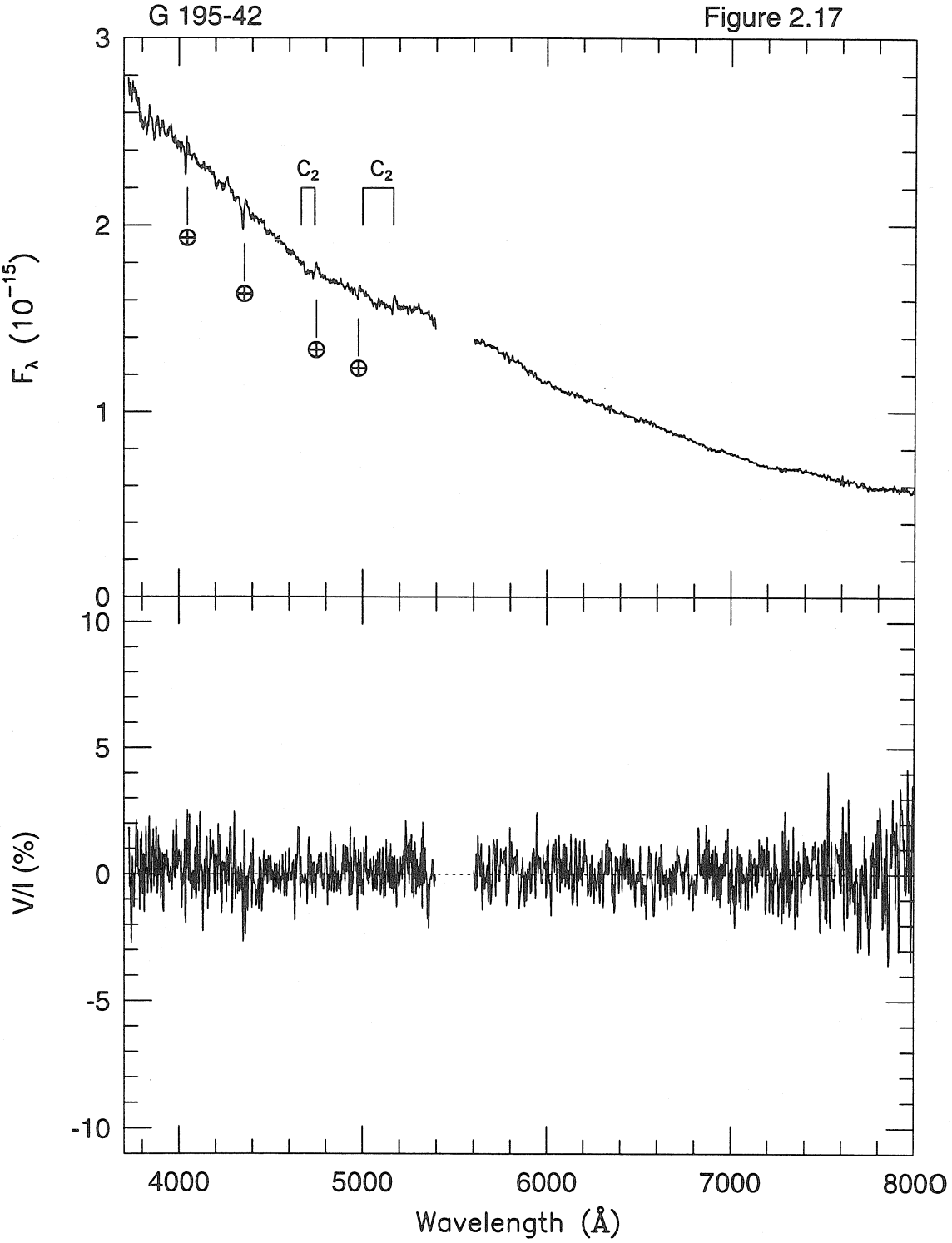
G 195-42
Figure 2.17
F_λ (10^{-15})
V/I (%)
C_2
C_2
Wavelength (Å)
4000
5000
6000
7000
8000

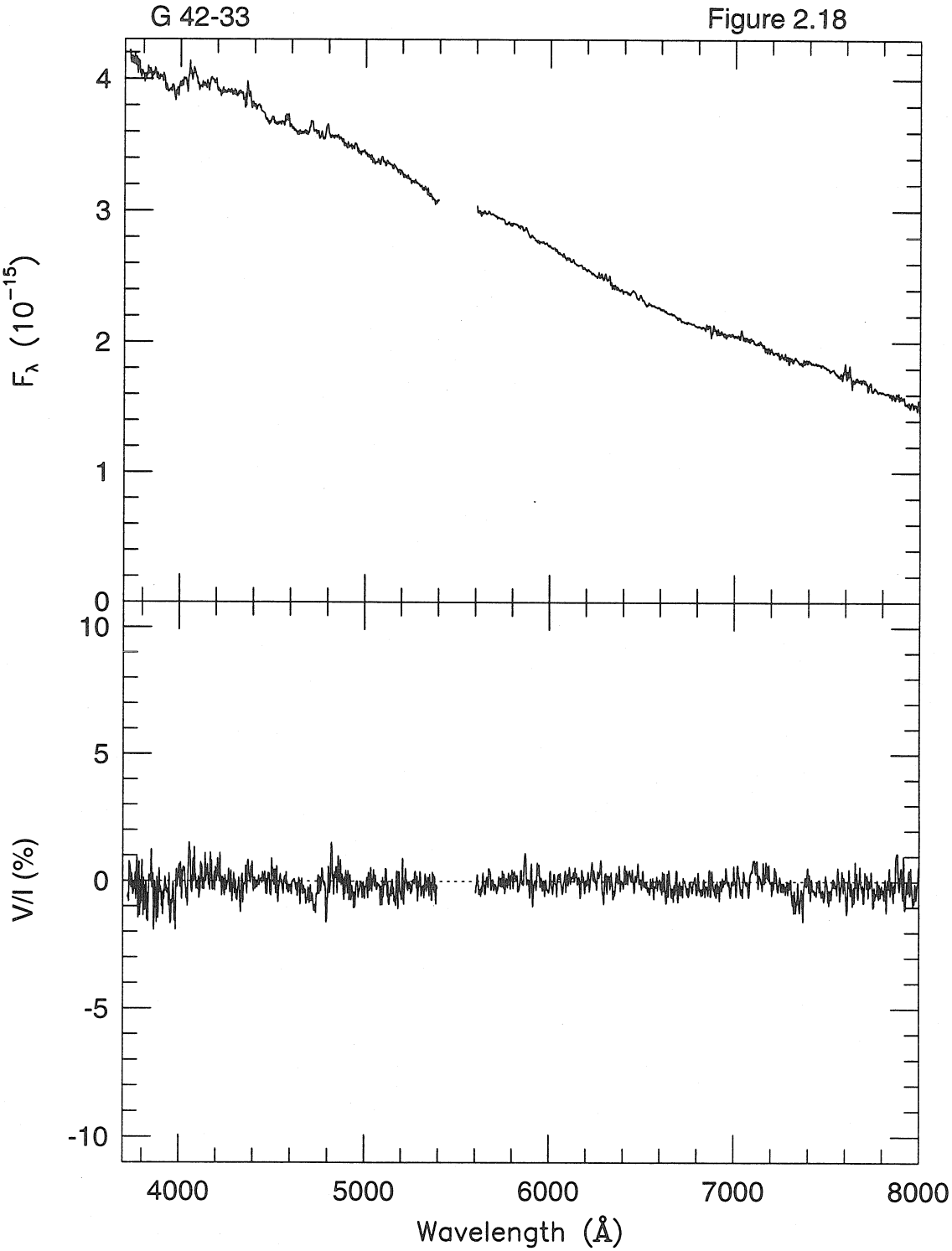
G 42-33
Figure 2.18
F_λ (10^{-15})
4
3
2
1
0
10
5
0
-5
-10
V/I (%)
4000
5000
6000
7000
8000
Wavelength (Å)

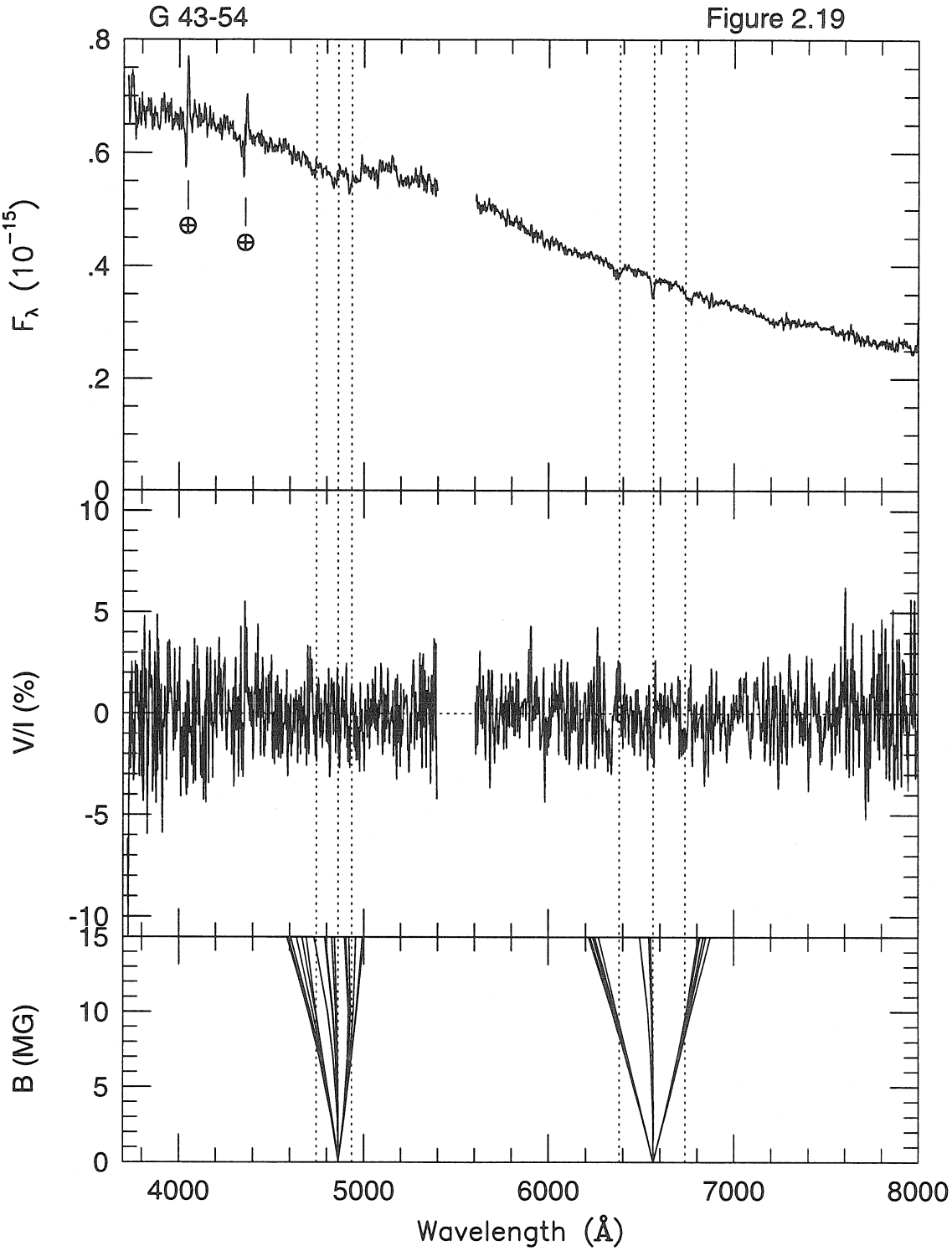
G 43-54
Figure 2.19
F_λ (10^{-15})
V/I (%)
B (MG)
Wavelength (Å)
4000
5000
6000
7000
8000

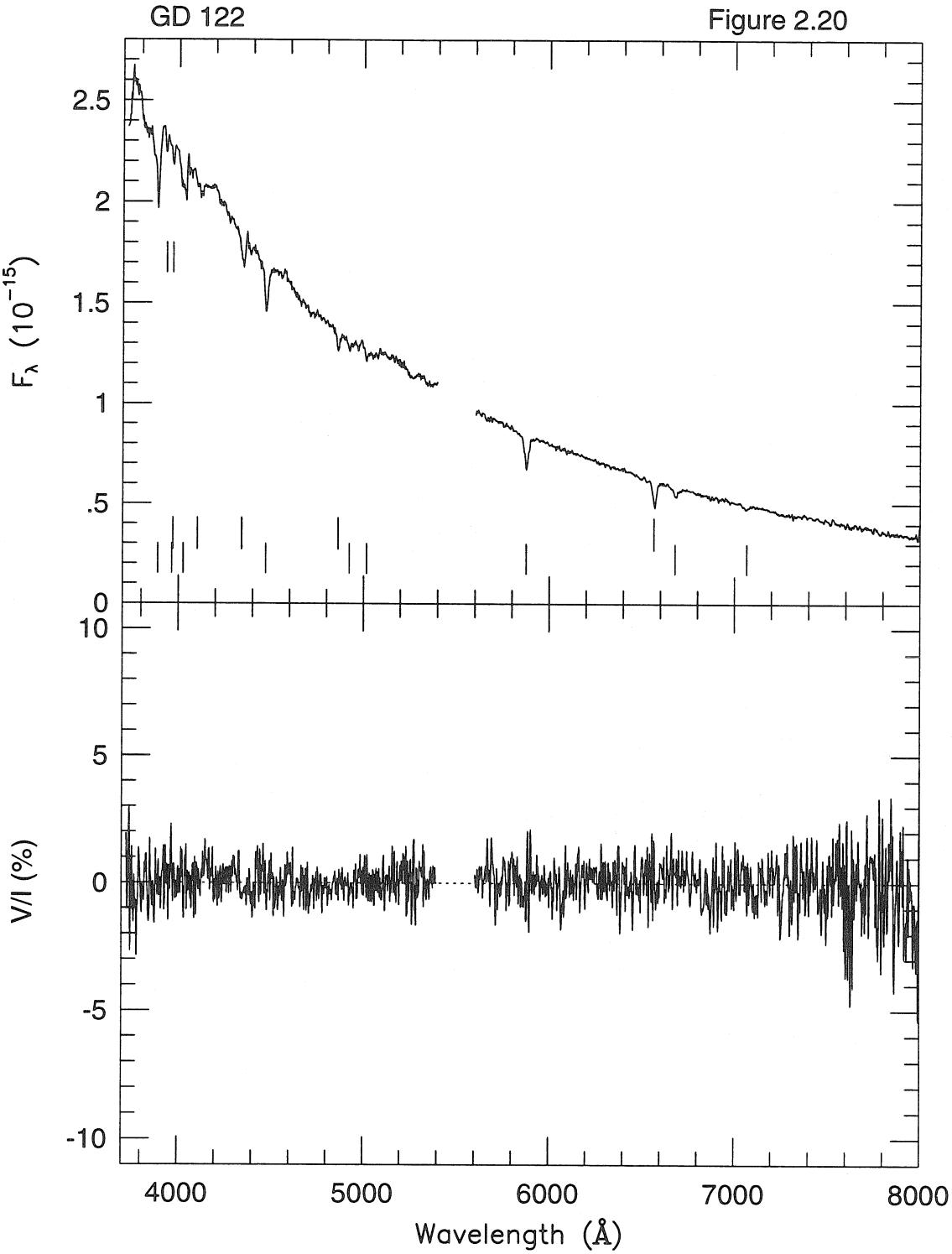
GD 122
Figure 2.20
2.5
2
1.5
1
.5
0
F_λ (10^{-15})
10
5
0
-5
-10
V/I (%)
4000
5000
6000
7000
8000
Wavelength (Å)

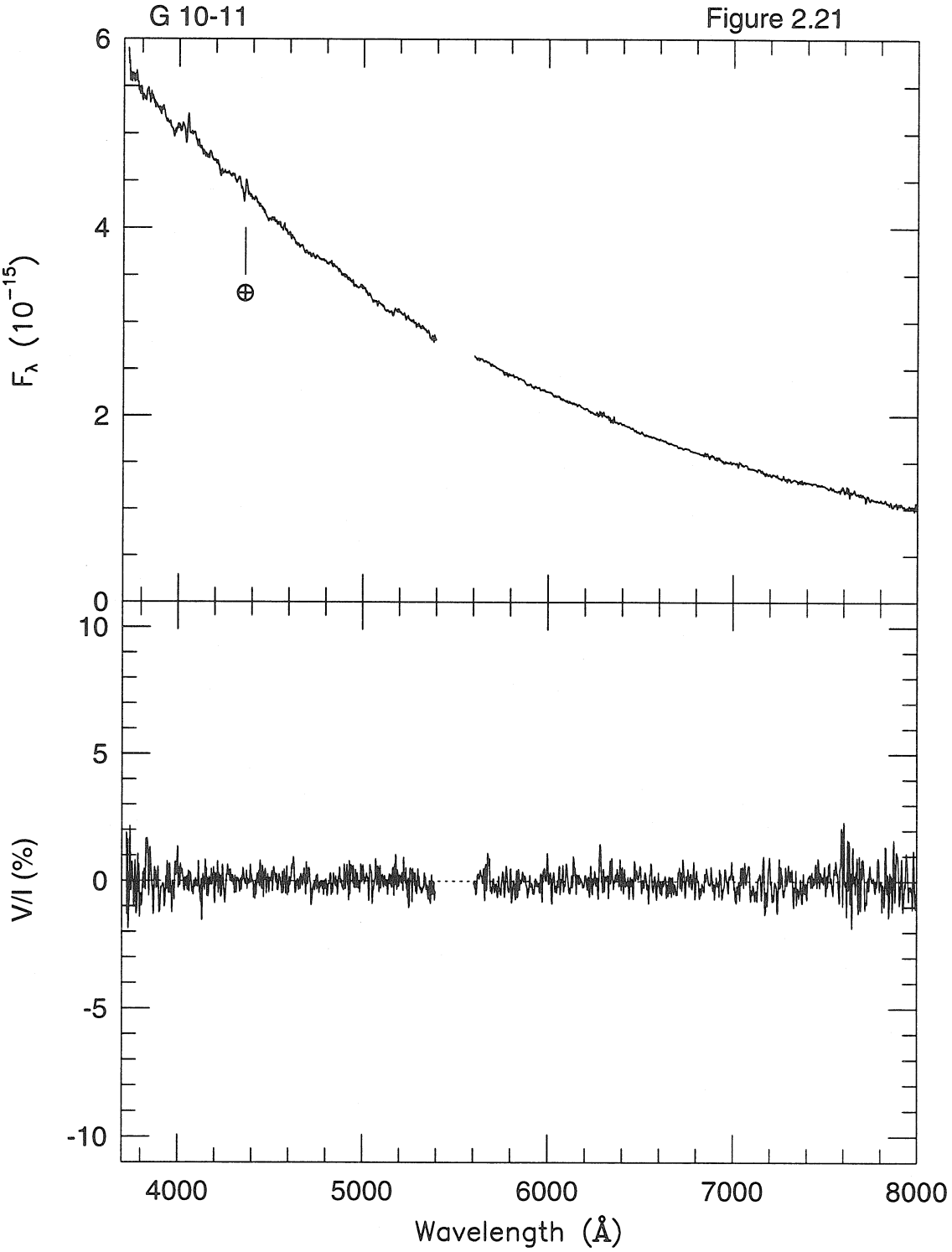
G 10-11
Figure 2.21
6
4
2
0
F_λ (10^{-15})
⊕
10
5
0
-5
-10
V/I (%)
4000
5000
6000
7000
8000
Wavelength (Å)

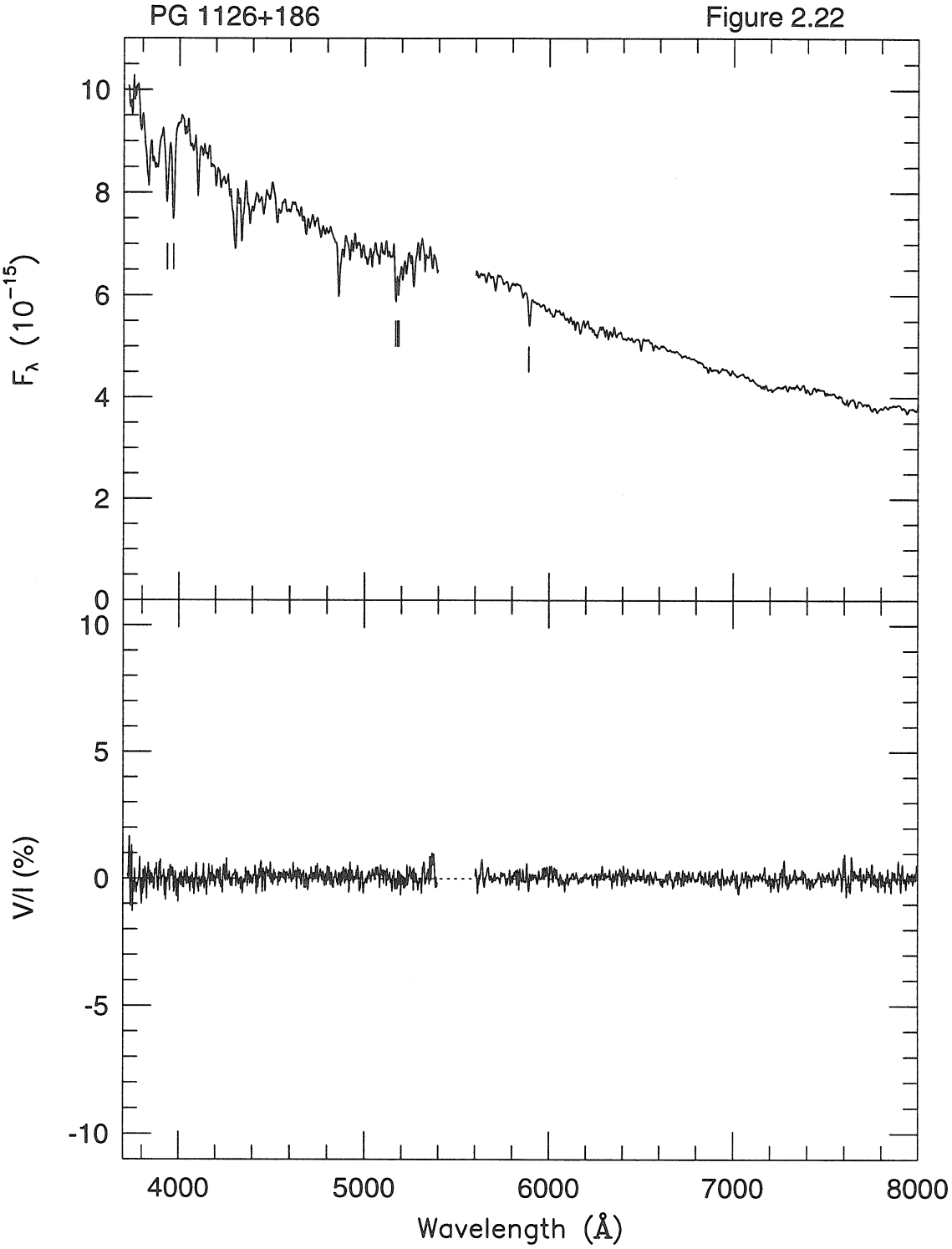
PG 1126+186
Figure 2.22
F_λ (10^{-15})
V/I (%)
Wavelength (Å)
10
8
6
4
2
0
5
-5
-10
4000
5000
6000
7000
8000

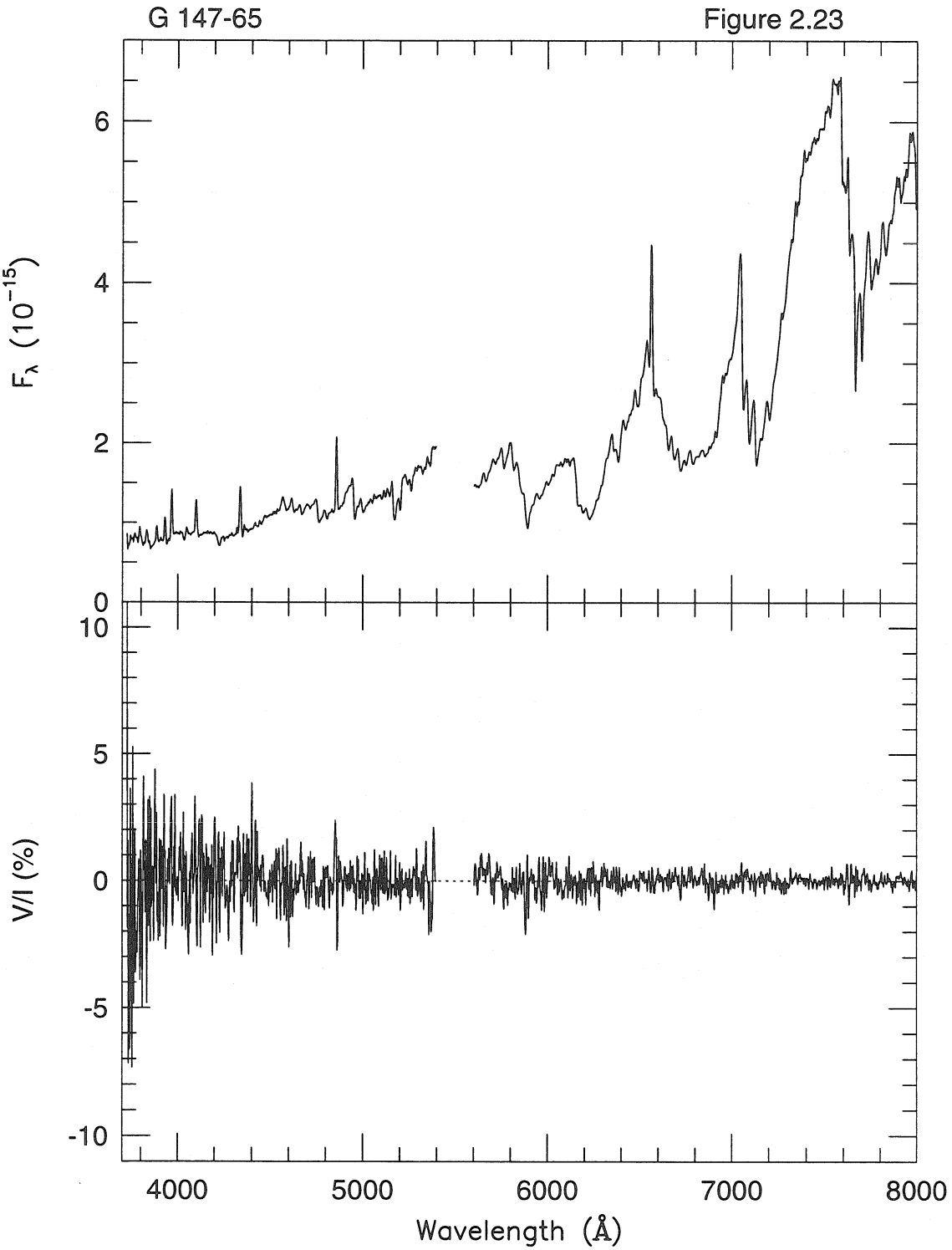
G 147-65
Figure 2.23
6
4
2
0
F_λ (10^{-15})
10
5
0
-5
-10
V/I (%)
4000
5000
6000
7000
8000
Wavelength (Å)

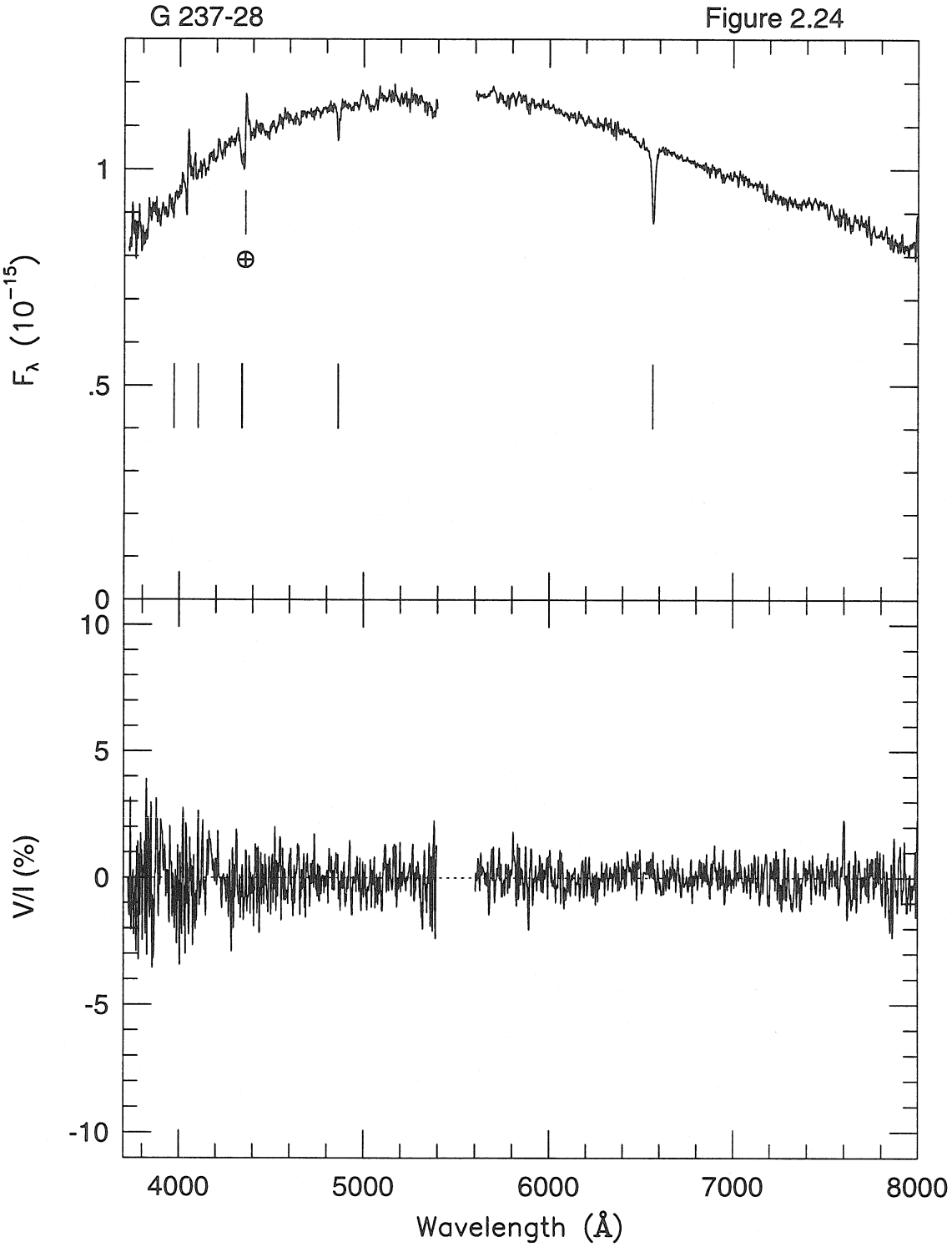
G 237-28
Figure 2.24
F_λ (10^{-15})
1
.5
0
⊕
10
5
0
-5
-10
V/I (%)
4000
5000
6000
7000
8000
Wavelength (Å)

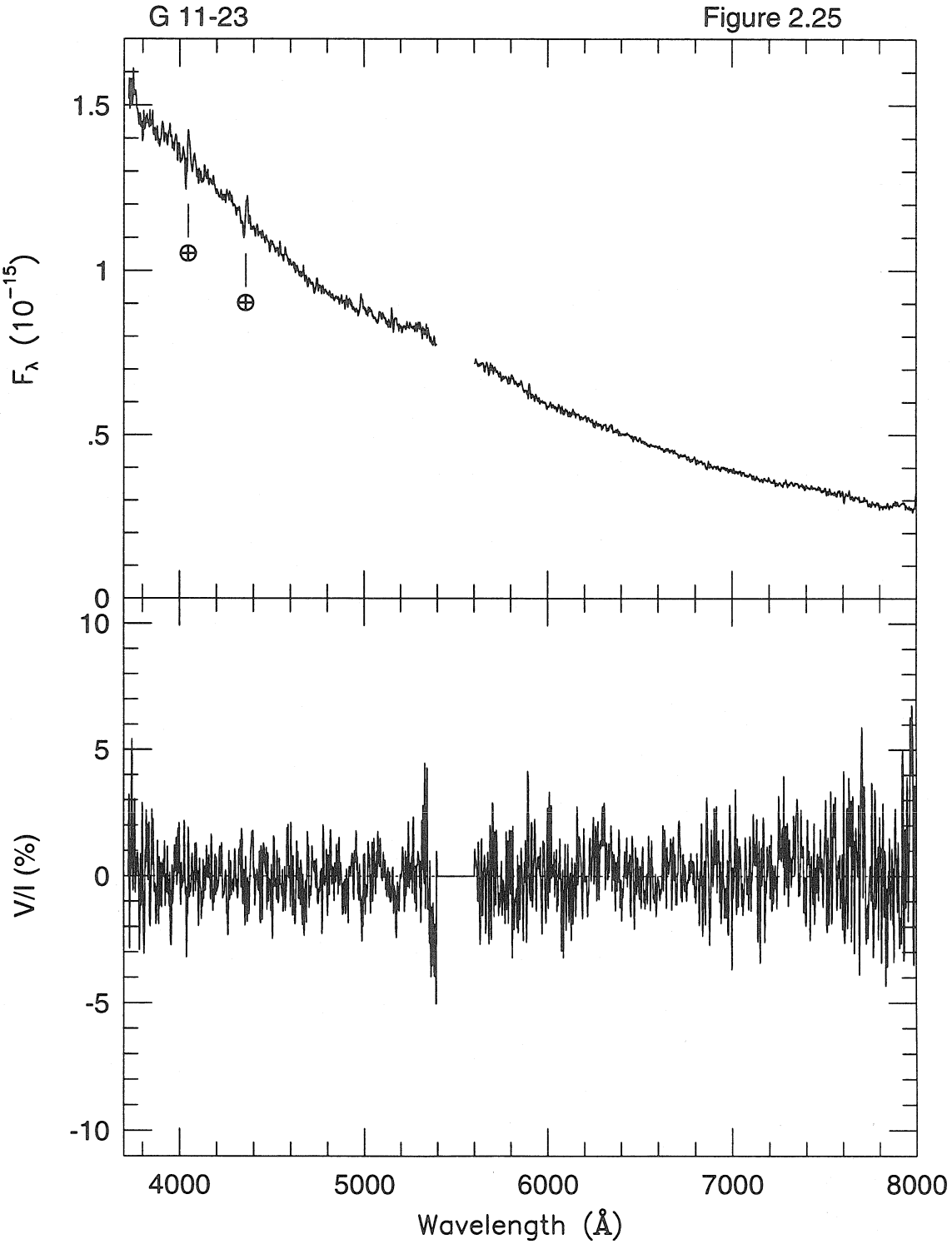
G 11-23
Figure 2.25
1.5
1
.5
0
F_λ (10^{-15})
⊕
⊕
10
5
0
-5
-10
V/I (%)
4000
5000
6000
7000
8000
Wavelength (Å)

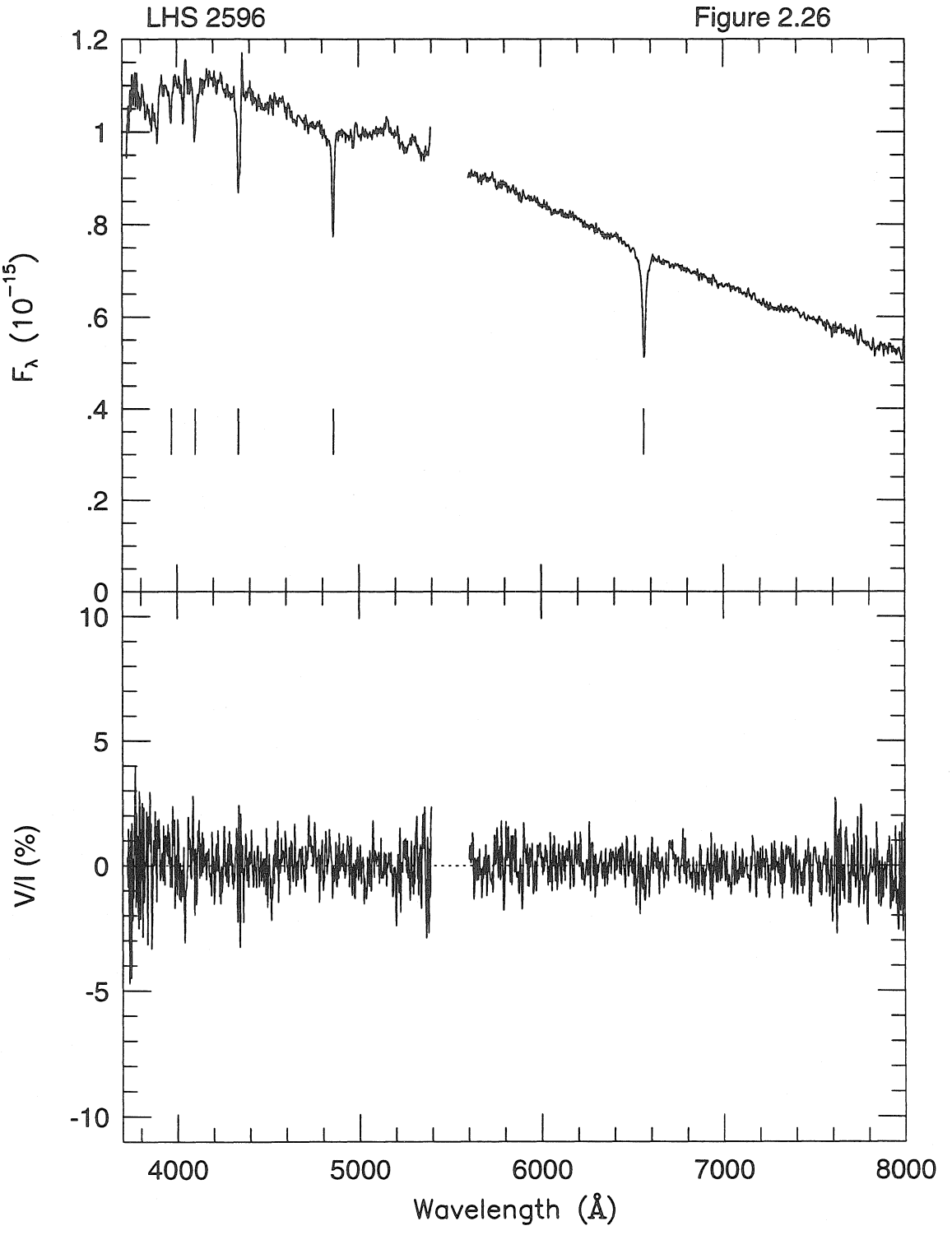
LHS 2596
Figure 2.26
1.2
1
.8
.6
.4
.2
0
F_λ (10^{-15})
10
5
0
-5
-10
V/I (%)
4000
5000
6000
7000
8000
Wavelength (Å)

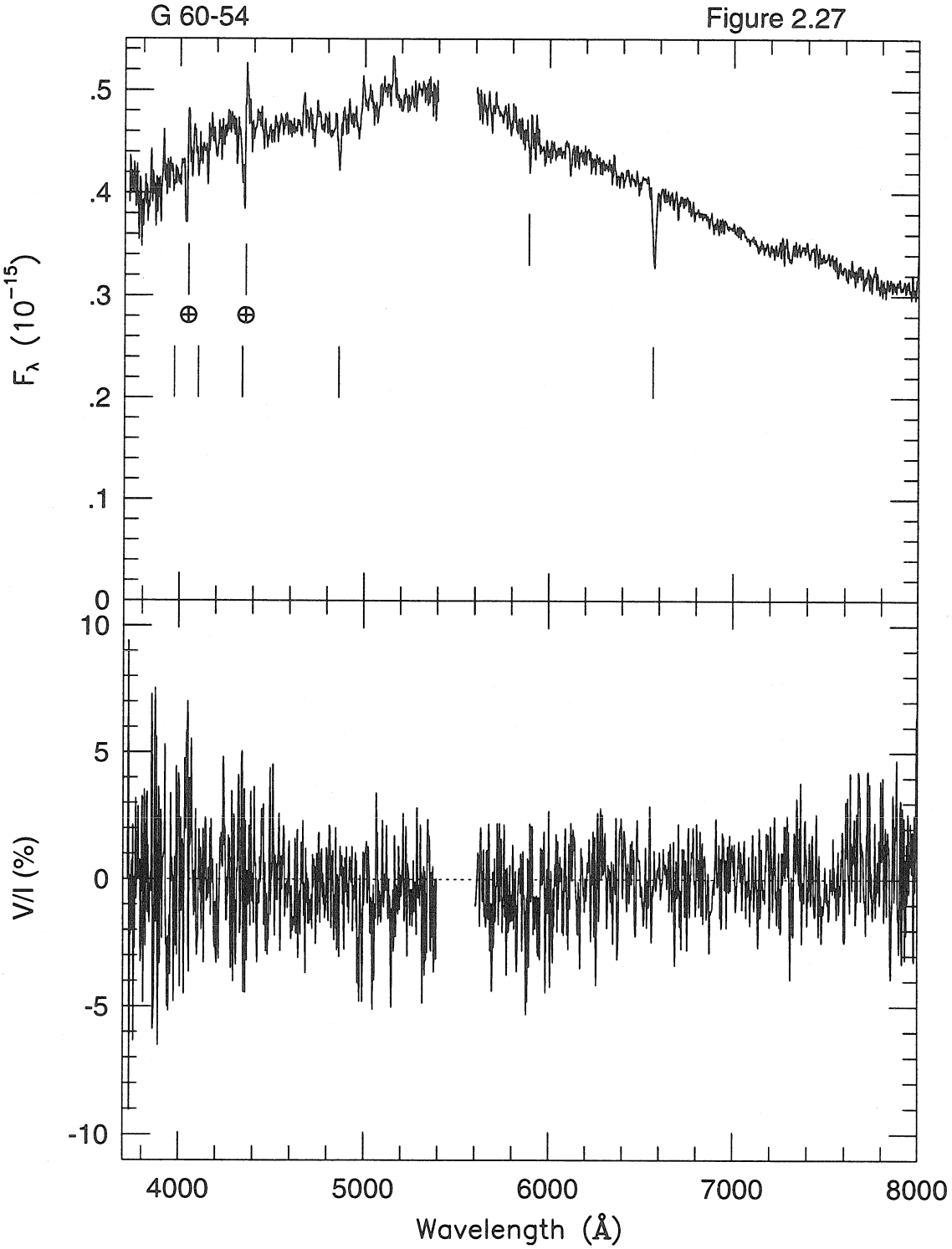
G 60-54
Figure 2.27
F_λ (10^{-15})
.5
.4
.3
.2
.1
0
10
5
0
-5
-10
V/I (%)
4000
5000
6000
7000
8000
Wavelength (Å)

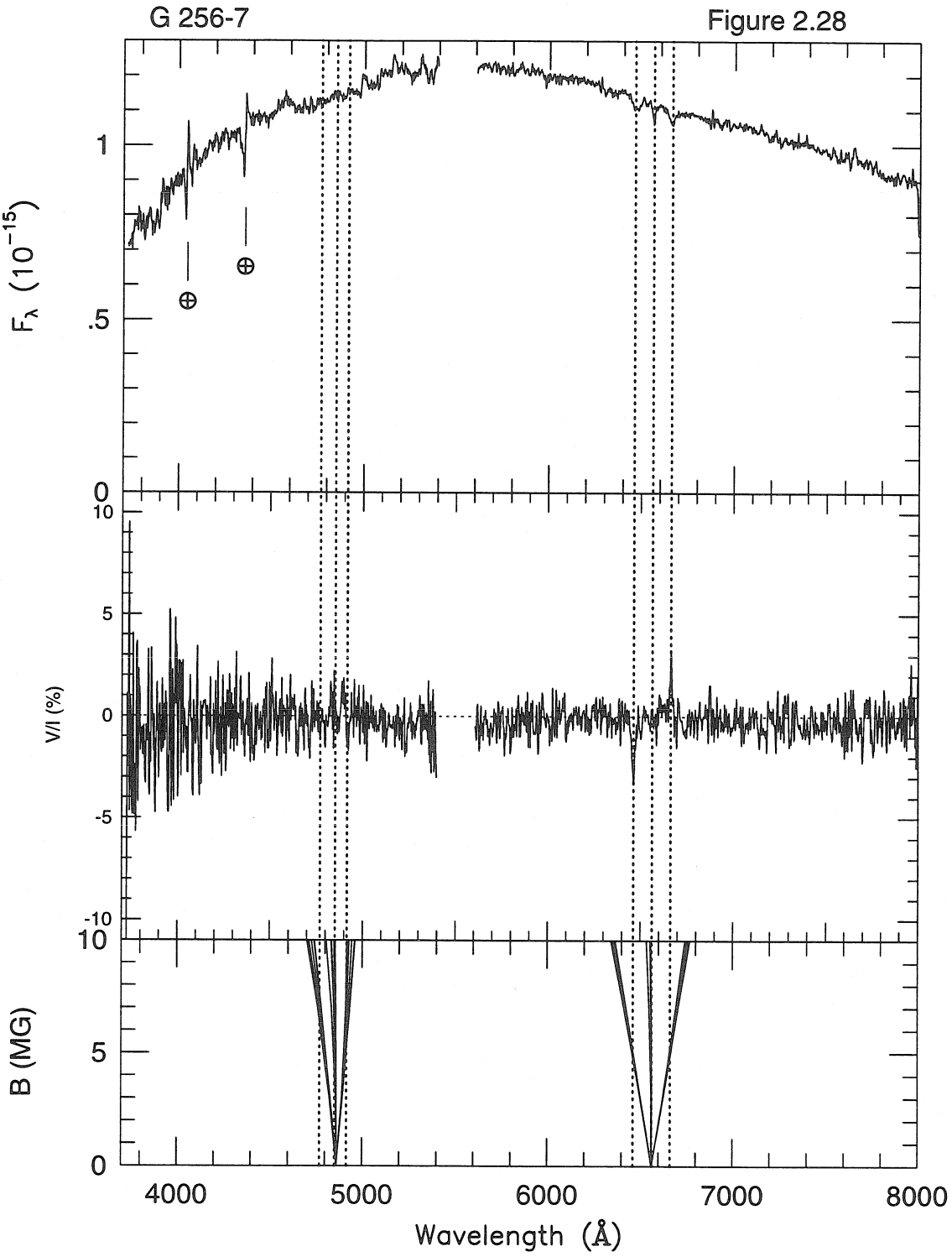
G 256-7
Figure 2.28
F_λ (10^{-15})
1
.5
0
⊕
⊕
10
5
0
-5
-10
V/I (%)
10
5
0
B (MG)
4000
5000
6000
7000
8000
Wavelength (Å)

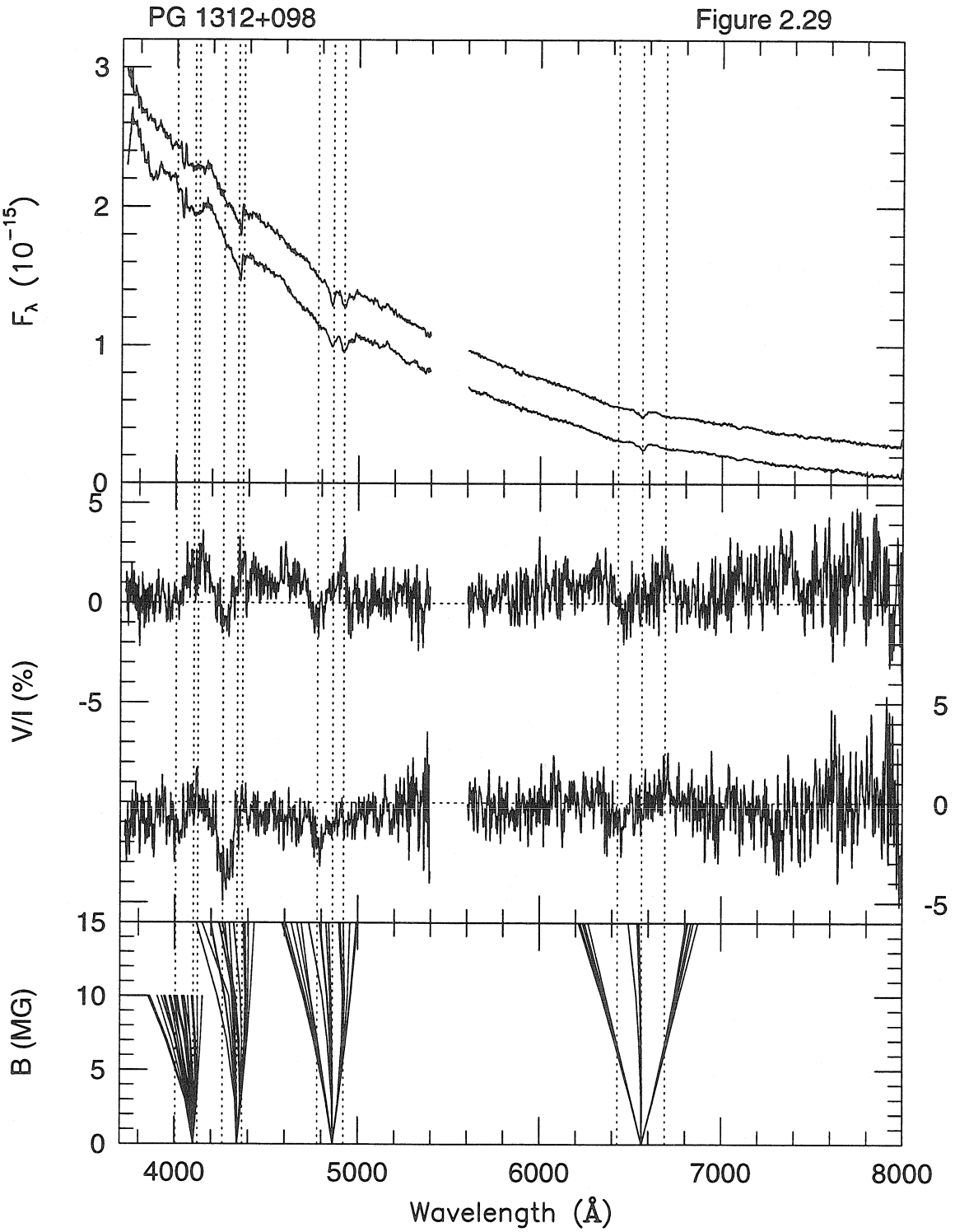
PG 1312+098
Figure 2.29
F_λ (10^{-15})
V/I (%)
B (MG)
Wavelength (Å)
4000
5000
6000
7000
8000

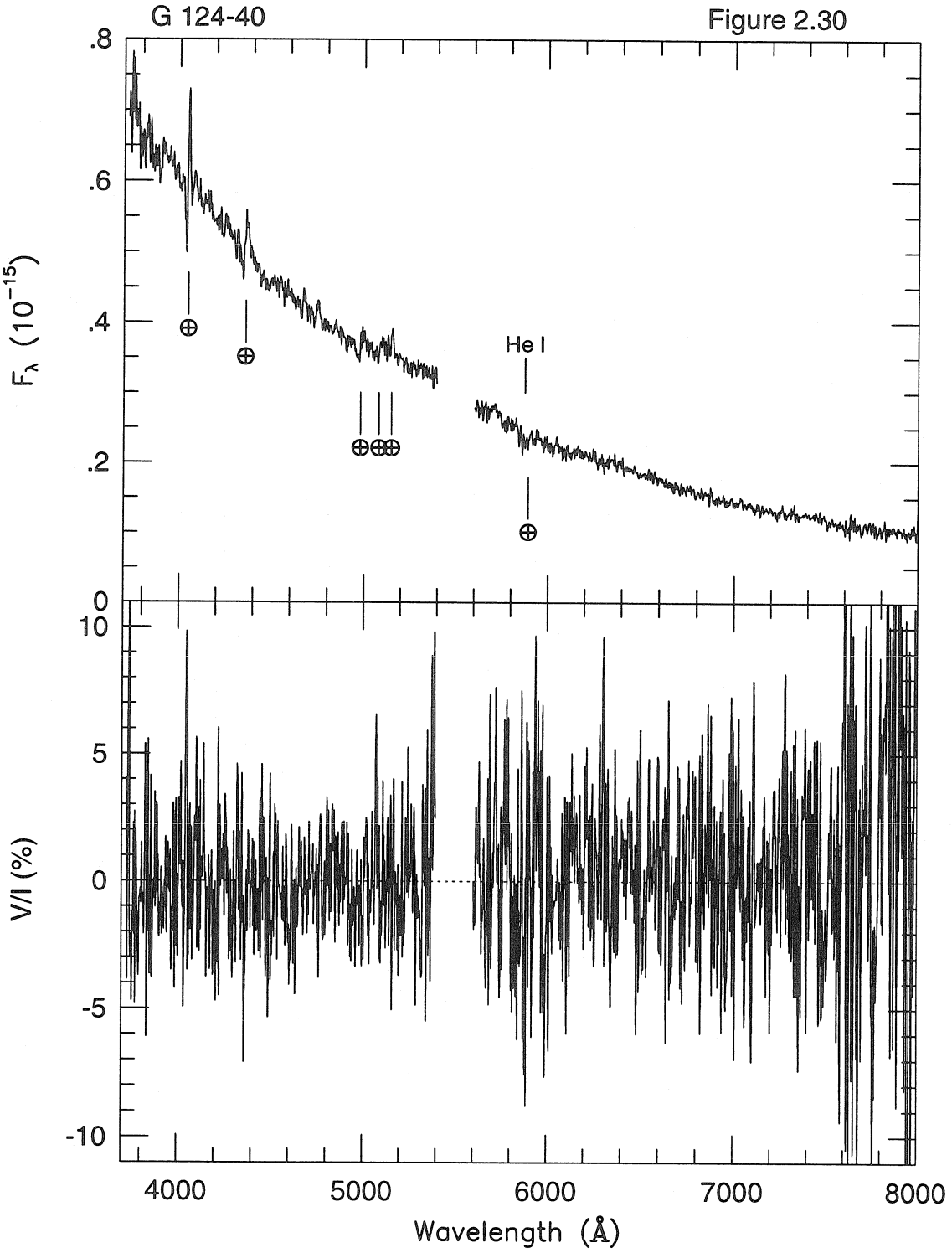
G 124-40
Figure 2.30
.8
.6
.4
.2
0
F_λ (10^{-15})
He I
10
5
0
-5
-10
V/I (%)
4000
5000
6000
7000
8000
Wavelength (Å)

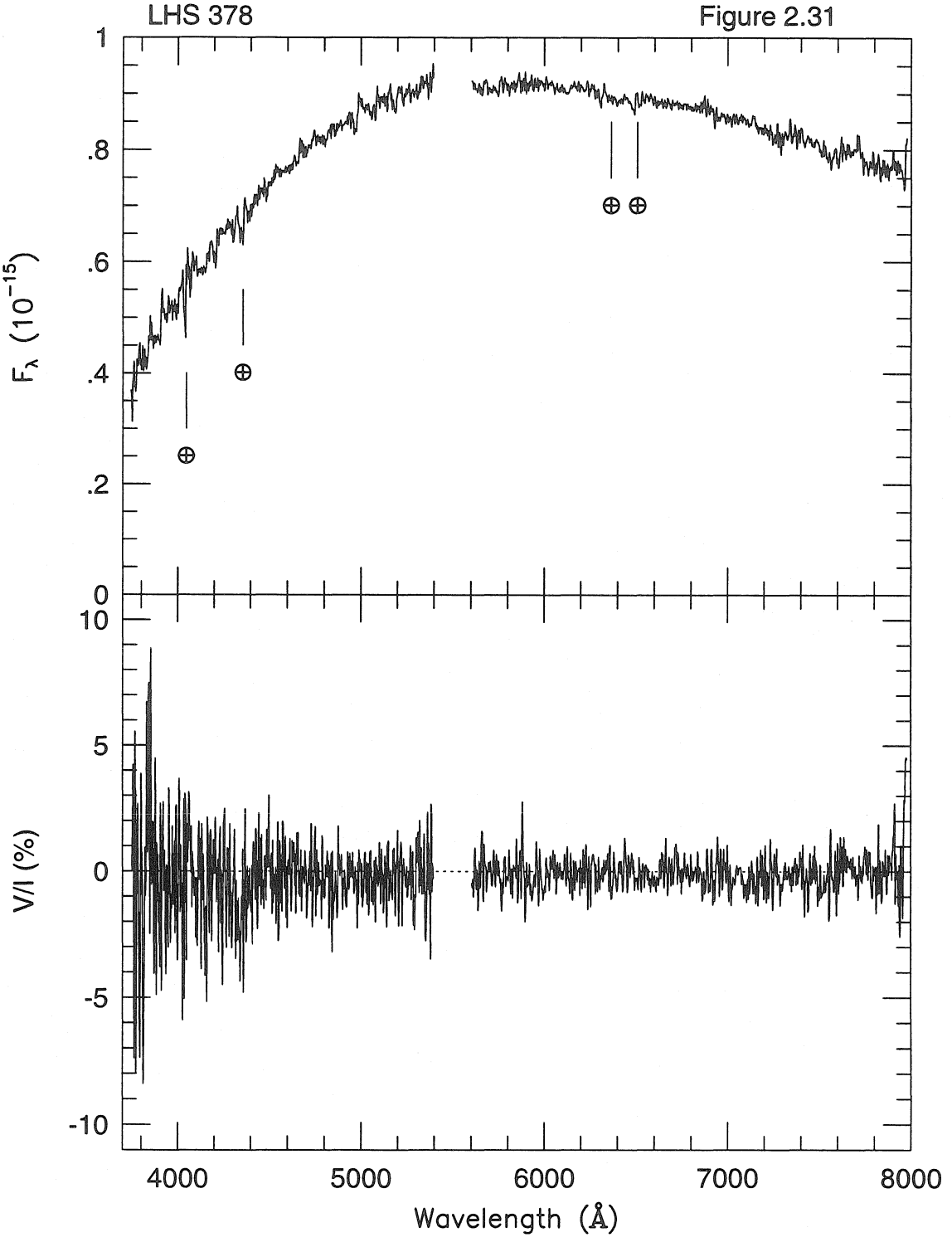
LHS 378
Figure 2.31
1
.8
.6
.4
.2
0
F_λ (10^{-15})
⊕
⊕
⊕ ⊕
10
5
0
-5
-10
V/I (%)
4000
5000
6000
7000
8000
Wavelength (Å)

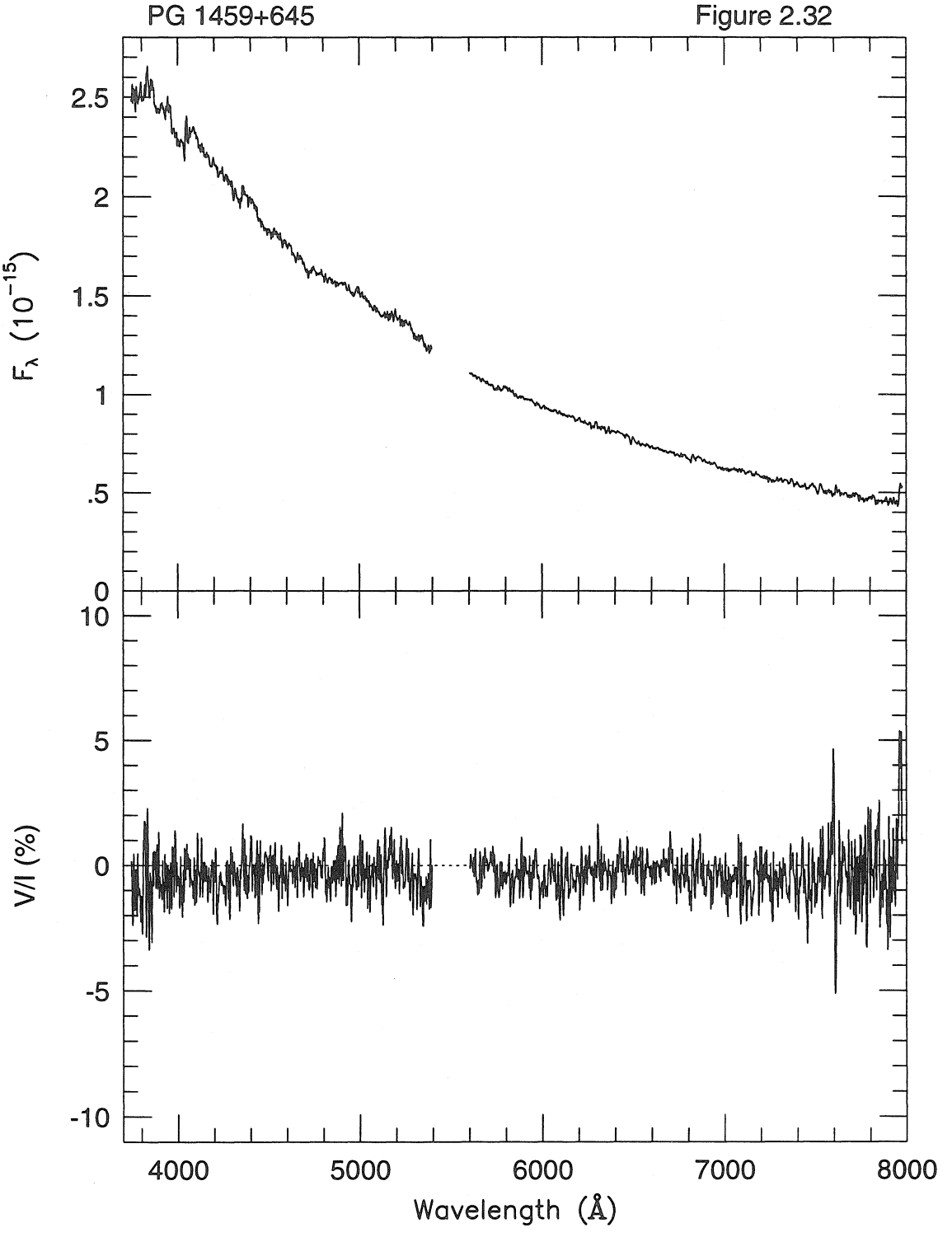
PG 1459+645
Figure 2.32
2.5
2
1.5
1
.5
0
F_λ (10^{-15})
10
5
0
-5
-10
V/I (%)
4000
5000
6000
7000
8000
Wavelength (Å)

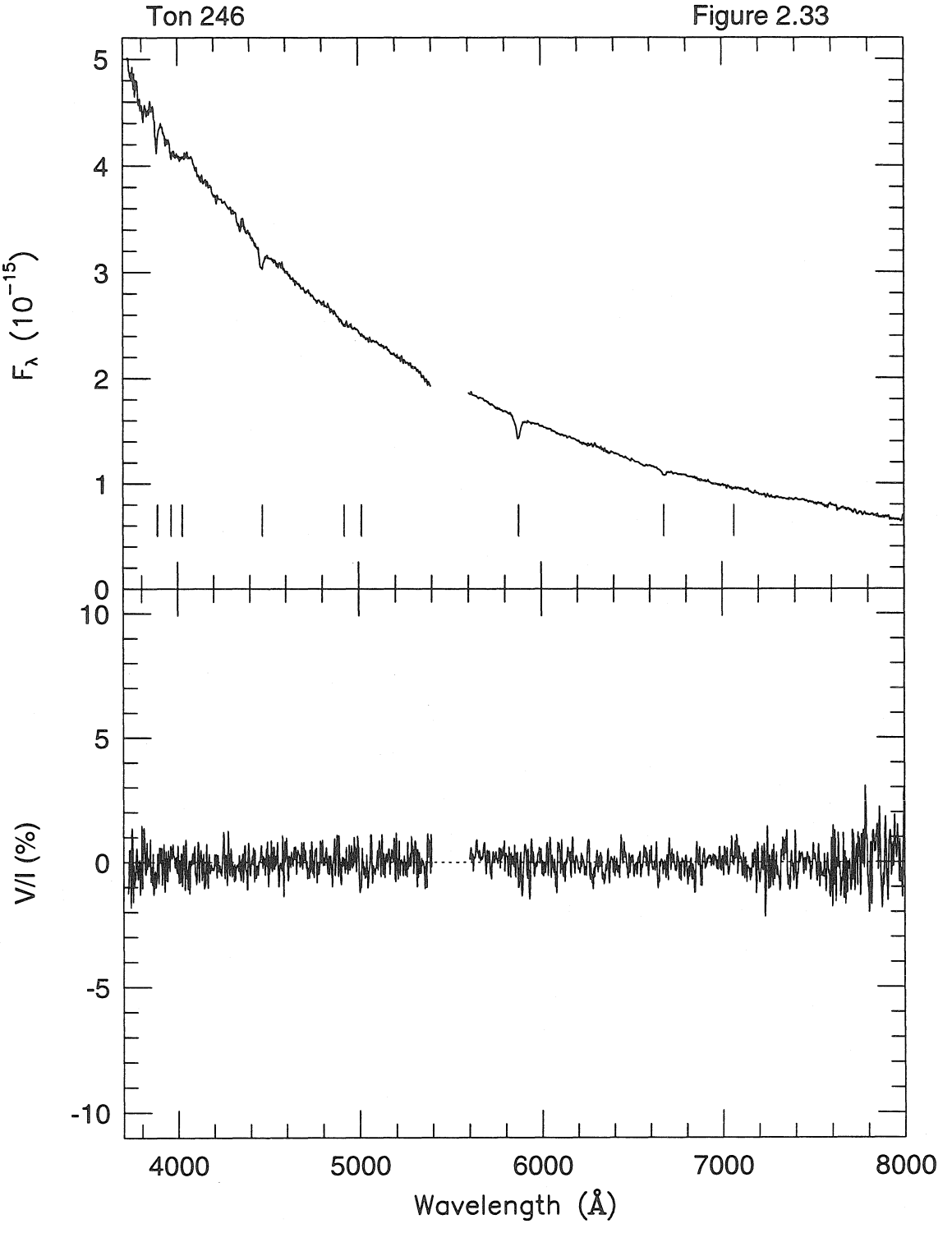
Ton 246
Figure 2.33
F_λ (10^{-15})
V/I (%)
Wavelength (Å)
5
4
3
2
1
0
10
5
0
-5
-10
4000
5000
6000
7000
8000

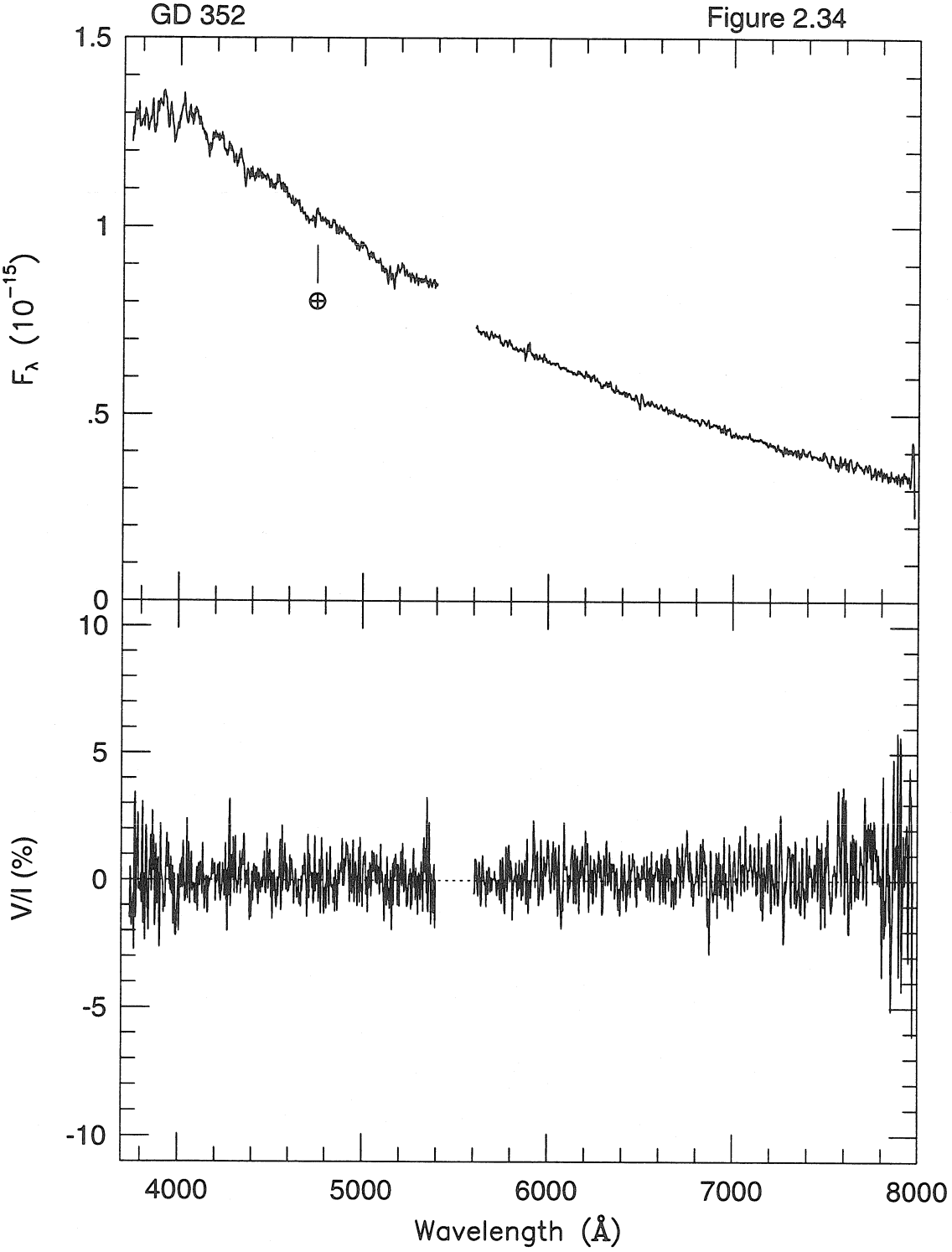
GD 352
Figure 2.34
1.5
1
.5
0
F_λ (10^{-15})
⊕
10
5
0
-5
-10
V/I (%)
4000
5000
6000
7000
8000
Wavelength (Å)

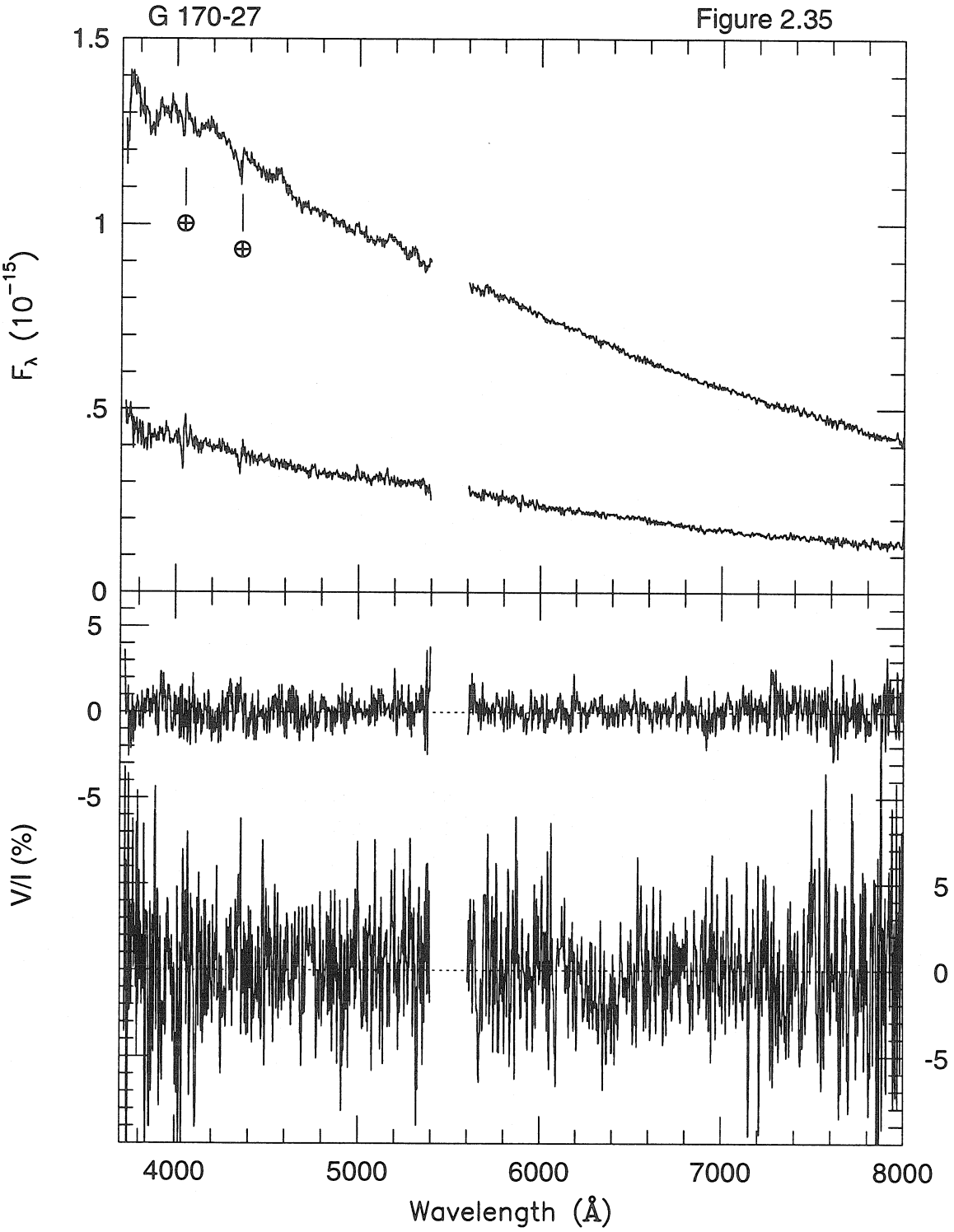
G 170-27
Figure 2.35
1.5
1
.5
0
F_λ (10^{-15})
⊕
⊕
5
0
-5
V/I (%)
5
0
-5
4000
5000
6000
7000
8000
Wavelength (Å)

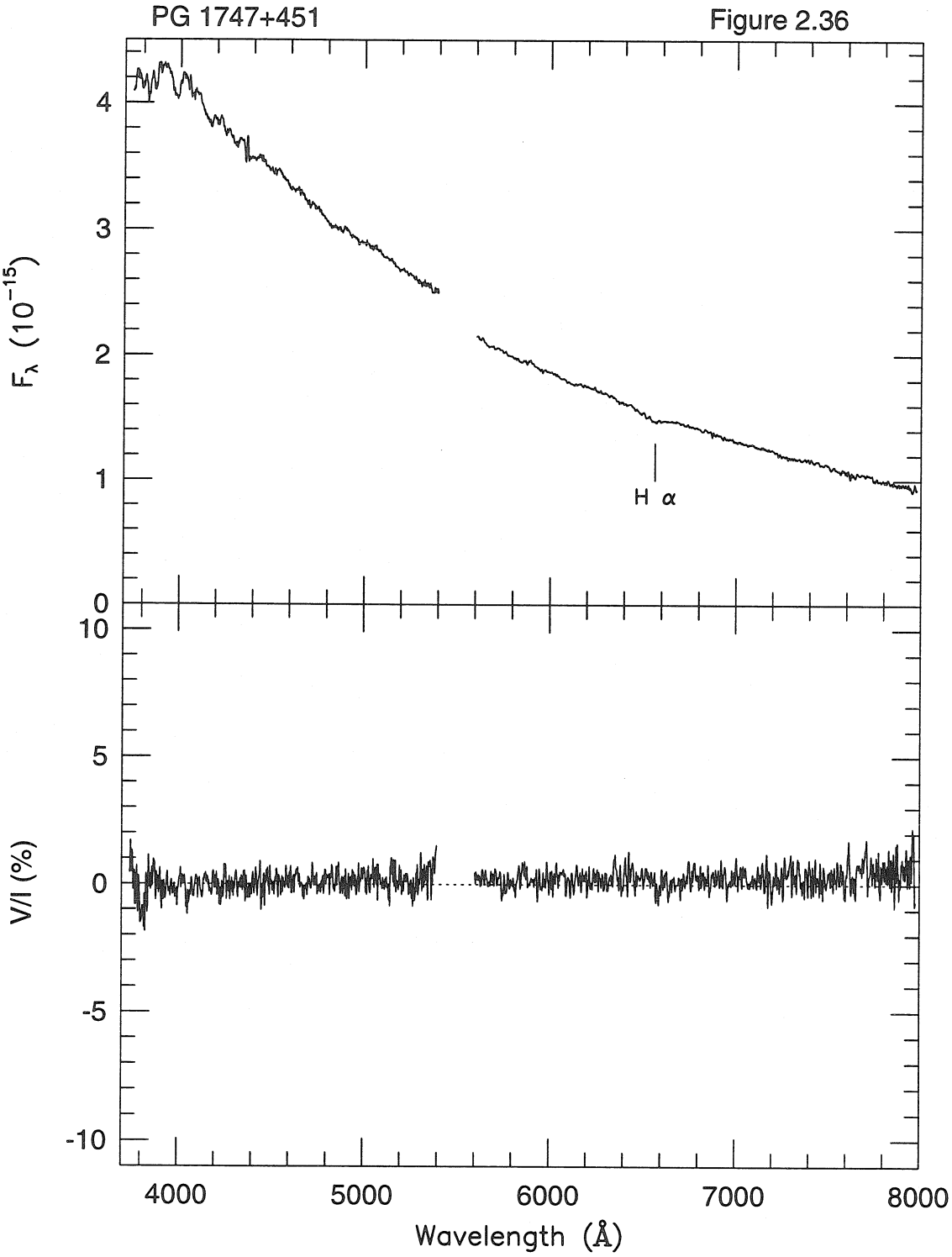
PG 1747+451
Figure 2.36
F_λ (10^{-15})
4
3
2
1
0
H α
10
5
0
-5
-10
V/I (%)
4000
5000
6000
7000
8000
Wavelength (Å)

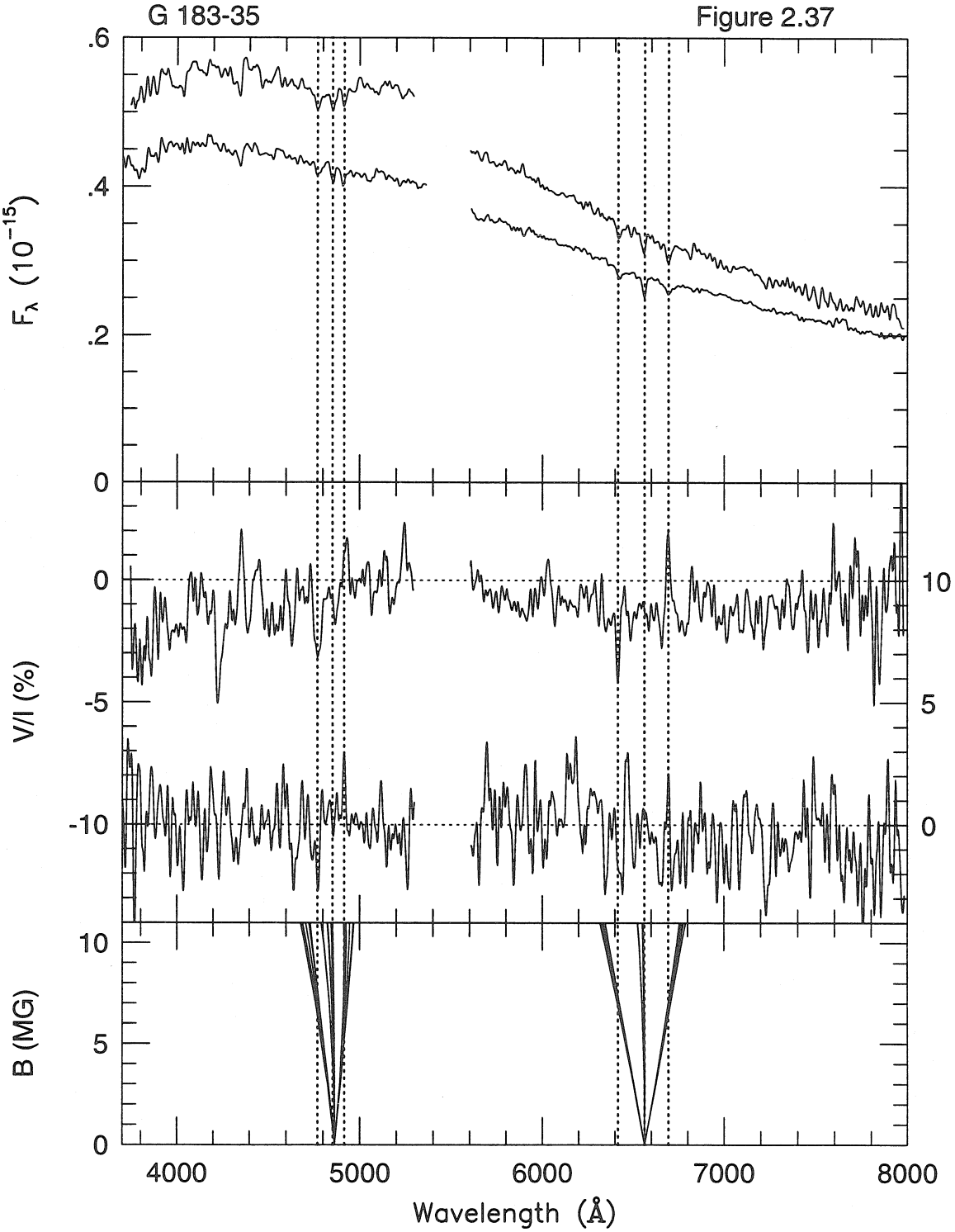
G 183-35
Figure 2.37
.6
.4
.2
0
F_λ (10^{-15})
0
-5
-10
V/I (%)
10
5
0
10
5
0
B (MG)
4000
5000
6000
7000
8000
Wavelength (Å)

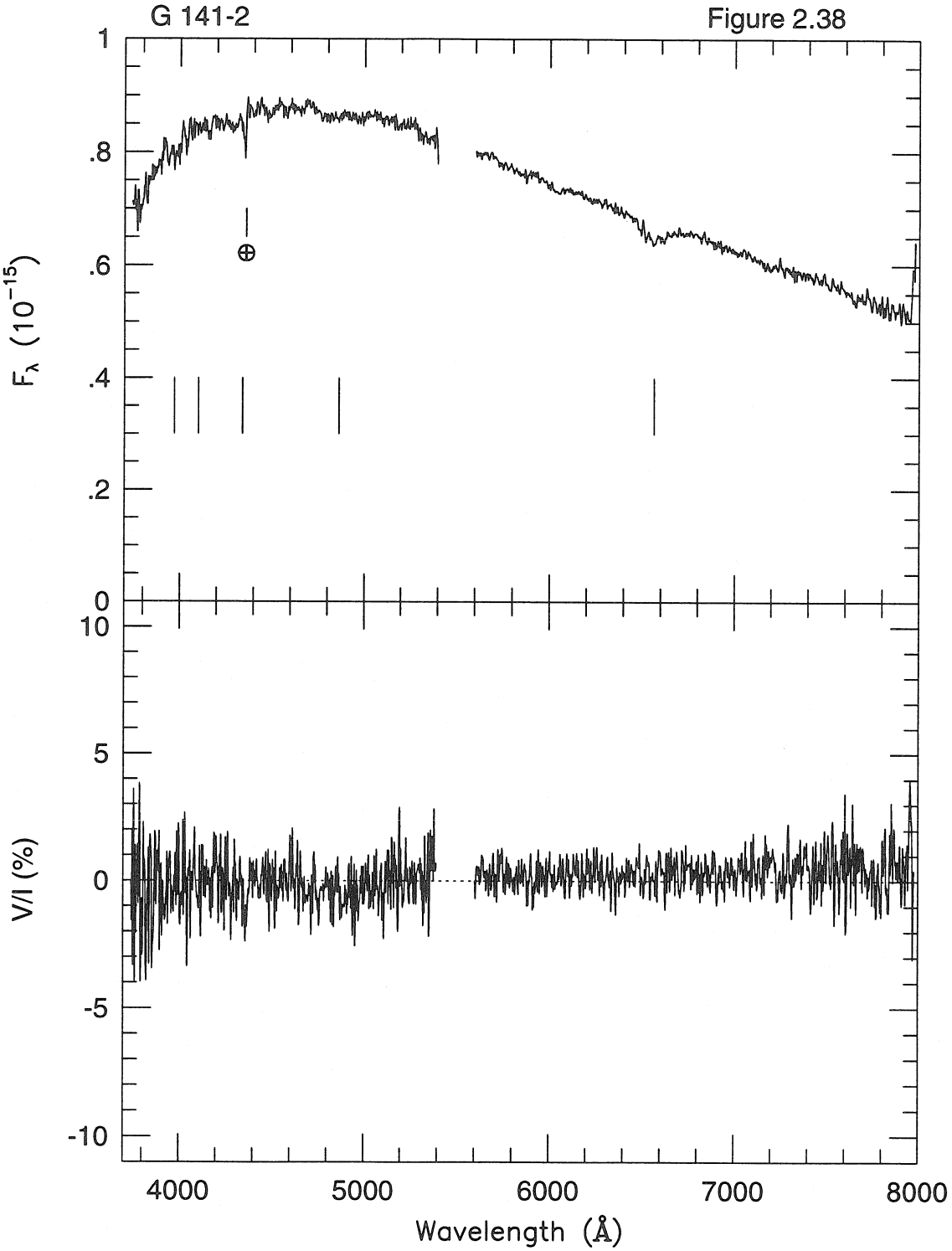
G 141-2
Figure 2.38
1
.8
.6
.4
.2
0
F_λ (10^{-15})
⊕
10
5
0
-5
-10
V/I (%)
4000
5000
6000
7000
8000
Wavelength (Å)

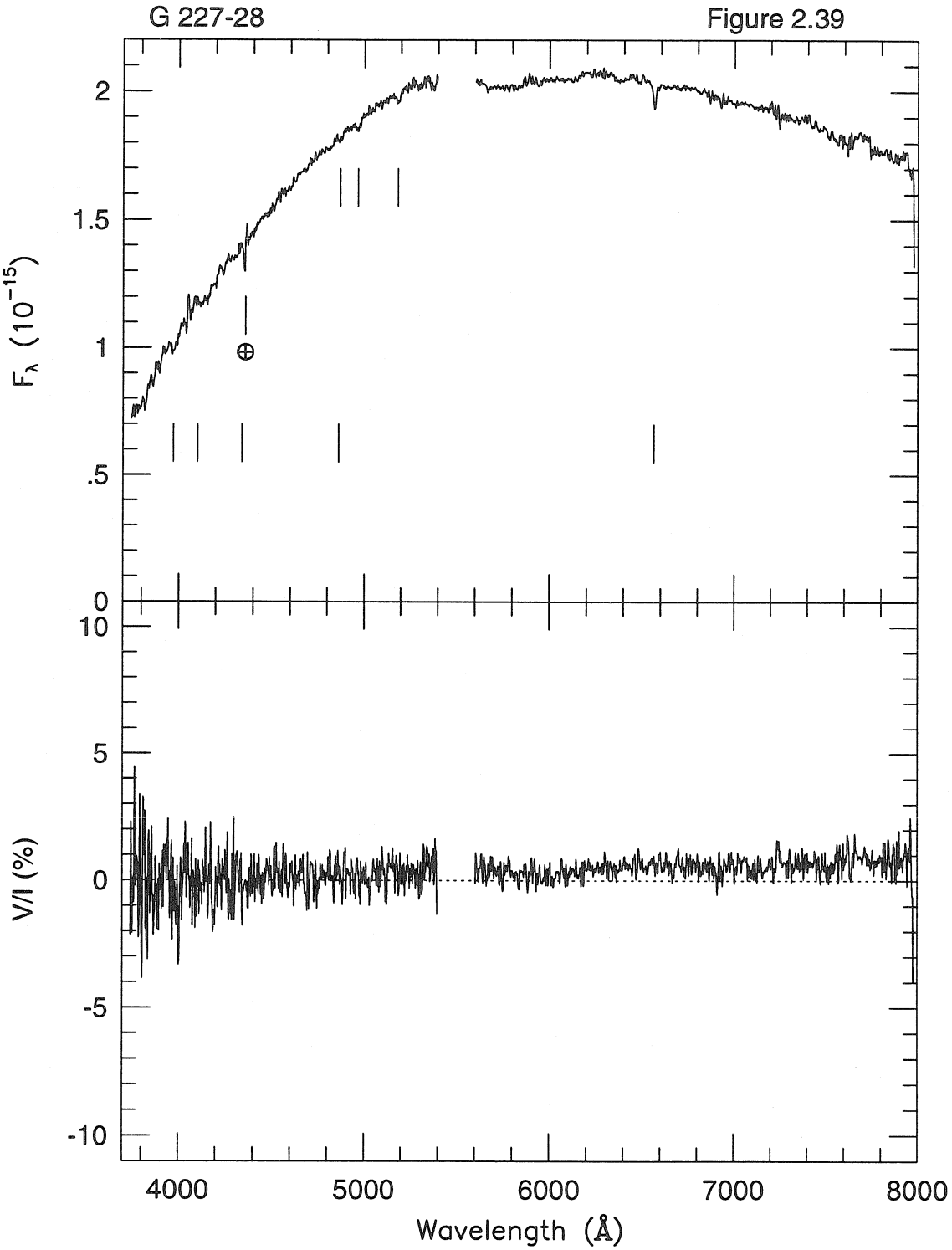
G 227-28
Figure 2.39
F_λ (10^{-15})
2
1.5
1
.5
0
⊕
10
5
0
-5
-10
V/I (%)
4000
5000
6000
7000
8000
Wavelength (Å)

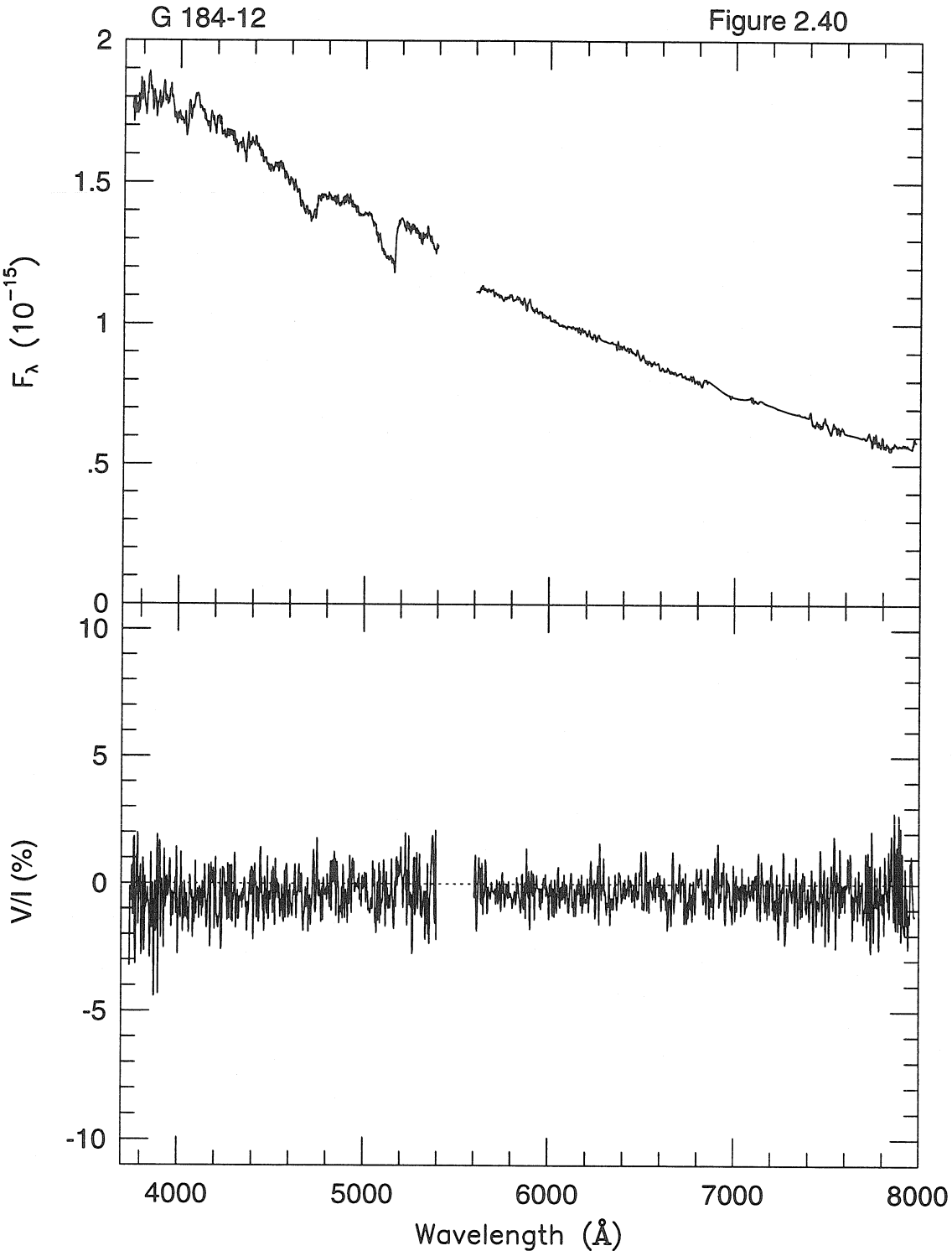
G 184-12
Figure 2.40
2
1.5
1
.5
0
F_λ (10^{-15})
10
5
0
-5
-10
V/I (%)
4000
5000
6000
7000
8000
Wavelength (Å)

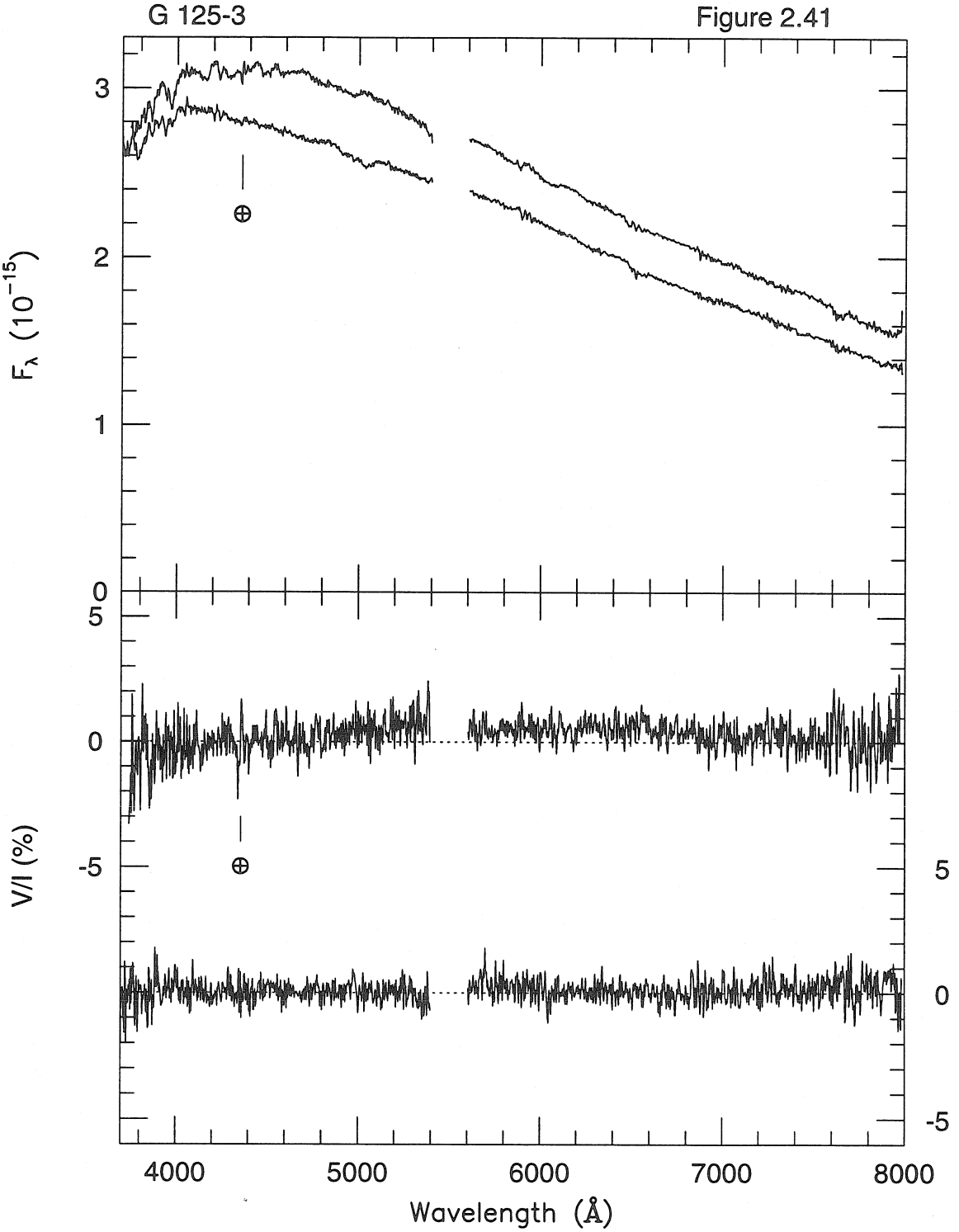
G 125-3
Figure 2.41
F_λ (10^{-15})
V/I (%)
Wavelength (Å)
4000
5000
6000
7000
8000
3
2
1
0
5
0
-5
5
0
-5
⊕
⊕

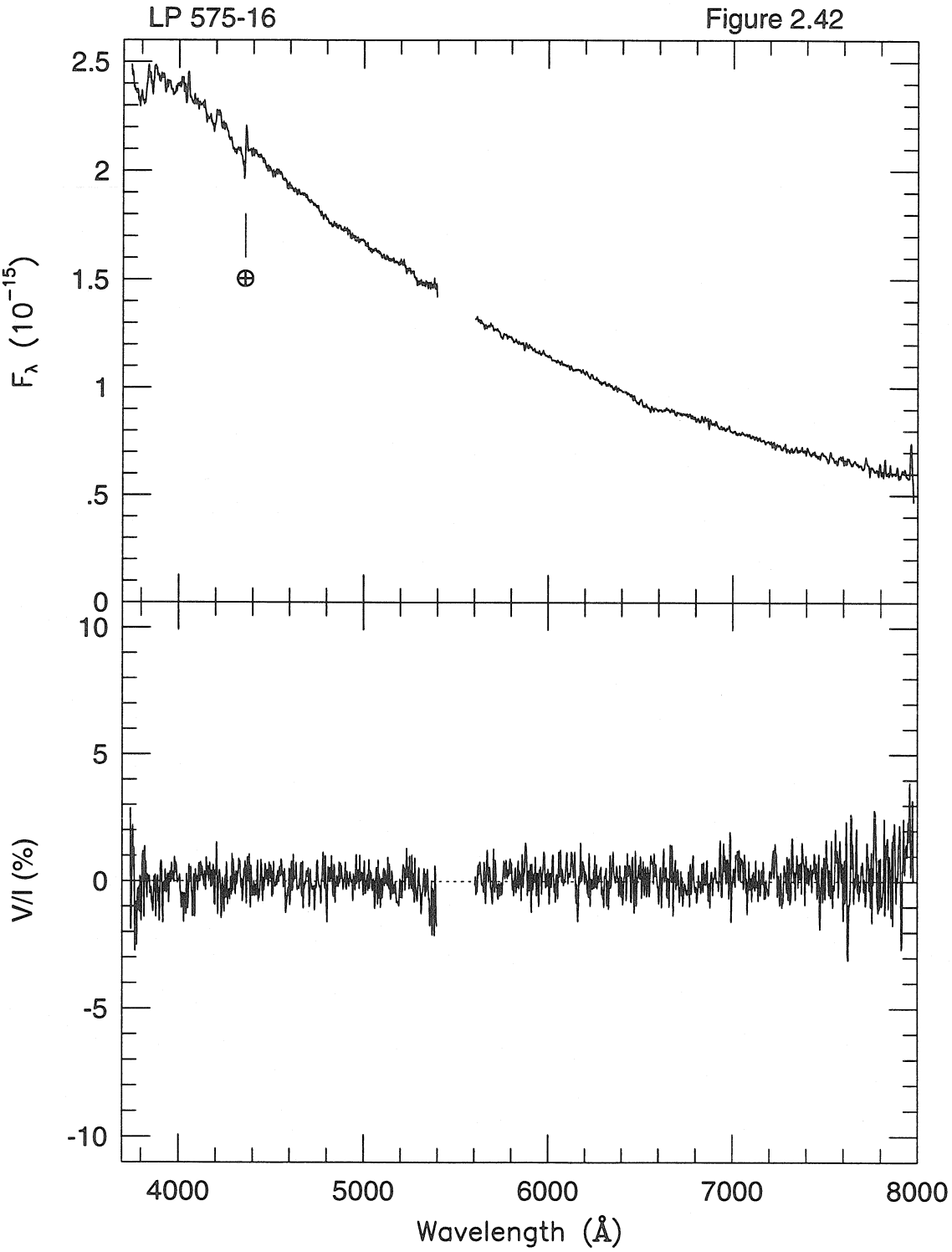
LP 575-16
Figure 2.42
2.5
2
1.5
1
.5
0
F_λ (10^{-15})
⊕
10
5
0
-5
-10
V/I (%)
4000
5000
6000
7000
8000
Wavelength (Å)

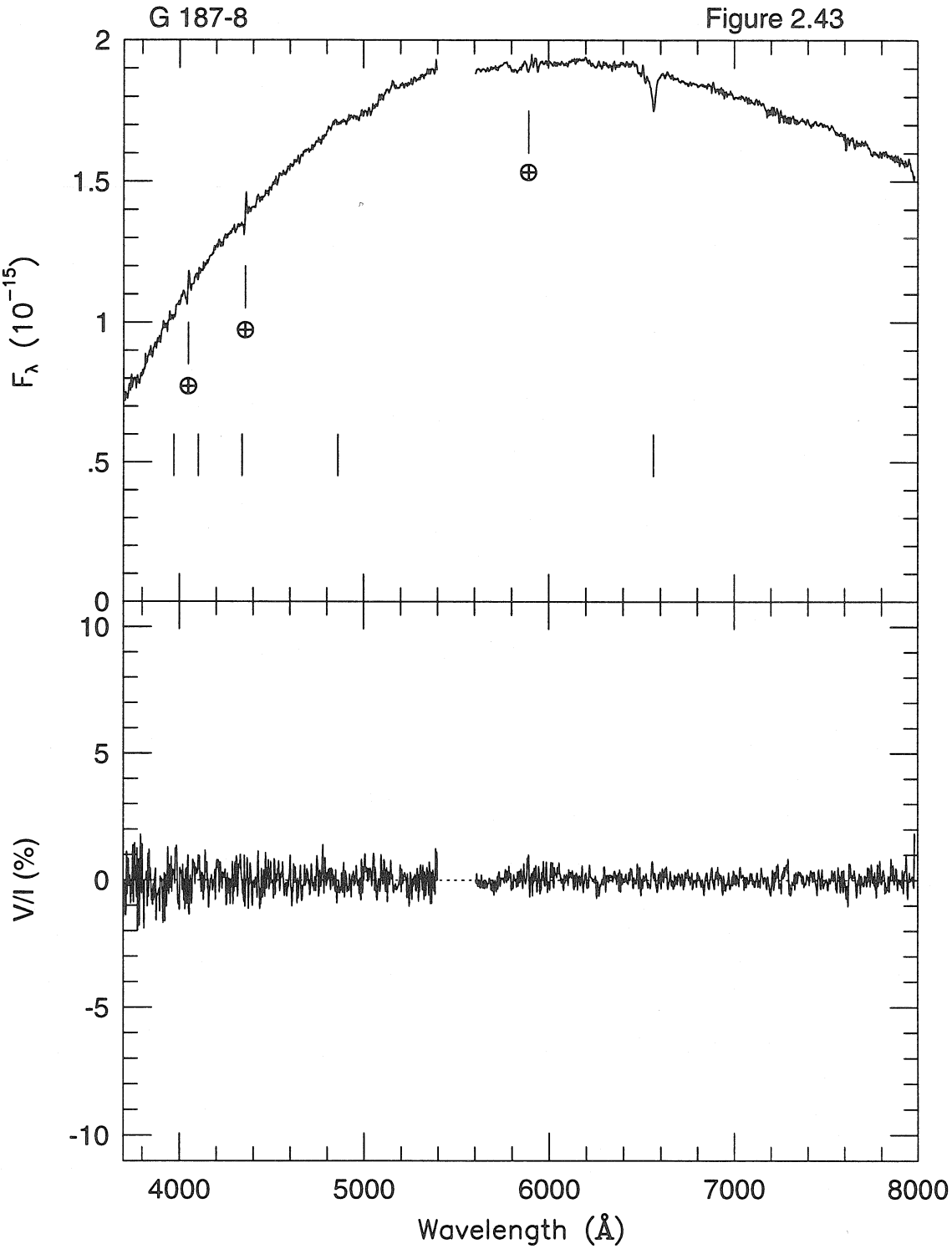
G 187-8
Figure 2.43
2
1.5
1
.5
0
F_λ (10^{-15})
10
5
0
-5
-10
V/I (%)
4000
5000
6000
7000
8000
Wavelength (Å)

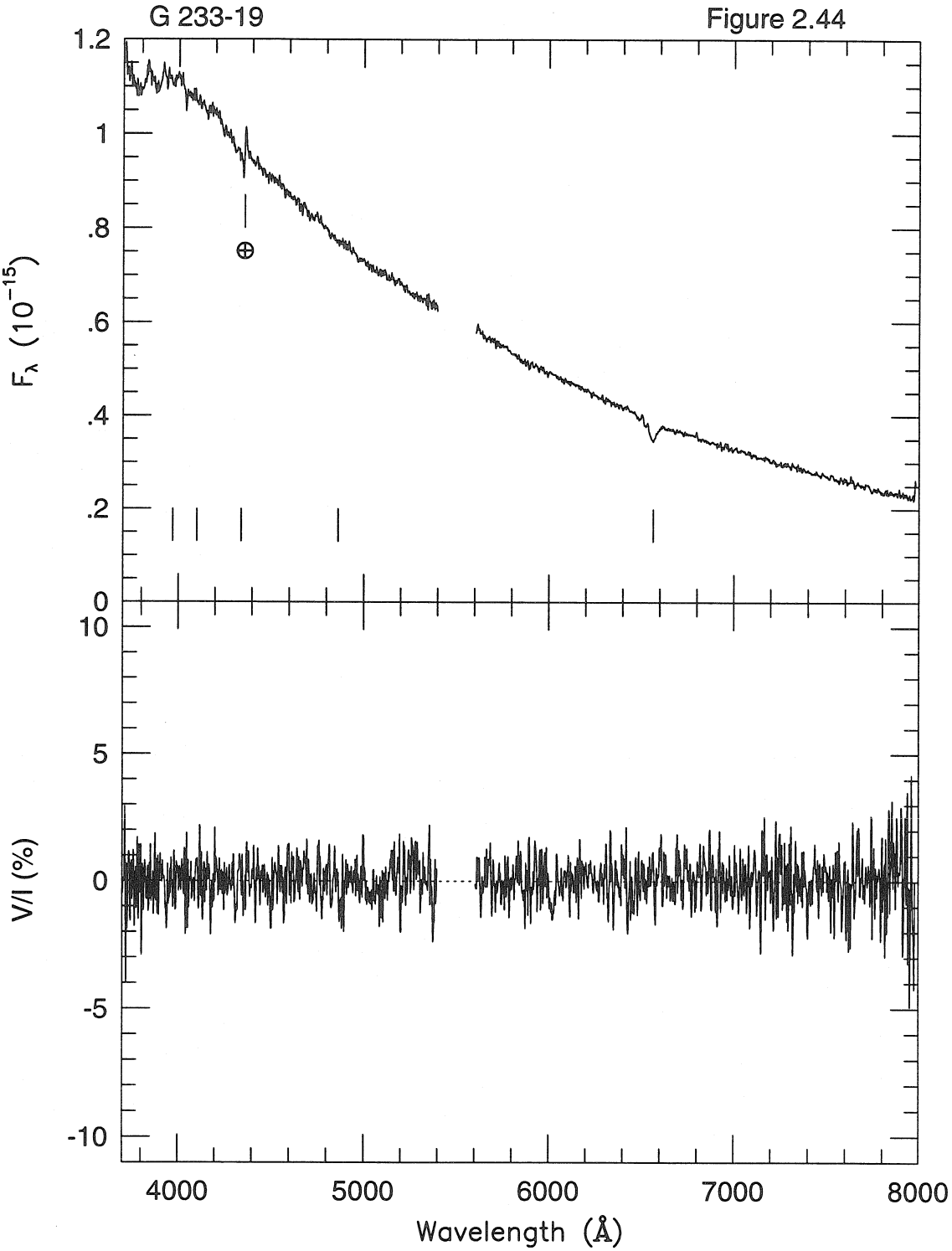
G 233-19
Figure 2.44
1.2
1
.8
.6
.4
.2
0
F_λ (10^{-15})
⊕
10
5
0
-5
-10
V/I (%)
4000
5000
6000
7000
8000
Wavelength (Å)

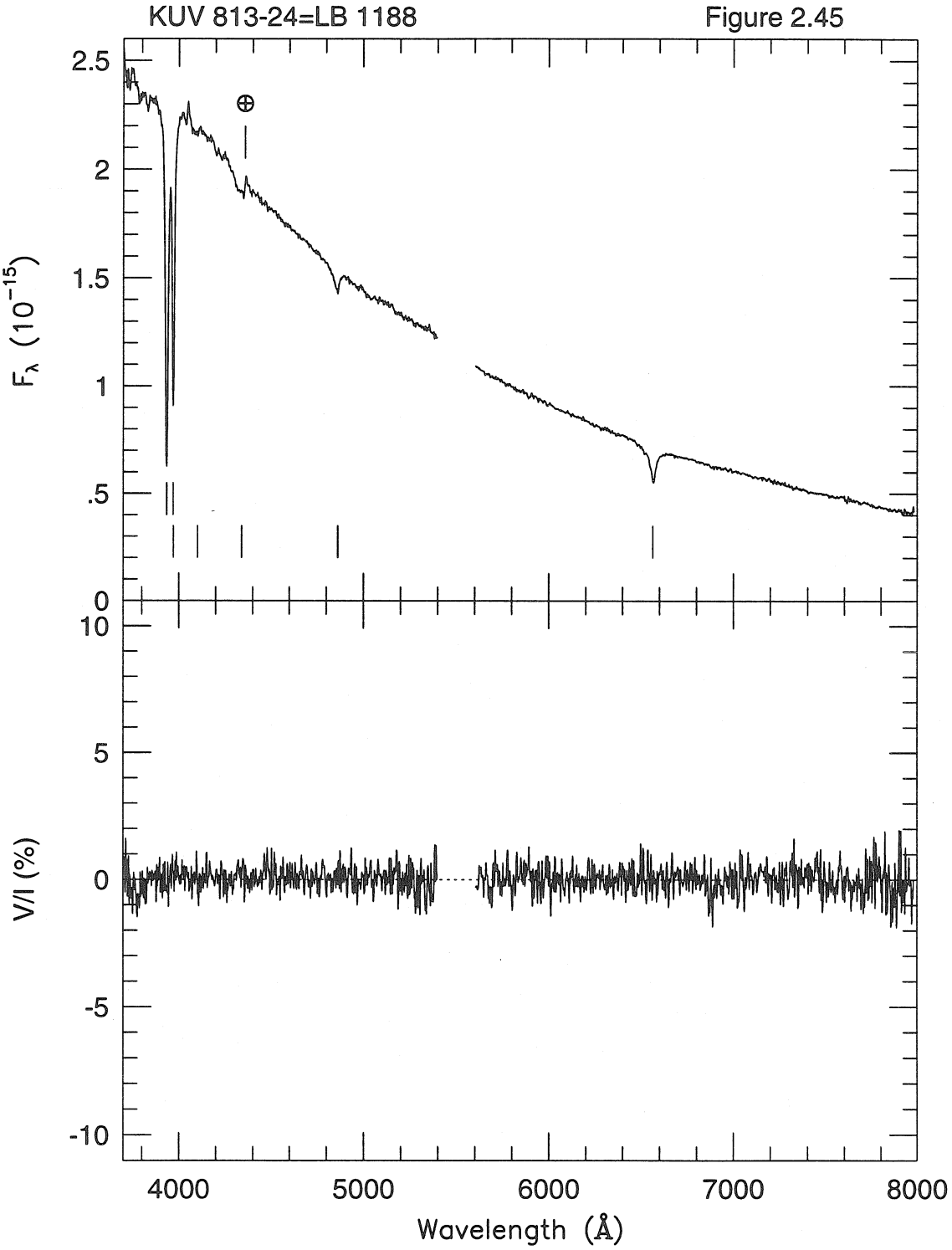
KUV 813-24=LB 1188
Figure 2.45
2.5
2
1.5
1
.5
0
F_λ (10^{-15})
⊕
10
5
0
-5
-10
V/I (%)
4000
5000
6000
7000
8000
Wavelength (Å)

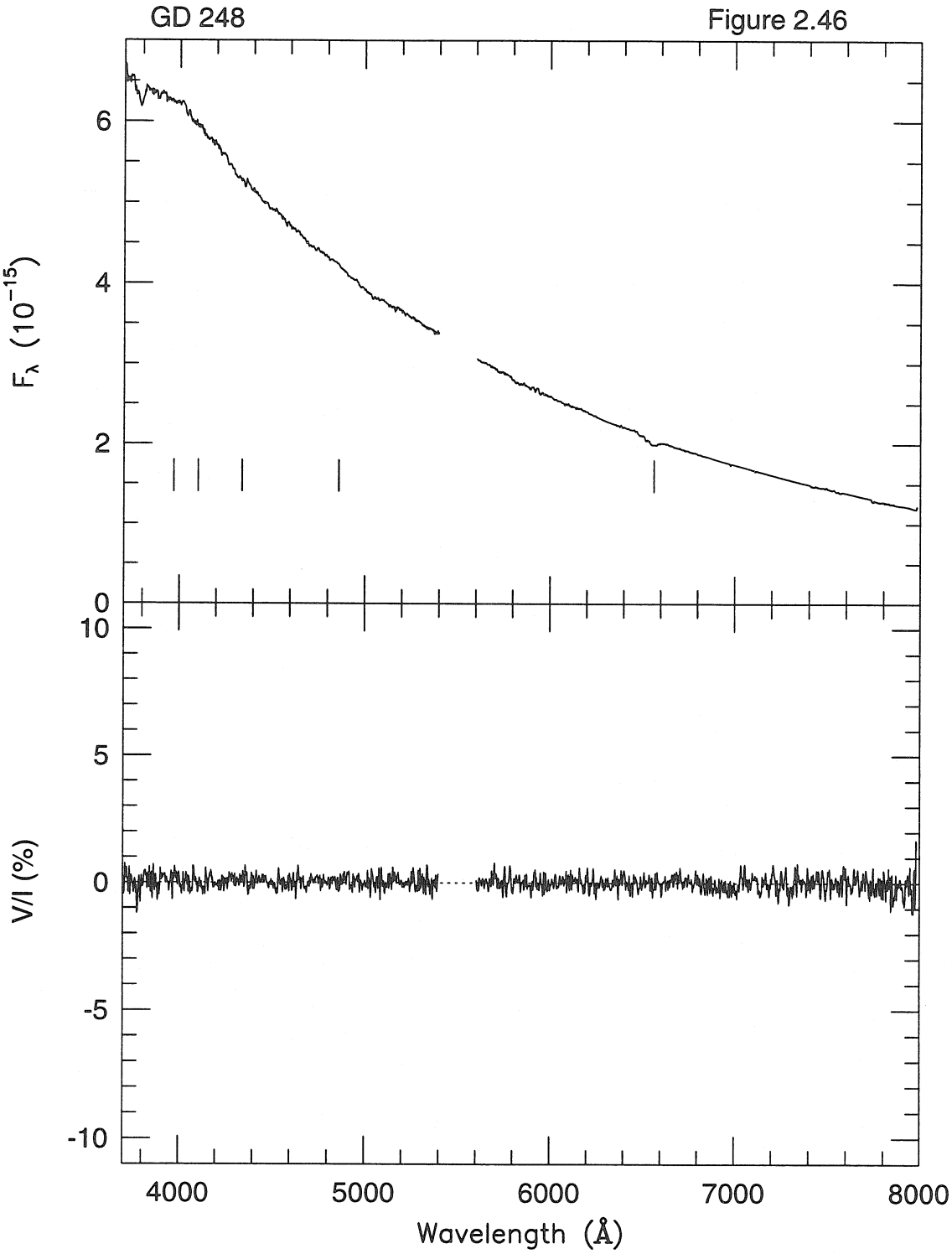
GD 248
Figure 2.46
6
4
2
0
F_λ (10^{-15})
10
5
0
-5
-10
V/I (%)
4000
5000
6000
7000
8000
Wavelength (Å)

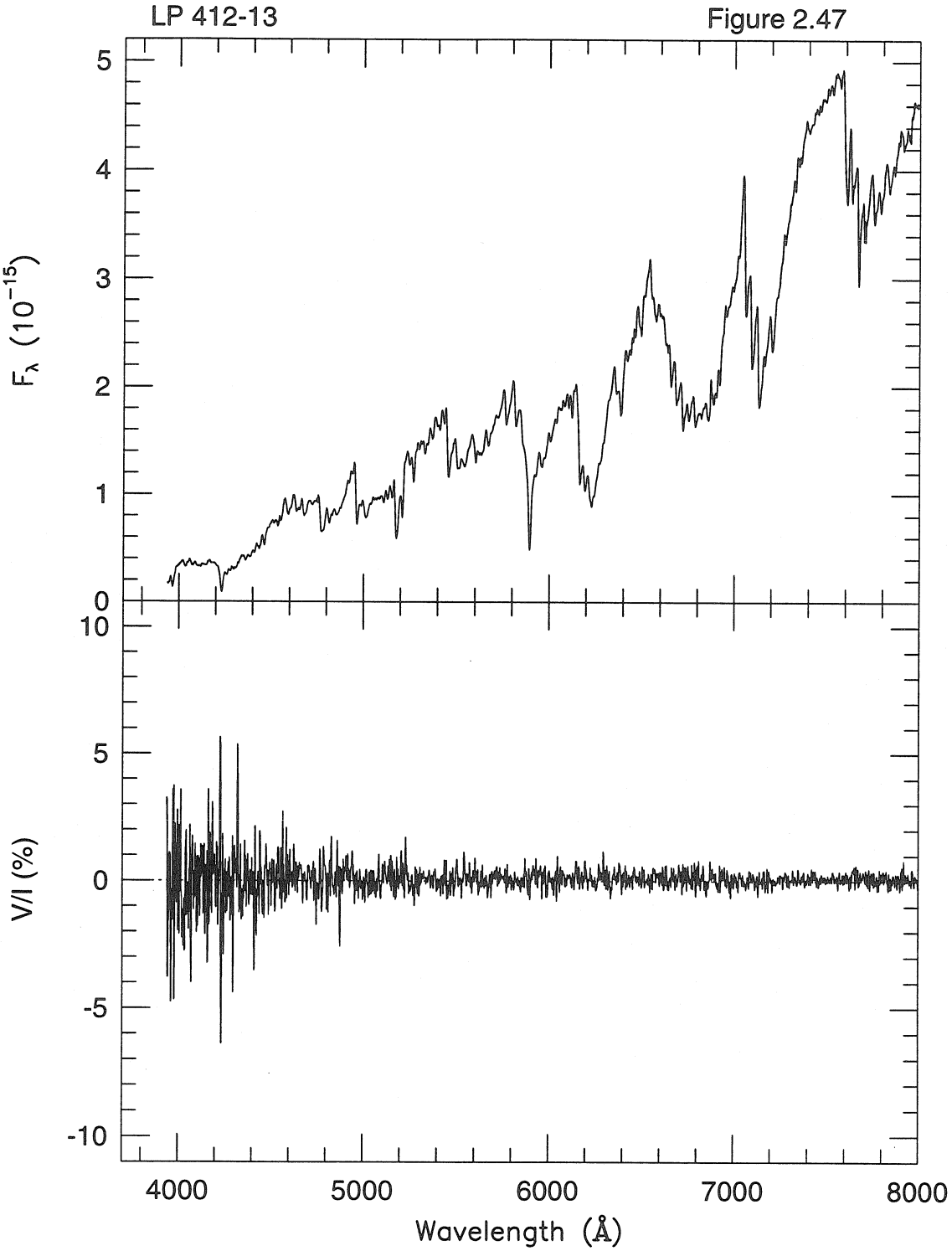
LP 412-13
Figure 2.47
F_λ (10^{-15})
V/I (%)
Wavelength (Å)
5
4
3
2
1
0
10
5
0
-5
-10
4000
5000
6000
7000
8000

Figure 2.48a

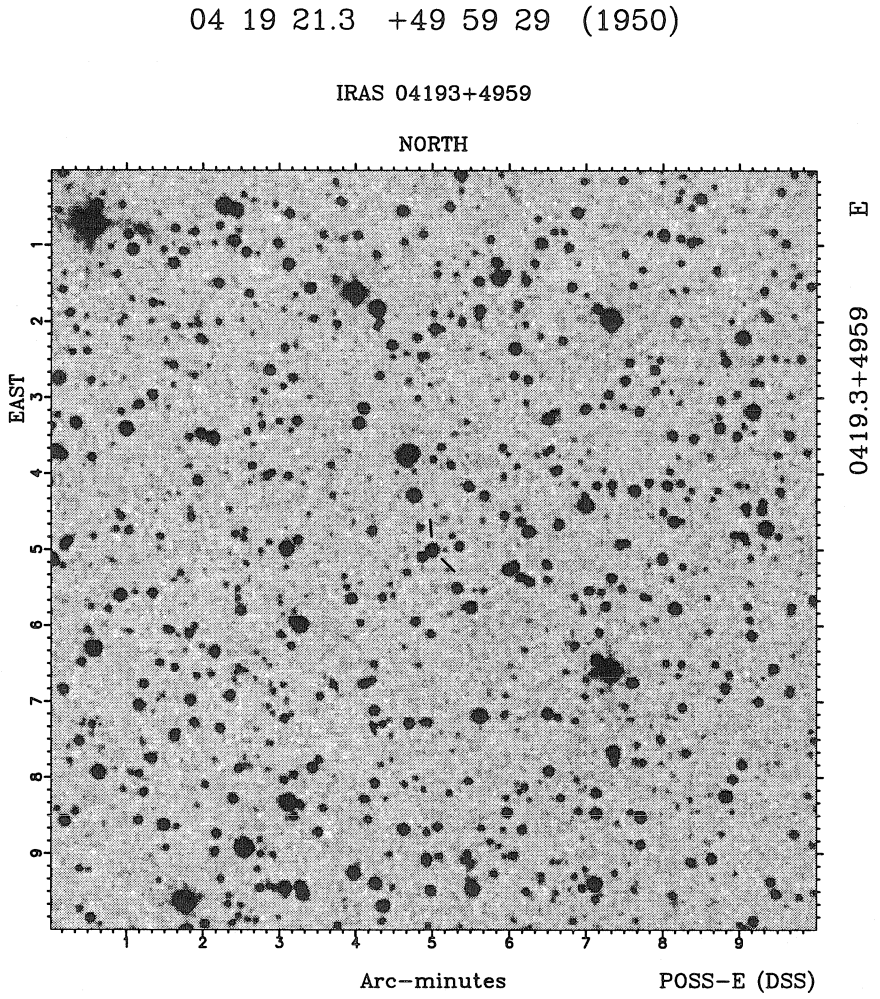
04 19 21.3 +49 59 29 (1950)
IRAS 04193+4959
NORTH
EAST
E
0419.3+4959
1
2
3
4
5
6
7
8
9
Arc-minutes
POSS-E (DSS)

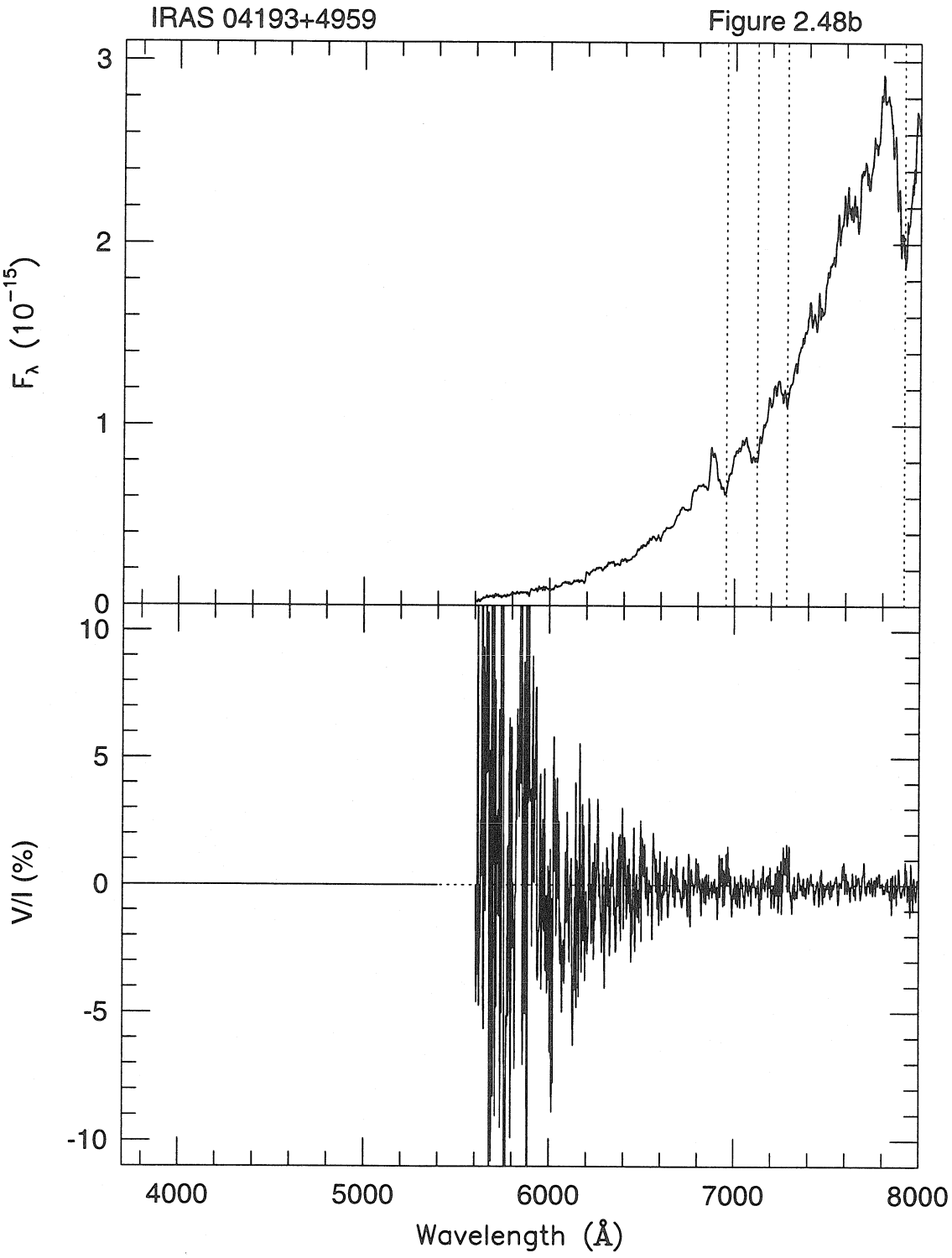
IRAS 04193+4959
Figure 2.48b
F_λ (10^{-15})
3
2
1
0
V/I (%)
10
5
0
-5
-10
4000
5000
6000
7000
8000
Wavelength (Å)

Figure 2.49a

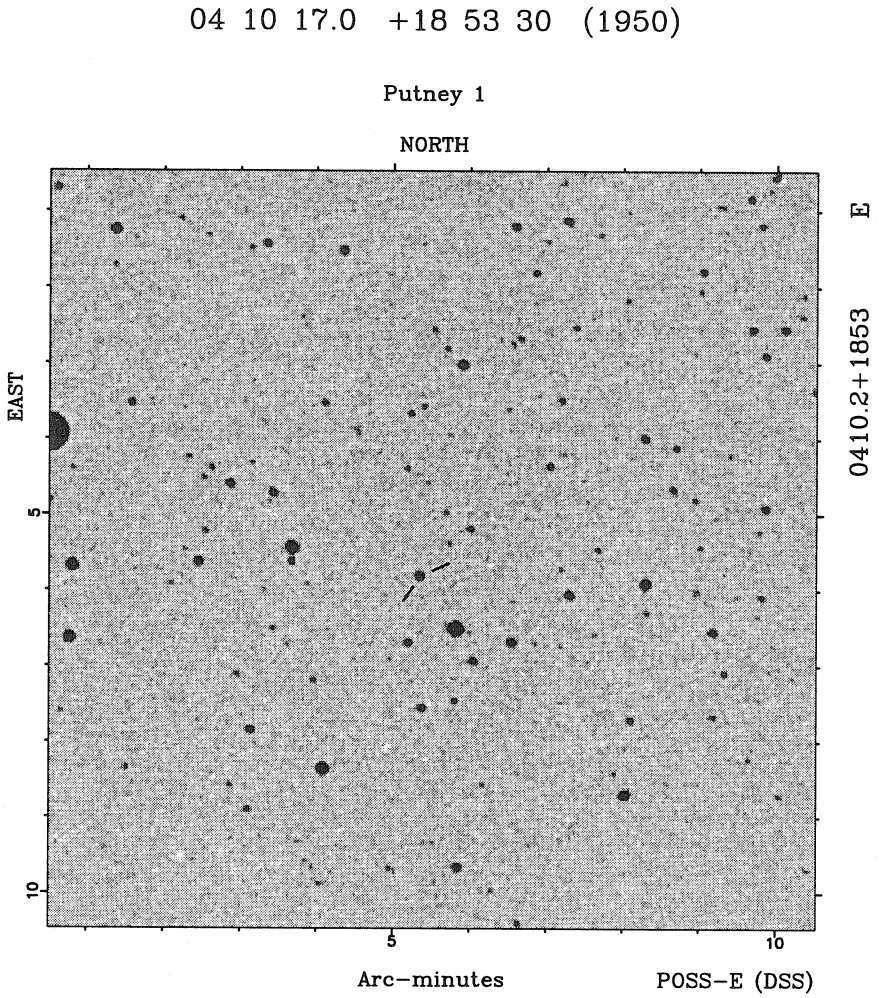
04 10 17.0 +18 53 30 (1950)
Putney 1
NORTH
EAST
E
0410.2+1853
5
10
5
10
Arc−minutes
POSS−E (DSS)

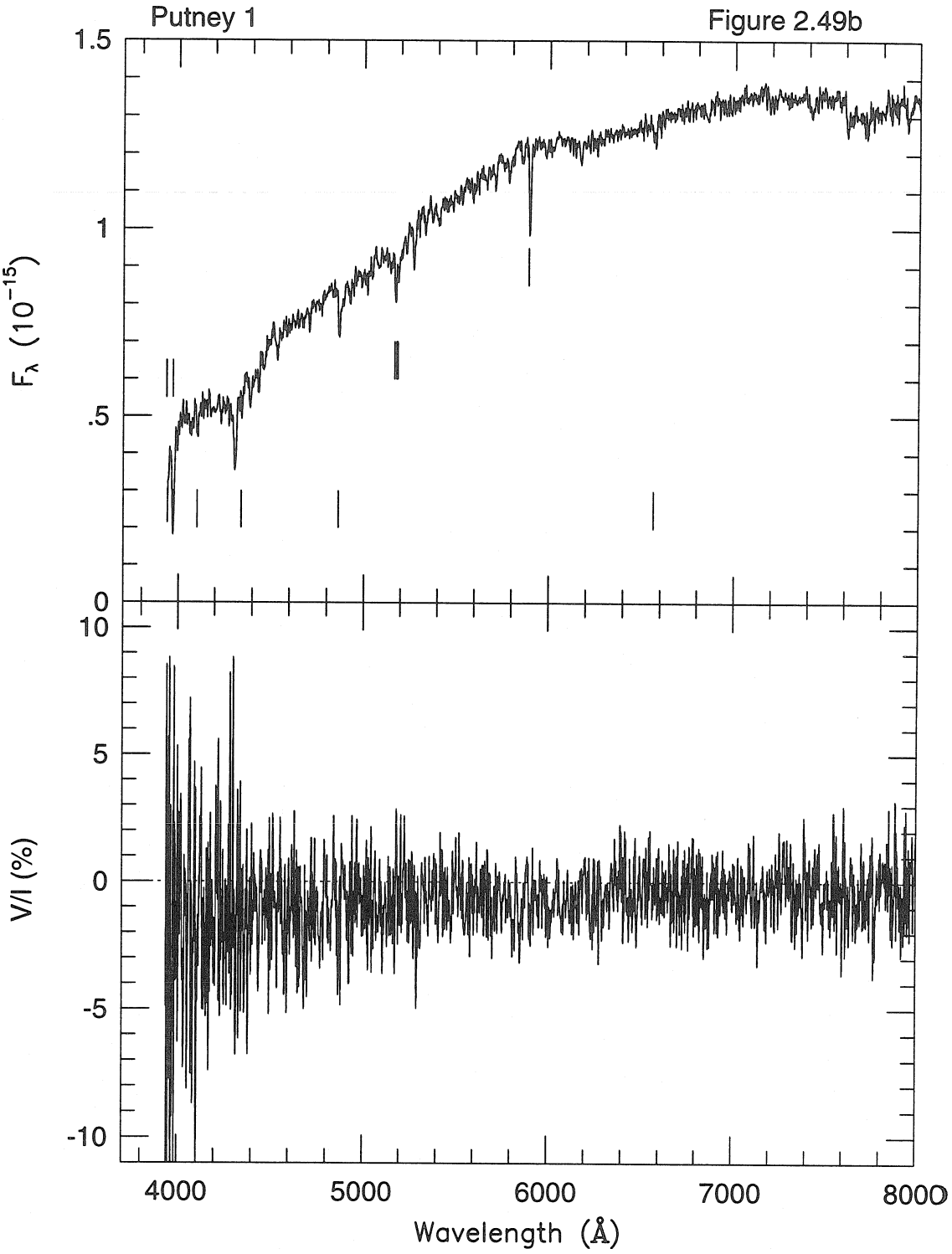
Putney 1
Figure 2.49b
1.5
1
.5
0
F_λ (10^{-15})
10
5
0
-5
-10
V/I (%)
4000
5000
6000
7000
8000
Wavelength (Å)

Figure 2.50a

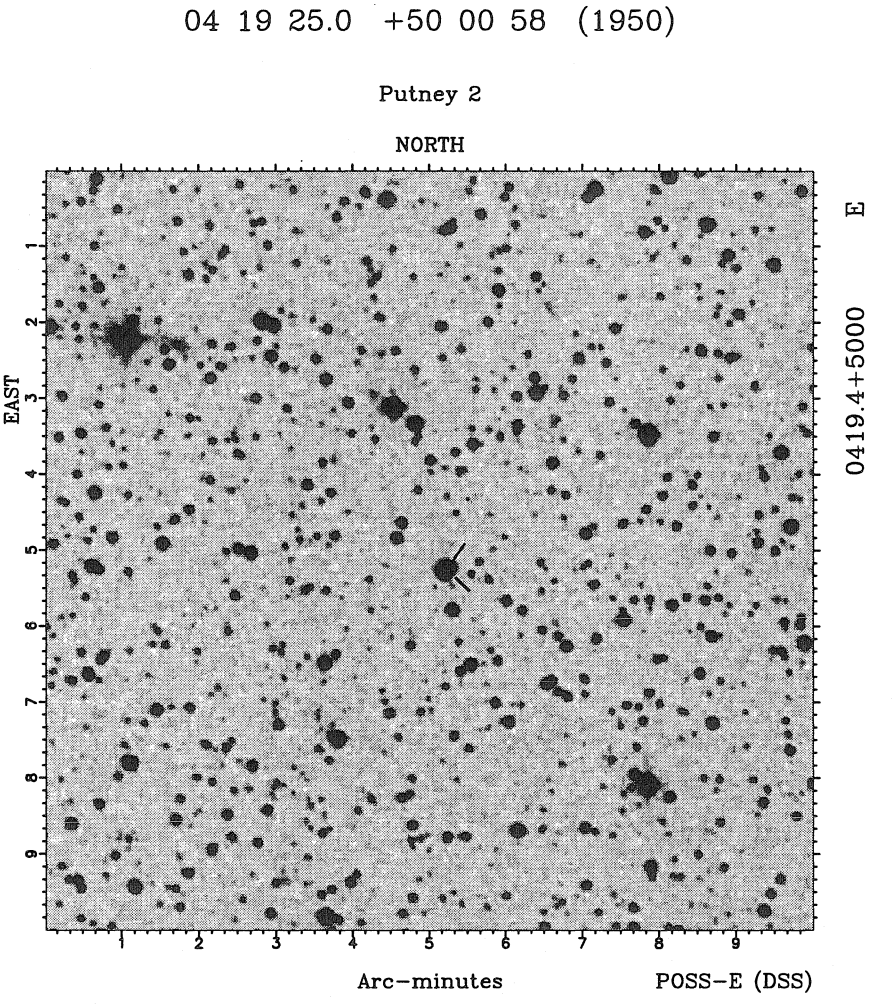
04 19 25.0 +50 00 58 (1950)
Putney 2
NORTH
EAST
E
0419.4+5000
1
2
3
4
5
6
7
8
9
Arc-minutes
POSS-E (DSS)

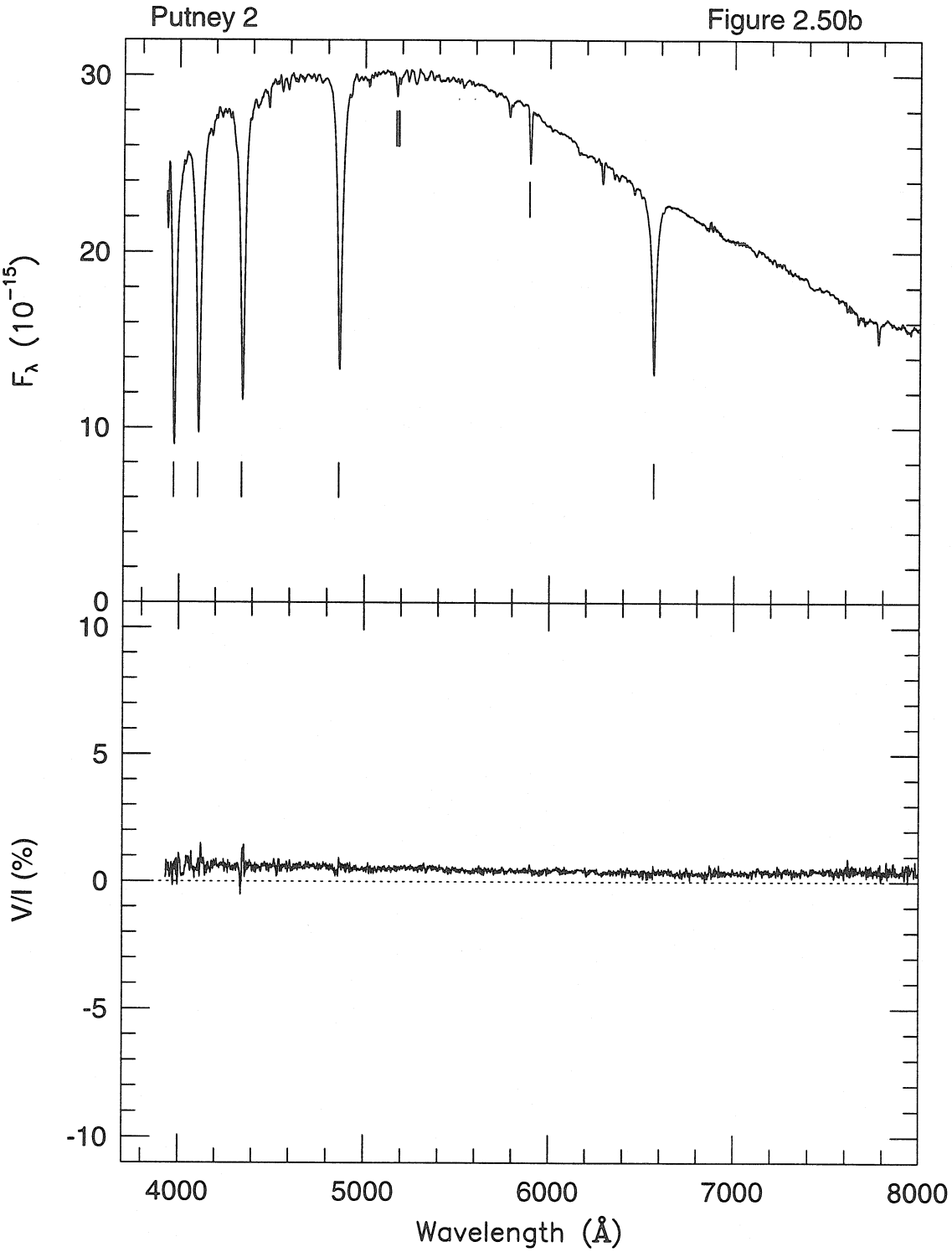
Putney 2
Figure 2.50b
30
20
10
0
F_λ (10^{-15})
10
5
0
-5
-10
V/I (%)
4000
5000
6000
7000
8000
Wavelength (Å)

Figure 2.51a

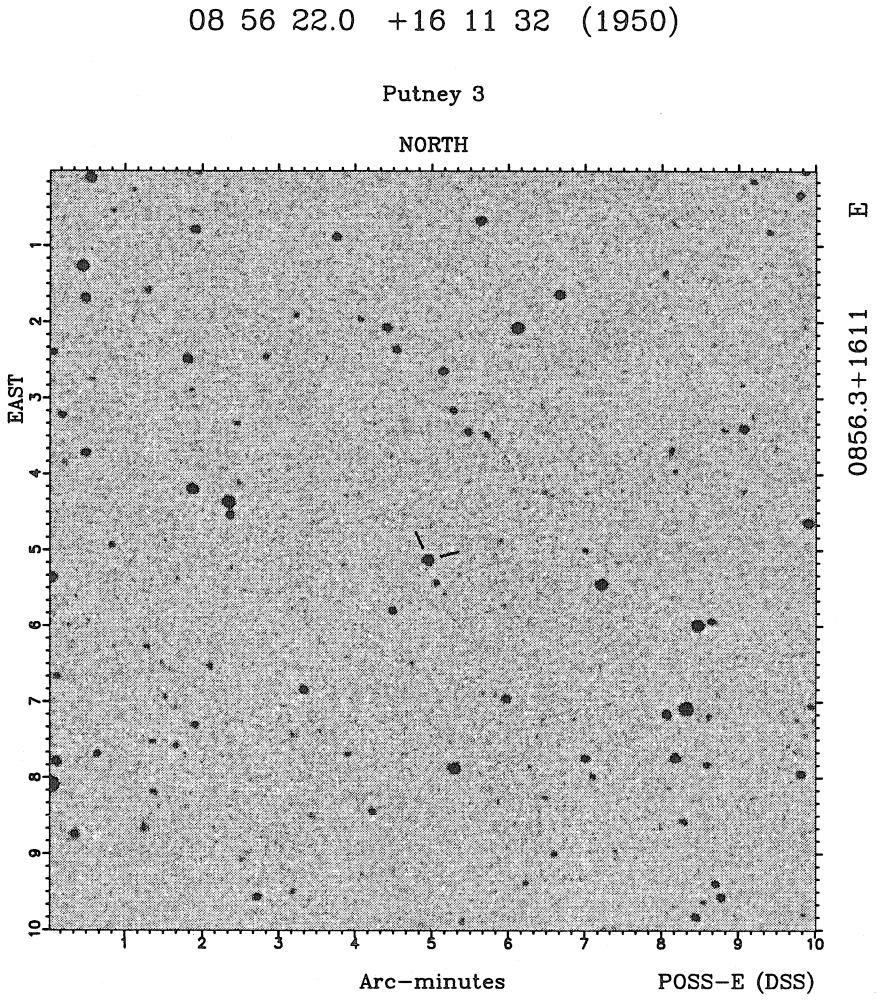
08 56 22.0 +16 11 32 (1950)
Putney 3
NORTH
EAST
E
0856.3+1611
1
2
3
4
5
6
7
8
9
10
Arc−minutes
POSS−E (DSS)

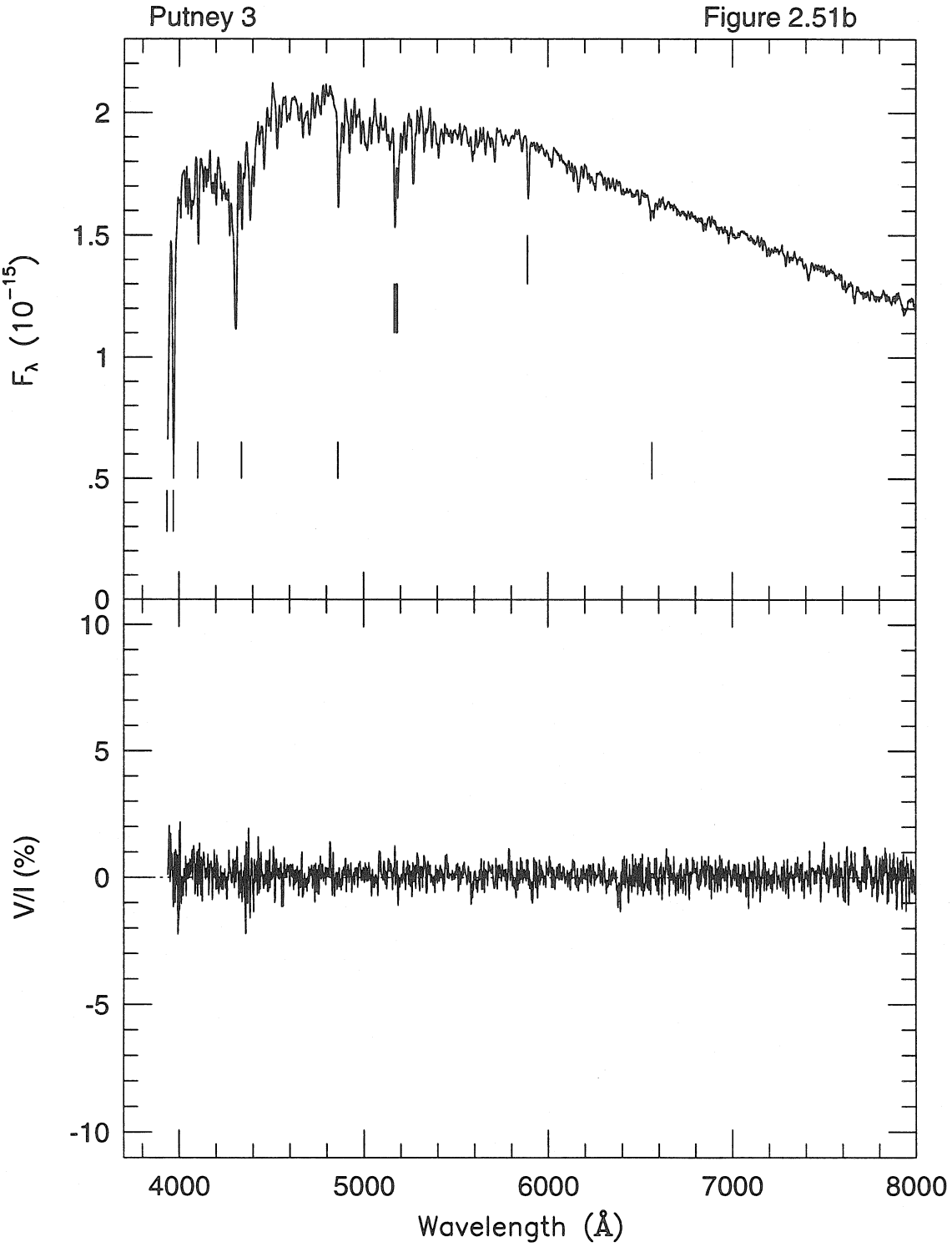
Putney 3
Figure 2.51b
F_λ (10^{-15})
2
1.5
1
.5
0
10
5
0
-5
-10
V/I (%)
4000
5000
6000
7000
8000
Wavelength (Å)

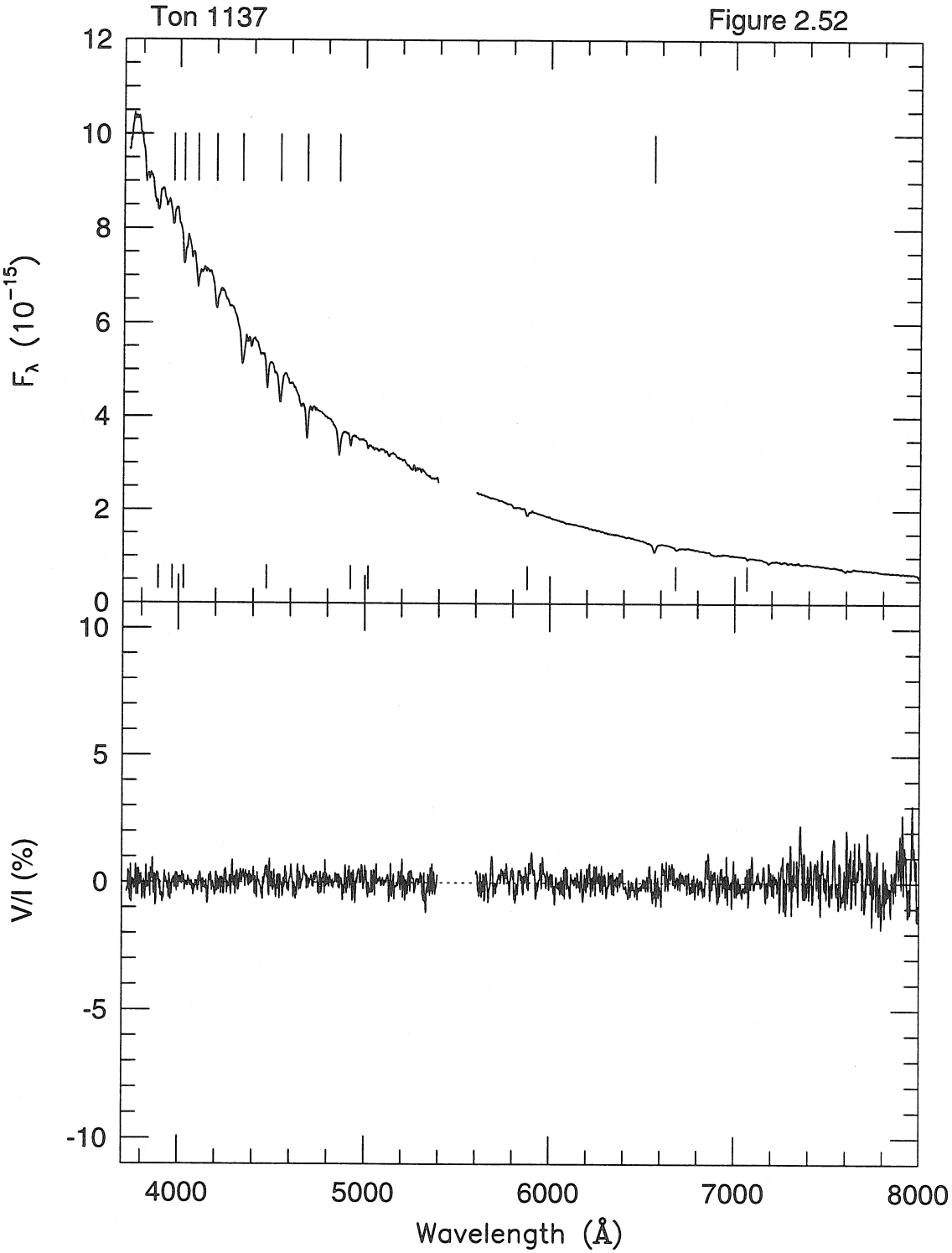
Ton 1137
Figure 2.52
12
10
8
6
4
2
0
F_λ (10^{-15})
10
5
0
-5
-10
V/I (%)
4000
5000
6000
7000
8000
Wavelength (Å)

Figure 2.53a

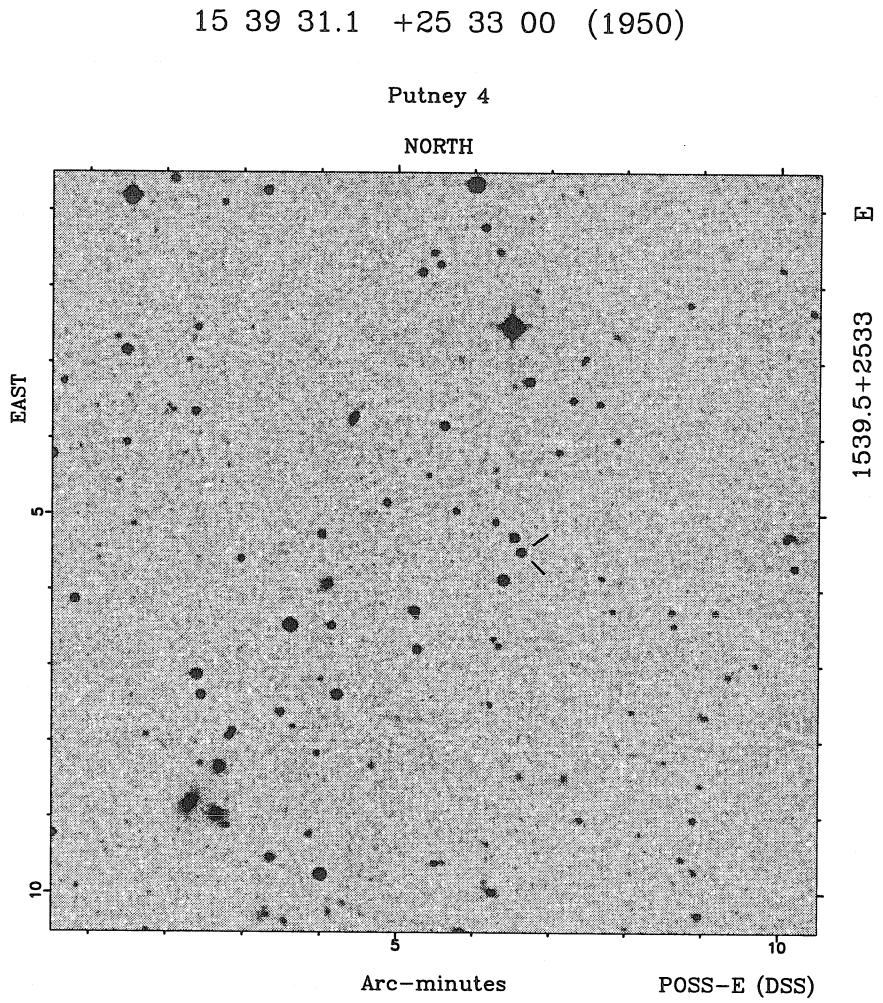
15 39 31.1 +25 33 00 (1950)
Putney 4
NORTH
EAST
E
1539.5+2533
5
10
5
10
Arc−minutes
POSS−E (DSS)

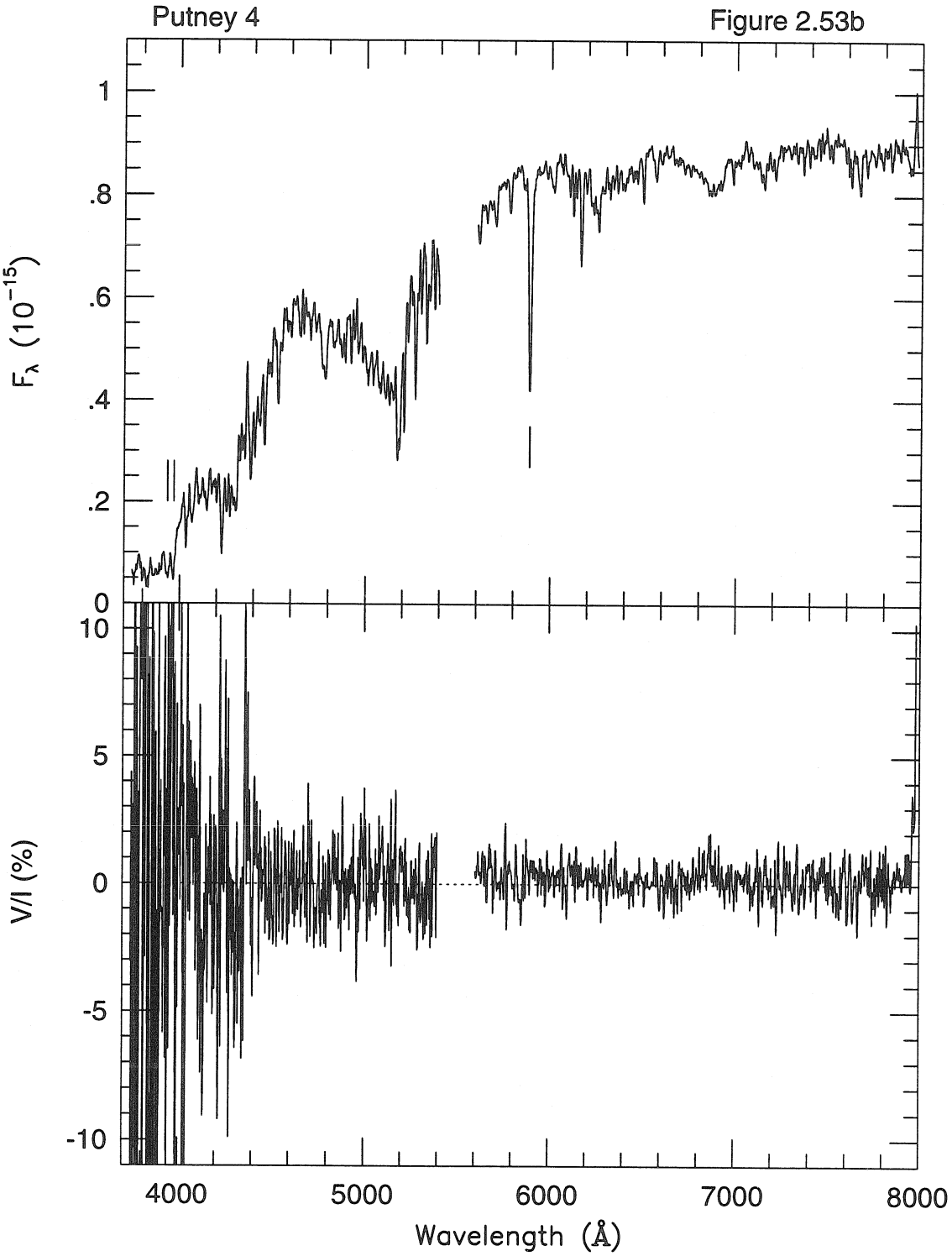
Putney 4
Figure 2.53b
1
.8
.6
.4
.2
0
F_λ (10^{-15})
10
5
0
-5
-10
V/I (%)
4000
5000
6000
7000
8000
Wavelength (Å)

Figure 2.54a

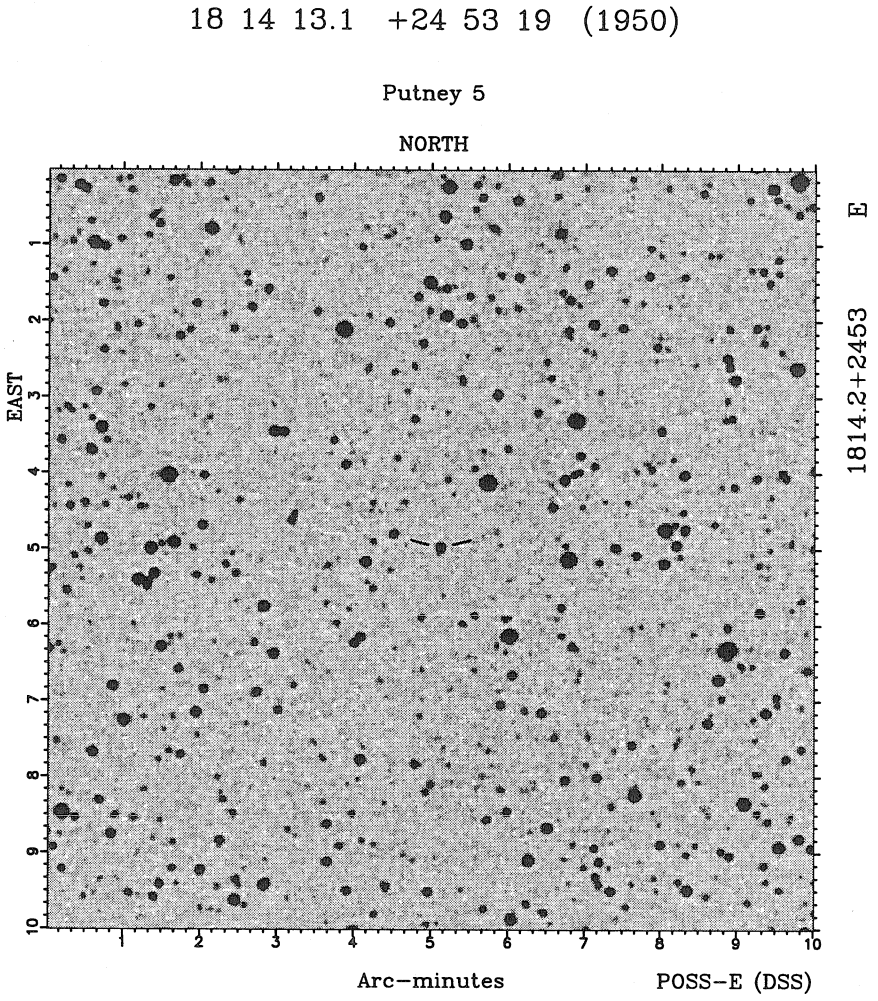
18 14 13.1 +24 53 19 (1950)
Putney 5
NORTH
EAST
E
1814.2+2453
1
2
3
4
5
6
7
8
9
10
Arc−minutes
POSS−E (DSS)

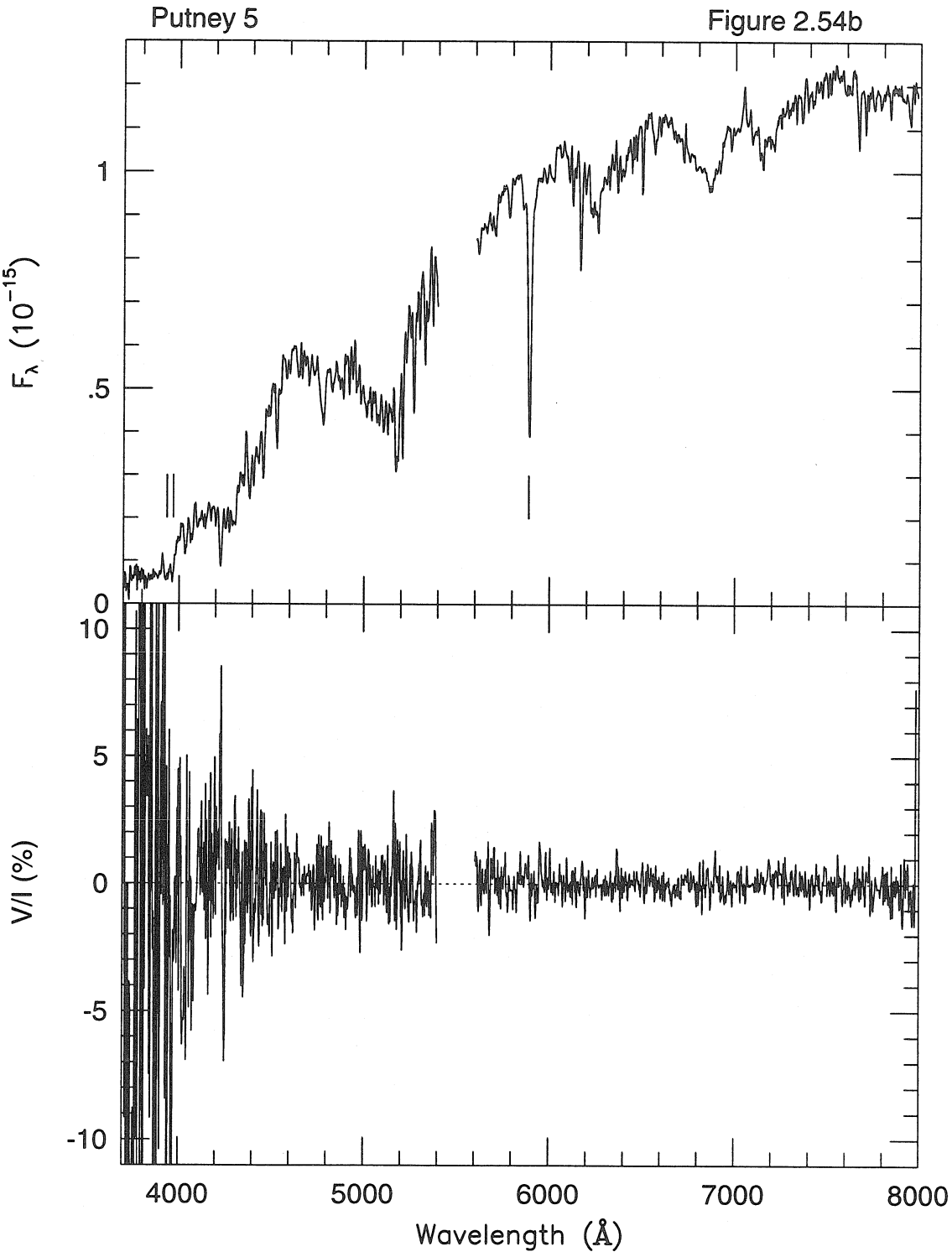
Putney 5
Figure 2.54b
F_λ (10^{-15})
1
.5
0
10
5
0
-5
-10
V/I (%)
4000
5000
6000
7000
8000
Wavelength (Å)

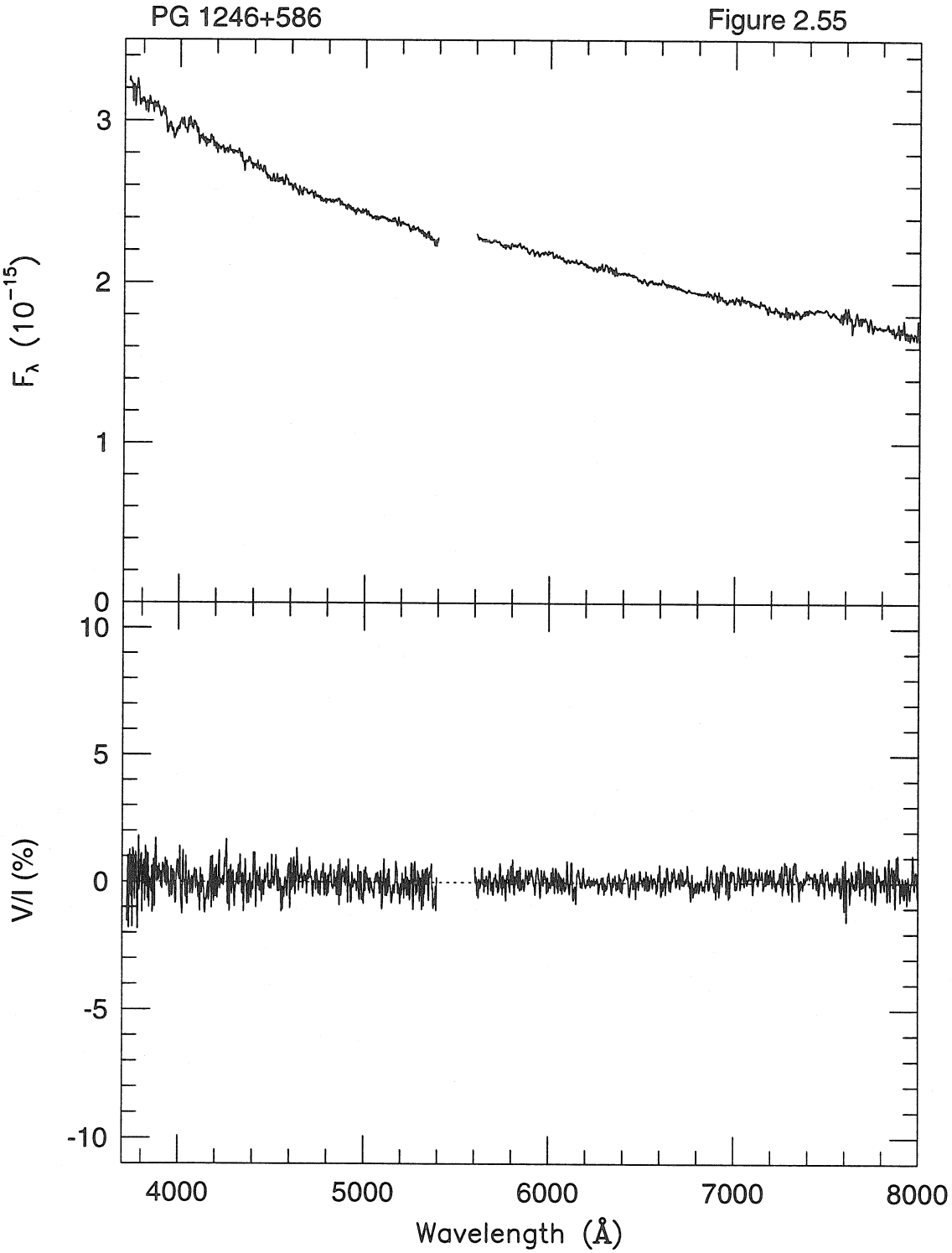
PG 1246+586
Figure 2.55
F_λ (10^{-15})
3
2
1
0
10
5
0
-5
-10
V/I (%)
4000
5000
6000
7000
8000
Wavelength (Å)

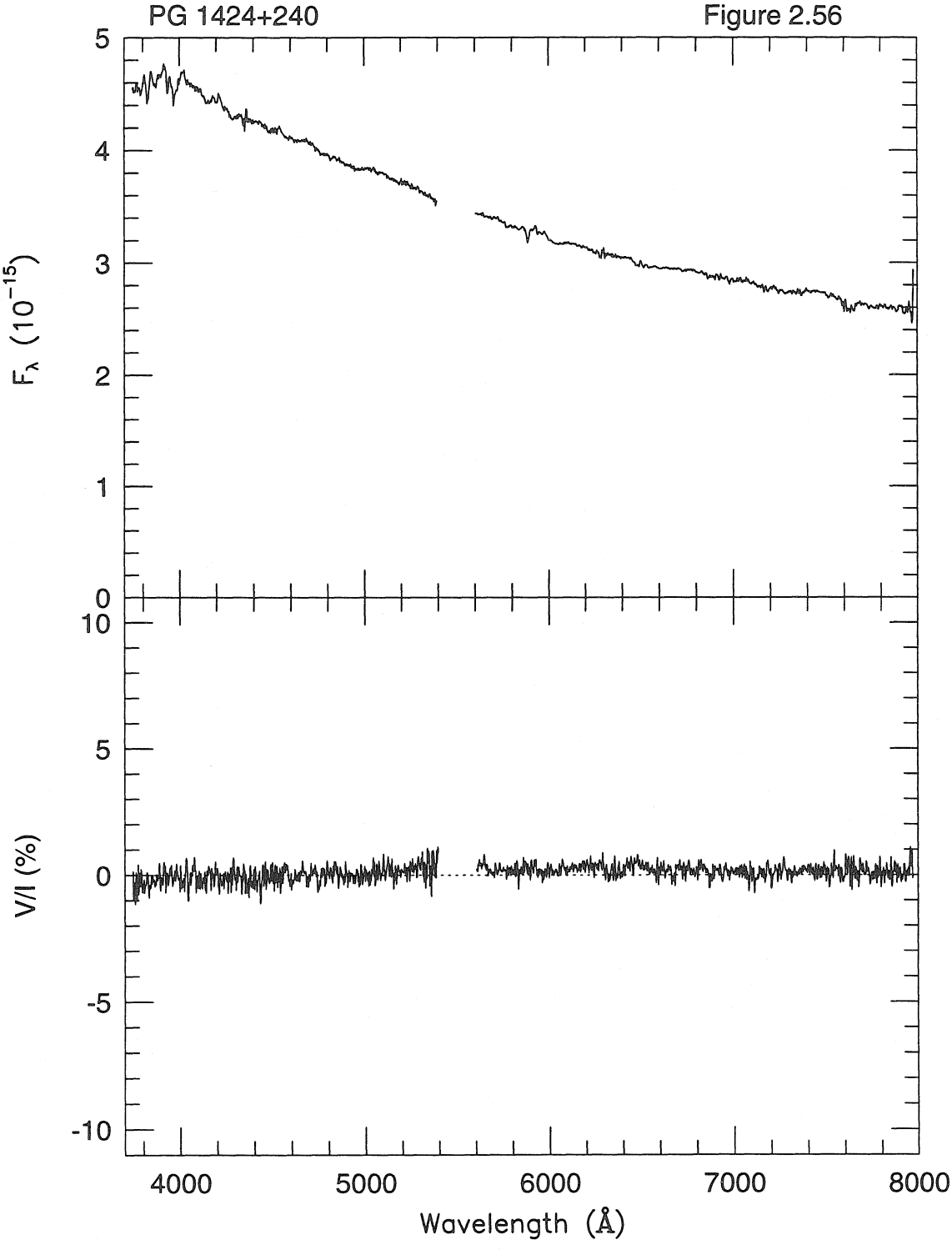
PG 1424+240
Figure 2.56
F_λ (10^{-15})
V/I (%)
Wavelength (Å)
5
4
3
2
1
0
10
5
0
-5
-10
4000
5000
6000
7000
8000

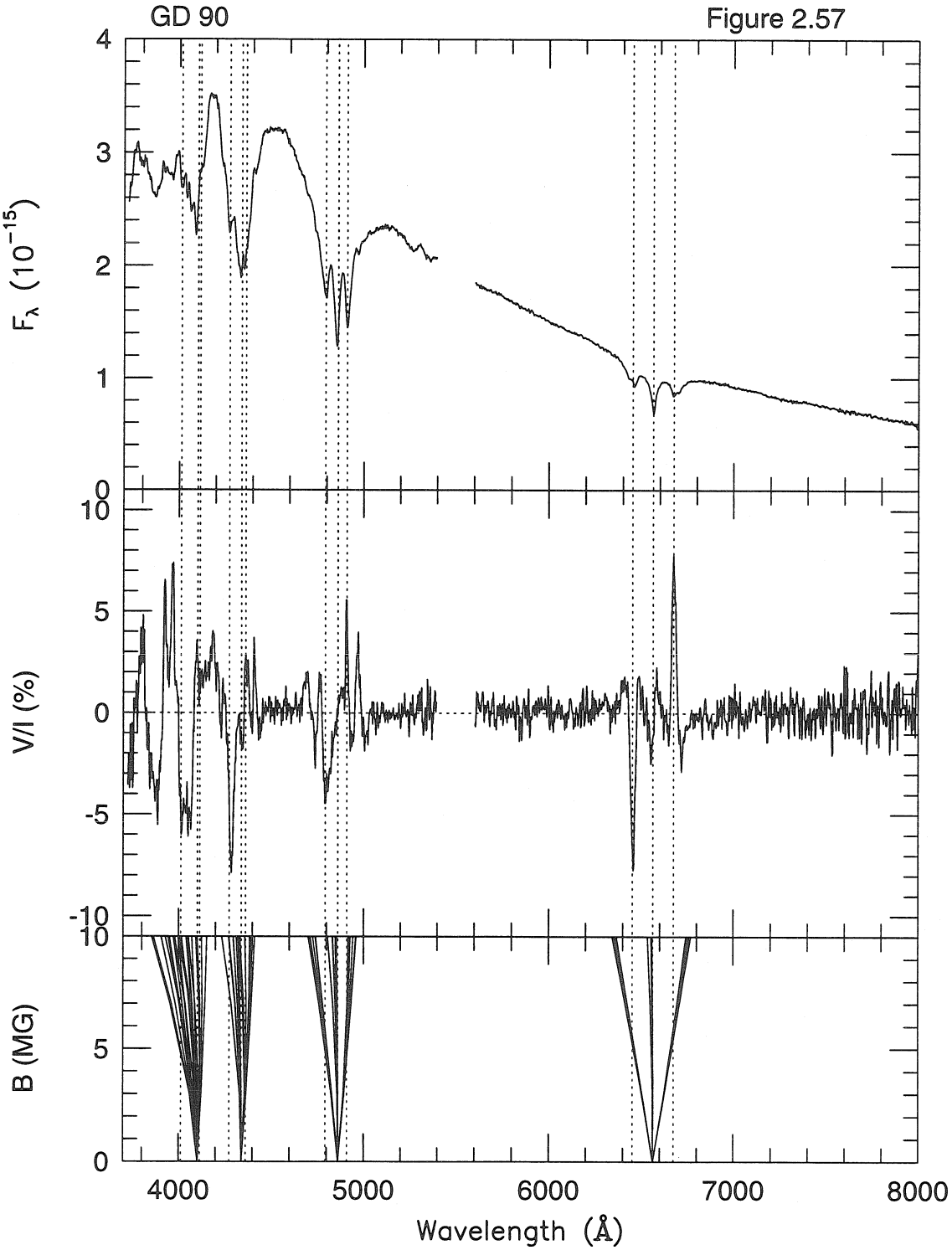
GD 90
Figure 2.57
F_λ (10^{-15})
V/I (%)
B (MG)
Wavelength (Å)
4000
5000
6000
7000
8000

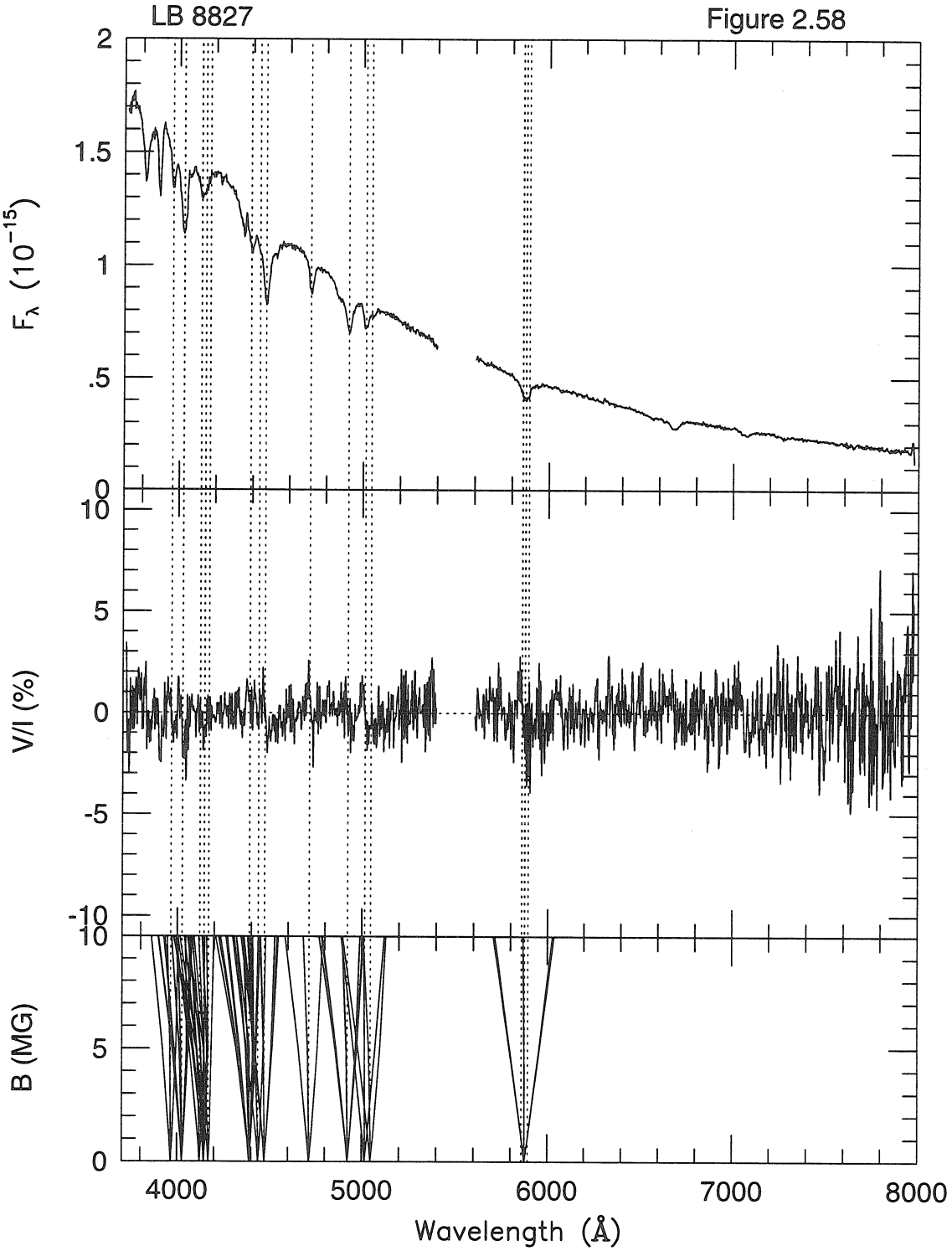
LB 8827
Figure 2.58
F_λ (10^{-15})
V/I (%)
B (MG)
Wavelength (Å)
2
1.5
1
.5
0
10
5
0
-5
-10
10
5
0
4000
5000
6000
7000
8000

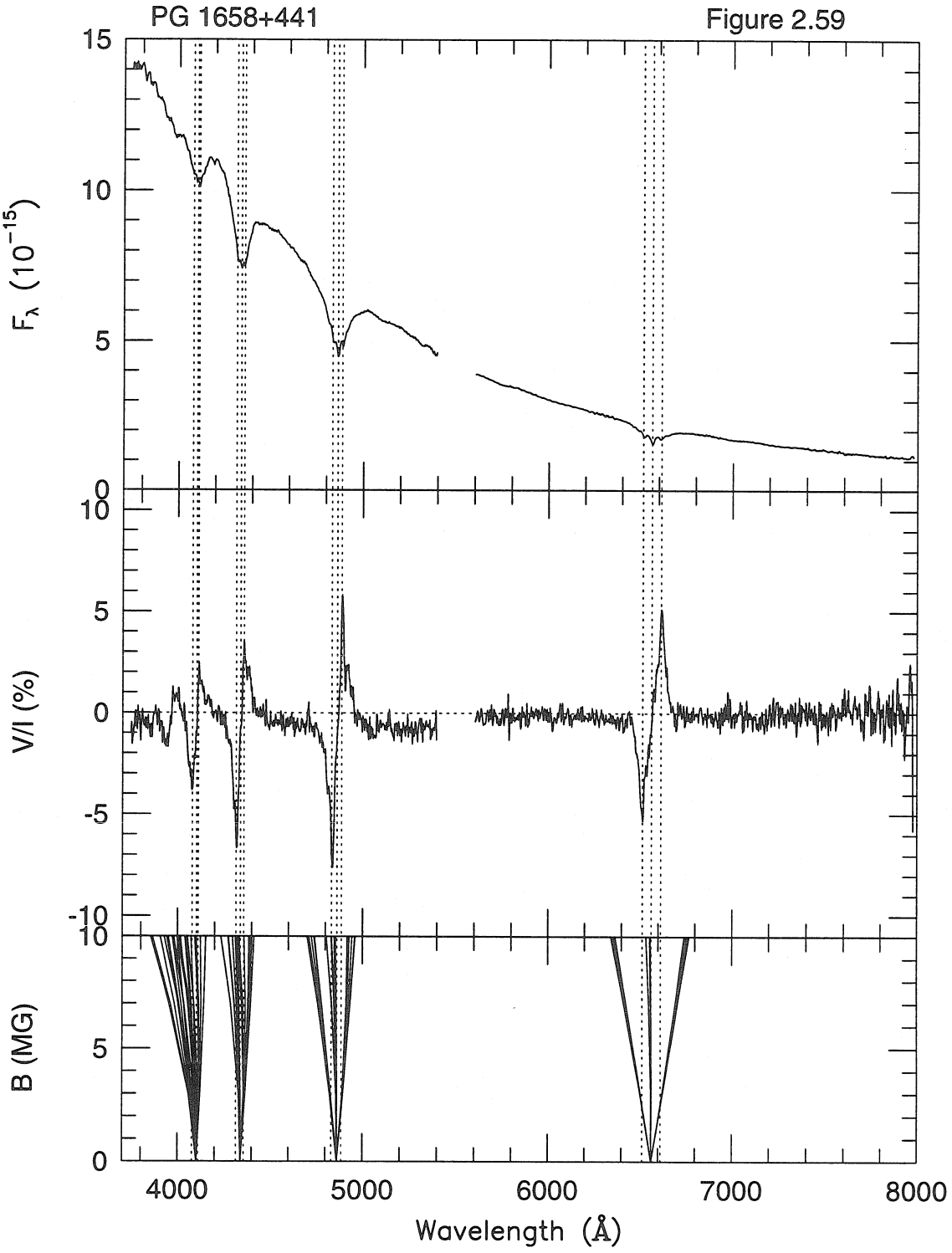
PG 1658+441
Figure 2.59
F_λ (10^{-15})
V/I (%)
B (MG)
Wavelength (Å)
15
10
5
0
10
5
0
-5
-10
10
5
0
4000
5000
6000
7000
8000

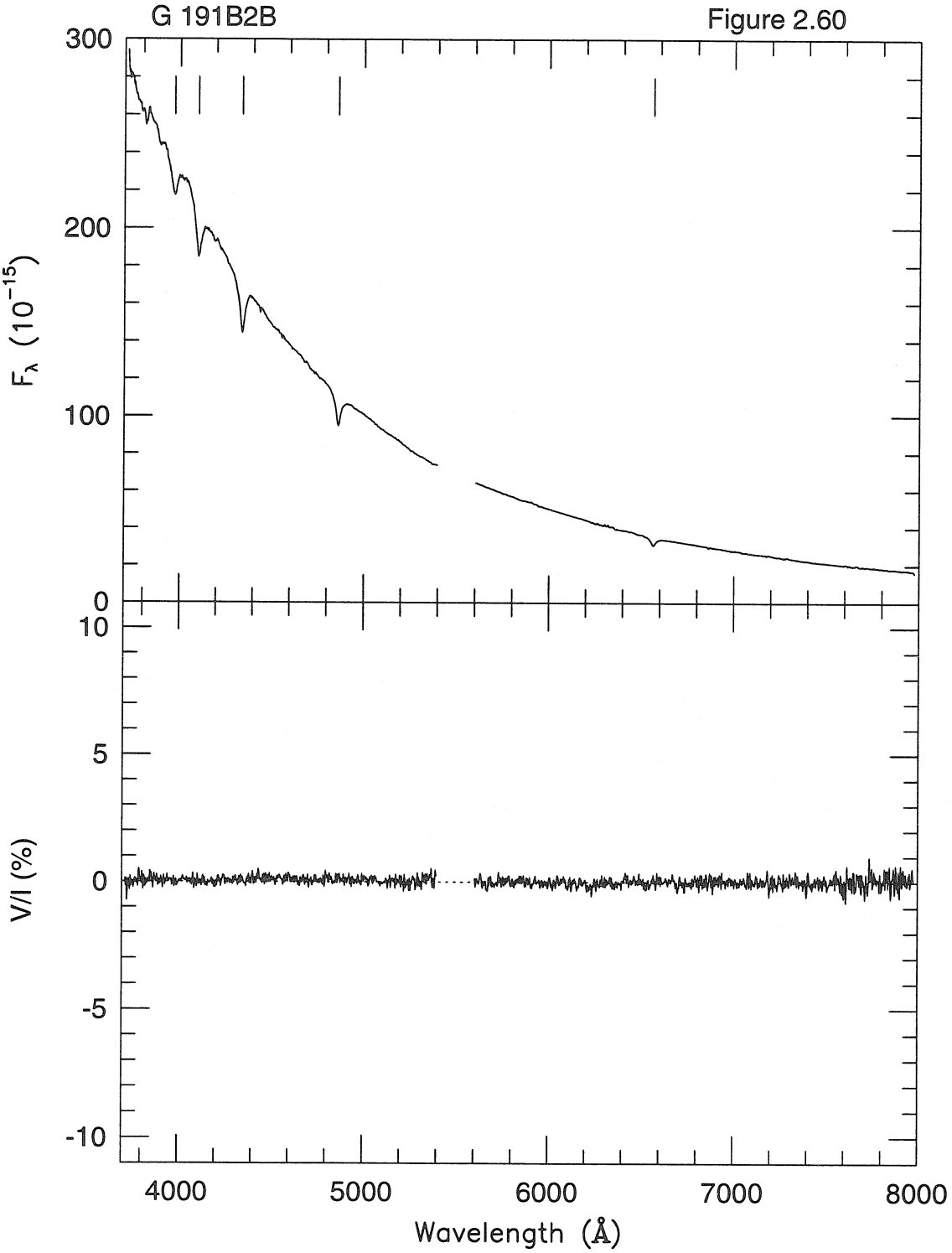
G 191B2B
Figure 2.60
300
200
100
0
F_λ (10^{-15})
10
5
0
-5
-10
V/I (%)
4000
5000
6000
7000
8000
Wavelength (Å)

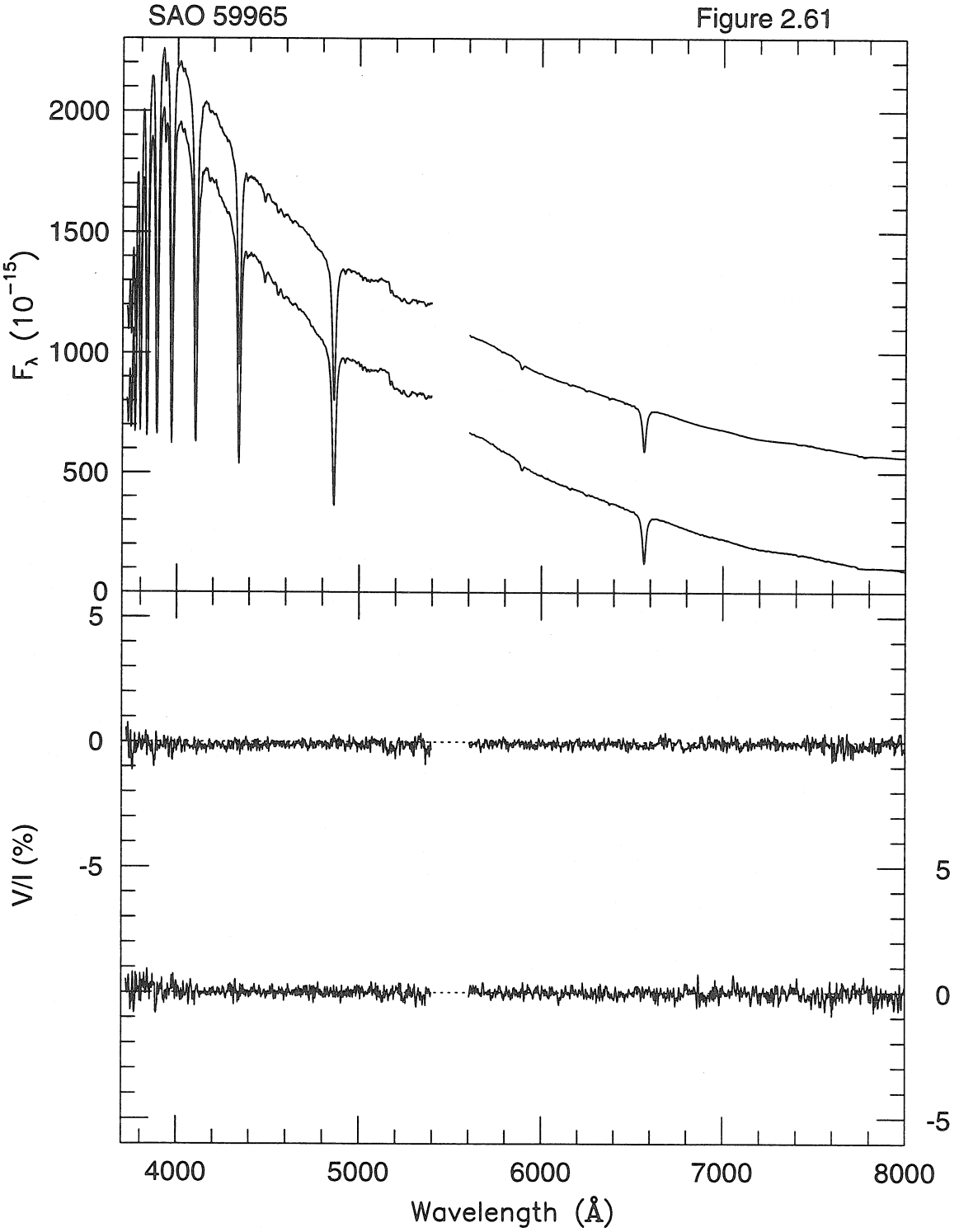
SAO 59965
Figure 2.61
2000
1500
1000
500
0
F_λ (10^{-15})
5
0
-5
V/I (%)
5
0
-5
4000
5000
6000
7000
8000
Wavelength (Å)

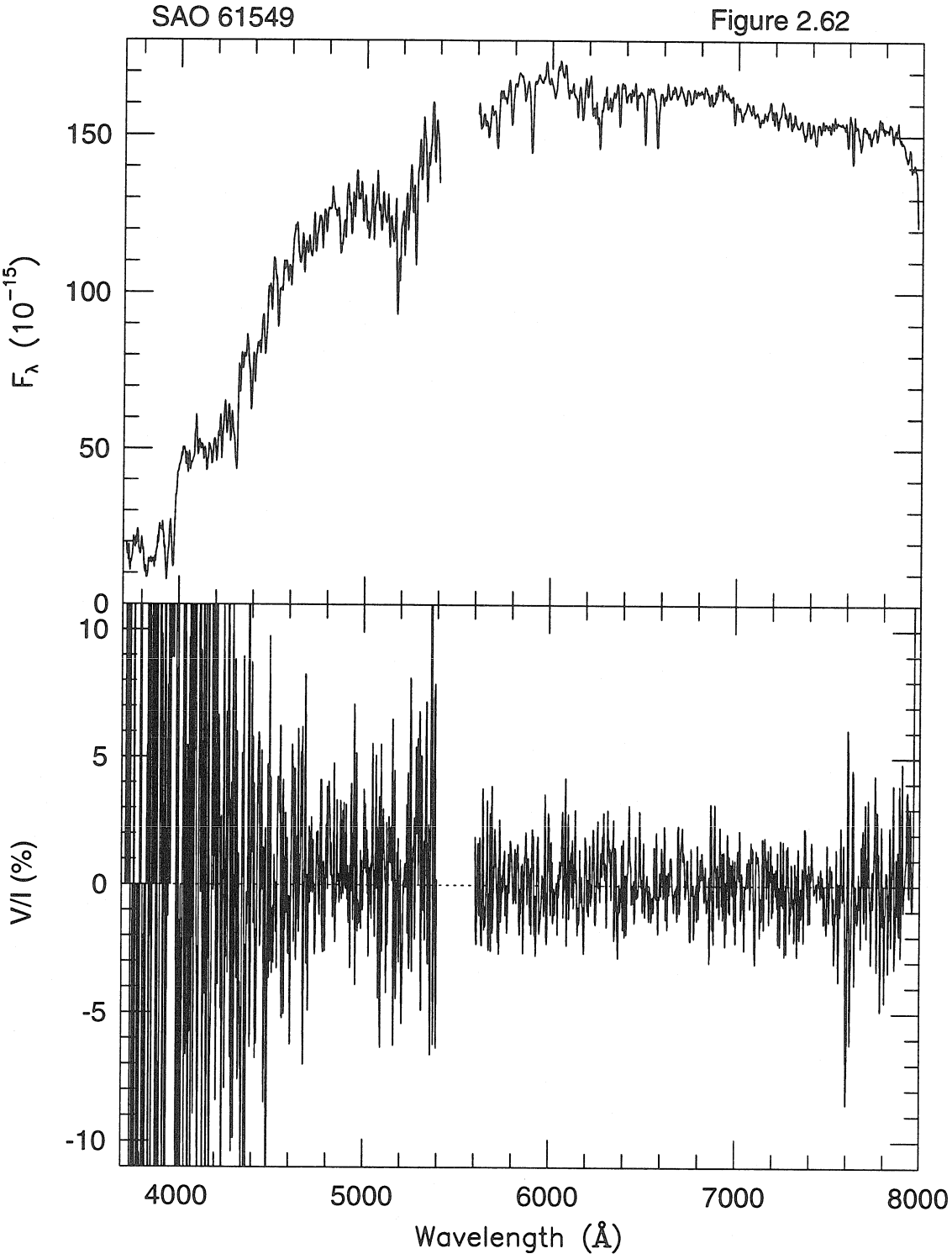
SAO 61549
Figure 2.62
150
100
50
0
F_λ (10^{-15})
10
5
0
-5
-10
V/I (%)
4000
5000
6000
7000
8000
Wavelength (Å)

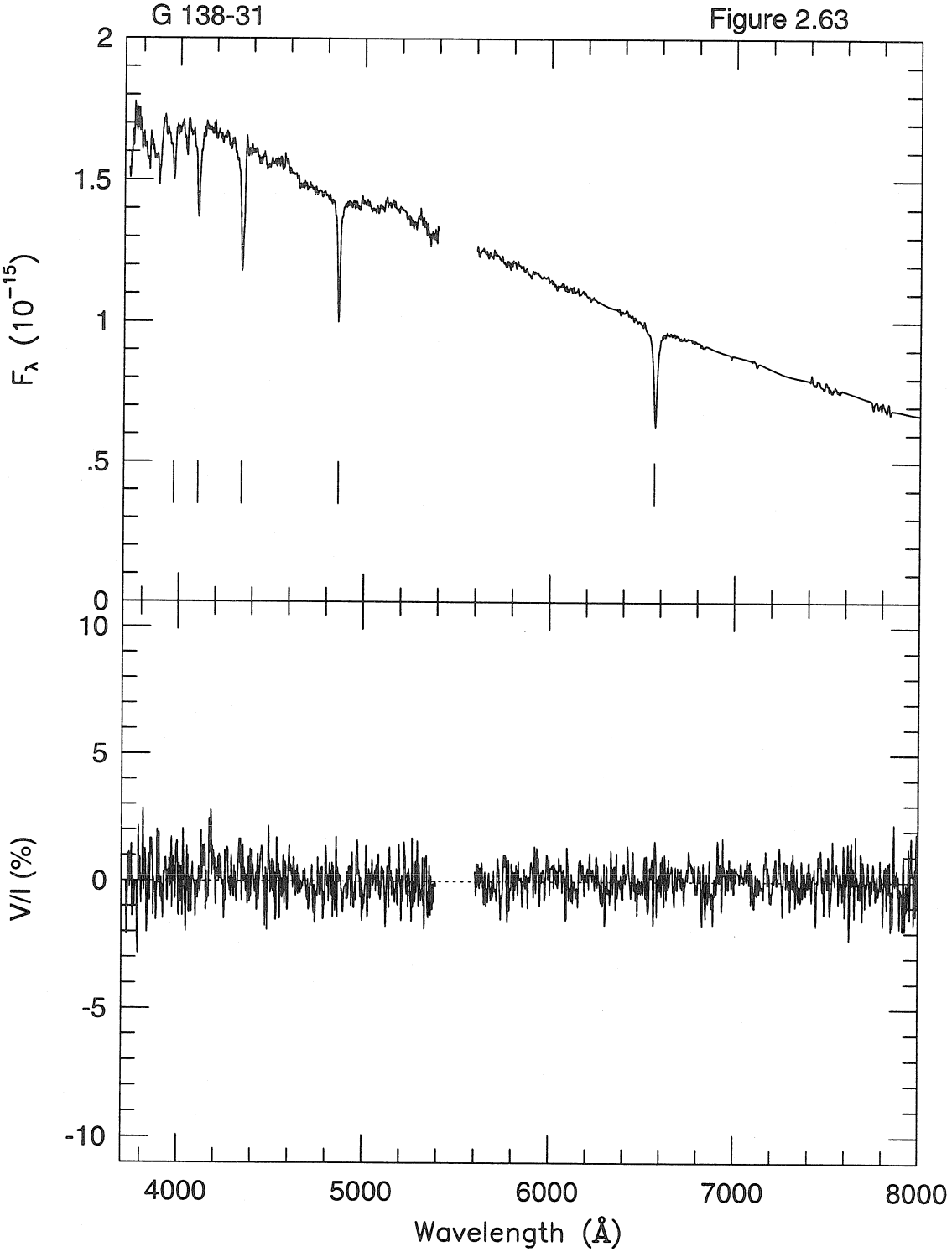
G 138-31
Figure 2.63
2
1.5
1
.5
0
F_λ (10^{-15})
10
5
0
-5
-10
V/I (%)
4000
5000
6000
7000
8000
Wavelength (Å)

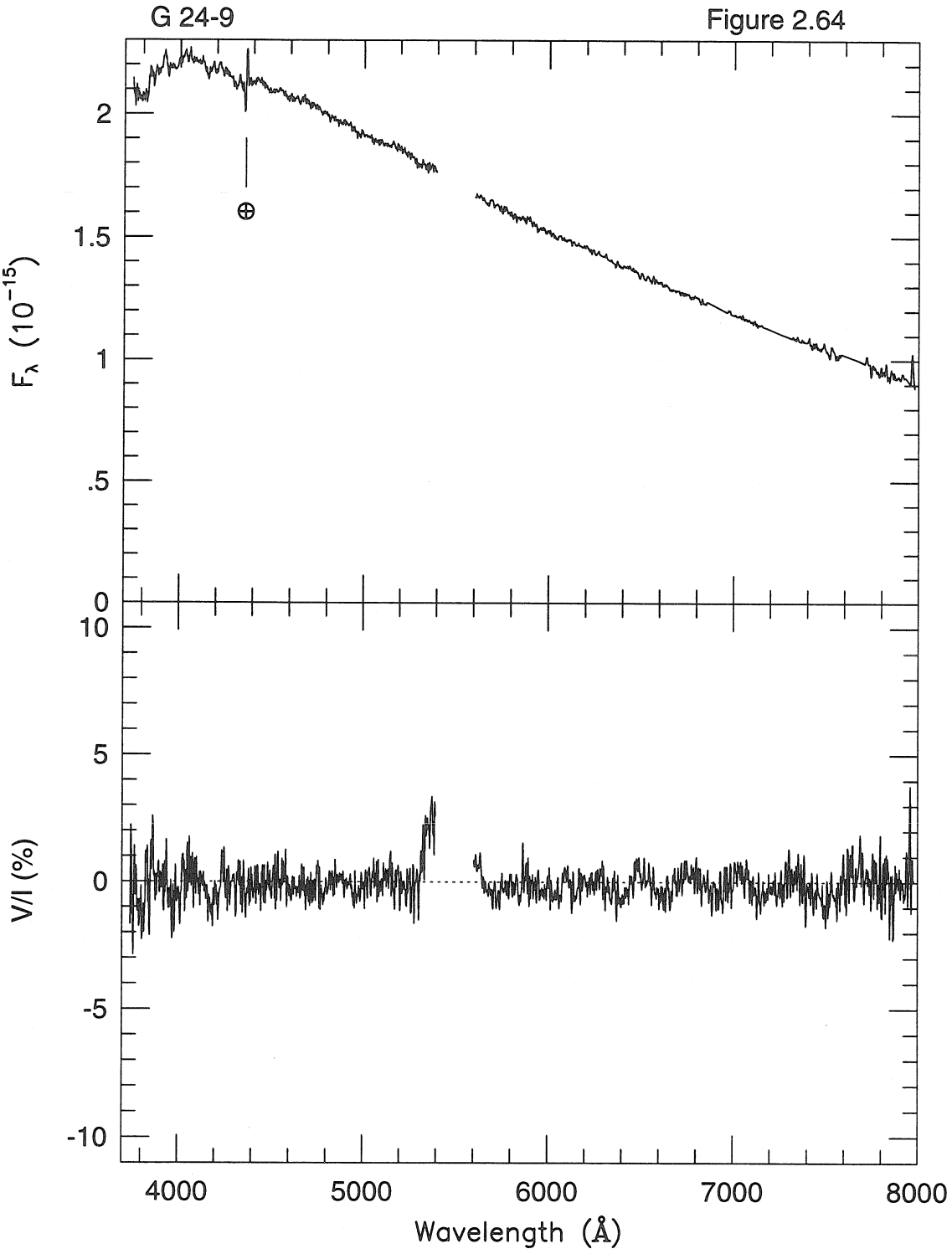
G 24-9
Figure 2.64
2
1.5
1
.5
0
F_λ (10^{-15})
⊕
10
5
0
-5
-10
V/I (%)
4000
5000
6000
7000
8000
Wavelength (Å)

Figure 2.65

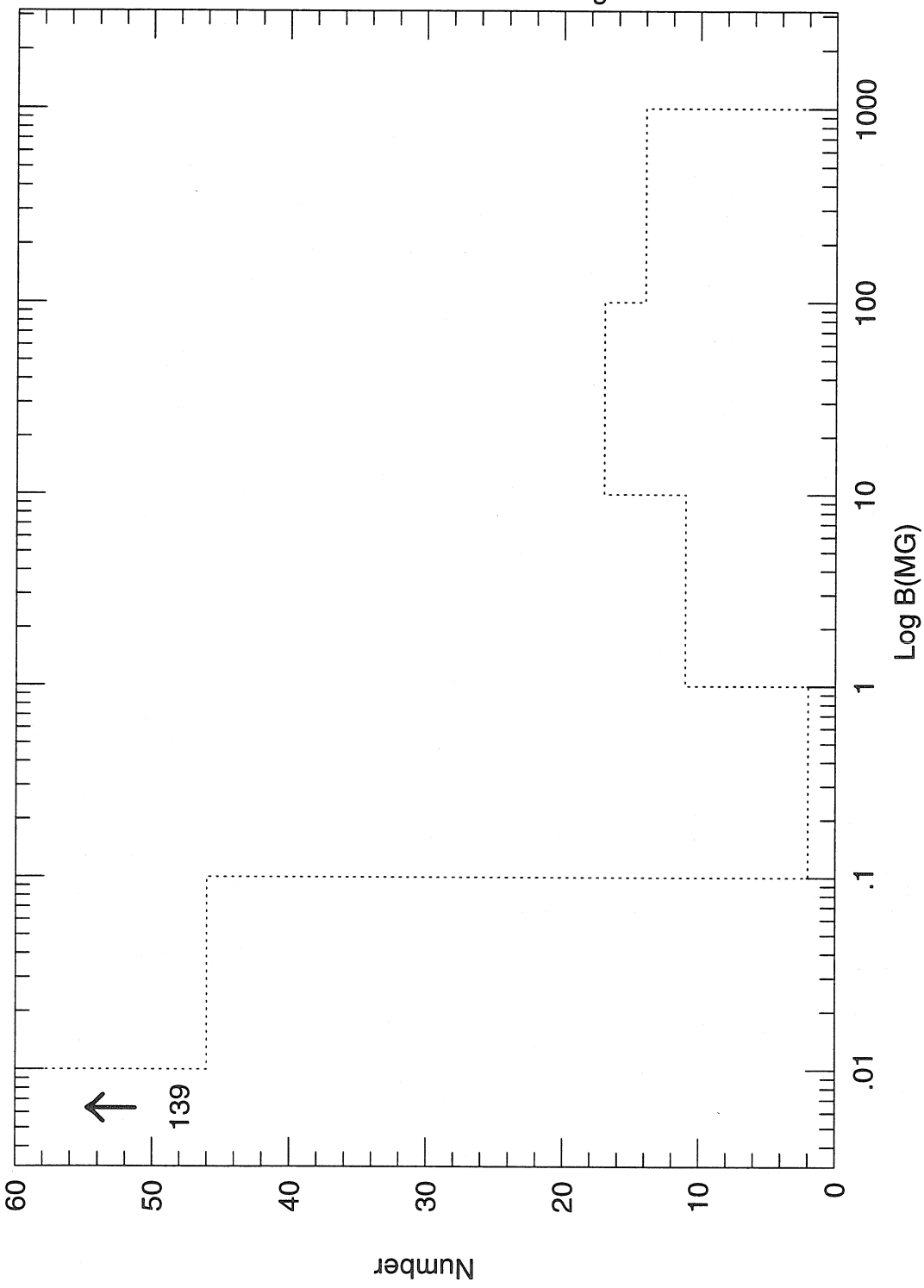

Figure 2.66

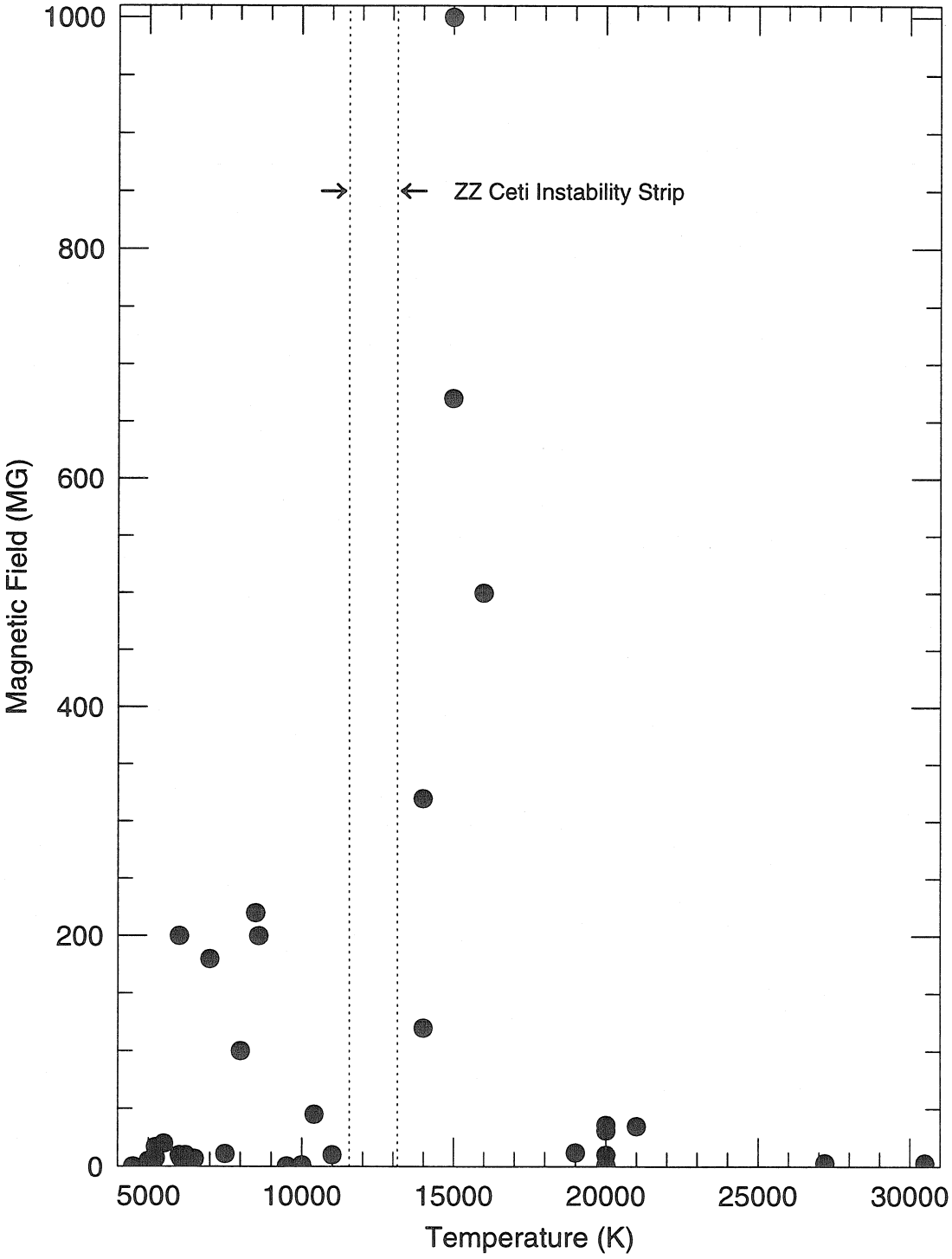
1000
800
600
400
200
0
Magnetic Field (MG)
ZZ Ceti Instability Strip
5000
10000
15000
20000
25000
30000
Temperature (K)

Figure 2.67

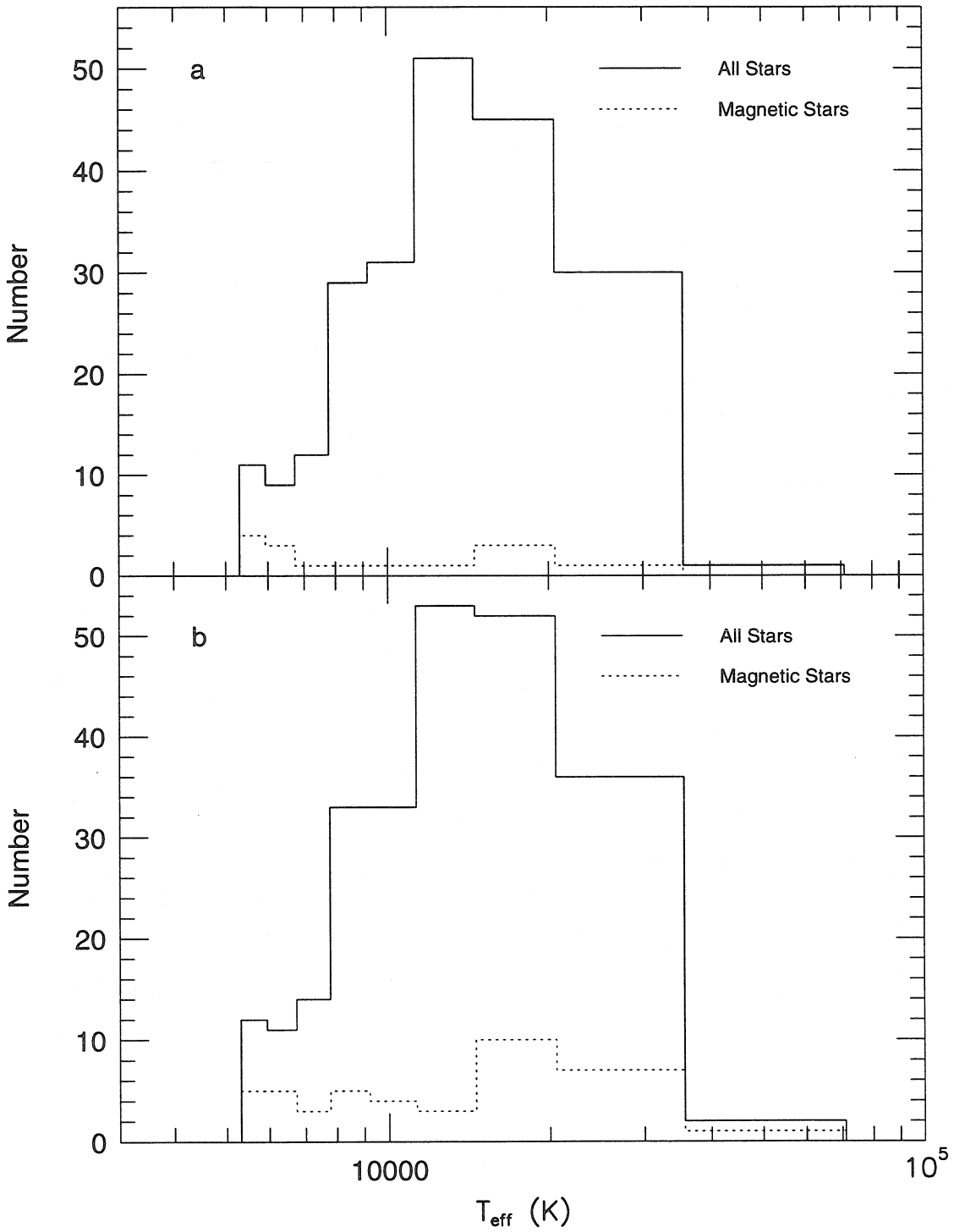
a
All Stars
Magnetic Stars
Number
50
40
30
20
10
0
b
All Stars
Magnetic Stars
Number
50
40
30
20
10
0
10000
10^5
T_{eff} (K)

CHAPTER 3

Rotation of Magnetic White Dwarf Stars

Abstract

Three magnetic stars from the DC white dwarf survey were re-observed to investigate the possibility of rotation. Two are definitely rotating: LHS 1734 with 16 min$\lesssim P <$1 yr and G 158-45 (=LHS 1044) with a probable period $P \sim 11$ hr but a definite period $P \leq 1$ day or $P \sim$ a few days. G 183-35 might be rotating with 50 min$\lesssim P <$ a few yr. From all the white dwarf rotations known, it is clear that angular momentum is lost before a star becomes a white dwarf. It is not clear that magnetic fields greatly enhance the angular momentum loss.

3.1 Introduction

Most stars rotate. In general, O, B, A, and early F stars are the only ones to rotate rapidly, $v \sin i > 50$ km/s, although typically with $100 < v \sin i < 200$ km/s (Tassoul 1978), and the later type stars generally rotate more slowly.[1] There are exceptions to these speeds, e.g., Be stars usually rotate with $v \sin i \sim 350$ km/s (Huang & Struve 1960), and Ap and Am stars with $v \sin i \sim 30$ km/s (Tassoul 1978). The rotation velocities are normally determined by measuring the line widths. This type of measurement is generally not possible for white dwarf stars since the line broadening due to the gravity is typically larger than broadening due to rotation; Stark broadening (pressure broadening) is typically 20 Å in a white dwarf, whereas rotational broadening for a white dwarf with a velocity, $v \sin i$, of 60 km/s ($\sim$ 730 s period) is about 1 Å. Some DA white dwarfs have been found with very sharp line cores and from these cores a rotation velocity has been measured

[1] A rotation velocity, v, is measured for some stars and a rotation period, P, for others. They are related by $P = v/(2\pi R_*)$, where R_* is the star's radius. I refer to the measured value and, for white dwarfs, calculate the other value.

(Greenstein & Peterson 1973; Pilachowski & Milkey 1984, 1987). However, this method cannot be used on most white dwarfs because their cores are not sharp enough, they are too faint, or they are not rotating fast enough. The only other way to measure the rotation of an isolated white dwarf is to measure the periodicity of a changing feature. The only white dwarfs to have changing features are ZZ Ceti stars and magnetic white dwarf stars (MWDs).

White dwarf rotation is a field where the data in hand are confusing, but there is very little data in hand. Only a small number of MWDs have known periods. The table of Schmidt & Smith (1995; SS) lists 42 stars and only 15 have rotation periods or limits on rotation periods. Five of these have not varied over periods of tens of years (actually, GD 229 has seen some variation over decades (Schmidt, Latter, & Foltz 1990)), and were therefore given the lower limit of 100 years ($v \sin i < 10^{-5}$ km/s). The others range from 1.5 hours ($v \sin i \sim 8$ km/s) to 18 days ($v \sin i \sim 0.3$ km/s) (see Table 3.5). There is a glaring gap in the rotation periods between several weeks and a century. Schmidt & Norsworthy (1991; SN) comment extensively on this gap. They could find no correlation between period and magnetic field strength nor period and temperature (age). However, it should be mentioned that all of the known white dwarfs with periods > 100 yr have fields above 100 MG, but not the converse. SN also point out the lack of white dwarfs with periods of less than 99 min, despite the technical ability to detect rotation periods of 10 min and greater. Barstow et al. (1995) recently discovered a MWD, RE J0317-853, which appears to be rotating with a period 725.4 s. At present, it is not possible to measure a rotation period near the breakup speed, which corresponds to a period of a few seconds (see Chapter 1). Three of the magnetic white dwarfs in my survey, G 158-45(=LHS 1044), LHS 1734, and G 183-35 (see Chapter 2), were observed more than once to check for rotation. All three show signs of rotation. The number of observations of these stars was insufficient to determine rotation periods, but limits can be placed on them. Adding these three stars to the list of rotating MWDs by no means explains the non-rotating objects, nor places them in a "very rare" category. It does, however, slowly increase the

number of stars known to rotate and demonstrate the profitability of this line of research.

3.2 Observations

The observations of these objects were taken on the 200 inch Palomar telescope and the 10 meter Keck telescope. All information regarding these observations are described in Chapter 2, Section 2.3. Table 3.1 lists observation data for the objects. Table 3.2 lists the magnetic field strengths measured for these stars in Chapter 2.

3.3 Analysis

Seven objects in the DC survey have a magnetic field above 1 MG. Four were observed on more than one occasion, although PG 1312+098 has had its period determined by SN. The remaining three, G 158-45(=LHS 1044), LHS 1734, and G 183-35, had never been monitored for rotation before. A precise rotation period cannot be found for any of these objects with the data taken, although there are strong limits on G 158-45(=LHS 1044). In all cases, only Hα will be discussed. The Hβ lines are either much weaker or non-existent. The whole wavelength range observed, including Hα and Hβ, can be viewed in Chapter 2.

3.3.1 G 183-35

Only two observations of this object were taken. Two observations are adequate to determine if a star is rotating; however, two are inadequate to determine the absence of rotation. Figure 3.1 shows the Hα region of the two observations in both flux and circular polarization. The data have been smoothed by 6.2 Å (= 2 pixels) for clarity. The σ-components have widened in the September data in flux and, more importantly, their shape has changed in polarization. In the June 1993 data, the σ-components are well pronounced and the continuum polarization is -1% (as is pointed out in Chapter 2, this value may be too high). Both of these

indicate a viewing angle closer to the magnetic pole than the magnetic equator (this conclusion remains the same even if the continuum polarization is actually null). The September 1994 polarization shows signs of being a nearly equator-on view of the magnetic field. The continuum polarization is nearly null and the σ-components might each have a "mixed" shape, although it is hard to be certain through all the noise. A "mixed" shape occurs when the parts of the σ-components closest to the π-component (central component) have a polarization corresponding to a magnetic field with, say, a positive sense, and the parts of the σ-components further from the π-component has the opposite sense, in this example, a negative sense.

This object is probably rotating. Due to the paucity of data, the length of the exposure time, and the length of time between observations, all that can be said about a possible rotation period is that it is 50 min $\lesssim$ P $<$ a few years. This star needs monitoring. Judging by the minor changes in flux absorption line shape, and low continuum polarization, this is best done in circular spectropolarimetry.

3.3.2 LHS 1734

Three observations were taken of this object. Figure 3.2 shows the Hα region in flux and polarization for all three observations. The shapes of the σ-components have changed slightly from one observation to the next in flux and they changed more drastically in polarization (the September data are very noisy). The October polarization data show a "mixed" shape in the σ-components whereas they are well defined in the December data.

From these observations, I must conclude that the object is rotating. Using the two clean (Keck) spectra, October 1994 and December 1994, I can place limits of 16 min $\lesssim$ P $<$ 1 year on the object. This object needs monitoring in circular spectropolarimetry.

3.3.3 G 158-45=LHS 1044

This is the best studied object of the three. Six observations were made from September 1994 through December 1994, including two sets of two observations taken on consecutive days. Figure 3.3 shows the Hα region for all six observations in both flux and polarization. In this case, not only do the flux features change shape from one observation to the next, but they also change position in wavelength. In polarization, there are sign reversals amongst the different observations. The two November observations show evidence of "mixing," although not as pronounced as for LHS 1734.

The number of observations and the close spacing of observations allows for a much tighter period range determination for G 158-45 than for the previous two objects. There were 24:07:09 hours between the two November observations. The wavelengths of the σ-components shifted in flux and polarization, and the polarization flipped sign, in both the features and continuum. Clearly, if the magnetic field is symmetric or nearly symmetric, the magnetic and rotational axes are not aligned, therefore allowing for a view of one magnetic hemisphere on one day and the other hemisphere on the next. Figures 3.4 a and b schematically show a possible alignment of the magnetic and rotational axes for the two November observations. Both circular polarization measurements show signs of "mixing," which implies that some of the other magnetic hemisphere is present. Figure 3.4 c shows some possible locations of the exposures on the rotation cycle. The "A"s represent possible time positions for the November 8 observations and the "B"s for November 9. The data could be separated by more than the half rotation shown. These two observations put limits of a few hours to a few days ($\sim$ 3 or 4) on the rotation period. The December data places a few more restrictions on the period. The December observations are 22:06:29 hr apart. The data from the two observations are nearly identical. This can mean that they represent the same phase of the rotation, implying either a $\sim$ 22 hr period, or some submultiple thereof. It can also mean that they come from very similar phases of the rotation, e.g., the first observation is of the phase just before maximum magnetic field

strength and the second observation is the phase directly afterwards. Figure 4d shows some of these possibilities. These additional data points place limits on the period of either ≤ 1 day or about 3 or 4 days.

The best way to determine a period would be to use a Fast Fourier Transform on the data, like those who study pulsars use. However, six points in four months are far too few data points to use this method. The time proximity of the two November data points and the two December data points gave strong limits within each run. A continuous sine curve of the form

$$\mathrm{A}(t) = \mathrm{A}_0 + \mathrm{A}_1 \sin(\omega(t + t_0)) \tag{3.1}$$

should pass through all six data points, where A can refer to the circular polarization or the disk averaged magnetic field strength, $\omega = \frac{2\pi}{P}$, and t_0 is the initial epoch, A_1 is the semi-amplitude, and A_0 is the mean polarization or magnetic field. To test out the possible periods, I made a grid search of the four variables in both circular polarization and disk averaged magnetic field strength and tested for a minimum χ^2 $(= \sum((\mathrm{A}_i - \mathrm{A}(t_i))/\sigma_i)^2)$ of equation (3.1). Table 3.3 lists the data points used. The polarization data are the average polarization from 6000 Å to 8000 Å (see Table 2.6). The magnetic field data points are not the B_e calculated in Chapter 2. The B_e are calculated from the flux measurements and are a mean line of sight magnetic field strength. The B in Table 3.3 are calculated from the polarization measurements and are a disk averaged field strength, e.g., three-quarters of the observed hemisphere of a star is covered in a field of ~ 8.5 MG and one-quarter in ~ -10.0 MG, thus the disk averaged field is $(0.75 \times 8.5) + (0.25 \times (-10.0)) = 3.9$ MG. The method of field determination used was similar to that of Section 2.4.2.2, except the gaussians were calculated and matched to the σ-components of the circular polarization data. In the cases of the two November observations, which showed "mixed" polarization, a magnetic field was fit to each of the "mixed" pieces of the σ-components. Then the percentage of the surface area covered by each field strength was determined from the equivalent width of each piece, and the disk averaged field strength was calculated. The

errors quoted are derived from the errors of the magnetic field strength from the dominant piece of the "mixed" σ-component. For both the V and B grid searches, periods from 0.005 days to 4.2 days and t_o from 0 to 8.95 days were searched. The polarization grid search covered V_0 from 0 to 0.26 % and V_1 from 0.36 to 0.41 %. The minimum χ^2 (= 15) occurred at P = 11.4 hours, V_1 = 0.41 %, V_0 = 0 %, and t_o = 0 days. The magnetic field grid search covered B_0 from -2 to 2 MG and B_1 from 10 to 15 MG. The minimum χ^2 (= 22) occurred at P = 10.8 hours, B_1 = 10.2 MG, $B_0 = -0.8$ MG, and t_o = 1.4 hours. Thus the most likely rotation period is $\sim$ 11 hours. A goodness of fit was also calculated for both grids using the incomplete gamma function (=χ^2 probability function; Press et al. 1989), which agreed that these were the best fits and not too unreasonable at that. I felt that errors assigned to the results would have little meaning due to the paucity of data, so I have not done so. There is a source of a possible error in the data used in the grid searches. The observations taken at Keck were approximately 12 min long and those at Palomar were 50 min long. The Palomar data points contain less information than the Keck points since they are an average over a larger fraction of the stellar surface. If the period were actually a submultiple of 11 hours, then the lack of information in the Palomar data could hide this from the present analysis. This was a simple exercise and may make it easier on future observers when they try to monitor this star for rotation. It might be worth noting that each grid has less significant χ^2 minima at $\sim$ 3 days (for V) and $\sim$ 4 days (for B).

3.4 Discussion

Like magnetic fields, rotation is often not included in stellar evolution schemes. Intuitively, one would expect a star to slow down as it expands and speed up as it shrinks, thus conserving angular momentum. A main sequence A0 star has an angular momentum $J \sim 10^{52}$ g cm^2 s^{-1}. If this were conserved until the white dwarf stage and the star became a 0.6 $M_\odot$, 10^{-2} $R_\odot$ white dwarf, it

would have a velocity of $V_e \sim 10^5$ km/s, which is 30 times faster than the break-up velocity! The fastest DA measured by Pilachowski & Milkey (1987; PM) is rotating at 60 km/s (see Table 3.4), implying a loss of a factor of 10^3 in angular momentum. Magnetic white dwarfs are typically rotating with 12 km/s ($P \sim 1$ hr) to 10^{-5} km/s ($P \sim 100$ yr) (see Table 3.5), although RE J0318 – 853 is as fast as the fastest PM object. These rotations imply losses of factors of 10^3 to 10^{10} in angular momentum for MWDs. Even if MWDs are descended from Ap stars, the losses are still large. An Ap0 star has an angular momentum $J \sim 10^{51}$ g cm^2 s^{-1}, so this places the losses at factors of 10^2 to 10^9.

The most probable explanation is that angular momentum is being transferred from the core to the envelope, at some stage in the star's life, and is then lost when the envelope is blown off. This leaves the white dwarf rotating with a smaller angular momentum than it had as a main sequence star. It is also expected that magnetic coupling of the core and envelope will increase the angular momentum transfer (SN). This implies that magnetic white dwarfs should rotate slowest.

Unfortunately, this is a regime of small number statistics. Figure 3.5 shows the known temperature vs. rotation period for MWDs (from SS and Barstow et al. 1995) and the DA stars of PM. There is no correlation of temperature (age) and rotation period, although it does appear that non-magnetic DAs might rotate more quickly than MWDs, but most of the measurements are lower limits. Figure 6 shows magnetic field strength vs. period for these same stars; all of the PM stars were included in the DA survey of SS (see Table 3.4). There is some correlation of increasing magnetic field strength and increasing rotation period. If this is true, PG 1015+014, PG 1031+234 and RE J0317 – 853 are clear outliers to the relation. It is also conceivable that the stars with $P \geq 100$ yr, the "century club," are special in some way.

There are two simple scenarios which could explain Figure 3.6. Both cases involve splitting up the white dwarfs into two classes. The first scenario has

one group of quickly rotating high magnetic field stars, e.g., PG 1015+014, PG 1031+234, and RE J0317 − 853, and the second group consists of all the remaining stars (these groups may appear arbitrary, but the "fast" group consists of all stars with B> 100 MG and $P \ll 100$ years, i.e., all stars which overlap in magnetic field strength with the century club). The idea behind this is that most stars follow the theory of increasing angular momentum transfer with increasing magnetic field strength. Thus the stronger the magnetic field, the longer the rotation period. Then the other group, the faster stars, are somehow spun up. Perhaps these stars had once been part of a close binary system with mass transfer causing the white dwarf to spin up. In this case, the secondary is too faint to be seen, e.g., a cooler white dwarf or a neutron star. It should be noted that RE J0317 − 853 might be part of a wide, ∼ 600 AU, binary (Barstow et al.).

Another scenario is where most stars, both with and without a strong magnetic field, lose a fraction of their angular momentum during the course of evolution. The magnetic stars might transfer a bit more than non-magnetic stars. However, there is a second group of stars – those in the century club. These may have lost much more angular momentum. They may be the descendants of the slowest Ap stars. They may all be viewed nearly pole-on, which is supported by the Wickramasinghe & Ferrario (1988) model of Grw+70°8247 wherein they fit the spectrum with an inclination angle of $i = 0°$ to $30°$ ($i = 0°$ = pole). Statistically, it is not plausible that the rotation axis of 1/3 of all MWDs is pointed towards the Earth. As more magnetic white dwarfs are found to rotate, it does become more plausible that this is the case for all (or some) of the members of the century club. From several works (Greenstein & Oke 1982; Liebert 1988; Sion et al. 1988; Schmidt et al. 1992), it has become clear that MWDs tend towards high masses, i.e., $M_{MWD} > 0.6$ $M_\odot$. Only two magnetic white dwarfs have had a mass determination, and both of these are heavier than 1 $M_\odot$, Grw+70°8247 has M > 1 $M_\odot$ (Greenstein & Oke) and PG 1658+441 has M= 1.31 ± 0.02 $M_\odot$ (Schmidt et al.). Perhaps all the stars in the century club are above some critical mass which

causes them to rotate even more slowly than the other stars (PG 1658+441 has not yet been determined to rotate).

In order to determine if the outliers to either theory are a true class of their own or just flukes, many more magnetic white dwarfs need to be monitored for rotation.

I would also like to point out that there are three other types of white dwarfs in which rotation periods can be determined. These are the variable white dwarfs, DOV (PG 1159 stars), DBV, and DAV (ZZ Ceti stars). Observations with the Whole Earth Telescope (Nather et al. 1990) have led to rotation period measurements in some of these stars. All the rotation periods measured have been a few hours to a few days. One star has had a magnetic field determination, GD 358 with $B = 1300 \pm 300$ G (Winget et al. 1994), and one has an upper limit, PG 1159−035 with $B < 6000$ G (Winget et al. 1991). All the other stars' magnetic fields are presumably lower since a magnetic field of the strengths of GD 358 and PG 1159−035 would have been detectable in the measured pulsations. These stars add a few more points in the left side of Figure 3.6. This lends more credence to the scenario of the century club stars being a separate group of stars, but the measured variable stars are too few to make a definite statement.

3.5 Conclusions

The DC survey (Chapter 2) has discovered 2 and possibly 3 new rotating magnetic white dwarf stars. No rotation period has been determined for any of the stars due to a lack of data. However, limits have been set. If G 183-35 is rotating, it is doing so with a period between 50 min and a few years. LHS 1734 has a period between 16 min and 1 year. G 158-45 (=LHS 1044) probably has a period of $\sim$ 11 hr, but more conservative limits of either 1 day or less or a period of a few days. These periods are all consistent with the other magnetic white dwarf rotation periods.

From all the data on white dwarf rotation, it is clear that factors of 10^3 to 10^{10} of angular momentum is lost during stellar evolution between the main sequence and the white dwarf stage. This is probably achieved through angular momentum transfer from the core to the envelope followed by the ejection of the envelope. It is not clear from the data that a magnetic field vastly increases this process. The data needed to make a more definite statement are obtainable, but would take several years to aquire.

The observations in this chapter were taken in collaboration with M.H. Cohen, R.W. Goodrich, P.M. Ogle, and H.D. Tran. I wish to thank M.H. Cohen for comments on the manuscript. I wish to thank G. Vashist, Y. Wu, and M.H. Van Kerwijk for discussions on white dwarf rotation. This research has made use of the Simbad database, operated at CDS, Strasbourg, France.

References

Allen, C.W. 1973, Astrophysical Quantities, 3rd edition (London: The Athlone Press), p. 213

Barstow, M.A., Jordan, S., O'Donoghue, D., Burleigh, M.R., Napiwotzki, R., & Harrop-Allin, M.K. 1995, MNRAS, in press

Greenstein, J.L. & Oke, J.B. 1982, ApJ, 252, 285

Greenstein, J.L. & Peterson, D.M. 1973, A&A, 25, 29

Huang, S. & Struve, O. 1960, in Stellar Atmospheres, ed. J.L. Greenstein (Chicago: The University of Chicago Press), 321

Liebert, J. 1988, PASP, 100, 1302

Nather, R.E., Winget, D.E., Clemens, J.C., Hansen, C.J., & Hine, B.P. 1990, ApJ, 361, 309

Pilachowski, C.A. & Milkey, R.W. 1984, PASP, 96, 821

——— 1987, PASP, 99, 836

Press, W.H., Flannery, B.P., Teukolsky, S.A., & Vetterling, W.T. 1989 (Cambridge: Cambridge University Press)

Schmidt, G.D., Bergeron, P., Liebert, J., & Saffer, R.A. 1992, ApJ, 394, 603

Schmidt, G.D., Latter, W.B., & Foltz, C.B. 1990, ApJ, 350, 758

Schmidt, G.D. & Norsworthy, J.E. 1991, ApJ, 366, 270 (SN)

Schmidt, G.D. & Smith, P.S. 1995, ApJ, 448, 305 (SS)

Sion, E.M., Fritz, M.L., McMullin, J.P., & Lalla, M.D. 1988, AJ, 96, 251

Tassoul, J.L. 1978, Theory of Rotating Stars (Princeton: Princeton University Press), pp 16

Wickramasinghe, D.T. & Ferrario, L. 1988, ApJ, 327, 222

Winget, D.E., Nather, R.E., Clemens, J.C., Provencal, J., Kleinman, S.J., Bradley, P.A., Wood, M.A., et al. 1991, ApJ, 378, 326

Winget, D.E., Nather, R.E., Clemens, J.C., Provencal, J., Kleinman, S.J., Bradley, P.A., Claver, C.F., et al. 1994, ApJ, 430, 839

Table 3.1 Summary of Observations

Name	Telescope	Date (UT)	Exposure	Exposure Start (UT)	Weather	Flux Standard
G 158-45	Palomar	94-Sep-29	50 min	07:01:41	cldy	GD 248
	Keck	94-Oct-28	16 min	11:10:33	clr	GD 248
	Palomar	94-Nov-8	50 min	03:37:51	fog	GD 248
	Palomar	94-Nov-9	50 min	03:45:00	clr	GD 248
	Keck	94-Dec-30	12 min	07:46:59	clr	G 193-74
	Keck	94-Dec-31	8 min	05:53:28	clr	G 191B2B
LHS 1734	Palomar	94-Sep-28	50 min	11:29:39	cldy	GD 248
	Keck	94-Oct-28	16 min	13:41:43	clr	GD 248
	Keck	94-Dec-31	16 min	09:03:10	clr	G 191B2B
G 183-35	Palomar	93-Jun-17	50 min	07:55:02	clr	G 138-31
	Palomar	94-Sep-29	50 min	03:09:21	vcdy	GD 248

Table 3.2 Magnetic Field Strengths of Observed Stars

Name	Date	B_e (MG)	Name	Date	B_e (MG)
G 158-45	94/9/29	$+8.8^{+1.2}_{-0.8}$	LHS 1734	94/9/28	$+3.9 \pm 0.4$
	94/10/28	$+8.2^{+0.6}_{-0.4}$		94/10/28	$+3.8^{+1.0}_{-0.5}$
	94/11/8	$-10.0^{+1.4}_{-0.2}$		94/12/31	$+3.8^{+0.4}_{-0.2}$
	94/11/9	$+8.7^{+0.9}_{-0.5}$	G 183-35	93/6/17	6.8 ± 0.5
	94/12/30	$-10.0^{+0.6}_{-0.4}$		94/9/29	
	94/12/31	$-10.0^{+0.6}_{-0.4}$			

Table 3.3 Date, Circular Polarization, and Magnetic Field for Grid Search

Date (JD-2440000)	$\langle V_{red} \rangle$ (%)	B (MG)
9624.7928	-0.106 ± 0.056	$+8.7 \pm 0.5$
9653.9788	-0.107 ± 0.022	$+8.2 \pm 0.5$
9664.6513	$+0.190 \pm 0.031$	-7.3 ± 0.4
9665.6563	-0.053 ± 0.024	$+4.4 \pm 0.5$
9716.8243	$+0.368 \pm 0.028$	-10.1 ± 0.4
9717.7455	$+0.270 \pm 0.020$	-10.1 ± 0.5

Table 3.4 Rotation Periods of Non-Magnetic DA Stars

Name	Period (min)	$v \sin i$ (km/s)	B (kG)	T (K)
WD 0205+25	15^{+9}_{-5}	50 ± 20	-10.5 ± 5.4	20300
WD 0401+25	24^{+9}_{-6}	30 ± 10	$+1.3 \pm 6.6$	13500
WD 0413 − 07	≥ 73	10 ± 10	$+1.2 \pm 0.9$	16900
WD 0425+16	≥ 73	10 ± 20	-5.1 ± 6.3	23900
WD 0644+37	≥ 73	10 ± 10	$+1.9 \pm 1.6$	22200
WD 0943+44	≥ 73	10 ± 20	-5.1 ± 8.1	14500
WD 1104+60	≥ 37	20 ± 20	$+2.9 \pm 8.1$	19200
WD 1105 − 04	≥ 33	22 ± 25	$+14.0 \pm 8.1$	15300
WD 1134+30	12^{+3}_{-2}	60 ± 10	-0.6 ± 2.2	23000
WD 1327 − 08	17 ± 3	42 ± 9	$+3.0 \pm 3.1$	16000
WD 1337+70	24^{+49}_{-9}	30 ± 20	$+1.1 \pm 2.1$	21000
WD 2032+24	≥ 73	10 ± 10	$+1.0 \pm 2.3$	21500
WD 2124+55	≥ 18	40 ± 40	$+14.2 \pm 9.6$	14100
WD 2126+73	18^{+19}_{-6}	40 ± 20	-8.8 ± 8.1	15400
WD 2149+02	≥ 73	10 ± 10	-4.6 ± 8.7	18300

All $v \sin i$ values from Pilachowski & Milkey (1987). Period calculated from $P \lesssim_{4.4 \times 10^4 (v \sin i)^{-1}}$, from Greenstein & Peterson (1973). All magnetic field values from Schmidt & Smith (1995).

Table 3.5 Rotation Periods of Magnetic White Dwarf Stars

Name	Period	B (MG)	T (K)
RE J0317 – 853	725.4 s	340	50000
PG 1015+014	1.65 h	120	14000
Feige 7	2.2 h	35	21000
LHS 1038	2 to 20 h	~0.1	6400
PG 1031+234	3.4 h	500-1000	15000
KPD 0253+5052	4.1 h	13	15000
PG 1312+098	5.43 h	10	20000
PG 1533-057	~ 1 d	31	20000
G 195-19	1.33 d	~100	8000
BPM 25114	2.8 d	36	20000
KUV 813-14	17.9 d	45	10400
G 227-35	$\gtrsim$100 y	180	7000
LP 790-29	$\gtrsim$100 y	~200	8600
G 240-72	$\gtrsim$100 y	~200	6000
Grw+70°8247	$\gtrsim$100 y	320	14000
GD 229	$\gtrsim$100 y	~1000	16000

All data from Schmidt & Smith (1995), except for RE J0317-853, which is from Barstow et al. (1995), and G 227-35 from Putney & Jordan (1995).

Figure Captions

Figure 3.1 G 183-35 The top panel contains the F_λ spectra for the two observations. The bottom panel contains the two circular polarization spectra. The dotted lines are the zero polarization lines for the respective spectra. The left ordinate describes the June data and the right ordinate describes the September data.

Figure 3.2 LHS 1734 Similar to Figure 1. Values for the polarization are on alternating sides of the lower panel. Note the change in the σ-components in polarization between the October and December observations.

Figure 3.3 G 158-45=LHS 1044 Similar to Figure 2.

Figure 3.4 A star's magnetic axis and rotational axis may not be aligned to one another. Thus as the star rotates around, the field visible to the observer changes.
(a) Possible orientation of the star's magnetic field on 1994 November 8.
(b) Possible orientation of the same field on 1994 November 9.
(c) Surface averaged magnetic field as a function of time on a star like that in (a) and (b). The points marked A and B represent possible positions of the star for the November 8 (A) and November 9 (B) observations. There are four possible combinations possible in this scenario. If the star is at A_1 on 11/8, then it can be at B_1 or B_2 on 11/9, and the same thing is true for A_2. The A's and B's can be separated by more than the half-rotation shown.
(d) Similar to (c), except for the nights 1994 December 30 (A) and 1994 December 31 (B). If the star is at A_1 on 12/30, then on 12/31, it can be at B_1, B_2, or B_3. If it is at A_m on 12/30, then it can be at B_m on 12/31. If it is at A_2 on 12/30, then it can be at B_2 or B_3. The separation between the A's and B's can be more than the one rotation shown.

Figure 3.5 This is a plot of temperature versus rotation period for all of the magnetic white dwarfs and non-magnetic DAs with measured rotation. The data for the non-magnetic DAs comes from Pilachowski & Milkey (1987). The arrows above a point indicates that the point is a lower limit on rotation period.

Figure 3.6 This is a plot of magnetic field strength versus rotation period. The magnetic field strengths for the Pilachowski & Milkey (1987) stars comes from Schmidt & Smith (1995). Three magnetic white dwarfs have been marked and are discussed in the text.

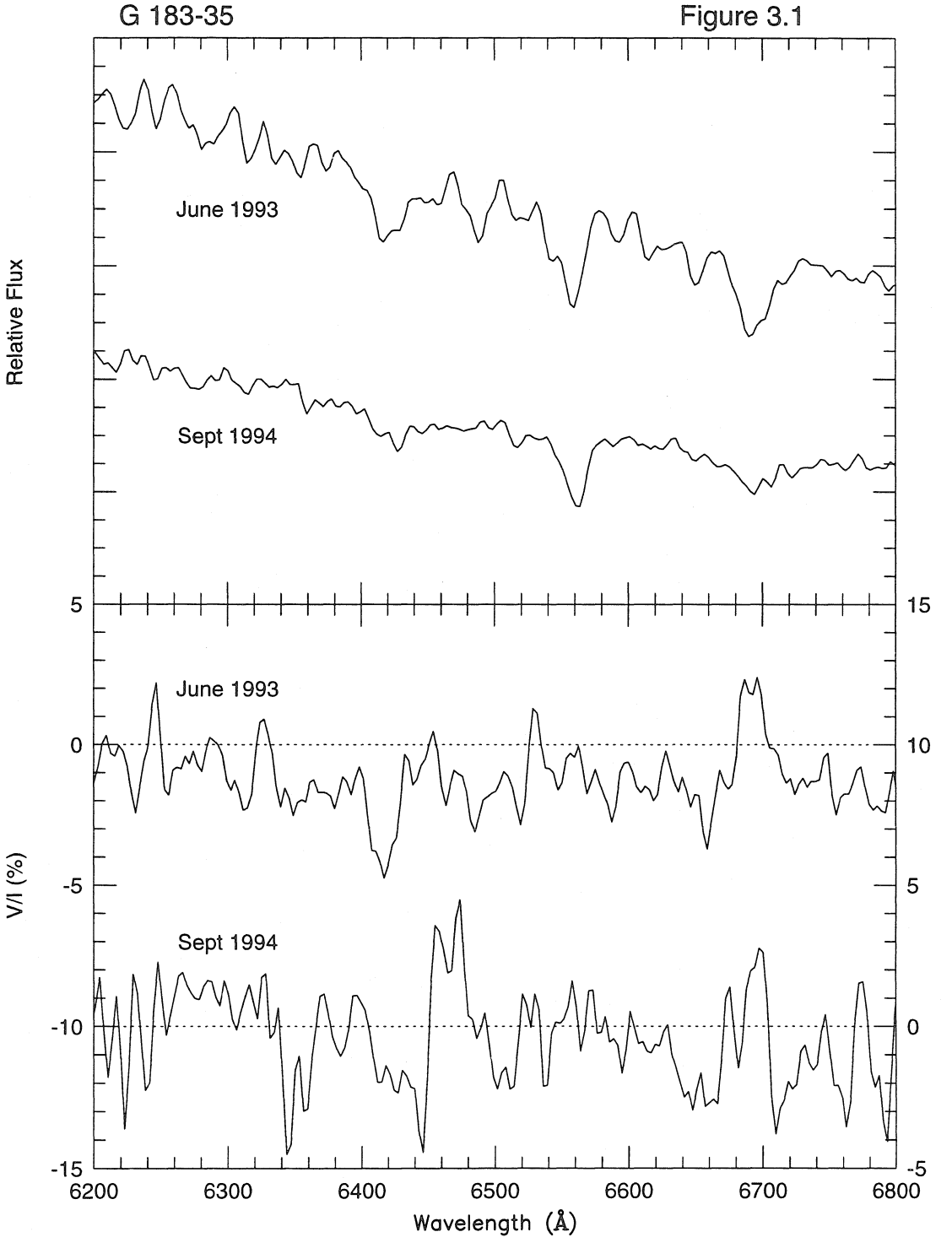
G 183-35
Figure 3.1
June 1993
Sept 1994
Relative Flux
5
15
June 1993
0
10
-5
5
Sept 1994
V/I (%)
-10
0
-15
-5
6200
6300
6400
6500
6600
6700
6800
Wavelength (Å)

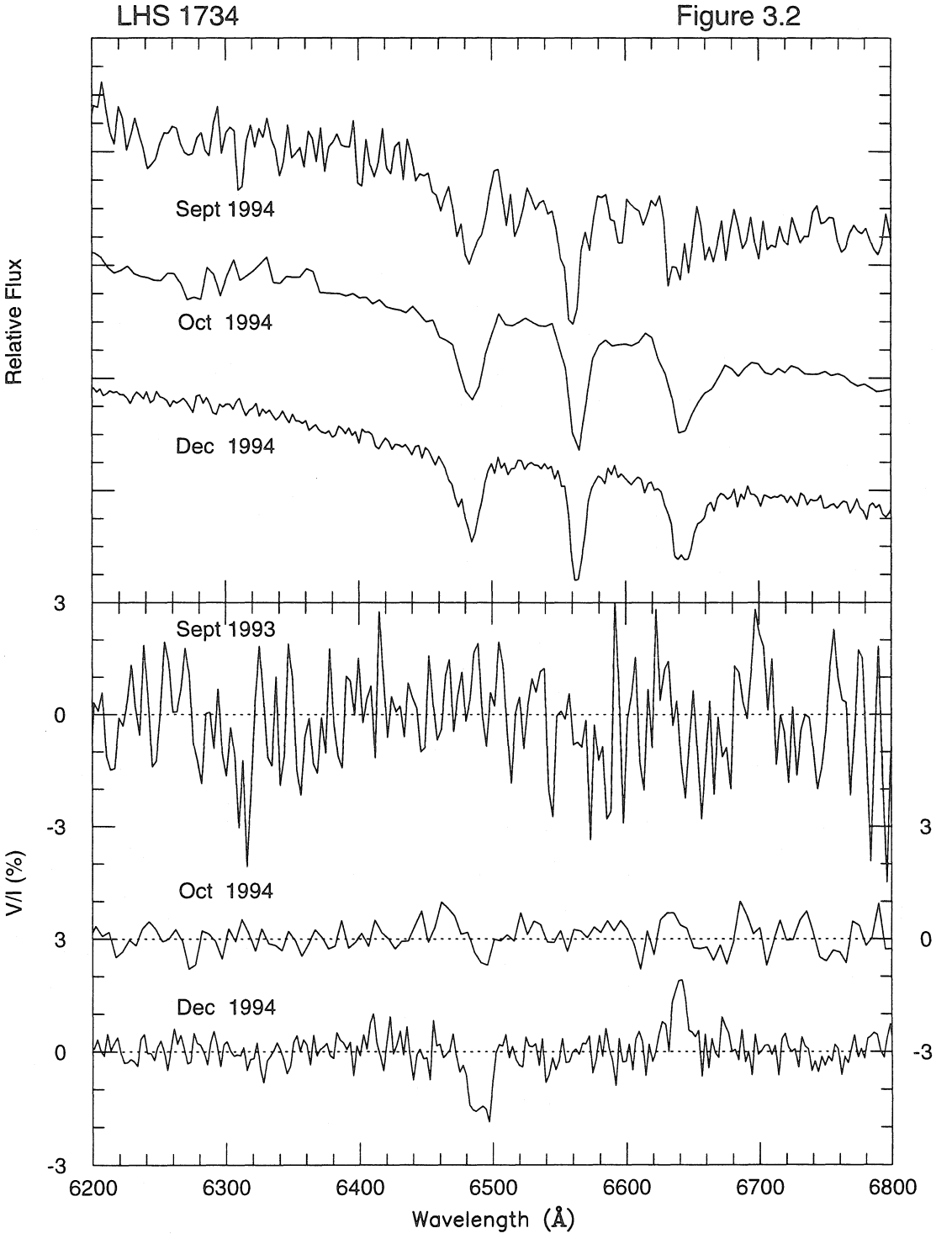
LHS 1734
Figure 3.2
Relative Flux
Sept 1994
Oct 1994
Dec 1994
Sept 1993
Oct 1994
Dec 1994
V/I (%)
3
0
-3
3
0
-3
3
0
-3
6200
6300
6400
6500
6600
6700
6800
Wavelength (Å)

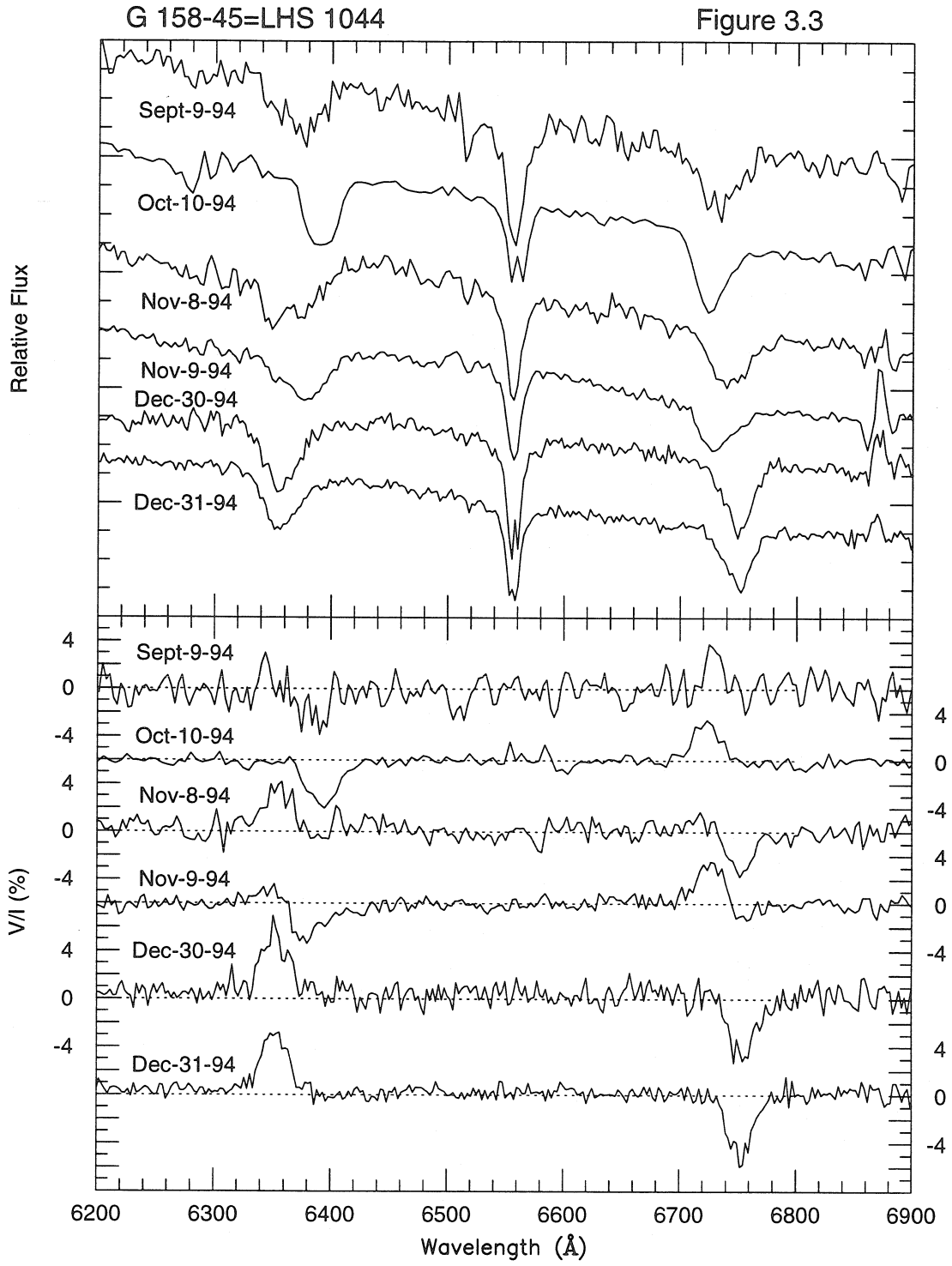
G 158-45=LHS 1044
Figure 3.3
Relative Flux
Sept-9-94
Oct-10-94
Nov-8-94
Nov-9-94
Dec-30-94
Dec-31-94
V/I (%)
4
0
-4
6200
6300
6400
6500
6600
6700
6800
6900
Wavelength (Å)

Figure 3.4

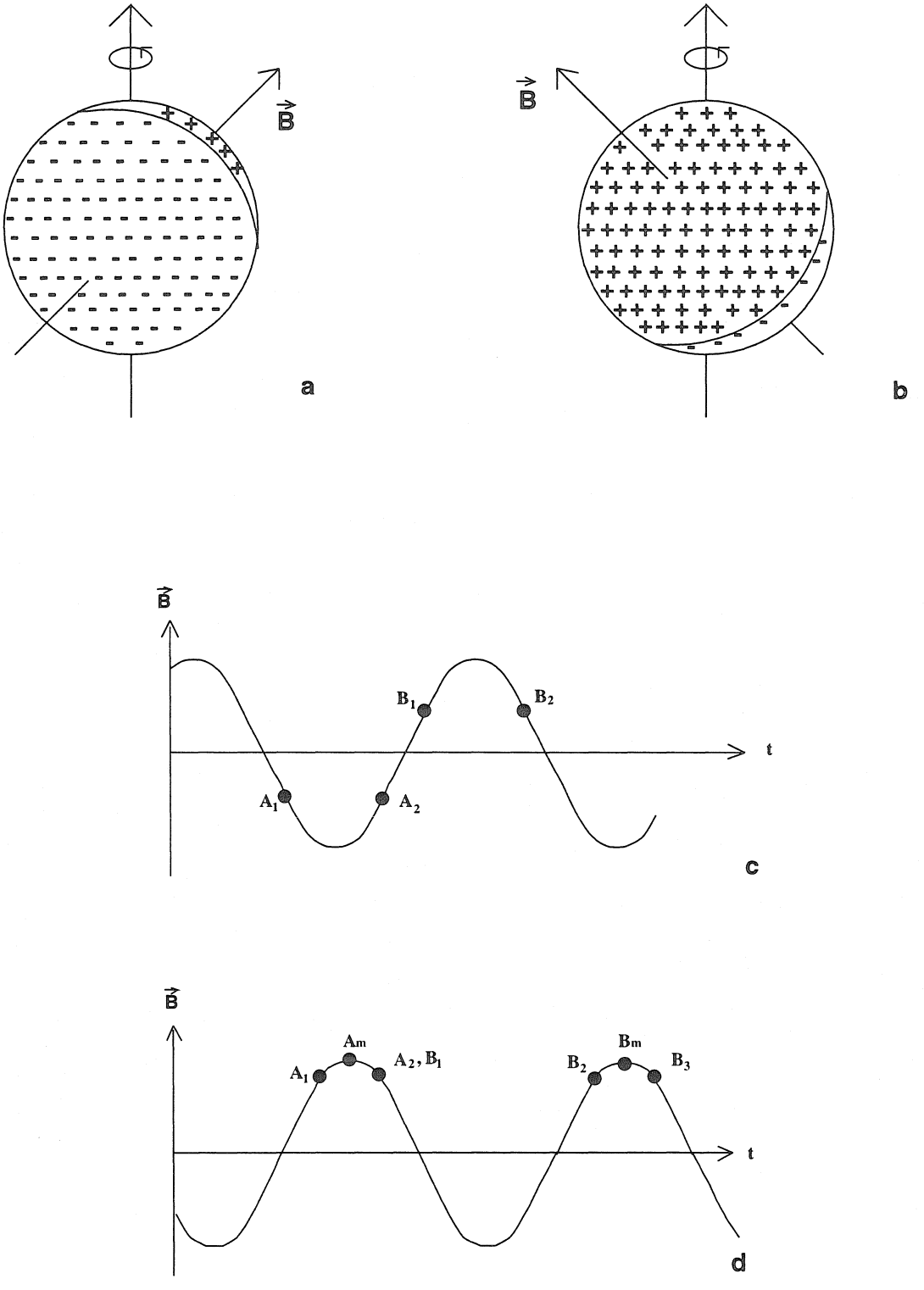

Figure 3.5

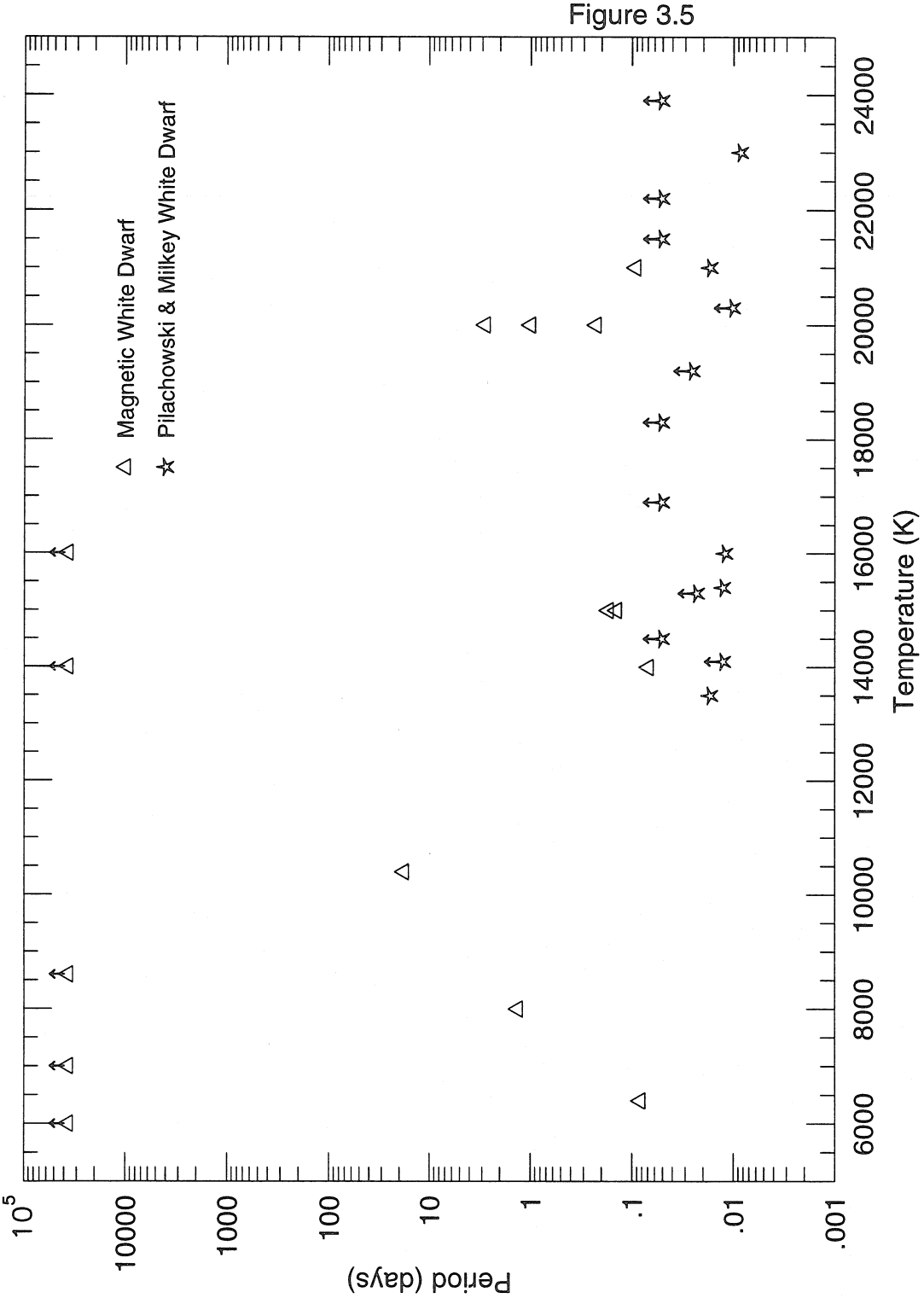
Magnetic White Dwarf
Pilachowski & Milkey White Dwarf
Period (days)
10^5
10000
1000
100
10
1
.1
.01
.001
6000
8000
10000
12000
14000
16000
18000
20000
22000
24000
Temperature (K)

Figure 3.6

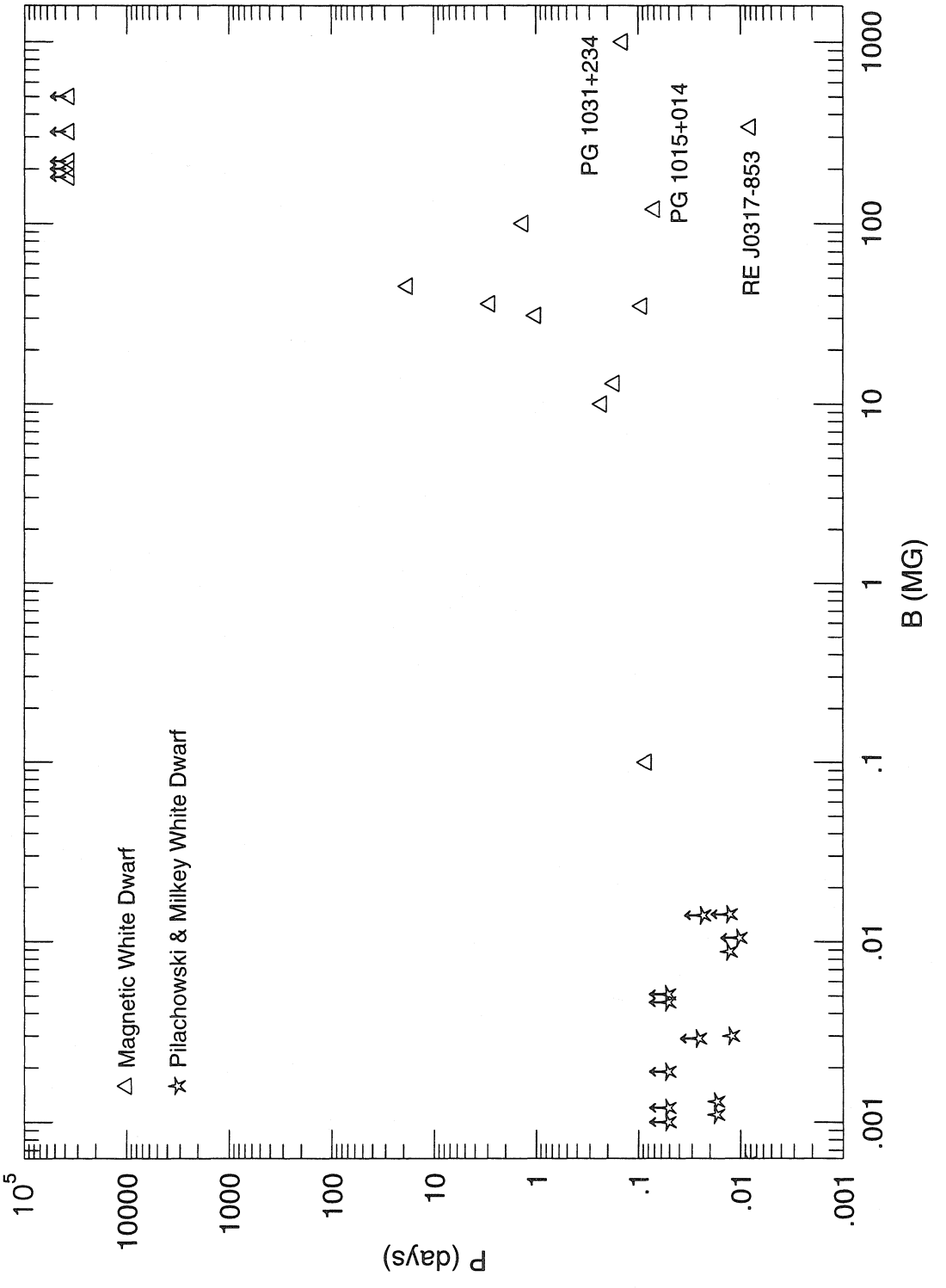
△ Magnetic White Dwarf
☆ Pilachowski & Milkey White Dwarf
PG 1031+234
PG 1015+014
RE J0317-853
P (days)
B (MG)
10^5
10000
1000
100
10
1
.1
.01
.001
.001
.01
.1
1
10
100
1000

CHAPTER 4

Off-Centered Dipole Models for 3 Isolated Magnetic White Dwarfs [1]

Abstract

The isolated magnetic white dwarfs G 99-47, KUV 813-14 (KUV 23162-1220), and G 227-35 were observed in linear and circular spectropolarimetry and then compared to calculated theoretical spectra to find a model for the magnetic field strength and structure. The comparisons were to Stokes' V/I (circular polarization) spectra in addition to total flux F_λ, and these add many constraints to the possible solutions. An off-centered dipole or a dipole+quadrupole configuration best fits the observations and this is consistent with the idea that the magnetic Ap and Bp stars — also showing deviations from a centered dipolar field — are the predecessors of the highly magnetic white dwarfs.

A good fit to the flux spectrum alone is possible in more than one region of parameter space. The addition of circular polarization data to our comparisons caused the parameters we found for G 99-47 and KUV 813-14 to be somewhat different from previous solutions.

4.1 Introduction

Circular polarization was first measured in the white dwarf Grw+70°8247 by Kemp et al. (1970). Kemp et al. pointed out that a magnetic field of 10^7 G could displace the hydrogen transitions to the wavelengths of the absorption bands first seen in this star by Minkowski (1938). Since that time, approximately 40 isolated white dwarfs have been found to have magnetic field strengths $> 10^6$ G (Chanmugam 1992; Landstreet 1992; Schmidt 1995). Most have absorption features (emission, in the case of GD 356; Greenstein & McCarthy 1985) that are

[1] This chapter has appeared as the article by A. Putney & S. Jordan in The Astrophysical Journal, volume 449, page 863.

identified as lines shifted by the linear and quadratic Zeeman effect of hydrogen and/or helium. In other cases, the absorption features were identified as hydrogen only with the aid of theoretical calculations of the displacements of the hydrogen lines in large ($> 10^8$ G) magnetic fields (Kemic 1974; Henry & O'Connell 1985; Wunner et al. 1985). A few stars are still a mystery. The features of GD 229 are still unidentified; Schmidt, Latter, & Foltz (1990) suggest that they might be due to helium, for which wavelengths and oscillator strengths for only a few line components have been calculated with a limited accuracy for large magnetic fields (Thurner et al. 1993).

After the initial discovery of white dwarf stars with large magnetic fields, searches of white dwarf stars in broadband circular polarization were begun (e.g., Angel & Landstreet 1970; Liebert & Stockman 1980; Angel, Borra, & Landstreet 1981). Such surveys are limited to detecting stars with mean longitudinal fields B $\gtrsim 10^6$G, due to the fact that the continuum polarization is not strongly affected until such strengths are reached. However, this is a very good method to find high magnetic field stars; Angel et al. (1981) listed 13 such stars, five of which were previously unknown to have large fields.

Several computer codes have been written to model the atmospheres of these stars (recent examples: Achilleos et al. 1992; Martin & Wickramasinghe 1992; Jordan 1992 and references therein). In general, these calculations were compared only to the observed flux spectra, although a few have been compared to polarization measurements as well (e.g., Schmidt et al. 1986; Wickramasinghe & Ferrario 1988; Achilleos & Wickramasinghe 1989a, b; Friedrich 1993a). However, calculated polarization spectra do not match the data well. The recent development of several spectropolarimeters (Goodrich 1991; Goodrich, Cohen, & Putney 1995; Schmidt, Stockman, & Smith 1992; Hough & Bailey 1994; Semel, Donati, & Rees 1991; Mathys 1991) now permits the models to be compared directly to sensitive polarization measurements of the same spectral resolution as the flux measurements.

The magnetic field of a white dwarf will vary in strength and direction over the surface of the star. The flux spectrum of such a star reveals the variations of field strength over the observable hemisphere, but gives no direct information about either the direction of the field or the orientation of the magnetic axis with respect to the observed hemisphere. If the magnetic white dwarf is rotating obliquely, e.g., Feige 7 or PG 1031+234, then the spectral line features will change during the rotation period and from this the structure of the whole magnetic field of the star is revealed – field strength, structure, and viewing angle. The circularly polarized spectrum (V/I) will give, in addition to field strength variations, the average direction of the visible field, which, in turn, tells us the inclination of the magnetic axis to the line of sight. The linearly polarized spectra (Q/I and U/I) should corroborate the information imparted to us by the circular polarization. For example, the polar view of a centered dipolar field B_{dp} and the equatorial view of a centered dipolar field of strength B_{de} can yield, for some $B_{de} > B_{dp}$, flux spectra similar enough to match the same observed flux spectrum but with very different polarization spectra. Off-centered dipolar and dipole+quadrupolar fields are mathematically very similar and therefore produce nearly the same spectra, which are different from the spectra from the simple centered dipolar fields. Thus comparing models only to a flux spectrum can yield a variety of good, but not necessarily "correct," fits, whereas including a comparison to a circular polarization spectrum will constrain the magnetic field configuration.

4.2 Observations

All observations were taken on the Hale 200 inch telescope at Palomar Observatory in 1992 and 1993 with the polarimeter (Goodrich 1991) mounted on the double spectrograph (Oke & Gunn 1982). Table 4.1 summarizes the observations. The 300 g/mm grating gives 2.2 Å/pixel, 316 g/mm gives 3.1 Å/pixel, and 158 g/mm gives 6.2 Å/pixel. When using the combination of the 300 g/mm grating in the blue with the 158 g/mm grating in the red, the wavelength coverage

is approximately 3700 Å to 10000 Å, and with the 316 g/mm grating in the red, the coverage ends at about 8000 Å. The slit width was 2″. All reductions were made with VISTA using procedures developed by Robert Goodrich.

Details of the methods used to take and reduce the linear polarization data are explained in Goodrich 1991 and for circular in Goodrich et al. (1995). Briefly, the light first passes through a wave plate ($\lambda/2$-plate for linear measurements and $\lambda/4$-plate for circular) which either rotates the plane of polarization ($\lambda/2$-plate) or converts between linear and circular polarization ($\lambda/4$-plate). Next the light passes through a calcite prism which splits the beam into two parallel, orthogonally polarized beams. Each Stokes' parameter requires two observations, each at a different angle of the wave plate fast axis (a 90° separation of the two angles for circular and 45° for linear). The four spectra produced from these two observations are extracted and combined to produce the Stokes' parameters Q, U, or V, in addition to I.

4.3 Modeling Technique

4.3.1 Radiative Transfer

The synthetic spectra of the Stokes' parameters were calculated with a computer program developed by Jordan (1989, 1992). For temperature and pressure structure zero field model atmospheres (see Koester, Schulz, & Weidemann 1979) were used. The equations of radiative transfer (Beckers 1969)

$$\mu \frac{\mathrm{d}I}{\mathrm{d}\tau} = \eta_I (I - B) + \eta_Q Q + \eta_V V, \tag{4.1}$$

$$\mu \frac{\mathrm{d}Q}{\mathrm{d}\tau} = \eta_Q (I - B) + \eta_I Q + \rho_R U, \tag{4.2}$$

$$\mu \frac{\mathrm{d}U}{\mathrm{d}\tau} = \rho_R Q + \eta_I U - \rho_W V, \tag{4.3}$$

and

$$\mu \frac{\mathrm{d}V}{\mathrm{d}\tau} = \eta_V (I - B) + \rho_W U + \eta_V V \tag{4.4}$$

were solved for the Stokes parameters I, Q, V and U with a semi-analytical algorithm similar to that of Wickramasinghe & Martin (1979). The optical depth scale is defined by $d\tau = -\kappa_{\rm R} {\rm d}z$, where $\kappa_{\rm R}$ is the Rosseland mean opacity. $\mu = \cos\vartheta$, with ϑ being the angle between the normal to the surface and the line of sight. According to Unno (1956), the monochromatic absorption coefficients η_l, η_p and η_r for transitions with respectively $\Delta m = -1, 0$ and $+1$ are combined to η_I, η_Q and η_V:

$$\eta_I = \tfrac{1}{2}\eta_p \sin^2\psi + \frac{1}{4}(\eta_l + \eta_r)(1 + \cos^2\psi), \tag{4.5}$$

$$\eta_Q = \tfrac{1}{2}\eta_p - \frac{1}{4}(\eta_l + \eta_r)\sin^2\psi, \tag{4.6}$$

$$\eta_V = \tfrac{1}{2}(\eta_r - \eta_l)\cos\psi; \tag{4.7}$$

ψ denotes the angle between the magnetic field direction and the line of sight. ρ_R (Faraday rotation) and ρ_W (Voigt effect) are the magneto-optical parameters originating from spectral lines and free electrons in a magnetic field (see Jordan, O'Connell, & Koester 1991).

In the outer layers ($\tau < 10^{-3}$) the Runge-Kutta method has been applied to equations (4.1)-(4.4) in case of numerical instabilities. We account for the variation of the magnetic field strength and direction (see next section) by calculating the Stokes' parameters on a large number of surface elements (up to about 10,000). Larger or variable sized surface elements, i.e., a smaller number of elements, could be used to follow the field gradients; however, the linear polarization is very sensitive to the field direction and decreasing the number of elements could corrupt the polarization calculations. The solutions to the radiative transfer equations of each element were added in order to obtain the spectrum and polarization from the whole visible hemisphere of the star. We considered line absorption by all Balmer components up to H_ϵ (Forster et al. 1984; Rösner et al. 1984; Friedrich 1993b). After the models were calculated, they were convolved with a Gaussian to match the instrumental resolution of 18 Å (for the red 158 g/mm grating).

A weak point of the modeling is still the treatment of the bound-free opacities. As described in Jordan (1989, 1992) the wavelengths of the absorption edges $\lambda_{\rm edge}$ are calculated with the help of the bound-state energies and the energy of the first Landau level that can be reached by a particular absorption process. Since the bound states are no longer degenerate and since not all transitions with $\Delta m > 0$ can reach the lowest Landau levels, the number of absorption edges increases; the Balmer threshold, e.g., splits into 15 individual transitions. In order to determine the photoionization cross sections at $\lambda < \lambda_{\rm edge}$, we still have to rely on shifted zero field values according to Lamb & Sutherland (1974). The situation may soon change when the newly calculated bound-free opacities from a group in Bochum will become available (Merani, Main, & Wunner 1995). However, a first application of these calculated data has not improved the situation as much as was hoped (Jordan 1994; Jordan & Merani 1995); only slight differences in flux and polarization occurred at 320 MG between the old models and the ones calculated with the new photoionization cross sections for high magnetic fields by Merani et al. (1995).

At fields higher than about 100 MG (e.g., on G 227-35), the cyclotron absorbing radiation, with Δm= +1 only, can become important at larger wavelengths. The frequency integrated cross section

$$\sigma_+ = \int_0^\infty \sigma'_+ d\omega \approx \frac{e^2}{\hbar c}\left(\frac{2\pi c}{\omega_c}\right)^2 \left(\frac{Be\hbar}{m^2c^3}\right) \frac{\omega_c}{1-e^{-\hbar\omega_c/k_BT}} \qquad (4.8)$$

has been calculated by Lamb & Sutherland (1974). $\omega_c = eB/m_ec$ is the cyclotron frequency; the other abbreviations have their usual physical meaning.

We use a Voigt profile in order to account for the (Gaussian) Doppler and magnetic broadening as well as the (Lorentzian) broadening by electron collisions. The term for the magnetic broadening for each element is determined from the variation of the magnetic field over the surface elements. For increased speed, the Voigt function is approximated by H = factor $\times\, a/(a^2+v^2)$ for large (a^2+v^2).

4.3.2 Geometry of the Magnetic Field

One goal of this work is to infer the detailed structure of the magnetic field. The observed spectrum and polarization is the superposition of the Stokes' parameters from the whole visible hemisphere of the star. Since the magnetic field strengths and the direction of the radiation relative to the magnetic field and the observer varies over the surface, it is possible to construct different field geometries that lead to the same observed spectrum and polarization. Recently, Donati et al. (1994) have demonstrated that this inverse problem can, in principle, be solved by applying a maximum entropy method. They calculated synthetic flux and circular polarization spectra for magnetic dipoles with different offsets and orientation and then tried to reconstruct the field geometry from this grid of theoretical Stokes' parameters I_λ and V_λ. Their study was limited to relatively low magnetic fields and to wavelengths in the Hα region. No perfect agreement between the assumed and reconstructed field distribution could be achieved. However, with a larger wavelength range and with observations at multiple rotational phases, this may be a rather powerful tool in the future.

In this paper we still use the traditional method to describe the field geometry in the framework of offset dipoles or combinations of dipoles and quadrupoles. After solving the equations of radiative transfer (see previous section), the predicted Stokes' parameters can be compared with the observation. In Cartesian coordinates, the components of the magnetic field of an offset dipole are given by

$$B_x = \frac{3}{2} B_p (x - x_{\rm off})(z - z_{\rm off})/r^5, \tag{4.9}$$

$$B_y = \frac{3}{2} B_p (y - y_{\rm off})(z - z_{\rm off})/r^5, \tag{4.10}$$

$$B_z = \frac{1}{2} B_p [3(z - z_{\rm off})^2 - r^2]/r^5, \tag{4.11}$$

with $r^2 = (x - x_{\rm off})^2 + (y - y_{\rm off})^2 + (z - z_{\rm off})^2$ (see Achilleos & Wickramasinghe 1989a). The z-axis defines the direction of the dipole and Figure 4.1a illustrates the geometry of the dipole coordinate system. $x_{\rm off}$, $y_{\rm off}$, and $z_{\rm off}$ define the dipole

offsets and B_p is the dipole strength. B_x, B_y, and B_z are calculated on the stellar surface ($r = 1$). The orientation of the field relative to the observer is described by the angle α ($\alpha = 0°$ corresponds to an equator-on view, $\alpha = 90°$ pole-on).

In addition to the dipole geometry, we also test some dipole+quadrupole combinations. The magnetic field strength of the quadrupole is given by

$$B_x^q = \frac{1}{2} B_p^q (5z^2 - 1)x, \tag{4.12}$$

$$B_y^q = \frac{1}{2} B_p^q (5z^2 - 1)y, \tag{4.13}$$

$$B_z^q = \frac{1}{2} B_p^q (5z^2 - 3)z. \tag{4.14}$$

The quadrupole is centered (as is the dipole in the dipole+quadrupole case) and B_p^q is the quadrupole field strength at the surface ($r = 1$). The dipole and quadrupole axes may not be aligned, in which case the quadrupole coordinate system is tilted by an angle θ and rotated azimuthally by an angle ϕ. ϕ is measured with respect to the plane defined by the dipole axis and the line of sight, in a right-handed coordinate system. Figure 4.1b illustrates the geometry of the quadrupole coordinate system.

As we will show, the flux spectrum can be reproduced by different combinations of offset dipoles or dipole+quadrupoles and the polarization is very sensitive to changes in the magnetic field parameters. In cases where a simple dipole is insufficient to reproduce the observed circular polarization, we will compare several models in order to find out which is the simplest model that can best reproduce the details of the observation.

4.3.3 Stark Broadening

Without a magnetic field, the lines in white dwarfs are broadened primarily by the Stark effect. For the hydrogen line components, the wavelength shift $\Delta\lambda$ of the individual components is given by (Schwarzschild 1916, Epstein 1916)

$$\Delta\lambda = 0.0192\lambda^2 n_k F \tag{4.15}$$

in cgs units. F is the local electric field strength and n_k, an integer determined by the initial and final state of the line transition. The total line profile is a superposition of all the individual Stark components shifted according to the different electric field strengths and directions caused by the ions and electrons at the locations of the absorbing atoms. In the presence of a magnetic field the situation becomes more difficult since the Hamiltonian operators describing the electric field and the magnetic field do not commute if the fields are not parallel or perpendicular. For the case of the magnetic and electric fields being parallel, Friedrich et al. (1994) calculated wavelength shifts for selected Balmer components, which turned out to be smaller than 5.5 Å. Unfortunately, no calculations exist for arbitrary angles between the electric and magnetic field.

If the magnetic field strength is strong ($B \gtrsim 100$ MG), one can expect that the linear and quadratic Zeeman splitting completely dominates the Stark broadening. However, at the field strengths of stationary components (where the wavelengths do not vary strongly with the magnetic field) and at lower field strengths, the inclusion of Stark broadening becomes important. We assume that the FWHM of the Lorentzian Stark profile is determined by

$$\Delta\lambda_S = 0.0192\lambda^2\overline{n_k}CF_0. \tag{4.16}$$

The $\overline{n_k}$ are intensity weighted means for the Balmer lines tabulated by Underhill & Waddell (1959), and $F_0 = 2.6eN^{2/3}$ (= normal field strength), with N being the particle density of the ions, and e the electric charge. We use a Voigt profile in order to account for the Stark broadening together with the Gaussian Doppler and magnetic broadening (Jordan 1992). The value of the free parameter C is not clear. One can, however, expect that $C \approx 0.1$ is probably a good choice when the l degeneracy, and therefore the Stark broadening, is strongly reduced by the quadratic Zeeman effect. At small magnetic fields a somewhat higher value of C may be more appropriate. Martin & Wickramasinghe (1984) have shown that different choices of the Voigt function damping parameter do strongly affect the depth and shape of the Hα line if a magnetic dipole field strength of only 10 MG

is assumed. For stars with relatively low magnetic fields (KUV 813-14 and G 99-47), we also varied the parameter C in order to find out if the the conclusions are different compared to the solutions we obtain with our standard value $C = 0.1$.

4.4 Results

4.4.1 Determining a "Best" Model

The decision as to which model is "best" is actually done by eye, that is to say, a model will be run and visually compared to data. Then the parameters will be altered and another model run until we are satisfied with the results. One or two hundred models may be run before a "best" model is found. On a Sparc 10/51, it takes about 6 hours to run through 3500 Å in 5 Å increments.

Choosing the "best" model from all the models calculated consists of a compromise of several factors. The most important is the position, in wavelength, and the width of the absorption features and their corresponding polarization features. The continuum polarization strength and shape is of secondary concern, particularly for the larger field strengths (e.g., G 227-35) since the theory describing continuum polarization breaks down as the field strength increases. The overall continuum shape in F_λ is important; in fact, a big compromise occurs between the overall shape of F_λ and the depth of the lines. In general, the morphology of the field is most important. The overall flux continuum shape and strength of the lines in flux and circular polarization can be easily changed by modifying the temperature. The strength of the lines can also be altered by using different values for our Stark parameter C or the gravity. These changes will not effect the magnetic field strength or structure chosen as "best."

Model parameters are selected from an ever changing grid. The grid starts out widely spaced and quickly narrows down and does not become regular until a "best" model is chosen (to determine uncertainties in the models; see Section 4.5.5). Before the first model is run, estimates are made for all the parameters. Effective temperature is taken from the literature or the shape of F_λ. Typical values are taken for log g (= 8.0), He/H (= 0), C (= 0.1), unless the literature or

the observations indicate otherwise. A comparison of the observed data to curves of magnetic field strength versus wavelength for hydrogen transitions yield a good approximation to the field strength. The continuum circular polarization may give a clue as to whether the orientation is closer to the pole or the equator. The necessity of a stronger or weaker field in the model is immediately obvious, as is an incorrect viewing angle or temperature. Eventually we got enough experience to be able to make a comparison of a model to the data and know that, e.g., the dipole needs a larger offset in a particular direction. Finally, a "best" model is chosen.

4.4.2 G 99-47

Of the three white dwarf stars investigated in this paper, G 99-47 has the weakest magnetic field strength and the lowest effective temperature. Greenstein (1974) observed G 99-47 with the multichannel spectrograph, found it to be featureless, and fit a 5600 K blackbody to the spectrum. Liebert, Angel, & Landstreet (1975) first detected Hα absorption in this star and noticed that it was shifted to the blue approximately 21 Å from the usual Hα position. They believed this to be the π-component of a Zeeman split line due to a field of 20-25 MG; they did not detect the σ-components. Greenstein and McCarthy's data (Greenstein & McCarthy 1985) clearly contained the σ-components. They calculated a field strength between 14 and 27 MG. Neither group detected Hβ absorption, creating an atypical Balmer decrement (Hα much stronger than Hβ) which can be explained by either high Helium content or high gravity (Hammond et al. 1993; Liebert & Wehrse 1983).

Liebert et al. (1975) also made circular polarization measurements in channels 160 Å wide from 3480 Å to 5720 Å, and 360 Å wide from 5320 Å to 10360 Å. Our data are consistent with theirs and show that the channels of high polarization (6020 Å to 6380 Å) and of low polarization (6740 Å to 7120 Å) are indeed real and significant and correspond to the σ_+ and σ_- components, respectively, of Hα. Angel & Landstreet (1972) measure both circular and linear polarization

for this object. Their circular polarization is consistent with ours and Liebert et al. As for linear polarization, they measure $\langle p \rangle_{3900-5550\text{Å}} = 0.26 \pm 0.09\%$ and $\langle p \rangle_{3500-8000\text{Å}} = 0.15 \pm 0.09\%$. We measure $\langle p \rangle_{5600-7500\text{Å}} = 0.37 \pm 0.1\%$, where most of the error is due to instrumental polarization. These measurements are consistent (less than 2σ), particularly if one looks at Angel & Landstreet's values of p_x and p_y (akin to Stokes' Q and U) and notices how they flip in sign between the two bands (implying a much higher value for p redward of 5500 Å). In general, null linear polarizations are extremely noisy and very sensitive to instrumental polarizations (in fact, the position angle θ is meaningless). Wickramasinghe & Martin (1979) and O'Donoghue (1980) each modeled G 99-47 and found fits of $T_{\rm eff}$ = 6000K, log g = 8, He/H = 0.1, B_d= 25 MG, and an inclination angle of 120°. They compared their models to the Liebert et al. data and they found their models to be consistent with the data in both flux and circular polarization.

We have run models varying effective temperature and gravity, in addition to the usual magnetic field configuration. We have also varied the helium abundance, but only to examine the effect on the temperature and pressure structure; helium has not been included in the calculations of the synthetic flux or polarization spectra since helium lines cannot be excited at temperatures below $\sim$ 10,000 K. Figure 4.2 shows how these changes affect the models, which are described in Table 4.2. We find that a model with the following parameters fits the observation best: $T_{\rm eff}$ = 5500 K, log g =8, He/H = 10^{-6}, B_p = 20 MG, $\alpha = -10°$ ($i = 100°$), $x_{\rm off} = 0.00$, $y_{\rm off} = -0.11$, $z_{\rm off} = +0.08$, and $C = 0.1$.

We also tried running models for a different value of our Stark factor C; namely we tried $C = 1.0$ instead of $C = 0.1$. Figure 4.2 shows one such model as well (model b). For this object, changing C made no noticeable difference. Our results differ slightly from those of Wickramasinghe & Martin (1979) and O'Donoghue (1980), mainly because the data we used has higher resolution and we used offset dipoles. The linear polarization data for this, and the following two objects, will be discussed in Section 4.4.5.

4.4.3 KUV 813-14

KUV 813-14 is the only object in this paper with a known rotation period. Of all the magnetic white dwarf stars with measured rotation rates (measurements are sensitive to periods 10 min $\lesssim$ P $\lesssim$ 100 yrs), it is rotating the slowest, at 17.856 days (Schmidt & Norsworthy 1991). The flux distribution of KUV 813-14 has been modeled by several groups. Liebert et al. (1985) deduced that it has a field strength of 29 MG with a (north) pole on view ($i = 0°$). Achilleos & Wickramasinghe (1989a,b) also determined a field strength of 29 MG but found an inclination angle $0° \leq i \leq 20°$ and the dipole to be offset along the z-axis as much as 10% of the stellar radius. Friedrich (1993a) modeled both the flux distribution and circular polarization, for the region of 4000 – 6200 Å, and she found the field strength to be 32-35 MG with an inclination angle of 170°.

As seen in Table 4.1, we observed KUV 813-14 on three consecutive nights and another night a year later. During the 1992 observations, the star moved through 0.12 of a rotation (43.2°) and the flux did not change noticeably. There was a significant change in the flux spectrum between the 1992 and 1993 observations which we assume to be entirely due to the 20.28 revolutions (100.8°) the star made between 1992 August 25 and 1993 August 22. Since the 1992 observations had both circular and linear measurements, we matched these against our models. Figure 4.3 shows several offset dipolar models, which are described in Table 4.3, and Figure 4.4 shows several offset dipolar+quadrupolar models, which are described in Table 4.4.

We find that there are two best dipolar models: model a, $B_p = 45$ MG, $\alpha = -13°$, $T_{\rm eff} = 11000$ K, $x_{\rm off} = +0.013$, $y_{\rm off} = -0.015$, $z_{\rm off} = +0.05$ and $C = 0.1$; model b, $B_p = 45$ MG, $\alpha = -10°$, $T_{\rm eff} = 11000$ K, $x_{\rm off} = +0.005$, $y_{\rm off} = -0.015$, $z_{\rm off} = +0.05$ and $C = 1.0$. The best quadrupolar model is $B_p = 43$ MG, $\alpha = -7°$, $T_{\rm eff} = 11000$K, with a quadrupolar field strength $B_p^q = 8$ MG, a tilt angle $\theta = +20°$, an azimuthal angle $\phi = -10°$, and $C = 1.0$ (model i). These parameters are different from previous groups' solutions. The strength of

the continuum circular polarization (i.e., weak) places the viewing angle closer to the equator than to the pole, but the width of the lines is larger than expected for an equator-on view of a centered dipole. Offsetting the dipole towards the observer will widen the line widths (change the surface field distribution) enough such that the near equator-on view matches in flux and leaves the circular polarization weak. Adding a quadrupolar field to a centered dipolar field has similar effects.

Another possible reason for the differences between the models chosen here and those found by others is that this object is rotating. Liebert et al.'s observations were possibly taken at a different phase of the rotation (they give no information on observing times), and Friedrich's observations were taken within 0.1 rotations of the data presented here. Having data at different rotational phases can be useful. The only star that can have its field completely mapped out is a rotating star. We can call a "true" field a magnetic configuration that, if seen from different angles via the rotational phase, matches the data at each observation. There are two ways to go about finding the "true" field, both by determining the rotation axis. The first is the method whereby the field is matched at one phase of the rotation and then the model is rotated about many different rotation axes until the "correct" axis is found. The second is where a model is matched for each of two phases and then a rotation axis is determined from the differences of the two models. Both methods assume that the only changes in the data of the two phases are due to rotation and not some other form of activity on the star.

Since we have flux measurements of this star separated by one-third of a rotation (using the ephemerides of Schmidt & Norsworthy 1991), we decided to try the first method to find the rotation axis. We took the best fit dipolar model and rotated it about different axes (chosen from a small grid) to see if the calculated spectra would still fit the data. Figure 4.5 shows the results of this exercise, and Table 4.5 describes the models. Narrowing down the rotation axis to an octant or so of the star is an easy task; however, determining a more precise vector is not. In the coordinate system of the magnetic field, a vector going through the origin and the point (0.018, 0.003, 0.08) defines the "best" rotation axis we could find

thus far. The star was rotated $-100.8°$ from the x-axis towards the y-axis (see Figure 4.6). These parameters indicate that the model $B_d = 45$, $T_{\rm eff} = 11000$ K, $\alpha = -2°$, $x_{\rm off} = 0.027$ $y_{\rm off} = 0.015$, and $z_{\rm off} = 0.04$ should "best" fit the 1993 observed spectrum, but it is a poor fit.

The major reason for the rotation models of Figure 4.5 not fitting as well as those in Figures 4.3 and 4 is that far fewer models have been run for this case. As compared to narrowing the "solutions" for the previous cases, finding the "best" axis to rotate the star about is a random process. Changing the field strength, the viewing angle, the offset either towards or away from the observer, etc., have very predictable results; e.g., in order to broaden the lines, yet keep the strength of circular polarization unchanged, the dipole needs to be offset towards the observer. Much this predictability comes from experience, and this has not yet been achieved for rotation about different axes.

4.4.4 G 227-35

G 227-35 has the highest magnetic field of the three stars in this paper. It was first classified as a DCP star (Hintzen & Strittmatter 1974) and later revised to a DQP7+ after high S/N spectra were obtained (Greenstein 1986; Greenstein & Liebert 1990). Its composition was again revised in 1993 to DAP (Cohen, Putney, & Goodrich 1993) when a prominent feature in circular polarization with a corresponding weak feature in flux was detected that corresponds to the 2p-1 – 3d-2 transition of Hα in a field of 117 MG.

It was recognized early that this star had a large magnetic field. Angel, Hintzen, & Landstreet (1975) observed it in broadband circular polarization and concluded from the continuum polarization that the magnetic field was in excess of 30 MG. West (1989) observed G 227-35 in broadband linear and circular polarization, but made no estimate of the magnetic field other than greater than 100 MG. Our polarization data are consistent with the previously observed data.

After running several models for this star, it became clear that the theory for continuum polarization is not well understood. Lamb & Sutherland (1974) calculated the effects of magnetic fields on the continuum opacity, and even though the calculations are now known not to be accurate, especially in stronger fields ($\gtrsim$ 50 MG), they are still used for lack of a better theory. After trying hundreds of different field configurations, Figure 4.7 shows the best models (Table 4.6 describes them) that we could achieve under the present treatment of continuum opacity, but it is clear that the line features can match up when the continuum does not. Furthermore, as previously mentioned, first test calculations by Jordan (1994) and Jordan & Merani (1995) indicate that the newly calculated photoionization cross sections (Merani et al. 1995) do not alter the flux and polarization much, even at 320 MG. It is also possible that the way we account for cyclotron absorption (see eq. (4.8)) is inadequate. At 180 MG, the cyclotron absorption wavelength, $\lambda_c = \frac{2\pi mc^2}{eB}$, is ~6000 Å. Thus, for wavelengths longer than 6000 Å, the flux and polarization continua are determined partly by the cyclotron absorption. Since the cyclotron absorption leads to a very sharp resonance peak with a high absorption coefficient, it is quite sensitive to changes of the broadening parameters (collision broadening and magnetic field variation). For the collision frequency we use a formula by Spitzer (1962, p. 78), which does not take into account a magnetic field. Test calculations show that slight changes of the polarization are introduced if the broadening parameters are varied.

4.4.5 Linear Polarization

When the above models were calculated and compared to the observed data, the linear polarization was ignored. One would expect that the best fit to the observations would be a model which fits flux, linear polarization, and circular polarization at the same time. However, the calculated linearly polarized spectrum never resembles the observed spectrum, even if one tries to fit the linear polarization instead of the circular polarization. Similar problems in reproducing the linear polarization also occur in the models calculated with the Achilleos &

Wickramasinghe code (1994). We expect that this is due to the numerical short comings of the Wickramasinghe & Martin (1979) algorithm. Whether one uses the Wickramasinghe & Martin algorithm or the more accurate, but highly CPU intensive, Runge-Kutta method, problems occur in the outer layers of the atmosphere. Tests have shown that negative fluxes and linear polarizations greater than 100% can be calculated in these regions. However, these problems appear to be attributable to the inability of any numerical method to approximate the fast varying opacities and magneto-optical parameters of the outer layers of the atmosphere, rather than problems with the atmosphere itself. Due to the manner in which the linear polarization relies on the calculations of the magneto-optical parameters, the linear polarization is affected to a far greater extent than the flux or the circular polarization. This means that the linear polarization is less reliable than the circular or the flux calculations.

Figure 4.8 shows the linear polarization spectra, P and θ, for the best fit model (in flux and V/I) of G 99-47. The $\langle\theta\rangle$ value for the model and the observed data will be different due to the definition of $\theta = 0$. For observations, the polarization angle zero point is defined from the North Celestial Pole towards East; for the models, it is defined from a position on the star which has no relation to the NCP, thus an offset by a constant angle is expected.

In general, the observed linear polarization spectra from the three stars investigated here are nearly featureless, whereas the model spectra show strong features. A pole-on view of a centered dipole has no features in linear polarization, but there is also no continuum linear polarization. All viewing angles of an off-centered dipole or dipole+quadrupole model have features in the linear polarization. Other magnetic white dwarf stars observed show features in linear polarization (e.g., Grw+70°8247, Angel, Liebert, & Stockman 1985 and our own, unpublished data), which implies that the problem is not with the observed data.

4.5 Discussion

4.5.1 Stark Factor

As mentioned in Section 4.3.3, we varied our Stark factor C for G 99-47 and KUV 813-14. This changed the depth of the lines and, therefore, the configuration that best matched the data also changed. Since it is unknown exactly how Stark broadening is affected by magnetic fields, it is hard to determine the proper value to be using for C. Even the trial and error method does not answer this question since a different model, with a slightly different magnetic field configuration and temperature, can always be found to match the data. In principle, the Stark factor could be varying from line to line, but it is not practical to account for this. For G 227-35, we feel justified in using $C = 0.1$ because, in fields of that strength, the linear and quadratic Zeeman effects are expected to completely dominate the Stark broadening. However, for the magnetic field strengths found in G 99-47 and KUV 813-14, it is not yet known how the magnetic field affects the Stark effect, although we are confident that $0.1 \leq C \leq 1.0$.

4.5.2 Offset Dipole versus Dipole+Quadrupole

Martin & Wickramasinghe (1984) made general tests of centered dipolar, off-centered dipolar, quadrupolar, and octopolar fields on a white dwarf star. They noted that an offset dipolar and a quadrupolar field give very similar results, and only superb observational data, in flux and polarization, might allow one to determine which one is correct. From the work done here, we would have to agree that distinguishing between the two is difficult. Mathematically, an offset dipole can be recreated by a centered dipole plus some combination of higher multipoles, and some offset dipoles can be closely approximated by dipole+quadrupole combinations. The decay time of a dipolar magnetic field in a white dwarf is $\sim 10^{10} - 10^{11}$ yr (Mestel 1965; Chanmugam & Gabriel 1972) and the higher multipolar fields will decay faster, although a quadrupole will decay faster by only a factor $\lesssim 10$,

and an octopole by $\sim$ 100. White dwarf stars tend to remain visible for approximately 10^{10} yr (D'Antona & Mazzitelli 1990), thus for most white dwarfs, a dipole+quadrupole model should be fairly accurate throughout most of its visible lifetime.

4.5.3 Convection

In zero-field atmospheres, the convection which occurs is due to hydrogen ionization. We can, however, assume that convection is at least partly suppressed in the presence of a magnetic field. Typically, the convection zones are located in layers of partial ionization, which would mean that the ions, at least, cannot move freely across the magnetic field lines. In this paper we have not studied this effect quantitatively, but we have analyzed the spectropolarimetry with both convective models and those where convection has been suppressed completely (see Figure 4.9). With the exception of G 227-35, the star with the highest magnetic field, the convective models fit best, an indication that convection is not completely suppressed. We do not want to give the impression that we believe that the convection is not heavily suppressed. A convective atmosphere has a smaller temperature gradient than a non-convective atmosphere. There are several influences of the magnetic field on the temperature and pressure structure that are not taken into account (see, e.g., Jordan 1992) in our calculations and these could lead to smaller temperature gradients. Thus, our use of convective atmospheres could be interpreted as our approximation to these missing factors rather than proof of convection in these stars.

4.5.4 Magnetic White Dwarf Precursors

It is presently believed that the magnetic Ap stars are the predecessors of the magnetic white dwarf stars (Angel et al. 1981; Landstreet 1992; Chanmugam 1992). If the total magnetic flux of a star ($\Phi \sim \pi R^2 B$) is conserved during its evolution, then the surface field of a white dwarf should be related to that of a main sequence star by $B_{\rm wd} \sim (\frac{R_{\rm ms}}{R_{\rm wd}})^2 B_{\rm ms}$. Thus, if a star shrinks by a factor of

100 between the main sequence and the white dwarf state, then its magnetic field will increase by a factor of $\sim 10^4$. Many magnetic Ap stars have field strengths between 10^3 and 10^4 G (Landstreet 1992) which would correspond to white dwarf magnetic field strengths between 10^7 and 10^8 G, which are the strengths of the high magnetic field white dwarf stars. Angel et al. (1981) suggested this evolution scenario and computed that the present space density and death rate of Ap stars, assuming that these values have been constant over time, predict a space density of magnetic white dwarf stars that, within a factor of 2 or 3, is consistent with the observed space density of magnetic white dwarf stars.

There are more than 100 known magnetic Ap and Bp stars (Landstreet 1992), at least 15 of which have been measured well enough to determine whether the field is a centered dipole or not (Stift 1975; Landstreet 1980 and references therein; Mathys 1993). None of the 15 stars analyzed thus far can be described as having a simple centered dipolar magnetic field. Landstreet (1980) summarizes 6 of these as offset along the dipole axis between 0.1 and 0.4 stellar radii. Mathys (1992) studied 10 in detail (one overlap between the two papers), but in only enough detail to determine that a centered dipole was insufficient.

Of the approximately 40 white dwarf stars with fields greater than 10^6 G, 11, including those studied in this paper, have been analyzed allowing for the possibility of a non-centered dipolar magnetic field. PG 1658+441 (Achilleos & Wickramasinghe 1989a) was determined to be consistent with a centered dipole, but the other 10 were found to be inconsistent with centered dipoles; several were found to require a dipole offset along the dipole axis by $\lesssim$0.2 stellar radii.

More than 30 solar and later type stars have detected magnetic fields (Landstreet 1992), all in the range of 1 - 5 kG. These fields are believed to be powered by dynamos (Hartman & Noyes 1987; Landstreet 1992 and references in both). Since there is no physical process known to maintain a dynamo in a white dwarf, one has to assume that once such a star left the main sequence and made its way to the white dwarf track, the dynamo will have vanished along with its convection

zone. Therefore, we have to assume that the magnetic fields in white dwarfs are fossil remnants.

If the magnetic field structure is "conserved" as well as the flux during evolution from main sequence to white dwarf, then a non-centered dipolar main sequence star should become a non-centered dipolar white dwarf star. The analyses of the magnetic Ap stars and the magnetic white dwarf stars are consistent with the former evolving into the latter.

4.5.5 Uncertainties in "Best" Models

As explained in Section 4.4.1, the "best" model is selected by eye. When a model is found which seems to match the flux and circular polarization data very well, an orderly search in a grid in all parameters is made around the "best" values. From this search a form of error can be determined by deciding at which point the model is no longer acceptable. For G 99-47 and KUV 813-14 the following values apply: $B_p \pm 3$ MG, $\alpha \pm 5°$, $\mathrm{x_{off}} \pm 0.01$, $\mathrm{y_{off}} \pm 0.01$, $\mathrm{z_{off}} \pm 0.01$, $T_{\mathrm{G99-47}} \pm 100$ K, and $T_{\mathrm{KUV813-14}} \pm 1000$ K. Also for KUV 813-14, $B_p^q \pm 5$ MG, $\theta \pm 10°$, and $\phi \pm 20°$. The "best" model for G 227-35 is not as good as those for G 99-47 and KUV 813-14 and consequently the errors are larger. All the models in Figure 4.7 are good fits for this star and give a good idea of the size of the errors.

4.6 Conclusions

We have calculated theoretical flux and polarization spectra and compared them to the observed flux and circular polarization spectra of G 99-47, G 227-35, and KUV 813-14. The best models we found for these objects are listed in Table 4.7.

Previous works on these stars found different parameters for the best fits. In these cases, however, the circular polarization data, if they existed, were not used in the determination of the magnetic field parameters. The inclusion of these data in the process of fitting a magnetic field model has now been shown to be

useful and necessary. G 227-35 has made it clear that work needs to be done on developing theories on continuum circular polarization, and all the objects have demonstrated the need for better treatment of the linear polarization.

All three objects were best fit with offset dipoles or dipole+quadrupoles, which brings the number of magnetic white dwarf stars with non-centered dipoles to 11. This is consistent with magnetic Ap stars being the precursors to white dwarf stars. However, little is known about the magnetic field structure of the other main sequence stars.

The observations reported were taken in collaboration with Marshall H. Cohen and Robert W. Goodrich. AP is grateful to M.H. Cohen for advice and to Jim McCarthy and Neill Reid for comments on the manuscript. We thank our referee, J.D. Landstreet, for several useful comments on the manuscript. AP is especially grateful to Prof. Weidemann and others at Kiel for their hospitality during visits in 1993 and 1994. This research has made use of the Simbad database, operated at CDS, Strasbourg, France. This work was partially supported by NSF grant AST91-21889.

References

Achilleos, N. & Wickramasinghe, D.T. 1989a, ApJ, 346, 444

— 1989b, PAS Australia, 8, 148

— 1994, private communication

Achilleos, N., Wickramasinghe, D.T., Liebert, J., Saffer, S.A., & Grauer, A.D. 1992, ApJ, 396, 273

Angel, J.R.P., Borra, E.F., & Landstreet, J.D. 1981, ApJSS, 45, 457

Angel, J.R.P., Hintzen, P., & Landstreet, J.D. 1975, ApJ, 196, L27

Angel, J.R.P. & Landstreet, J.D. 1970, ApJ, 160, L147

— 1972, APJ, 178, L21

Angel, J.R.P., Liebert, J., & Stockman, H.S. 1985, ApJ, 292, 260

Beckers, J.M. 1969, Sol. Phys., 9, 372

Chanmugam, G. 1992, ARAA, 30, 143

Chanmugam, G. & Gabriel, M. 1972, A&A, 16, 149

Cohen, M.H., Putney, A., & Goodrich, R.W. 1993, ApJ, 405, L67

D'Antona, F. & Mazzitelli, I. 1990, ARAA, 28, 139

Donati, J.F., Achilleos, N., Matthews, J.M., & Wesemael, F. 1994, A&A, 285, 285

Epstein, P.S. 1916, Ann. Phyz., 50, 489

Forster H., Strupat W., Rösner W., Wunner, G., Ruder, H., & Herold, H. 1984, J. Phys. B, 17, 1301

Friedrich, S. 1993a, Dissertation, Tübingen

——. 1993b, private communication

Friedrich, S., Ostreicher, R., Ruder, H., & Zeller, G. 1994, A&A, 282, 179

Goodrich, R.W. 1991, PASP, 103, 1314

Goodrich, R.W., Cohen, M.H., & Putney, A. 1995, PASP, 107, 179

Greenstein, J.L. 1974, ApJ, 194, L51

——. 1986, ApJ, 304, 334

Greenstein, J.L. & Liebert, J.W. 1990, ApJ, 360, 662

Hammond, G.L., Sion, E.M., Aannestad, P.A., & Kenyon, S.J. 1993, in White Dwarfs: Advances in Observation and Theory, ed. M.A. Barstow (Dordrecht: Kluwer Academic Publishers), 253

Hartmann, L.W. & Noyes, R.W. 1987, ARAA, 25, 271

Henry, R.J.W. & O'Connell, R.F. 1985, PASP, 97, 333

Hintzen, P. & Strittmatter, P.A. 1974, ApJ, 193, L111

Hough, J. & Bailey, J. 1994, AAO UM 24.2

Jordan, S. 1989, in White Dwarfs, Lecture Notes in Physics 328, ed. G. Wegner (New York: Springer-Verlag), 333

——. 1992, A&A, 265, 570

——. 1994, Astronomische Gesellschaft Abstract Series, 10, 133

Jordan, S. & Merani, N. 1995, in preparation

Jordan, S., O'Connell, R.F., & Koester, D. 1991, A&A, 242, 206

Kemic, S.B. 1974, Joint Inst Lab Astrop Rep, 113

Kemp, J.C., Swedlund, J.B., Landstreet, J.D., & Angel, J.R.P. 1970, ApJ, 161, L77

Koester D., Schulz H., & Weidemann V. 1979, A&A, 76, 262

Lamb, F.K. & Sutherland, P.G. 1974, in Physics of Dense Matter, ed. C.J. Hansen (Dordrecht: D. Reidel Publishing Company), 265

Landstreet, J.D. 1980, AJ, 85, 611

——. 1992, A&ARev, 4, 35

Liebert, J., Angel, J.R.P., & Landstreet, J.D. 1975, ApJ, 202, L139

Liebert, J., Schmidt, G.D., Sion, E.M., Starrfield, S.G., Green, R.F., & Boroson, T.A. 1985, PASP, 97, 158

Liebert, J. & Stockman, H.S. 1980, PASP, 92, 657

Liebert, J. & Wehrse, R. 1983, A&A, 122, 297

Martin, B. & Wickramasinghe, D.T. 1984, MNRAS, 206, 407

——. 1986, ApJ, 301, 177

Mathys, G. 1991, A&ASS, 89, 121

——. 1993, in Peculiar versus Normal Phenomena in A-Type and Related Stars, eds. M.M. Dwaretsky, F. Castelli, and R. Faraggiana (San Fransisco: Astronomical Society of the Pacific), 232

Merani, N., Main, J., & Wunner, G. 1995, A&A, 298, 193

Mestel, L. 1965, in Stars and Stellar Systems, eds. L.H. Aller and D.B. McLanchlin (Chicago: University of Chicago Press), 297

Minkowski, R. 1938, Ann Rep Mt Wilson Obs, 28

O'Donoghue, D.E. 1980, Ap&SS, 68, 273

Oke, J.B. & Gunn, J.E. 1982, PASP, 94, 586

Rösner W., Wunner G., Herold H., & Ruder H. 1984, J. Phys. B, 17, 29

Schmidt, G.D. 1995, in Reviews in Modern Astronomy., ed. G. Klare, in preparation

Schmidt, G.D., Latter, W.B., & Foltz, C.B. 1990, ApJ, 350, 758

Schmidt, G.D. & Norsworthy, J.E. 1991, ApJ, 366, 270

Schmidt, G.D., Stockman, H.S., & Smith, P.S. 1992, ApJ, 398, L57

Schmidt, G.D., West, S.C., Liebert, J., Green, R.F., & Stockman, H.S. 1986, ApJ, 309, 218

Schwarzschild, K. 1916, Sitzber. Berliner Akad. 548

Semel, M., Donati, J.-F., & Rees, D.E. 1993, A&A, 278, 231

Spitzer Jr., L. 1956, Physics of Fully Ionized Gases (New York: Interscience Publishers), p.78

Stift, M.J. 1975, MNRAS, 172, 133

Thurner, G., Körbel, H., Braun, M., Herold, H., Ruder, H., & Wunner, G. 1993, JPhysB: AtMolPhys, 26, 4719

Underhill, A.B. & Waddell, J.H. 1959, NBS Circular 603

Unno, W. 1956, PAS Japan, 8, 108

West, S.C. 1989, ApJ, 345, 511

Wickramasinghe, D.T. & Ferrario, L. 1988, ApJ, 327, 222

Wickramasinghe, D.T. & Martin, B. 1979, MNRAS, 188, 165

Wunner, G., Rösner, W., Herold, H., & Ruder, H. 1985, A&A, 149, 102

Table 4.1 Summary of Observations

Object	Date	Stokes' Parameter	Exposure Length (minutes)	UT Start	Dichroic Cutoff (Å)	Blue Grating (g/mm)	Red Grating (g/mm)
G 99-47	28 Jan 1992	V	4x 6	04:26	5500	300	158
	16 Dec 1993	Q,U	4x10	09:26	5500	300	316
KUV 813-14	23 Aug 1992	V	2x20	08:13	5500	300	158
	24 Aug 1992	V	2x25	08:16	5500	300	158
	25 Aug 1992	Q,U	8x12	07:23	5500	300	158
	22 Aug 1993	Q,U	4x15	08:47	5200	300	158
G 227-35	23 Aug 1992	V	2x15	00:13	5500	300	158
	24 Aug 1992	V	2x25	04:07	5500	300	158
	25 Aug 1992	Q,U	4x12	03:50	5500	300	158
	22 Aug 1993	flux only	20	03:57	5200	300	158

Table 4.2 G 99-47: Model Parameters

Model	B_{dipole} (MG)	α	x_{off}	y_{off}	z_{off}	log g	[He] (%)	C	T_{eff} (K)
a	20	$-10°$	0.00	-0.11	$+0.08$	8.0	0	0.1	5500
b	20	$-10°$	0.00	-0.11	$+0.08$	8.0	0	1.0	5500
c	40	$-0°$	0.00	$+0.15$	$+0.10$	8.5	0	0.1	5500
d	40	$-0°$	0.00	$+0.15$	$+0.10$	9.0	0	0.1	5500
e	20	$-10°$	0.00	-0.11	$+0.08$	8.0	10	0.1	5500
f	20	$-10°$	0.00	-0.11	$+0.08$	8.5	0	0.1	5500
g	20	$-10°$	0.00	-0.11	$+0.08$	9.0	0	0.1	5500
h	20	$-10°$	0.00	$+0.00$	$+0.00$	8.0	0	0.1	5500
i	20	$-10°$	0.00	-0.11	$+0.08$	8.0	0	0.1	5800
j	20	$-10°$	0.00	-0.11	$+0.08$	8.0	50	0.1	5500

Table 4.3 KUV 813-14: Offset Dipole Model Parameters

Model	B_{dipole} (MG)	α	T_{eff} (K)	x_{off}	y_{off}	z_{off}	C
a	45	−13°	11,000	+0.013	−0.015	+0.050	0.1
b	45	−10°	11,000	+0.005	−0.015	+0.050	1.0
c	45	−13°	11,000	+0.013	−0.015	+0.050	1.0
d	45	−10°	10,000	+0.005	−0.015	+0.050	1.0
e	45	−10°	12,000	+0.005	−0.015	+0.050	1.0
f	45	−10°	11,000	+0.000	+0.000	+0.000	1.0
g	50	−10°	11,000	+0.005	−0.015	+0.050	1.0
h	40	−10°	11,000	+0.005	−0.015	+0.050	1.0

Table 4.4 KUV 813-14: Dipole + Quadrupole Model Parameters

Model	B_{dipole} (MG)	α	B_{quad} (MG)	θ	ϕ	C
i	43	−7°	8	+20°	−10°	1.0
j	43	−7°	8	+20°	−10°	0.1
k	43	−7°	8	+0°	+0°	1.0
l	43	−7°	13	+20°	−10°	1.0
m	43	−7°	3	+20°	−10°	1.0

Table 4.5 KUV 813-14: Rotated Model Parameters

Model	β	P(x,y,z)	α	x_{off}	y_{off}	z_{off}
a	−100.8°	(0.018, 0.003, 0.08)	−2°	0.027	0.015	0.04
b	−100.8°	(0.020, 0.000, 0.05)	+10°	0.034	0.003	0.04
c	−100.8°	(0.020, 0.000, 0.10)	−2°	0.024	0.015	0.05
d	−100.8°	(0.000,−0.008, 0.063)	−21°	0.018	0.016	0.05
e	+100.8°	(0.000,−0.008, 0.063)	−21°	−0.023	−0.010	0.05
f	−100.8°	(0.018, 0.008, 0.08)	−6°	0.030	0.013	0.05

Table 4.6 G 227-35: Model Parameters

Model	B_{dipole} (MG)	α	x_{off}	y_{off}	z_{off}
a	170	+15°	0.000	0.000	−0.100
b	170	+25°	0.000	0.000	−0.150
c	170	+15°	0.000	−0.015	−0.150
d	180	+8°	0.000	−0.005	−0.050
e	180	+8°	0.000	−0.010	−0.050
f	180	+8°	0.000	−0.015	−0.050
g	180	+15°	0.000	−0.015	−0.100

Table 4.7 Summary of Best Models

Object	B_p (MG)	α	T_{eff} (K)	x_{off}	y_{off}	z_{off}	C	B_p^q (MG)	θ	ϕ
G 99-47	20	-10°	5500	0.000	-0.110	+0.08	0.1			
KUV 813-14	45	-13°	11000	+0.013	-0.015	+0.05	0.1			
	45	-10°	11000	+0.005	-0.015	+0.05	1.0			
	43	-7°	11000				1.0	8.0	+20°	-10°
G 227-35	$\geq$170 $\leq$180	$\geq$+8° $\leq$+25°	7000	+0.000	$\geq$0.000 $\leq$−0.015	$\geq$−0.05 $\leq$−0.15	0.1			

Figure Captions

Figure 4.1

Geometrical representation of the coordinate systems used by the computer program on a star. The eye is the observer who is facing the $x - z$ plane and is rotated an angle α in the $y - z$ plane.

(a) Dipole coordinate system showing offsets.

(b) Quadrupole coordinate system showing the angles θ and ϕ which describe the relationship between the dipole (d) and the quadrupole (q).

Figure 4.2

G 99-47. The top panel shows the observed flux spectrum and 10 dipolar models; the 0 marks the zero point for the observed flux spectrum (top spectrum) and the models are shifted for clarity. The bottom panel shows the corresponding circular polarization spectra, again with the top spectrum being the observed spectrum and the models shifted for clarity; the dotted lines define zero for each spectrum and each tick mark is 1% polarization (values are indicated for the observed and first model spectra). The break in the observed spectrum is due to the spectrograph's dichroic. Table 4.2 lists the different models for this figure. All models are convective. B_{dipole} is the magnetic field strength the centered dipole would have at the polar surface; the angle α is the viewing angle and is defined such that $+90°$ is the north magnetic pole and $-90°$ is the south pole; and the offsets are in units of stellar radii and represent the position off center of the dipole, where the z-axis is the dipole axis and the x-axis is in the plane of the sky. The model with the heavier line weight is the best fit model.

Figure 4.3

KUV 813-14. The top and bottom panels are similar to those in Figure 4.2: the zero next to the upper panel marks the zero point of the observed flux and the models are shifted for clarity; the dotted lines in the lower panel mark V/I=0 for

each spectrum and each tick mark is 1% circular polarization (values are indicated for the observed and first model spectra). The observed data is an average of the 1992 data. Table 4.3 lists the different models for this figure. The models all have log g= 8.0 and are convective.

Figure 4.4

KUV 813-14. Similar to Figure 4.3, except these models are dipole + quadrupole. Table 4.4 lists the different models for this figure. All models have an effective temperature of 11,000K. B_{quad} is the quadrupolar field strength and both the quadrupolar dipolar fields are centered on the star. The angle θ is the angle between the dipole and the quadrupole. The angle ϕ is the azimuthal angle of the quadrupole rotated about the dipole axis.

Figure 4.5 *KUV 813-14.* Similar to the top panels of Figures 4.2-4.4 – the zero indicates the zero point of the observed spectrum and the models are shifted for clarity. The observed data is from 1993, the models are models whose parameters are calculated from rotating Figure 4.3's model a by 100.8° about different axes. Table 4.5 lists the different models for this figure. β and P are as described in Figure 4.6.

Figure 4.6

Geometrical representation of the parameters used to describe the axis about which the "best" fit model is rotated. The vector OP describes the rotation vector itself. β is the angular amount of rotation.

Figure 4.7

G 227-35. Similar to Figure 4.2; the zero next to the upper panel marks the zero point of the observed flux and the models are shifted for clarity; the dotted lines in the lower panel mark V/I=0 for each spectrum and each tick mark is

1% circular polarization. Table 4.6 lists the different models for this figure. The models are all 7000 K, non-convective, and the Stark factor $C = 0.1$.

Figure 4.8

Linear Polarization. These are the linear polarization spectra for G 99-47. The top panel is the percent linear polarization. The bottom panel is the position angle of the linear polarization. The numbers and letters mark the figure number and model to which these curves correspond.

Figure 4.9

Convection versus Non-convection. The top panel shows F_λ for a convective and a non-convective model, where the rest of the parameters are those of G 99-47 model a (see Table 4.2). The lower panel shows the circular polarization for these models.

Figure 4.1

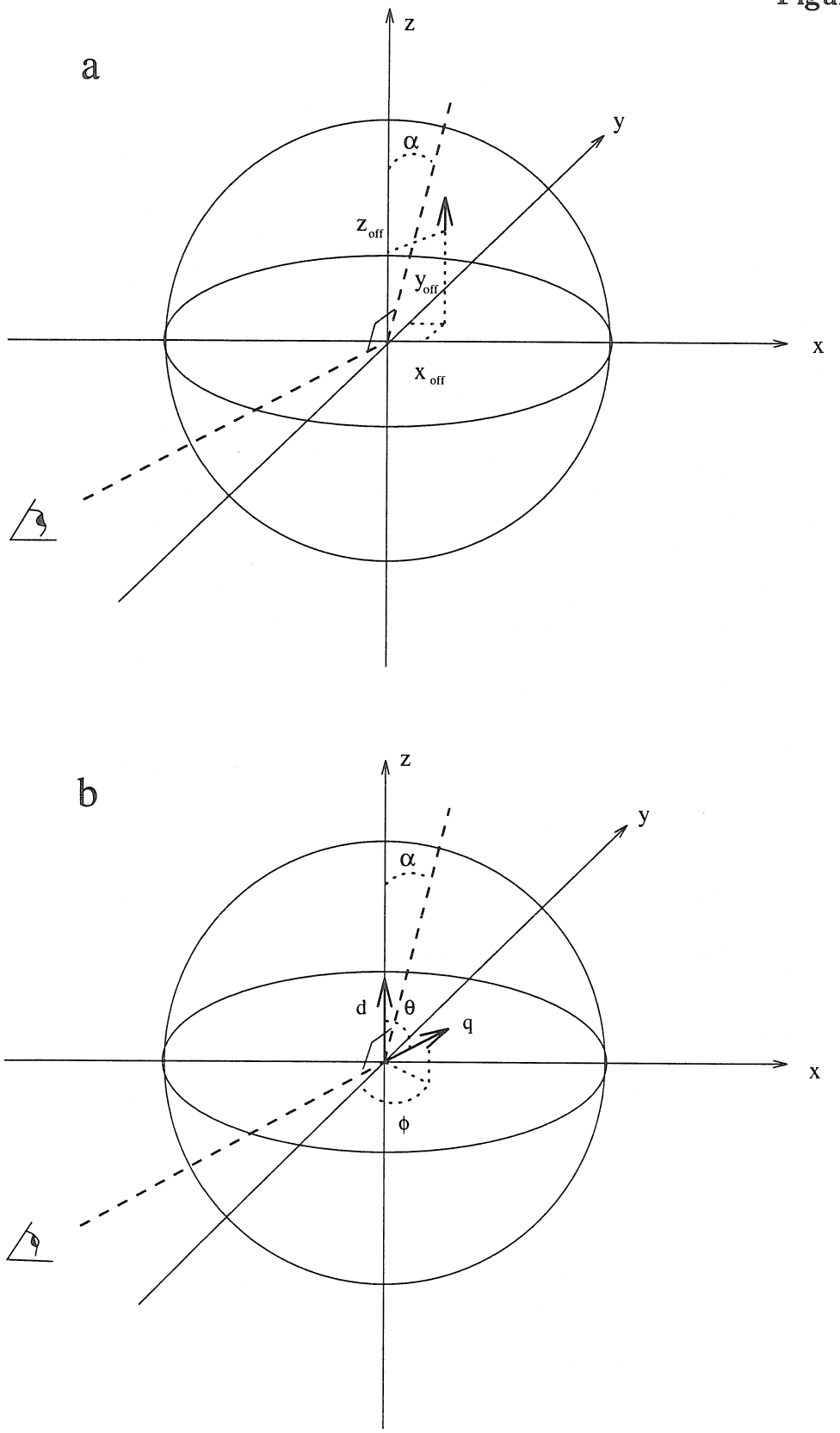

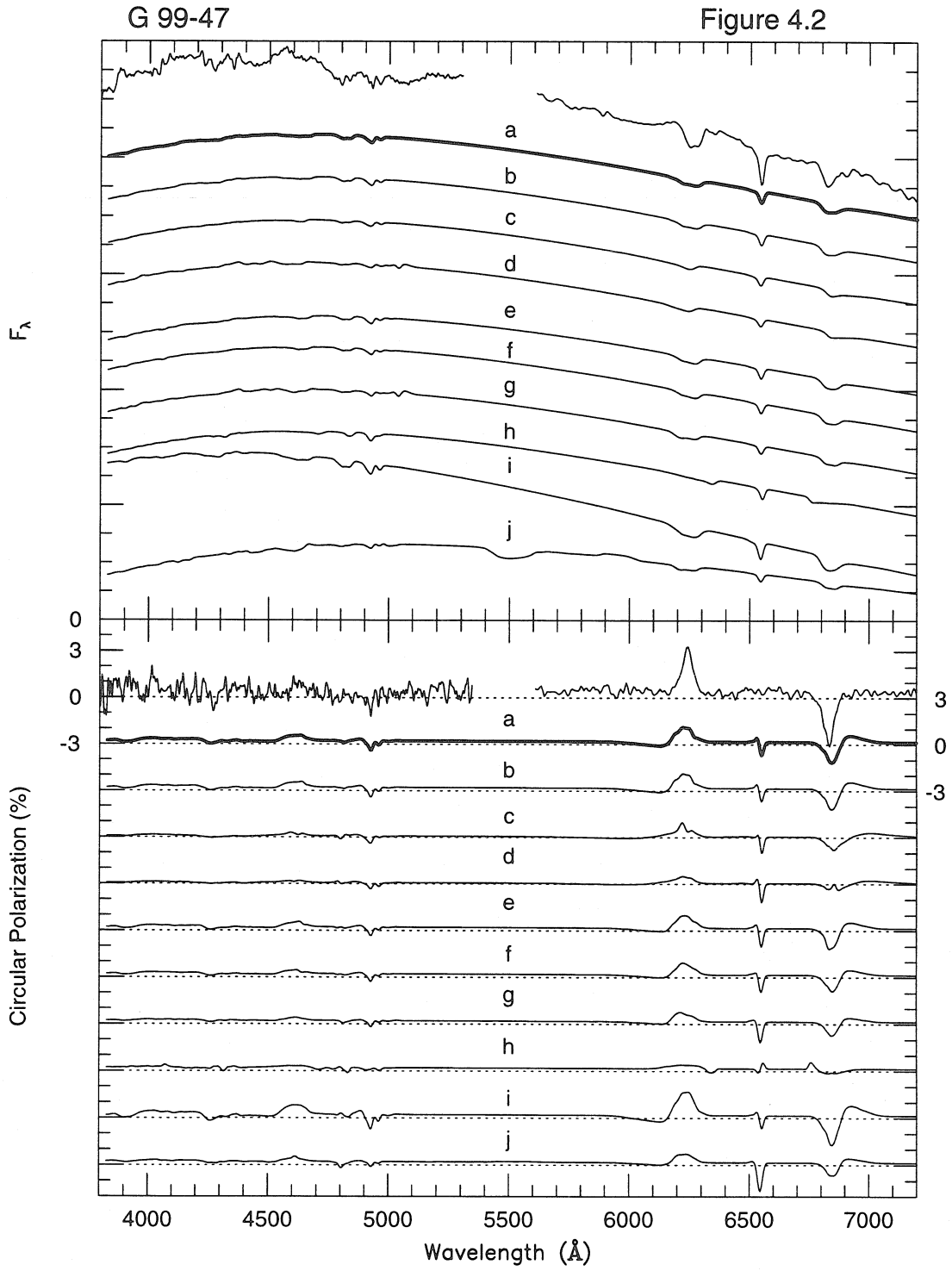
G 99-47
Figure 4.2
F_λ
a
b
c
d
e
f
g
h
i
j
0
3
0
-3
Circular Polarization (%)
4000
4500
5000
5500
6000
6500
7000
Wavelength (Å)

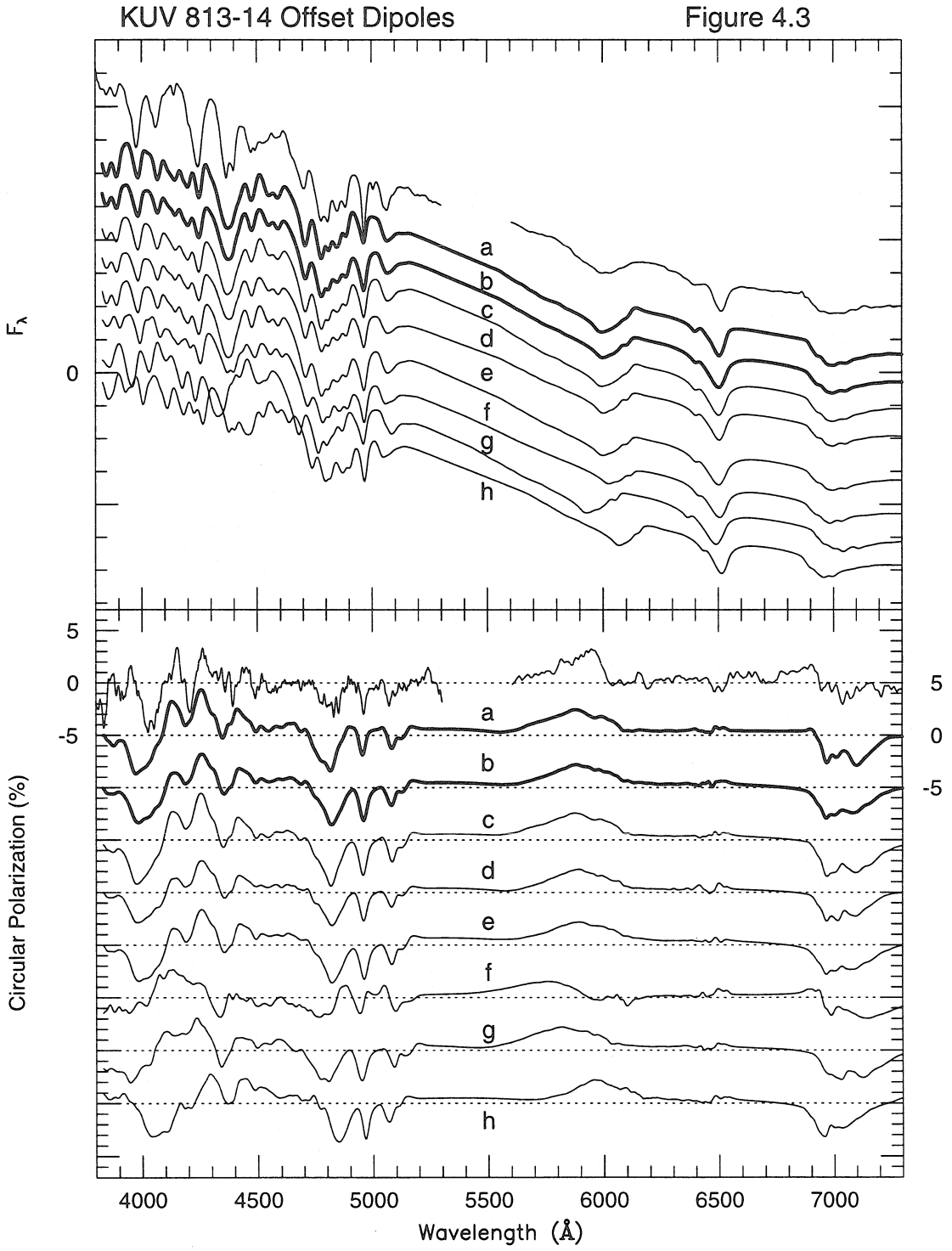
KUV 813-14 Offset Dipoles
Figure 4.3
F_λ
0
a
b
c
d
e
f
g
h
5
0
-5
Circular Polarization (%)
4000
4500
5000
5500
6000
6500
7000
Wavelength (Å)

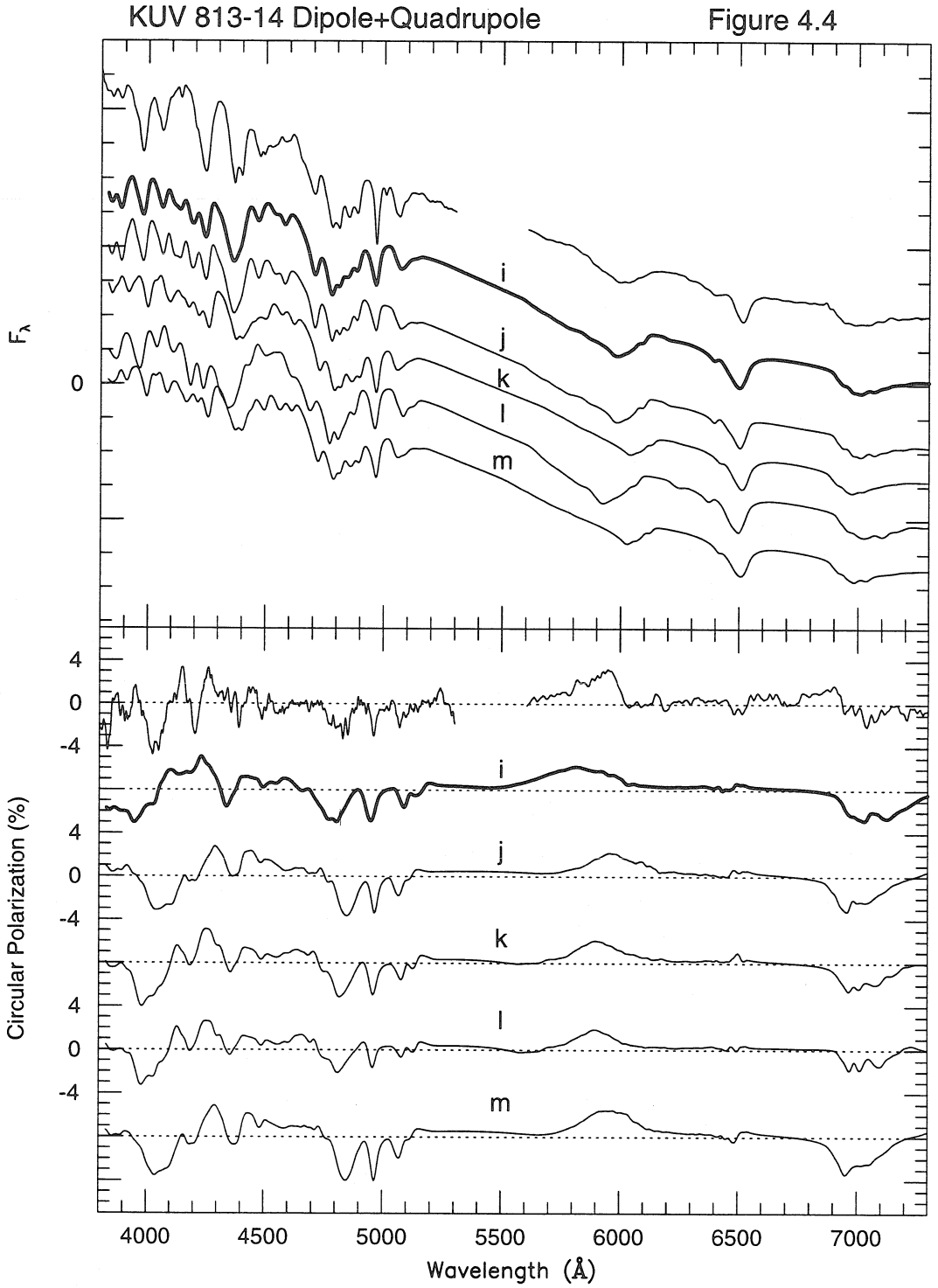
KUV 813-14 Dipole+Quadrupole
Figure 4.4
F_λ
0
i
j
k
l
m
Circular Polarization (%)
4
0
-4
4000
4500
5000
5500
6000
6500
7000
Wavelength (Å)

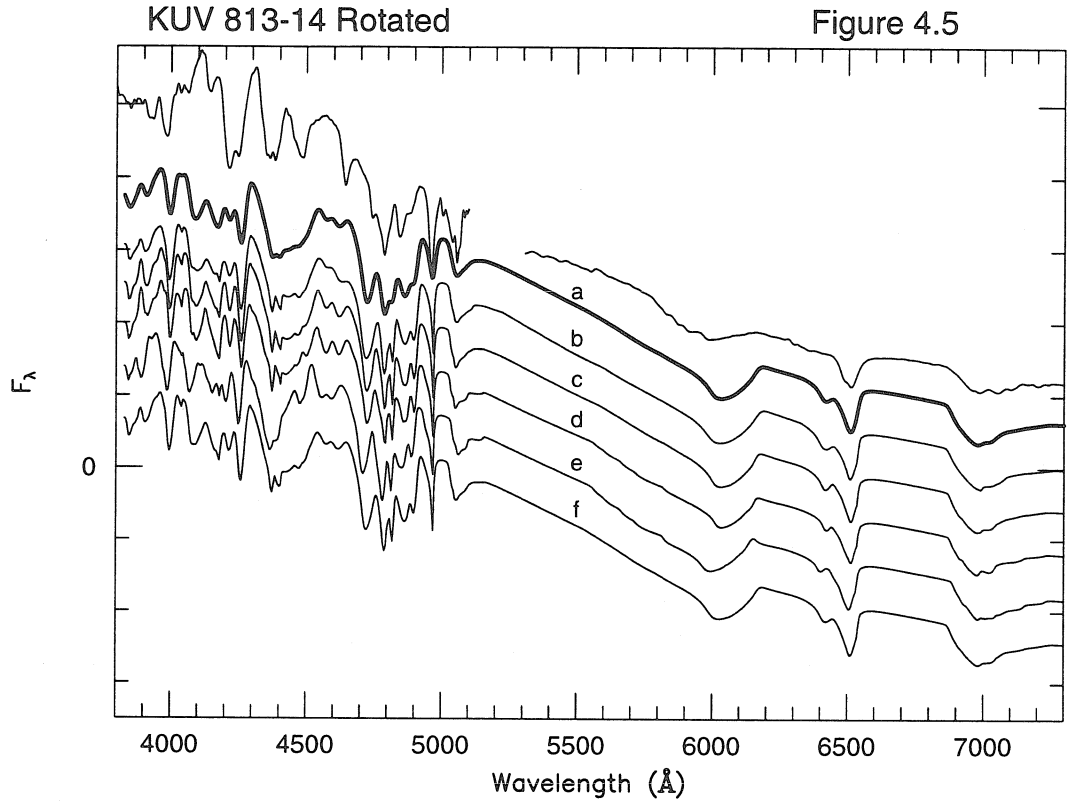
KUV 813-14 Rotated
Figure 4.5
a
b
c
d
e
f
0
F_λ
4000
4500
5000
5500
6000
6500
7000
Wavelength (Å)

Figure 4.6

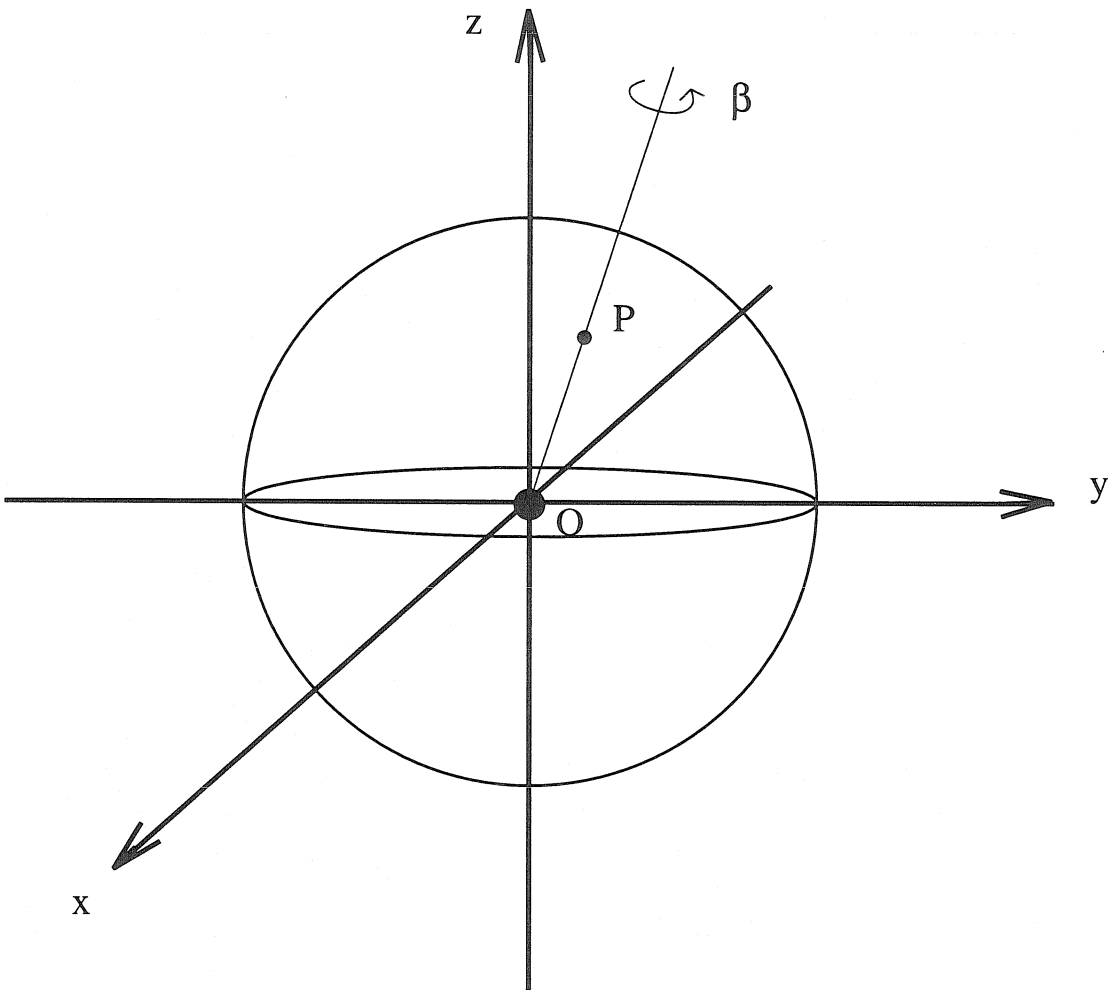

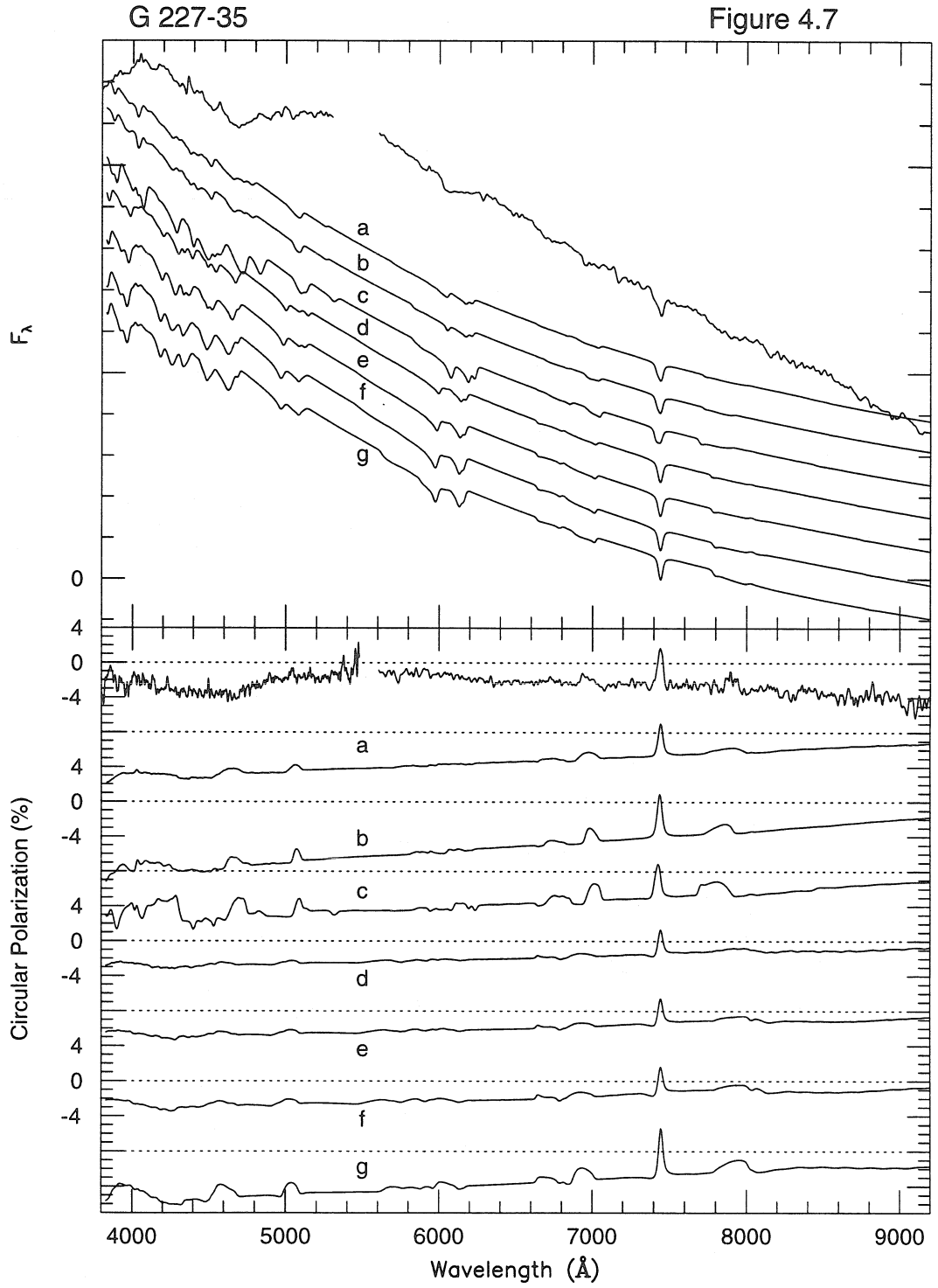
G 227-35
Figure 4.7
F_λ
a
b
c
d
e
f
g
0
4
0
-4
Circular Polarization (%)
4000
5000
6000
7000
8000
9000
Wavelength (Å)

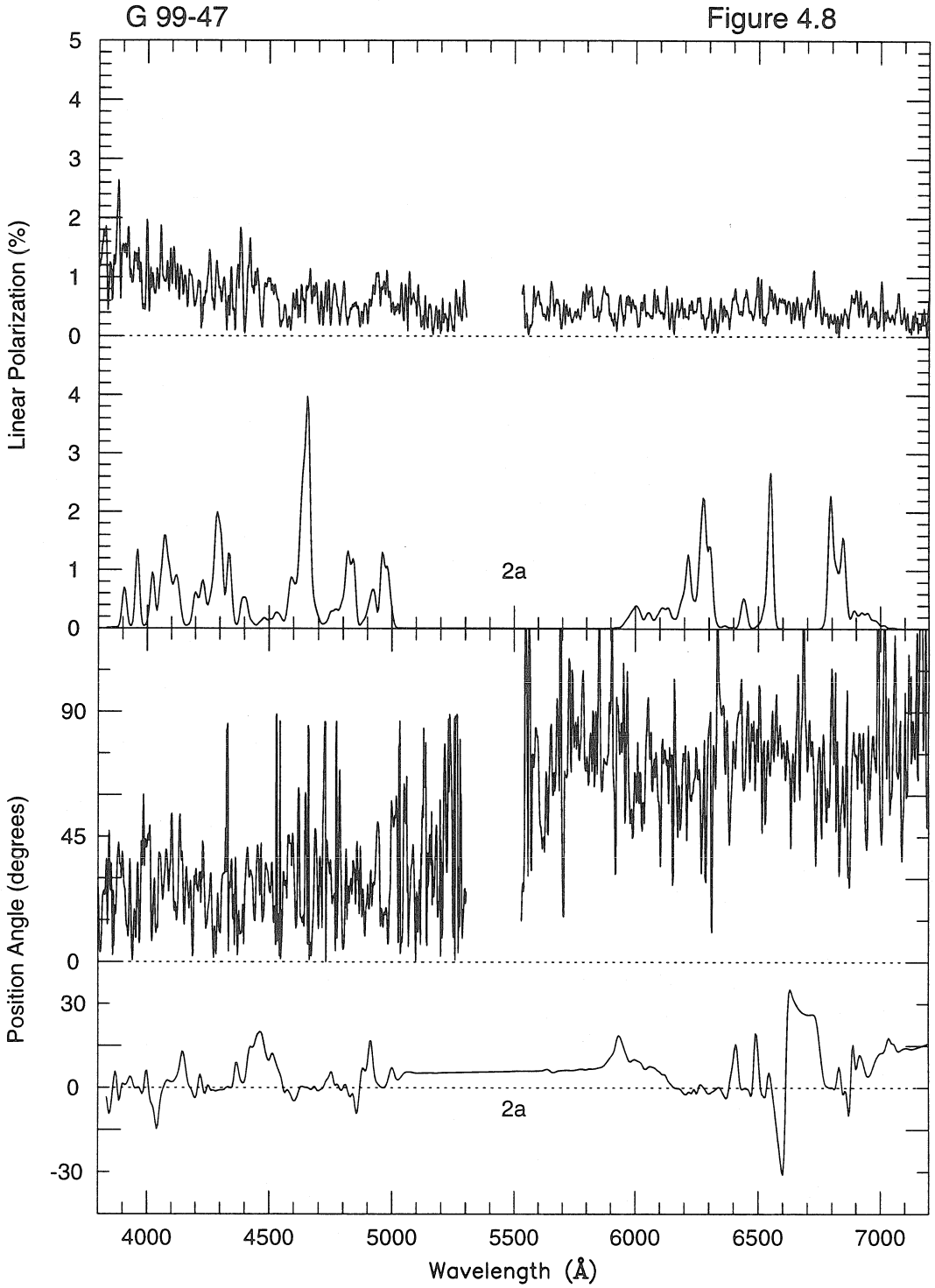
G 99-47
Figure 4.8
Linear Polarization (%)
5
4
3
2
1
0
4
3
2
1
0
2a
Position Angle (degrees)
90
45
0
30
0
-30
2a
4000
4500
5000
5500
6000
6500
7000
Wavelength (Å)

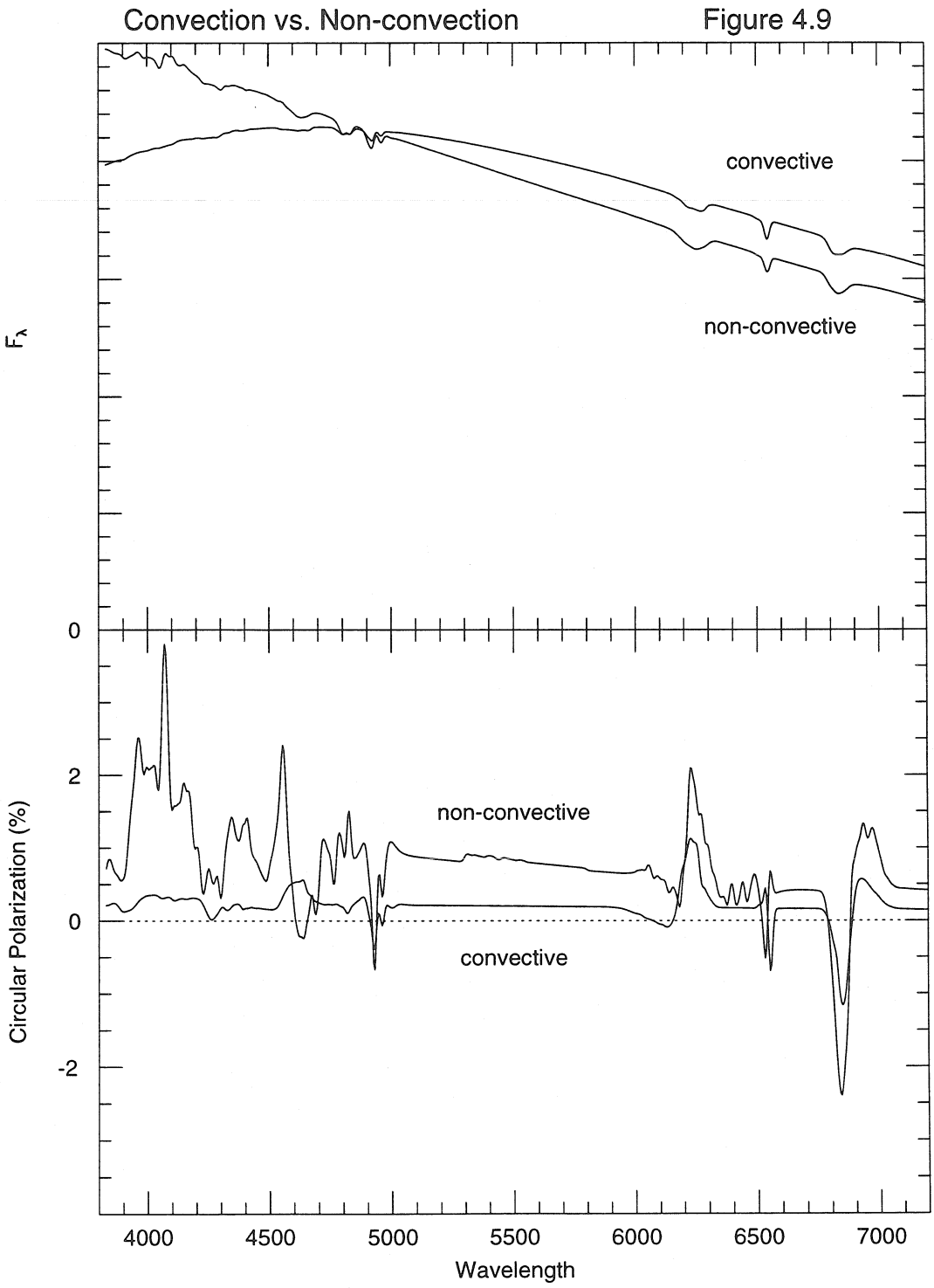
Convection vs. Non-convection
Figure 4.9
convective
non-convective
F_λ
0
2
0
-2
non-convective
convective
Circular Polarization (%)
4000
4500
5000
5500
6000
6500
7000
Wavelength

CHAPTER 5

Conclusions and Future Research

The preceding chapters have studied three aspects of magnetic white dwarf stars — the number of them, their rotation, and their magnetic field structure. A general summary is that they are few in number ($\sim$ 3% of all white dwarf stars with fields $>$ 1 MG), 14 rotate with periods between hours and weeks and 5 with periods on the order of a century, and these magnetic field structures tend to be off-set dipoles or dipoles+quadrupoles.

In Chapter 2 we saw that the distribution of magnetic fields in white dwarf stars is apparently bimodal. One peak of the distribution is around 10 - 100 MG and the other peak is less than 30 kG. This is analogous to the main sequence magnetic field distribution. There, one peak is at $\sim$ 10 kG and the other less than 100 G. If the magnetic flux of a star is conserved during evolution from a main sequence star to a white dwarf star, and there is no known mechanism to destroy the flux, then the white dwarf magnetic field distribution is the evolved version of the main sequence distribution. The 10 kG peak in the main sequence distribution is composed of magnetic Ap stars. This supports the theory of the magnetic Ap stars being the ancestors of the magnetic white dwarf stars. Chapter 4 discusses further support of this theory. Both magnetic Ap stars and magnetic white dwarf stars typically have offset dipolar magnetic field structures. This fact is not proof that they are related, but were it not true, then either the magnetic white dwarfs are not descended from the Ap stars or there is some other aspect of stellar evolution not understood.

In Chapter 3, the riddle of rotation was discussed. Some magnetic white dwarfs rotate quickly and others barely rotate at all. There is no correlation between rotation period and either temperature (age) or magnetic field strength. There is no good theory to explain this bimodal distribution. However, the distribution may be an artifact of small number statistics.

The work presented here has by no means exhausted this highly intriguing field. It is clear that there are several paths where future research on magnetic white dwarf stars should be directed. Solving the rotation riddle is one path to take. First, the distribution of rotation periods must be firmly established. This is done by monitoring all magnetic white dwarfs for rotation. Also, more non-magnetic white dwarfs should have their rotational velocities measured, perhaps through the use of high resolution spectrographs on large telescopes, e.g., the Keck 10 meter telescope. Another path to take is to calculate better atmospheric models of magnetic white dwarf stars. This requires improved theories of opacities in large magnetic fields as well as a better understanding of the atmospheric temperature structure. An added bonus from improved models is that rotation periods, in theory, could be determined with fewer observations by fitting models to the data and rotating the models. At present, approximately 100 observations are required for an accurate period determination. If an accurate model for the magnetic white dwarf can be calculated, then an accurate model can be calculated for each rotational phase and matched to the data at each observed phase. Observations could be decreased by a factor of 3 or 5 with this method. A third path of research to follow would be to make high resolution spectropolarimetric observations of the low field white dwarfs to better determine the magnetic field distribution below 30 kG. This particular path is very rugged at the moment. One reason is the lack of high resolution spectropolarimeters. A second reason is that white dwarfs tend to be faint, thus making these measurements feasible on bright white dwarfs only.

Like all puzzles, the magnetic white dwarf can be solved. It will just take more observations.